UNIVERSITY OF NAIROBI

HUMAN HEALTH RISKS ASSOCIATED WITH RADIOACTIVITY AND HEAVY METALS AROUND MRIMA HILL AND THE KWALE HEAVY MINERAL SAND MINE, KENYA

By

Pamella Kageliza Kilavi-Ndege

I80/52972/2018

A Thesis Submitted in Fulfilment of the Requirements for Award of the Degree of Doctor of Philosophy in Physics of the University of Nairobi.

© December, 2023

DECLARATION

I declare that this thesis is my original work, and it has not previously been submitted to any other University either in whole or in part for an award of a degree or publication. Where other people's work or my own work has been used, this has properly been acknowledged and referenced in accordance with the University of Nairobi's policy requirements.

Signed: …………………………………… Date: 1st December 2023 …………………………

Pamella Kageliza Kilavi-Ndege

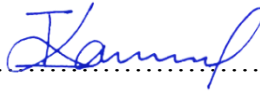I80/52972/2018
Department of Physics
Faculty of Science and Technology
University of Nairobi

This thesis has been submitted for examination with our approval as research supervisors:

	Signature	Date
Dr. Muchai Ian Kaniu		1st December 2023

Department of Physics
University of Nairobi
P.O. Box 30197-00100, Nairobi, Kenya
ikaniu@uonbi.ac.ke

Prof. Patel Jayanti P — 1st December 2023

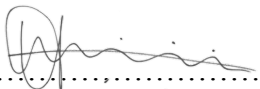School of Physics and Earth Science
Technical University of Kenya
P.O. Box 52428-00200, Nairobi, Kenya
jaypy.patel@gmail.com

Prof. Usman T. Iyabo — 1st December 2023

School of Physics
University of Witwatersrand
Private Bag X3, WITS 2050, Johannesburg, South Africa
iyabo.usman@wits.ac.za

"And when the time is right I, the Lord will make it happen."

Isaiah 60:22

ACKNOWLEDGEMENTS

My apologies to anyone I have unintentionally not mentioned.

ABSTRACT

This study addresses global health concerns from heightened environmental radioactivity and heavy metal exposure. Despite extensive research on the dynamics and health risks of heavy metal pollution from various mining activities, a significant knowledge gap persists, particularly in understanding the impact on human health from heavy mineral sand (HMS) mining. This research focuses on the ecological and human health risk assessment resulting from exposure to heavy metals and naturally occurring radioactive materials in soil and drinking water around Mrima Hill and the Kwale HMS deposit, utilizing the Agilent 7700s ICP-MS technique. Water quality indices were used to evaluate the quality of drinking, while the geo-accumulation index (I_{geo}), enrichment factor (EF), and pollution index (PI) were used to evaluate the extent of soil pollution. The USEPA model was used to evaluate the non-carcinogenic (NCR) and carcinogenic (CR) health risks. The total effective dose equivalent (TEDE) and the incremental lifetime cancer risk (ILRC) from exposure to environmental radioactivity were assessed using the RESRAD OFFSITE code. Cr and Cd in water samples exceeded the maximum contaminant levels of 0.1 and 0.005 mg/L in drinking water, with Cd contributing the highest percentage to the WQI. However, the soil was strongly polluted by Cr, As, and Cd. Mean Cr, As, and Cd concentrations in soil samples from Mrima Hill were ~500, ~7, and ~9 times higher than the maximum allowable concentration (MAC) of 200 mg/kg Cr, 20 mg/kg As, and 5 mg/kg. The EF of Cr, As, and Cd for soil samples from Mrima Hill were ~700, ~5, and ~224 higher than the EF threshold value of 1.5. The NCR assessment showed that the population was more susceptible to the effects of As in soil and Cr in drinking water. As contributed ~67% to the hazard indices (HI) from exposure to soil, while Cr contributed ~60% to the HI in drinking water. The CR assessment showed that both As and Cr values from ingestion and dermal exposure to water and soil were above the threshold value of 10^{-4}. The TEDE assessment showed that the dose values for inhabitants from the Kwale HMS deposit and Mrima Hill environs were highest (67.72 µSv and 504.7 µSv, respectively) in the 74th year of exposure. The ILCR values from external exposure to ^{228}Ra and ^{228}Th in the soil were above the regulatory limit of 10^{-4}. However, the ILCR from ingesting soil particles was within the tolerable limit of 10^{-6} to 10^{-4}, while the ILCR from inhaling the soil particles was below the recommended value

of 10^{-6}. Thus, the populations in the surveyed areas are prone to health risk from exposure to natural radioactivity and heavy metals. There is therefore need for stringent mechanisms to monitor, control, and mitigate soil pollution from future mining activities. Epidemiological studies from exposure to these metals could be done to assess the occurrence and distribution of the health risks from exposure to these metals.

Table of Contents

List of Figures

List of Tables

Acronyms and Abbreviations

AAS	Atomic absorption spectroscopy
CRM	Certified Reference Materials
DNA	Deoxyribonucleic acid
EC	Electrical conductivity
EDXRF	Energy dispersive x-ray fluorescence
HMS	Heavy mineral sand
HPGe	High purity germanium
ICP MS	Inductively coupled plasma mass spectrometry
NORM	Naturally occurring radioactive material
RESRAD	RESidual RADioactive
ppm	Parts per million
ppt	Parts per trillion
RIBE	Radiation induced bystander effect
REE	Rare earth elements
RNA	Ribonucleic acid
USEPA	United States Environmental Protection Agency
WASREB	Water Service Regulatory Board
WHO	World Health Organization

CHAPTER 1

Introduction

1.1   Background to the Study

The unique properties such as non-corrosiveness, high melting points, high resistivity to wear and tear, low weight with high specific strength, and biocompatibility (Kamachi *et al.*, 2003; Bilčíková *et al*., 2018; Alves and Coutinho, 2019)   make titanium (Ti) and niobium (Nb) highly sought-after metals. Ti is used in dye-sensitized solar cells (O'Regan and Gratzel, 1991), as a pigment in cosmetics and food (McNulty, 2007), and in the production of aerospace components and cryogenics devices (Henriques, 2009). Ti is also used in biodevices to aid in healing, correct deformities, or restore the function of the original body part (Kamachi *et al*., 2003). On the other hand, Nb is used to make superconducting magnets, commemorating coins, and medical equipment, in the nuclear, electronics, and jewelry industries (Bilčíková *et al.*, 2018; Alves and Coutinho, 2019).

Ti exists in the environment as rutile, ilmenite, leucoxene, sphene, perovskite, anatase, and brookite ores (Kabata-Pendias, 2010). The Ti ores are deposited in igneous and related rocks, metamorphic rocks, or are part of unconsolidated heavy mineral sand deposits and shoreline beach placers (Woodruff *et al*., 2017). The unconsolidated heavy mineral sand deposits contain other high-density and erosion-resistant minerals such as monazite, zircon, chromite, garnet, staurolite, kyanite, and tourmaline (Van Gosen *et al*., 2014; Woodruff *et al*., 2017). However, ores like pyrochlore, tantalite, and niobite contain a substantial amount of Nb, while biotite, rutile, sphene, and zircon have traces of Nb (Sutliff-Johansson *et al*., 2021). The Nb ores occur exclusively in carbonatites and alkaline intrusions rocks (Verplanck et al., 2014). Both Nb and Ti ores co-exist with radioactive elements uranium (U), thorium (Th), and other elements such as chromium (Cr), iron (Fe), lead (Pb), manganese (Mn), zirconium (Zr), the rare earth elements (REE), among others (Zack *et al*., 2002; Abuodha and Hayombe, 2006; Van Gosen *et al*., 2014; Woodruff *et al*., 2017; Sabu and Rejith, 2020).

Mining and mineral processing activities of Nb and Ti ores produce large quantities of waste such as dust, sand tails, sludge, and mine water, which may contain the naturally

occurring radionuclides (Th and U), and other heavy metals (Lottermoser, 2010; Ramasamy *et al*., 2014; Alves and Coutinho, 2019). The radionuclides and heavy metals may be transported to far-off places through run-off, erosion, and atmospheric deposition polluting the water, soil, and air (Pokhrel and Dubey, 2013). But since soils have filtering and buffering properties (Kabata-Pendias and Mukherjee, 2007), it acts as a sink for radionuclides and heavy metals from mining and other anthropogenic activities (Horta *et al*., 2015). The heavy metals and radionuclides do not undergo microbial action or chemical degradation (Wuana and Okieimen, 2011), but they accumulate in the soils. These metals and radionuclides may exceed their respective geochemical background levels in soil, polluting it. They then percolate through the soil into groundwater, contaminating it (Kabata-Pendias, 2010).

The radionuclides and metals contaminated environmental media may be ingested, inhaled, or come in to contact with the skin. Thus, the general population may be exposed to radionuclides and heavy metal-contaminated soil, water, or air via gastrointestinal tract, respiratory tract, or dermal contact (Kabata-Pendias and Mukherjee, 2007). The radionuclides and heavy metals then passively or actively diffuse through the cell membrane into specific organelles or cells for metabolism, storage, and excretion, or they are transported further within the body (USEPA, 1992). The inorganic metals are non-biodegradable. They react with functional groups that play essential roles in biomolecules such as nuclei acids, proteins, and lipids (Briffa *et al*., 2020). The metals may displace critical endogenous metals from the biomolecules leading to modification of proteins and change in enzymatic activities or disruption of the functions of the organelles (Rump *et al*., 2019).

Heavy metals such as Mn, Cu, Ni, Zn, and Fe are essential for the growth and normal functioning of the immune system, the formation of the skeletal structure, and the maintenance of the colloidal system (Tchounwou *et al*., 2012). However, these metals become detrimental to human health when they exceed a prescribed threshold concentration (Kabata-Pendias and Mukherjee, 2007). For instance, excessive intake of Fe and high Fe stores has been associated with increased oxidation and initiation of free radicals in healthy people (Zacharski *et al.*, 2000). The free radicals are toxic to

biomolecules (Phaniendra, *et al.*, 2015). They initiate carcinogenesis and pathogenesis of other diseases, such as diabetes mellitus and atherogenesis (Zacharski *et al.*, 2000). Metals such as Cu are involved in several oxidation-reduction reactions and cycles between an oxidized state and a reduced state. Cu becomes potentially toxic during this transition since superoxide and hydroxyl radical, which play a role in mutagenesis and carcinogenesis, is generated (Tchounwou *et al.*, 2012).

Other metals such as Cr, Cd, As, and Pb are non-essential, and exposure to these metals, even at low concentrations, produces multiple organ damage. The metal ions interact with biomolecules such nuclear proteins and DNA, damaging or altering the shape and structure of the biomolecules (Tchounwou *et al*., 2012). They produce radicals, which play a role in mutagenesis and carcinogenesis. For instance, Cd, which has a similar ionic radius and chemical behavior with calcium (Kubier *et al*., 2019), interferes with calcium metabolism leading to weakened bones and severe joint pain and renal dysfunction (Aoshima, 2016). When ingested over a prolonged period, it selectively accumulates in the renal cortex causing irreversible renal dysfunction (Aoshima, 2016). In addition, prolonged exposure to Cd may lead to various types of cancer, including breast and lung cancer (Kubier *et al*., 2019).

Ingestion of Pb and As contaminated drinking water also causes systemic health issues, including cognitive and neurobehavioral development anomalies, irreversible changes in vital organs, and cancer development (Wuana and Okieimen, 2011; Tchounwou *et al.*, 2012). Smith *et al.* (2018) linked lung, kidney, and blood cancer death of a population in Northern Chile to ingestion of As-contaminated water. Other studies showed that dermatitis and skin ulcers were due to exposure to Cr, As, and Ni-contaminated soils (Bagdon and Hazen, 1991; Zhang *et al*., 2009; Genchi *et al.,* 2020), while nasal or lung cancers were associated with inhalation of Cr, U, Ni, As, and Th contaminated dust particles; (Pinkerton *et al.,* 2004; Belluck *et al*., 2003; Martin *et al.,* 2014). However, the enormity of the human health risk depends on the chemical form of the metal, the particle size of inhaled particles, the solubility, and the biotransformation of the metal (Tchounwou *et al.*, 2012).

Besides the chemotoxicity on human health from exposure to U and Th as heavy metals, these metals are also radiotoxic. The radioactivities of U and Th are very low while in their natural state (Ma *et al.*, 2020). However, mining activities disturb their secular equilibrium and specific activities and initiate the mobilization of the radionuclides in the environment. They decay to stable nuclides through the emission of alpha (α), beta (β), and gamma (γ) radiation. When ingested or inhaled, the emitted radiations interact with and deposit energy into cells, breaking the DNA strands (Prise and O'Sullivan, 2009). The radiations may also indirectly interact with the water molecules in the cells and form free radicals such as hydrogen peroxide, hydroxyl, and alkoxy, which also break the DNA strands (Desouky *et al.*, 2015). Residual or unrepaired DNA double strands could cause chromosomal aberration, loss of genetic material, and death of cells, while incorrectly paired DNA double strands may induce mutations that leading to mutagenesis (Prise and O'Sullivan, 2009). Even though the damage to the DNA has been linked to high doses of radiation, a review by Desouky *et al.* (2015) showed that the radiation-induced bystander effect (RIBE) was due to exposure to low doses of radiation. RIBE has been linked to induced mutations, chromosome instability, exchange of sister chromatids, cell differentiation, and altered gene expression (Desouky *et al.,* 2015)

Despite the well-documented dynamics and human health risks assessment associated with environmental radioactivity and heavy metal pollution in the environment from gold mining activities (Bortey-Sam *et al.*, 2015; Kamunda *et al.*, 2016; Xiao *et al.*, 2017; Bello *et al*., 2019; Jiménez-Oyola *et al.*, 2021), uranium mining activities (Haribala *et al*., 2016; Wang *et al*., 2019; Haakonde et al., 2020; Raghavendra *et al*., 2020; Chen *et al*., 2022), and other metals (Huang *et al.*, 2009; Qu *et al.*, 2012 Li *et al.*, 2014; Adamu *et al.,* 2015), scanty information on human health risk assessment from mining and mineral processing activities of Ti and Nb is available. This research, therefore, presents a typical case study of the health risk assessment from exposure to chromium (Cr), manganese (Mn), nickel (Ni), copper (Cu), zinc (Zn), arsenic (As), cadmium (Cd), lead (Pb, thorium (Th) and uranium (U) in soil and water samples collected at the Kwale HMS deposit, where Ti ore mining is ongoing, and Mrima Hill, a prospecting area for mining of Nb and rare earth elements (REE), both located in Kwale County, south coast of Kenya.

1.2   Statement of the Problem

Despite the well-documented dynamics and human health risks associated with heavy metal pollution of soil from other mining activities, such as gold mining activities (Kamunda *et al*., 2016; Xiao *et al.*, 2017; Bello *et al.*, 2019; Jiménez-Oyola *et al.*, 2021), uranium mining activities (Haribala *et al.*, 2016; Haakonde *et al.*, 2020; Chen *et al.*, 2022), and other metals (Huang *et al.*, 2009; Qu *et al.*, 2012; Li *et al.*, 2014; (Adamu *et al.*, 2015), a substantial knowledge gap exists in understanding soil and water pollution and its impact on human health, particularly in the context of heavy mineral sands (HMS) mining. While some studies delved into the radiological effects of HMS mining (Zaman *et al.*, 2012; Carvalho *et al.*, 2014; Ramasamy *et al.*, 2014), there is limited research on heavy metal pollution from HMS and associated human health risks. This study aims to address this gap by evaluating soil and water pollution in the vicinity of the Kwale HMS mine (six years after the initiation of titanium mining operations) and Mrima Hill (a high background radiation area earmarked for Nb and REE mineral mining) on the south coast of Kenya. The research study demonstrates how the USEPA model embedded in the EnviroPRA Monte Carlo simulation package can be used assess the carcinogenic and non-carcinogenic risks from exposure to heavy metals via dermal and ingestion pathways.

1.3   Objectives

1.3.1   Main Objective

To assess the human health risk from exposure to environmental radioactivity and heavy metals by general population residing at the environs of the Kwale HMS sand and the Mrima Hill, in Kwale County, south coast of Kenya.

1.3.2   Specific Objectives

(i)   To determine the concentration of ^{232}Th, ^{238}U, and other heavy metals in water and soil from the study area.

(ii)   To assess the impact of mining on drinking water quality and soil pollution levels by heavy metals,

(iii)   To evaluate the non-carcinogenic and the carcinogenic health risk from exposure to Th, U, and heavy metals of interest,

(iv) To estimate the total effective dose equivalent (TEDE) and the incremental lifetime cancer risk (ILCR) from exposure to ^{238}U, ^{234}U, ^{230}Th, ^{226}Ra, ^{210}Pb, ^{210}Po, ^{232}Th, ^{228}Th, and ^{228}Ra by area inhabitants.

1.4 Justification and Significance of the Study

Economic activities such as mining and mineral processing, oil and gas exploration, coal and fuel combustion, and geothermal energy production are some of Kenya's Vision 2030 flagship projects (Ministry of Energy and Petroleum, 2015; Ministry of Mining, 2013). These activities cause changes in the chemical and physical properties of heavy metals and the specific activities of NORMs, leading to the mobilization and redistribution of the heavy metals and radionuclides in soil, water, air, and biota. As a result, exposure of the population to heavy metals and radionuclides via ingestion, inhalation, and dermal contact is increased, exacerbating human health risks.

Continuous and prolonged exposure to the radiation emitted by the NORM and heavy metals, such as arsenic, even at low doses, could induce cancer (Belluck *et al*., 2003; Cember and Johnson, 2012). Thus, there is a need to assess the chemical and radiological toxicity from exposure to heavy metals and radionuclides in environmental media for long-term management or proper disposal of wastewater and tailings associated with such economic activities. In addition, most of the available guidelines and regulations at both national and international levels are do not address the human health risks from exposure to enhanced naturally occurring radionuclides but clear on radiation safety and protection from enhanced naturally occurring radionuclides (Nabhani *et al*., 2015). Therefore, this study will provide baseline data on the concentration of heavy metal and radionuclides in soil and water sampled at the environs of Kwale HMS deposit, where Ti mining is ongoing, and Mrima Hill, where there is economic value Nb and rare earth minerals. The baseline data will help design policies and regulations based on human health risks assessment from exposure to heavy metals and enhanced naturally occurring radionuclides from mining and mineral processing activities in Kenya.

CHAPTER 2

Literature Review

2.1 Chapter Overview

This chapter examines the co-occurrence and distribution of Ti, Nb, Th, U, and other heavy in environment, impact of mining and mineral processing of the ores on quality of water and soil some studies on human exposure to heavy metals and the health risk associated with exposure to these metals. A summary of the literature review and the knowledge gap is also provided.

2.2 Origin of Radioactivity and Heavy Metals in Terrestrial Environment.

Carbonatite mineral ores such pitchblende (U_3O_8) , monazite (Ce,La,Nd,Th)(PO_4,SiO_4), becquerelite ($2UO_3.3H_2O$), uraninite (UO_2), thorianite [(Th.U)O_2] contain substantial amount of ^{238}U and ^{232}Th (Johansson, 2008). These ores contain distinct concentration of phosphate, titanium, niobium, fluorite, rare earth minerals (REEs) among others (Verplanck et al., 2014). On the other hand, heavy mineral sands originate from weathered inland carbonatite rocks washed by water or glacier, sorted depending on size and density and deposited by wind, waves and tides under water or in dunes (Johansson, 2008). These sands contains substantial amount of zircon ($ZrSiO_4$), ilmenite (FeO.TiO_2), rutile (TiO_2), garnet ($A_3B_2Si_3O_{12}$), sillimanite (Al_2SiO_5), monazite (Ce,La,Nd,Th)(PO_4,SiO_4) among other REEs (Van Gosen et al., 2014). Thus, Nb and Ti ores co-exists in terrestrial environment with radioactive elements; U, and Th, and other elements such as Cr, Fe, Pb, Mn, Zr, and rare earth elements among others (Zack et al., 2002; Abuodha and Hayombe, 2006; Van Gosen et al., 2014; Woodruff et al., 2017; Sabu and Rejith, 2020).

2.3 Effects of Mining Activities on Water and Soil Quality

Mining and mineral processing activities produce an appreciable amount of waste, such as spoils, sludge, tailings, mining and mill water, and atmospheric emissions (Lottermoser, 2010). Xu (2019) indicated that solid waste accounted for approximately 97% to 99% of the mineral ore, with only 1% to 3% of the mineral ore being the concentrate. The quantity of mine waste has increased exponentially over the years due to the growing need for industrial and gauge minerals. These wastes contain elevated

concentrations of uranium, thorium and heavy metals such as Cu, Fe, As, Pb, Zn, and Cd, which may be transported to far-flung areas through run-off, erosion, and atmospheric deposition polluting nearby environmental media, i.e., soil, air and water (Pokhrel and Dubey, 2013). Due to its filtering and buffering properties, the soil is a sink for radionuclides and heavy metals (Kabata-Pendias and Mukherjee, 2007. Since the metals do not undergo chemical or microbial degradation, they accumulate in the soil, polluting it (Wuana and Okieimen, 2011). They then percolate into underground water, contaminating it (Kabata-Pendias, 2010) . In addition, surface water nearby could also be contaminated by mine waste through run-off from mining and mineral processing activities (Lottermoser, 2010).

Several studies on the effect of mining and mineral processing activities on the quality of water and soil pollution levels around mining sites have been conducted in many countries. In China, a study done on agricultural land by Wang *et al.* (2019) around the Xinzhuang uranium mine showed that U, Th, Pb, Cd, Zn, and Mn polluted the topsoil. The pollution indices of these metals were 6.31 (U), 4.20 (Th), 2.52 (Pb), 2.36 (Cd), 1.52 (Zn), and 1.39 (Mn). Another study by Zhang *et al.* (2018) showed enrichment of Cr, Cu, Pb, and Cd in soils and groundwater near the iron mining site in Anshan. An earlier study that had been done by Zhuang *et al*. (2009) in four sampling sites around the Dabaoshan mineral deposit in Guangdong province, South China, showed that the agricultural soils in Fandong village, located on the mountaintop of this mine site, were highly polluted by Cu, Zn, Pb, and Cd due atmospheric deposition of the dust from the mine. The concentrations of these metals in mg/kg were 703, 1100, 386, and 5.5 for Cu, Zn, Pb, and Cd, respectively, values that exceeded the maximum allowable concentration of 150 mg/kg of Cu, 300 mg/kg of Zn and Pb, and 5 mg/kg of Cd.

Manna and Maiti (2017) reported an exacerbated level of Cu, Ni, Zn, and Zr in soil and groundwater around a Raniganj coalfield in India. Another study in India along the Chevara- Neendakara coastline of Kollam, Kerala, showed that mining heavy mineral sand affected the area's water, soil, and air quality (Humsa and Srivastava, 2015). The soil sampled around this mining site was highly enriched and contaminated with Fe, Cu, Ni, Zn, Pb, and Cr, with contamination factors of 1.37, 3.10, 1.96, 1.60, 4.61, and 2.09,

respectively, with an average pollution index of 5.69. The enrichment factors of these metals in the soil samples were 13.75, 2.97, 1.87, 1.53, 4.41, and 2.00, respectively. The study by Humsa and Srivastava (2015) further evaluated water quality indices from open wells and tapped water. The water quality index, WQI, of water from the open well was 81, a sign of extreme contamination, while the tap water was moderately contaminated (WQI = 70). Water samples from the paddy field (WQI = 692) and the heavy mineral sand processing plant (WQI = 741) were severely contaminated and unsuitable for domestic use.

In Africa, some studies also showed exacerbated concentrations of heavy metals in soil, groundwater, and surface water sampled near mining and mineral processing activities. For instance, a preliminary study on the impact of uranium mining on drinking water sources near a uranium mine in Siavonga District by Haakonde et al. (2020) showed an elevation in uranium levels in water sampled around this mine. The median estimate of U in water samples was approximately four times higher than the safe limits of U in drinking water. The concentration of U in borehole water ranged between 16.86 μg/L and 263.24 μg/L with a median of 113.1 μg/L, while in wells, the U levels ranged between 6.62 μg/L and 199.14 μg/L with a median of 110.03 μg/L. The median concentration of U in dam water was 115,62 ranging from 85.09 μg/L to 146.15 μg/L. The highest level of U was observed in water from the stream. The concentration ranged between 90.64 μg/L and 207.7 μg/L, with a mean of 135.3 μg/L.

Other studies done in Africa, way after the closure of the mining site, showed that heavy metals continued to threaten the quality of water and soil sampled from the vicinity of the mining sites. For instance, the contamination factor (CF) of Cd, As, Cr, Ni, Pb, and Zn on in the soil samples near a legacy gold mine in Allqi Wadi Aswan, Egypt, which was closed in 1948, were above 1 (Rashed, 2010). Of concern was As and Pb, whose CF value was 94.59 and 4.14, respectively, an indication of extreme pollution of the soil with these heavy metals of concern. Another study on drinking water in Western Uganda sourced from River Nyamwamba and community wells near a legacy copper mine in Kalembe showed that approximately 42% of the drinking water exceeded the threshold value of 200 for Fe in drinking water (Mwesigye and Tumwebaze, 2017). The level of Fe

in the water samples ranged between 4.5 μg/L to 7200 μg/L. However, the level of other metals, i.e., Cr, Ni, Mn, Zn, Cu, Cd, As, and Pb, in the drinking water samples were within the maximum allowable limits defined by the World Health Organization (WHO, 2011). In southwestern mining areas of Ghana, the study by Kazapoe *et al.* (2022) on soil quality of Prestea-Huni valley and Wassa areas, showed that the level of As in 43% in the 300 soil samples exceeded the threshold value of 15 mg/kg As in soil. The concentration of As ranged between 2.00 mg/kg and 246.00 mg/kg, with a mean of 18.37 mg/kg. The concentration of Zn in 71% of the soil samples from the mining areas exceeded the maximum contaminant threshold of 20.00 mg/kg in soils, while Ni in 54% of the samples exceeded the value of 8.67 mg/kg in soil.

In Kenya, information on the effect of mining and mineral processing on soil and water quality is scanty. However, Maina *et al.* (2016) study conducted before titanium mining and mineral processing in Kwale County commenced provided baseline information on the state of the heavy metals in soil. Although Mwashinga *et al.* (2019) conducted a study on heavy metal contamination of the Mkurumudzi River, a river adjacent to the mine, when the titanium mining and mineral processing had commenced, the study also showed that the river was unpolluted.

Regardless of these studies, water and soil pollution decrease soil productivity, leading to food security (Xiao *et al.*, 2017). For example, a review by Pourrut *et al.* (2011) on the uptake and translocation of lead (Pb) in plants showed that Pb inhibited the germination of seeds and elongation of the roots and impaired the photosynthesis process and plant growth. Likewise, excessive chromium (Cr) in soil inhibited the uptake of essential metals such as iron (Fe), copper (Cu), zinc (Zn), phosphorous (P), and magnesium (Mg), which are vital in plant growth (Sharma *et al.*, 2020). Furthermore, the uptake, translocation, and accumulation of other heavy metals such as thorium (Th), uranium (U), arsenic (As), and zirconium (Zr) in plants also inhibit plant growth and development (Shtangeeva *et al.* 2006; Finnegan and Chen 2012; Shahid *et al.* 2013). Even though other metals such as copper (Cu), nickel (Ni), titanium (Ti), iron (Fe), manganese (Mn), and zinc (Zn) are critical for the growth and development of plants (Kabata-pendias 2011; Yusuf *et al.* 2011; Shahid *et al.* 2013; Lyu *et al.* 2017; Pietrini *et al.* 2019), an

excessive uptake and accumulation of some of these essential metals may become deleterious to plants. For instance, chlorosis and necrosis, discoloration of leaves, and stunting of plants are due to excessive uptake of Cu and Zn by plants (Kabata-pendias 2011; Pietrini *et al.* 2019). Likewise, excess Mn in poorly drained and acidic soil hinders the absorption, utilization, and translocation of Fe, P, Mg, and Ca (El-Jaoual and Cox, 1998).

2.4   Human Health Risk from Exposure to U, Th, and Heavy Metals.

Besides the effect of heavy metal pollution to plants, exposure to the metals is also a human health concern. A population may be exposed to heavy metals in soils and water via ingestion, dermal contact, inhalation pathways, or through the food chain. For instance, lung, kidney, and bladder-related mortality in Northern Chile was due to exposure to drinking water contaminated with arsenic (Smith *et al.*, 2018). The cancer mortality was manifest 40 years after exposure to high As levels in drinking water. Guol *et al.* (2001) observed basal cell carcinoma among individuals in southwestern Taiwan exposed to As-contaminated water above 0.64 mg/L, while those exposed to As-contaminated water whose concentration ranging from 0.32 mg/L to 0.64 mg/L suffered from the squamous cell carcinoma.

In Northwest Iran, Dastgiri *et al.* (2010) investigation on chronic exposure to As-contaminated drinking water showed higher incidences of hyperkeratosis among the exposed group than the unexposed group. The study showed that the exposed population had dermatological lesions. In addition, 25% of the exposed group showed chromosomal abnormalities. In other studies, exposure to As-contaminated water caused spontaneous abortion, an increase in stillbirth, high infant mortality rates, and reduced birth weight (Bozsonyi *et al.*, 1992; Ahmad *et al.*, 2001; Milton *et al.*, 2005) due to the increased frequency of dormant point mutations and chromosomal aberrations (Borzsonyi *et al.*, 1992). Besides the human health risks from exposure to As-contaminated drinking water, Zhang *et al.* (2009) also observed that dermal exposure to As-contaminated soil could lead to skin and liver cancer.

Exposure to U accounts for 36.22%, 19.48%, 17.58%, 13.90%, 7.24%, and 5.58% of kidney, bone, liver, reproductive system, lung, and nervous system-related diseases, respectively (Minghao *et al.,* 2020). Uranium triggers these health problems through oxidative stress, metabolic disorder, protein interaction damage, cell death, genetic damage, and inflammation (Minghao *et al.,* 2020). For instance, Banning and Benfer (2017) found cases of liver, skeletal, tumors, genito-urinary diseases, and thyroid among the residents of the Northern part of Bavaria State in German due to continuous exposure to U-contaminated drinking water. Residents exposed to more than 10 µg/L of U in drinking water suffered from tumors and liver diseases, while those exposed to drinking water with a U concentration of more than 2 µg/L had thyroid. Kurttio *et al.* (2002) observed an altered proximal tubular function among 325 residents in southern Finland exposed to drinking water with a median U concentration of 28 µg/L. Uranium is a bone seeker; it impairs normal bone metabolism and functions by replacing calcium on the bone surface and depositing in the skeletons (Minghao *et al.*, 2020). Increased fractional excretion of calcium and phosphate among the subjects under study was observed by (Kurttio *et al*., 2005). The excretion of calcium is a predisposing risk factor for osteoporosis.

Secondary bone abnormalities and osteoporosis have also been observed among patients with renal tabular dysfunction from exposure to Cd. For instance, residents of the Jinzu River basin in Toyama, Japan, who depended on the Jinzu River for farming, continued to experience the effect of environmental Cd-contamination from the Kamioka Pb-Zn mine and smeltery (Aoshima, 2016). Severe joint pain, weak bones, and spine dysfunction were observed among the population residing in the Jinzu River basin. These Jinzu River basin residents also suffered from renal tubular dysfunction. In an earlier study at the Jinzu River basin, Aoshima *et al.* (2003) observed a significant correlation between all markers of bone turnover, indicating that bone formation and resorption were coupled and increased in Cd-induced renal tabular dysfunction.

Renal dysfunction was also observed among approximately 50% of 1595 residents of Xiaoguang in Hubei province, China, who were exposed to the high level of Cd released from a smelting factory in its vicinity (Li *et al.*, 2020). The urinary Cd in the subjects was above the maximum national value of 5.000 μg/g creatinine, a biomarker for urinary Cd burden. Renal tubular disorder and bone damage have also been observed in persons exposed to prolonged low-concentration occupational or environmental Cd (Järup *et al.*, 2000; Åkesson *et al.*, 2006).

Like other non-essential elements, Pb generates free radicals that trigger oxidative stress, leading to human cell and tissue damage (Collin *et al.*, 2022). In addition, Pb affects the nervous system by substituting calcium in activating calmodulin-dependent phosphodiesterase and protein kinase C which plays a role in spatial learning (Bressler and Goldstein, 1991). For instance, a study conducted by Choudhari *et al.* (2010) among 432 school-going children living within a 2.5 km radius of a Zn-Pb mine showed that 22.8% of the children exposed to Pb showed central nervous system symptoms. However, the Pb-blood level in 80% of these children was below the 10 mg/dl threshold for central nervous breakdown. Furthermore, Lee *et al.* (2022) observed a decline in attention between the ages of 64 and 71 and language function among persons of 64 years exposed to Pb during childhood. Another follow-up study in Port Pirie showed a continuous deterioration of intellectual functions into adulthood among persons exposed to Pb during childhood (Searle *et al.*, 2014). This intellectual incapacitation has also been observed among persons chronically exposed to water contaminated with arsenic (Tsai *et al.*, 2003; Wasserman *et al.*, 2004; von Ehrenstein *et al.*, 2007; Tolins *et al.*, 2014).

Studies have also shown that several organs, including the lung, kidney, liver, gastrointestinal tract, and skin, are targets of Cr carcinogenicity (Linos *et al.*, 2011). Hexavalent chromium [Cr (VI)] is soluble, and when converted to trivalent chromium [Cr (III)], it gives rise to reactive intermediates of reactive oxygen species, Cr (V) and (IV) (ATSDR, 2012). The reactive oxygen species are responsible for the deleterious effect of Cr, including lipid peroxidation and alteration in cellular communication, signaling pathways, and cytoskeleton (ATSDR, 2012). In addition, lung cancer was due to Cr-induced instability (Holmes *et al.*, 2006). Linos *et al.* (2011) noted a high mortality rate

among residents of Oinafita, Greece, from liver and lung due to exposure to Cr-contaminated drinking water. Sharma *et al.* (2012) observed gastrointestinal tract distress, hematological disorder, and dermatological ailments among the residents of Kanpur who were exposed to Cr-contaminated groundwater. Ulceration, abdominal pain, ingestion, and vomiting were also observed among 155 people in the People's Republic of China exposed to Cr-contaminated drinking water (ATSDR, 2012).

Besides health effects from the non-essential metals; Pb, Cr, As, and Cd, exposure to high to essential metals such as Ni, Cu, Zn, Mn, and Fe are detrimental to health. For instance, Mn is a co-factor of several enzymes, including arginase, glutamine synthetase, mitochondria superoxide dismutase, and pyruvate decarboxylase (Bouabid *et al.*, 2016). In addition, Mn is responsible for the development and functioning of the brain (Takeda, 2003), and it is vital for the growth and maintenance of nerve and immune cell function (O'Neal and Zheng, 2015). However, chronically Mn-overexposed individuals have had adverse cognitive, psychiatric, and motor disorders (Bouabid *et al.*, 2016). Studies by Wasserman *et al.* (2006) in Araihazar, Bangladesh, and Oulhote *et al.* (2016) in southern Quebec, Canada, showed that school-going children exposed to high levels of Mn exhibited intellectual challenge.

Cu plays a vital role in fetal and infant growth and development, bone strength, iron, glucose, cholesterol metabolism, brain development, and immune function (Taylor *et al.*, 2020). However, it participates in producing reactive oxygen species via the Fenton reactions when in excess (Valko *et al.*, 2005). The hydroxyl produced reacts with biomolecules within their proximity through hydrogen abstraction leading to lipid peroxidation (Valko *et al.*, 2005). Valko *et al.* (2005) also noted that the free reactive radicals formed during the oxidation and reduction of the Cu could induce DNA strand breakage, and its effect was more active than the effects of Fe. Incidents of gastrointestinal upset and liver impairment, including Indian childhood cirrhosis, were reported among those exposed to high levels of Cu in drinking water (National Research Council, 2000; ATSDR, 2022). However, the toxicity of Cu depends on the level of Fe and Zn in the body. Zn inhibits the absorption of Cu, which can be used to treat Wilson's

disease, while deficiency of Fe promotes Cu overload in the central nervous system leading to neurological disorders (Taylor *et al.*, 2020).

2.5 Evaluation of Carcinogenic and Non-carcinogenic Health Risks

Exposure to heavy metals is a current global human health concern. Besides pedogenic and other anthropogenic activities such as agriculture, industrialization, and urbanization, mining is the highest heavy metal source (Li *et al.*, 2014). Thus, several recent studies have been done on non-carcinogenic and carcinogenic health risks from exposure to heavy metals contaminated soil and drinking water due to mining and mineral processing activities. For example, the non-carcinogenic health risk, which is estimated using the average values of the hazard indices (HI), which is a sum of the target health quotient (THQ) of individual metals of the population living near lead-zinc (Pb-Zn), manganese (Mn), and tungsten (W) mines were approximately 10, 7.5, and 5, respectively, values that much higher than 1, an acceptable HI value (Li *et al.*, 2014). Pb, As, Cd, and Ni accounted for 54%, 25.8%, 13.8%, and 3.5% of the HI values at the Shenzhou Pb-Zn mine (Li *et al.*, 2014). The carcinogenic risk estimates at eight sites that Li *et al.* (2014) evaluated were much higher than the threshold cancer risk value of 1.0E-04 (USEPA, 1989). In addition, Qu *et al.* (2012) risk assessment study at the Pb-Zn mining site showed that the workers were susceptible to non-carcinogenic risk from exposure to Pb and As. The HI values were 16.4, with Pb and As accounting for 90% and 9% of the HI values. However, the carcinogenic risk values were within the threshold USEPA cancer risk values of 1.0E-04 and 1.0E-06 (USEPA, 1989).

The residents of Sewakht-Chiltral, Pakistan, living in a rich mineral area, are also susceptible to non-carcinogenic and carcinogenic risks from exposure to Co, Cr, Cd, Mn, Cu, Fe, Pb, Ni, Zn, and Mo (Rehman *et al.*, 2018). The health risk assessment done by Rehman *et al.* (2018) showed that the child's THQ values from exposure to Fe in soil for children were 4.49, while that of adults was 2.68. However, these residents were more prone to the effects of exposure to heavy metal contamination since the THQ values from exposure to Cd, Co, Mo, and Cu in water for children were 15, 10.5, 6, and 1.55, respectively, while the adults' THQ values were 7.84 for Cd, 5.49 for Co, and 3.18 for Mo, values that were above the safe limits of 1. In addition, the carcinogenic estimates

showed that the children living around this rich mineral area of Sewakht-Chiltral were prone to human health effects due to exposure to Co, Ni, Cd, and Cr in soil, whose cancer risks were 4.65E-03, 2.88E-04, 1.65E-04, and 1.62E-04, respectively. However, the child's cancer risk from exposure to the metals in water was 1.45E-01, 1.13E-01, 2.53E-03, and 2.42E-03 for Co, Cd, Cr, and Ni, respectively. Adults were less susceptible to carcinogenic risks since the cancer risk value from exposure to heavy metals in soil was 2.18E-04 and 7.53E-02, 5.88E-02, 1.32E-03, and 1.26E-03 for Co, Cd, Cr, and Ni, respectively in water.

Giri *et al*. (2020) estimated the carcinogenic and non-carcinogenic health risks from exposure to selected heavy metals in groundwater samples in the mining areas of the Singhbhum Copper Belt, India. The risk from ingesting the heavy metals was higher than dermal exposure to and inhalation of the metals. The THQ values for Mn, Ni, Mn, Co, and As in some samples where geological enrichment or mining activities were observed exceeded 1 for children and adults. Another study by Kamunda *et al.* (2016) around a Goldfield mine in Witwatersrand, South Africa, showed that children were more prone to carcinogenic and non-carcinogenic effects from exposure to heavy metals. The children's HI values were 43.80, with As and Cr contributing more to the HI values.

Although Haribala *et al.* (2016) assessed the annual effective dose rate from exposure to ^{40}K, ^{137}Cs, ^{226}Ra, ^{232}Th, and ^{238}U in soils around a uranium mine in Tongliao, China, the health risks from exposure to As, Zn, Hg, Cd, Cu, and Pb in surface soils were also evaluated. The annual effective dose ranged between 4.14 μSv/year to 68.33 μSv/year with a mean of 57.13 ± 6.54 μSv/year, values much less than the mean global exposure of 2.4 mSv/year. Haribala *et al.* (2016) study also showed that the residents of Tongliao were not prone to the non-carcinogenic and carcinogenic cancer risks from exposure to heavy metals. The child's mean HI value was 6.46E-02, while HI average value for an adult was 7.85E-03, far less than the non-carcinogenic safe limit of 1. Furthermore, the mean cancer risk from exposure to As for a child was 1.65E-05 while that of an adult was 1.84E-06, values lying within the acceptable cancer risk of 1.0E-06 and 1.0E-06. However, Haakonde *et al*. (2020) study focused on the chemotoxicity effect of exposure to U-contaminated drinking water sources from boreholes, shallow wells, streams, and

dams near a uranium mine in Sivonga, Zambia. The drinking water from all the sources was contaminated with uranium with U-mean concentrations ranging from 110.03 μg/L to 135.30 μg/L values that were higher than the maximum permissible U level of 30 μg/L (WHO, 2011; USEPA, 2018). Thus, the Sivonga residents were prone to both carcinogenic and non-carcinogenic risk due to exposure to U in the drinking water, the HI values ranged between 11.98 and 49.17, while the cancer risk values ranged between 1.86E-05 and 1.38E-02, an indication of carcinogenic risk.

Some human health risk assessment studies from exposure to heavy metals due to mining activities were based on deterministic techniques. However, Monte Carlo simulation, commonly known as the probabilistic technique, quantifies variation and uncertainty from the input parameters providing a range and likelihood of risks (Washburn *et al.,* 1998). Probabilistic risk assessment provides a range of values for decision-making on environmental remediation, protecting a population from heavy metal contamination (Hu *et al.*, 2019). For instance, Rivera-Velasquez *et al*. (2013) study on carcinogenic and non-carcinogenic risk assessment of As, Cd, and Zn showed that the corresponding deterministic values were higher than the probabilistic values. However, studies by Saha *et al.* (2017) and Giri *et al*. (2020) showed that the high-end (95th percentile) values from the probabilistic health risk assessment were higher than the deterministic values due to the variation in the input parameters. In Saha *et al.* (2017) study, the high-end probabilistic THQ estimates for children and adults were 1.65 to 2.05 and 3.38 to 4.1 times higher than the respective deterministic THQ values.

On the other hand, a study by Giri *et al*. (2020) showed that the deterministic HI values for males, females and children during the pre-monsoon season were 1.80, 1.55, and 2.87, respectively, while during the monsoon season, the HI values were 1.38, 1.19, and 2.20 respectively, and 1.60, 1.38, and 2.56 during the post-monsoon season. However, the 95th percentile values were 2.87, 2.16, and 2.38 for males during the pre-monsoon, monsoon, and post-monsoon seasons; 2.54, 1.88, and 2.02 for females, and 4.57, 3.49, and 3.75 for child for the respective seasons. The 50th percentile (median) values from probabilistic estimation were lower than the respective deterministic values. In this study, we

estimated and compared the values from deterministic and probabilistic risk assessment from exposure to U, Th, Pb, Cd, As, Zn, Cu, Ni, Mn, and Cr in soil and water samples.

2.6 Evaluation the TEDE and ILRC from Exposure to NORMs using RESRAD-OFFSITE

External dose at the point of contact to NORMs can easily be measured using dosimeters. However, internal dose can either be reconstructed using biomarkers such as fluid, tissue, and breath or estimated by modeling exposure scenarios using codes (USEPA, 1992). Code such as RESRAD (RESidual RADioactive)-OFFSITE is used to model different exposure scenarios: worker, recreational, rural resident farmer, and urban resident, from both primary and secondary contamination (Shhub, 2021). The code can further be used to estimate both external and internal doses and the cancer risk due to exposure to residual radioactive materials and their progenies (Yu *et al.*, 2009). The internal dose is modeled following the emission of alpha particles from the inhaled radioactive contaminated particulates and ingested vegetables, grains, fruits, meat, milk, aquatic food, water, and soil, while the external dose is simulated from exposure from the emission of beta and gamma radiations (Shhub, 2021).

Some researchers have used RESRAD OFFSITE to estimate the radiological dose and cancer risk resulting from exposure to NORMs. For instance, Ziajahromi *et al.* (2015) estimated the cancer risks for an offsite resident farmer at an agricultural site experiencing high levels of natural radiation in Khak-Sefid, Ramsar, using RESRAD OFFSITE. The results showed that the farmer was at high risk to exposure from ^{226}Ra in the second year of exposure compared to ^{232}Th, and ^{40}K. Mathuthu *et al.* (2016) predicted the radiological dose and risk from exposure to ^{40}K, ^{232}Th, and ^{238}U of a hypothetical offsite resident at the gold mine tailing in Wonderfonteinspruit catchment area in South Africa. The prediction showed that the maximum total effective dose equivalent (TEDE) was 0.0135 mSv/year at the 30th year, a value that was below the public exposure limit of 1 mSv/year (Lecomte *et al.*, 2019), while the highest excess cancer risk was 3.04E-05 at the 15th year, a value that was within the acceptable regulatory range of 1.0E-04 to 1.0E-06 (USEPA, 1989). Another radiological dose rate assessment using this code done by Nandutu and Kim (2021) at landfill disposal of consumer products containing NORM in

South Korea showed that the exposure dose was below the public limit dose of 1 mSv/year. Shhub (2021) used RESRAD OFFSITE to evaluate the absorbed doses from exposure to artificial radioactivity of ^{137}Cs, ^{241}Am, and ^{252}Cf at hypothetical well-logging rapture incidents of a rural resident farmer. The results showed that the health risk from exposure to ^{241}Am was 22 times higher than risks from exposure to ^{137}Cs and ^{252}Cf.

Several studies on exposure to environmental radioactivity have been done in the coastal region of Kenya (Osoro *et al.*, 2011; Kebwaro *et al.*, 2011; Kaniu *et al.*, 2018; Odongo *et al.*, 2021). However, the researchers evaluated the annual effective dose equivalent (AEDE) using either absorbed dose values obtained from either dosimeter readings or by converting the activity concentration obtained from HPGe detector measurements to dose. The incremental lifetime cancer risk (ILCR) in these studies was a product of the AEDE, the average lifespan, and the risk. In this study, we used the RESRAD OFFSITE code to estimate the TEDE and ILCR from exposure to ^{232}Th and ^{238}U contaminated soil by a rural resident farmer at the environs of a titanium mine in Kwale County, Kenya. The rural resident farmer was assumed to be self-sufficient since most of the dietary needs were met at the site of residence (Shhub, 2021). The exposure pathways considered in this work were incidental ingestion of soil, inhalation of soil particles, and external exposure to ^{232}Th and ^{238}U and their progenies.

19

2.7　Summary on Literature Review and Knowledge Gap

The surveyed literature has demonstrated that mining and mineral processing produces waste containing appreciable amounts of NORM and heavy metals such as Cr, Cd, As, and Pb, which could be transported to far-flung areas, polluting water, soil, and air. The health of persons close to such mining areas may be compromised. Although several studies have been conducted in Kenya on the concentrations of ^{232}Th, ^{238}U, Nb, and related metals in soils sampled around Mrima Hill, the annual effective dose equivalent (AEDE) was assessed. However, the human health risks from exposure to NORM and heavy metals in soils and drinking water have not been evaluated. In this study, the USEPA model embedded in the EnviroPRA Monte Carlo simulation was used to assess the non-cancer and cancer risk from exposure to heavy metals in soils and drinking water sampled not only in the environs of Mrima Hill, a prospecting Nb and REE mining site but also in the environs of the Kwale HMS deposit, where Ti mining is ongoing. RESRAD OFF-SITE code was also used to assess the internal and external dose from exposure to ^{232}Th and its progenies (^{228}Th, ^{228}Ra), ^{238}U and its progenies (^{234}U, ^{230}Th, ^{226}Ra, ^{220}Pb, and ^{210}Po), and the cancer risk estimates due to exposure to these NORM.

CHAPTER 3

Theoretical Framework

3.1 Chapter Overview

This chapter presents the mass spectrometric technique used in the study, the radioactive decay series, internal dose, the interaction of radiation emitted during the decay of NORM and by the heavy metals with biological matter, and their effects on human health. Summaries on the exposure scenarios and health risk assessment techniques will also be presented.

3.2   Mass Spectrometric Techniques

Mass spectrometric techniques such as resonance ionization mass spectrometry (RIMS), accelerator mass spectrometry (AMS), inductively coupled plasma mass spectrometry (ICP-MS), glow discharge mass spectrometry (GDMS), thermal ionization mass spectrometry (TIMS), and secondary ion mass spectrometry (SIMS), , can be used to measure the number of radioactive atoms and more often long-lived atoms (Lariviere *et al.*, 2006; Hou and Roos, 2007). They can differentiate the isotopes of elements based on their masses. In this study, ICP-MS was used for analysis of ^{47}Ti, ^{54}Cr, ^{55}Mn, ^{56}Fe, ^{60}Ni, ^{63}Cu, ^{66}Zn, ^{75}As, ^{90}Zr, ^{93}Nb, ^{112}Cd, ^{208}Pb, ^{232}Th, and ^{238}U.

An inductively coupled plasma mass spectrometer, ICP-MS, counts the number of radioactive atoms (Lariviere *et al.*, 2006). The atoms' molar mass, relates to the activity concentration of the radionuclide, A, of the atom through Eqn. 3.25

$$m = \frac{A}{In2} \frac{M}{N_A} t_{1/2}$$
(3.25)

Where, N_A is the Avogadro's constant, M is the molar mass, and $t_{1/2}$ is the half-life of the radionuclide. Since the mass of the atom is proportional to the half-life and molar mass of the atom, mass spectrometric techniques are often used to determine long lived radionuclides.

ICP-MS consists of the sample introduction system, ion extraction interface, ion lenses, mass analyzer, and detector (see Fig. 3.5). Argon gas, which is chemically inert and has high ionization energy of 15.76 eV, is used to create singly ionized plasma. A high-temperature plasma is generated when argon gas tangentially flows into a quartz torch surrounded by a copper coil, as shown in Fig. 3.6, through which a radiofrequency current is passed. The plasma is generated and sustained by the radiofrequency current by allowing the argon gas to be seeded with electrons generated by a Tesla coil. A vortex created at the base of the plasma weakens it allowing punching of the plasma by a nebulizer gas flow carrying the sample aerosol to the center of the annular-shaped plasma (Vanhaeck *et al.*, 2007). The solvent vaporizes, and the dry aerosol decomposes into individual molecules before entering the axial channel. The molecules are then atomized and ionized at the tail of the plasma (Taylor, 2001).
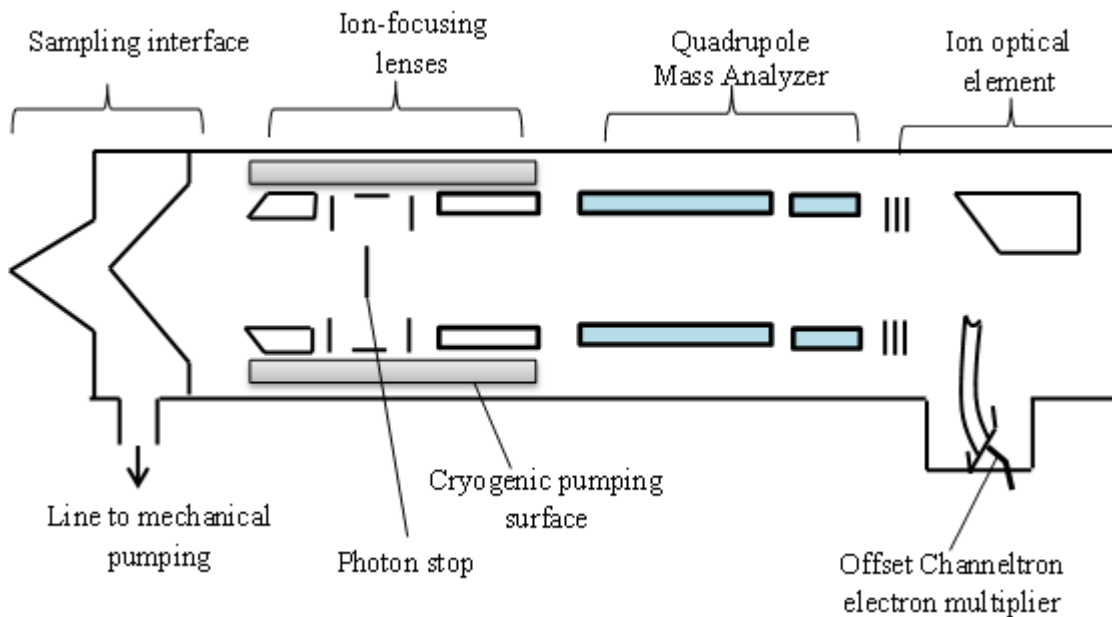
Fig. 3.1: A schematic diagram of a mass spectrometer (Adapted from: Houk, 1986)
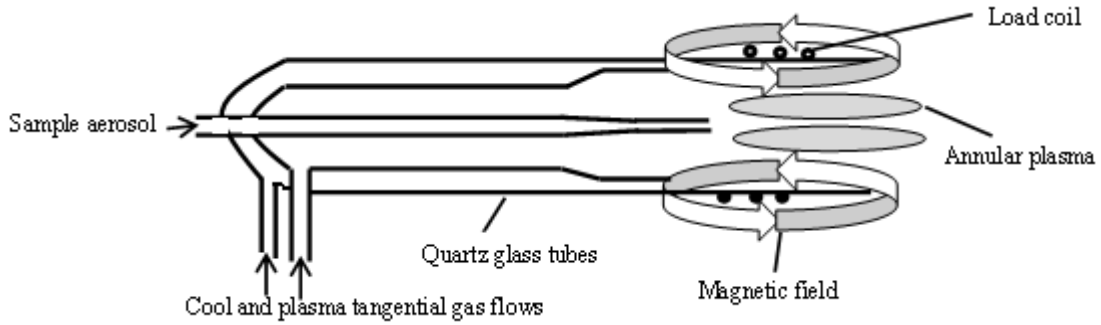
Figure 3.2:A cross section of gas introduction system (Adapted from: Hill, 2007)

The analyte atom can be ionized thermally or undergo penning ionization. In thermal ionization, the ions, the analyte atoms, and the free electrons in the plasma collide, attaining a thermal equilibrium whose degree of ionization is described by the Eqn. 3.26 (Vanhaeck *et al.*, 2007).

$$\frac{n_i n_e}{n_a} = 2 \frac{Z_i}{Z_a} \left(2\pi m_0 k \frac{T}{h^2} \right)^{\frac{3}{2}} e^{\left(-\frac{E_i}{kT} \right)} \qquad (3.26)$$

where, n_i, n_e and n_a are number of densities of ions, electrons, and atoms; Z_i, and Z_a are ionic and atomic partition functions; m_0 is mass of electron; h is the Planks' constant; k is Boltzmann constant; T is the thermal temperature and E_i is the first ionization potentials. Therefore, the degree of ionization depends on the electron density, thermal temperature, and ionization energy of the elements in the analyte. Since the temperatures at the center of the plasma range from 8,000 K to 10,000K, instant desolvation and ionization of the sample aerosol occurs. Thus, over 80% of elements are singly thermally ionized by the ICP with an efficiency of over 90% (Niu and Houk, 1996; Lariviere *et al.*, 2006). On the other hand, penning ionization occurs when the analyte atom's ionization energy is equal to the colliding species' energy. It involves charge exchange between plasma gas metastable species and the analyte atoms producing an analyte ion. Experimental work by Niu and Houk (1996) indicates that the contribution of ions due to penning ionization is insignificant.

The ions produced at atmospheric pressure in the ICP are sampled through an interface into a vacuum for mass analysis. The interface consists of two orifices: the skimmer and sampler made of either nickel or platinum. The interface maintains the integrity and composition of the ion beam by limiting the kinetic energy spread of the ion beam and the production of the polyatomic atoms. As the plasma passes through the sampler into a low-pressure zone, it expands adiabatically and forms a supersonic jet. (Niu, 1994) observed a decrease in the density and temperature of the supersonic jet. The jets' density was also proportional to the inverse square of the distance from the source. The positively charged ions in the plasma relative to the earthed orifice are then accelerated across this potential with high kinetic energy. The free jet expansion terminates at the Mach disk, located at an axial distance from the sampler, determined by the pumping speed at the near-end nozzle of the sampler. The internal energy of the source is therefore converted into a directional motion causing the central flow of the ions to pass through the skimmer orifice to the ion lenses.

The equipotential fields formed around ion lenses are set at specific potentials to serve as refractive surfaces and collimators. They focus the ion beam on the mass analyzer. However, in a multi-elemental analysis mode, the differences in ion masses of the elements may cause the ions to respond differently to the lens voltage in different ways. The lens voltage is, therefore, optimized in the middle of the mass range to provide for maximum ion transmission (Hu *et al*., 1993; Linge and Jarvis, 2009). In addition to the lenses, either a photon stop aligned with the ion beam or a multipole system placed at a slight angle is used to intercept photons and energetic neutrals so that they do not reach the analyzer and, allowing only the ions to be deflected on to the axis providing a low background across the entire range (Taylor, 2001; O'Connor and Evans, 2007).

Currently, the ICP-MS systems have collision/reaction cells (CRC) containing a multipole (2n +2 rods) positioned between the interface and the quadrupole (Vanhaeck *et al.*, 2007).. The cells are pressurized with reactive gases such as oxygen, hydrogen, and hydrocarbons and non-reactive collision gases such as helium and other halogens. The reactive gases neutralize the more intense chemically ionized species in the beam. They also shift the isobar of the analyte ion from each other in the mass-charge ratio through

different reaction methods described by (Koppenaal *et al.,* 2004). The kinetic energy of polyatomic ions, which are larger than the analyte ions (Linge and Jarvis, 2009), are reduced when they collide with inert gases such as helium. A bias voltage placed at the exit of the cell excludes the slow polyatomic ions from reaching the mass analyzer.

The ions extracted from the ICP are then sorted by the mass analyzer into a discrete mass-to-charge ratio (m/z) depending on the ions' kinetic energy, velocity, and momentum. (O'Connor and Evans, 2007) describe the different structural designs of mass analyzers. These designs include quadrupole, magnetic sector field mass analyzer, time of flight mass analyzer, and ion trap mass analyzer. In this research, we utilized the quadrupole mass analyzer.

Quadrupole mass analyzer has four parallel conducting rods connected to a direct current potential, U, and radio frequency alternating current potential, V. A combined electrical potential of is applied to a pair of rods while simultaneously applying - to the other oppositely positioned pair of rods such that the pairs are out of phase as they oscillate. The electrical field is created due to the electrical potential interacting with the ion beam causing the ions to oscillate with varying frequency and amplitude depending on the mass and charge of the ion. Extreme oscillations neutralize the unstable ions as they strike the rods. However, at any given voltage combination, singly ionized charge m/z passes through the center of the quadrupole and is sequentially filtered at the exit (Linge and Jarvis, 2009). The quadrupole can scan the entire mass range from 2 amu to 260 amu as the voltage rapidly changes. Each of the ions is converted into a discrete electrical pulse, which is then counted by the pulse counting detectors.

3.3 Radioactive Decay Series

Decay of radioactive nuclear is spontaneous. The unstable nuclide is transformed into a stable nuclide through different processes including alpha (α) decay, beta minus (β^-) or (β^+) decay, gamma (γ) emission, electron capture, protons or neutrons decay, isomeric transition, and spontaneous fission. The decay does not depend on the chemical and physical state of the nuclide but it depends on the neutron to proton ratio and on the mass-energy relation between the parent, progenies and emitted particles (Magill and

Galy, 2005). The probability of the radioactive nuclide undergoing decay in a time interval t is given as

$$N = N_0 e^{-\lambda t} \tag{3.1}$$

where N_0 is the number of radioactive atoms at $t = 0$, and λ is the decay constant of a given nuclide. The radioactive decay of and element can also be described in terms of activity, A, such that $A = \lambda N$. Therefore

$$A = \lambda N_0 e^{-\lambda t} = A_0 e^{-\lambda t} \tag{3.2}$$

The product of the radioactive decay of many nuclides is usually radioactive. Therefore, the product is continuously transformed into another radioactive product until stability is achieved. The relative activities of a radioactive parent and its radioactive product is given as

$$A_2(t) = \frac{\lambda_2}{\lambda_2 - \lambda_1} A_0 \left(e^{-\lambda_1 t} - e^{-\lambda_2 t} \right) \tag{3.3}$$

Naturally occurring radioactive atoms, ^{238}U and ^{232}Th, undergo a series of decay before attaining stability with different lead (Pb) isotopes: ^{206}Pb and ^{208}Pb as shown in Appendix A. They exhibit secular equilibrium where the half-life of the parent nuclide is greater than that of the daughter nuclide. A gradual ingrowth of the daughter nuclide is observed, and the relative activity of the daughter reaches approximately 99% that of the parent nuclide at approximately 7 half-lives (Martin, 2006) such that at equilibrium, the activity of parent is equal to that of the daughter. The decay constants of parent and daughter are the inverse ratio of the equilibrium concentration of the parent and daughter as shown in Fig. 3.1 (a). When the half-life of the daughter nuclide is approximately of the same order but smaller than that of the parent, the activity of the daughter nuclide rises from zero to maximum and decays with the same half-life with a pure parent as shown in Fig. 3.2 (b). The activity concentration of the daughter nuclide is thus given as

$$A_2 = \frac{\lambda_2}{\lambda_2 - \lambda_1} A_1 \tag{3.4}$$
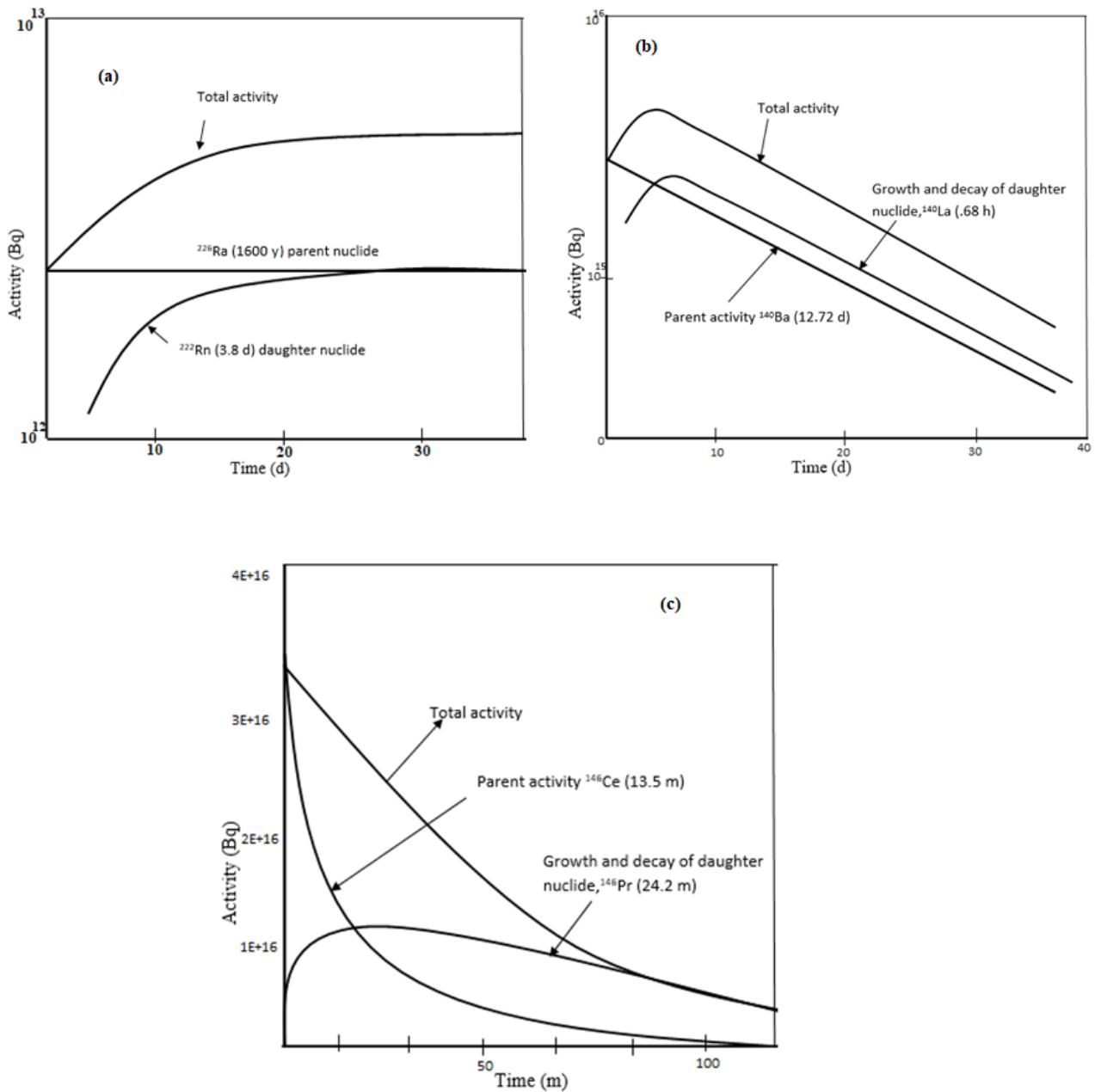
Figure 3.3(a) No Equilibrium (b) Secular Equilibrium (c) Transient Equilibrium decay

series (Shabaan, 2018)

Transient equilibrium occurs at the end of the ^{232}Th series, where ^{212} Pb (T = 10.6 h) decays by β- emission to ^{21}Bi (T = 61 min), of which 35.6% of the decay is through α-emission to ^{208}Te $(T = 3.1\ min)$ and 64.6% by β-decay to ^{212}Po (T = 33.0E − 7 s). ^{208}Te and ^{212}Po then decays to a stable ^{208}Pb nuclide, as shown in Appendix A-1. The no

equilibrium decay mode occurs when the half-life of the parent nuclide is less than that of the daughter nuclide. The activity of the daughter nuclide reaches maximum and then decays at its own characteristic rate, while the parent, whose half-life is shorter disintegrates. However, the total activity does not increase, rather it decreases exponentially, as shown in Fig. 3.1 (c).

3.4   Interaction of Radiation with Biological Matter

Radiation interacts with biological matter directly through ionization or excitation of molecules and atoms. The radiation may eject an inner shell electron of the atom through a process called photoelectric absorption or transfer part of the energy to a loosely bound electron, and the remaining photon scattered in a different direction through a process called Compton scattering, or an electron and positron may be produced when the photon energies are more than 1.022 MeV through a process called pair production. The positron and electron annihilate, and the two photons produced during annihilation are emitted in opposite directions, depositing their energies elsewhere in the biological matter. The radiation or secondary electrons produced during interaction of radiation with biological matter may break the DNA double strands leading to point mutations of germ and somatic cells, as shown in Fig. 3.4. Thus, information originally in the parent gene may not be transmitted to the next generation leading to genetic change among the irradiated individuals (Cember and Johnson, 2012).

The radiation may also interact with biological matter indirectly through radiolysis of water molecules. The water absorbs the radiation and dissociate, producing highly reactive oxygen species (ROS) of OH and H_2O^+, hydrogen radical, H^+, OH^- and electrons, e^-, as indicated in Eqns. 3.5 (a) to (d).

$$H_2O + h\nu \rightarrow H_2O^+ + e^-$$ 3.5 (a)

$$H_2O^+ \rightarrow H^+ + OH^*$$ 3.5(b)

$$H_2O + e^- \rightarrow H_2O^-$$ 3.5(c)

$$H_2O^- \rightarrow H + OH^-$$ 3.5(d)

The free radical OH^* may, especially in cases where particles are of high specific ionization such as alpha particles, recombine to produced hydrogen peroxide, while H recombine to form gaseous hydrogen, which in turn combine with oxygen to form hydroperoxyl radical (Cember and Johnson, 2012), see Eqns. 3.6 and 3.7.

$$OH^* + OH^* \rightarrow H_2O_2 \qquad\qquad (3.6)$$

$$H + O_2 \rightarrow HO_2 \qquad\qquad (3.7)$$

Hydroperoxyl, HO_2, has a longer lifetime and may combine with H to form hydrogen peroxide, H_2O_2 (Cember and Johnson, 2012). Hydrogen peroxide is stable and has a long lifetime. It decomposes to hydroxyl and alkoxy radicals during the Fenton reaction with cuprous ions (Valko *et al*., 2005). Hydrogen peroxide, hydroxyl, and alkoxy radical could break the DNA single or double strands (Desouky *et al*., 2015), as shown in Fig. 3.4. Residual or unrepaired DNA double strands could cause chromosomal aberration, loss of genetic material, and death of cells, while incorrectly paired DNA double strands inducing mutations and carcinogenesis (Prise and O'Sullivan, 2009; Asic *et al.*, 2017). Furthermore, in the presence of metal ions, the radicals could be involved in the modification of DNA backbone and base lipid peroxidation and alteration of calcium and sulfhydryl homeostasis (Valko *et al*., 2005), aggravating the radiogenic cancer effects.

Even though the damage to the DNA has been linked to high doses of radiation, a review by Desouky et al. (2015) showed that the radiation-induced bystander effect (RIBE) was due to exposure to low doses of radiation. RIBE is associated with induced mutations, chromosome instability, exchange of sister chromatids, cell differentiation, and altered gene expression (Desouky *et al*., 2015).
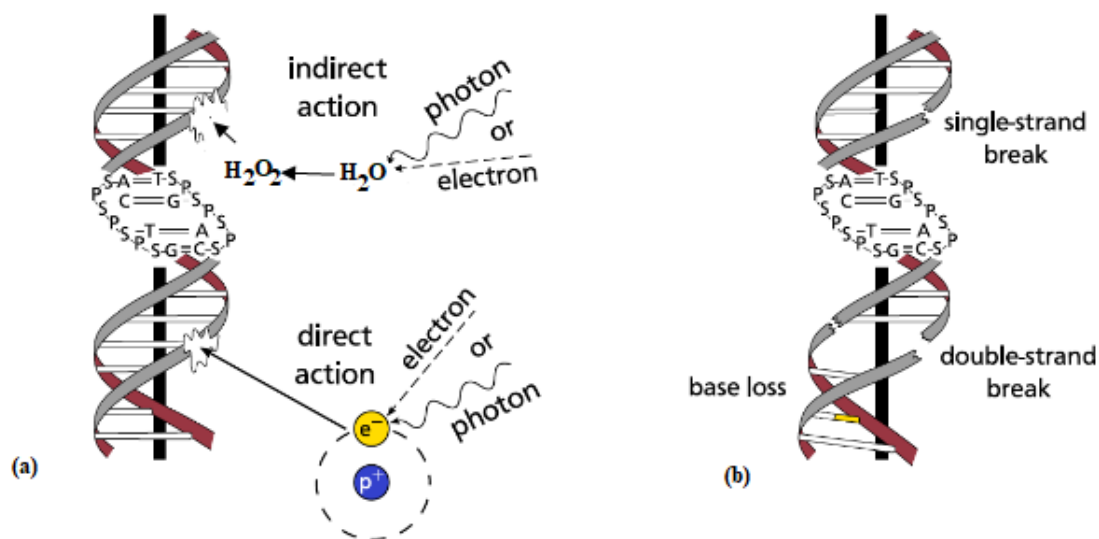
Fig. 3.4: (a) Indirect and direction interaction of radiation, secondary electrons, or products of hydrolysis with the DNA. (b) Damage of DNA caused by radiation or hydrolysis (adapted from: Erlangung, 2014)

3.5 Chemical Toxicity of Heavy Metals

Besides other heavy metals such as Cd, Pb, Fe, Cr, Ni, and Cu, the chemical toxicity from exposure to Th and U has also been recognized (Asic *et al.*, 2017; Rump *et al*., 2019; Bjørklund *et al.*, 2020). These metals are involved in Fenton and Heber-Weiss-type reactions to produce reactive nitrogen species (RNS) and reactive oxygen species (ROS), which interact with biomolecules initiating mutagenic, carcinogenic, and non-carcinogenic effects.

During the synthesis of adenosine triphosphate (ATP), some oxygen gas molecules are partially reduced to form superoxide, which in turn is catalyzed by superoxide dismutase, SOD, to form hydrogen peroxide and oxygen (Wardman and Candeias, 1996), as shown in Eqn. 3.8 (a) and (b). Although hydrogen peroxide plays fundamental roles in biological processes such as cell proliferation, neuronal protection, and anti-bacterial defense (Guo *et al.*, 2014), when in excess and in the absence of chelating agents, it is involved in the Fenton reactions with transition metal ions such as Fe(II), Co(II), Cu (I), Cr(V), and Ti(III), and to produce reactive hydroxyl radicals and intermediate metal ions (Prousek, 2007), as illustrated in Eqn. 3.9. The hydroxyl radical reacts with biomolecules near it via hydrogen abstraction leaving behind carbon-centered radicals such as the formation of

30

lipid radicals from unsaturated fatty acids (Valko *et al.*, 2005), which could initiate carcinogenesis and pathogenesis of other diseases (Tchounwou *et al.*, 2012; Zacharski *et al.*, 2000). As discussed earlier, the radicals may also modify the DNA backbone and DNA base and alter the calcium and sulfhydryl homeostasis.

$$O_2 \rightarrow O_2^{\cdot -} \qquad\qquad\qquad\qquad 3.8\ (a)$$

$$2O_2^{\cdot -} + 2H^+ + SOD \rightarrow H_2O_2 \qquad\qquad 3.8\ (b)$$

$$H_2O_2 + M^{+n} \rightarrow M^{(n+1)} + HO^* + HO^- \qquad\qquad 3.9$$

3.6 Human Health Risk Assessment from Exposure to Th, U and Heavy Metals

Health risk assessment estimates the probability of adverse health effects from exposure to life-threatening materials, including environmental contaminants such as NORM and other heavy metals. Health risk assessment processes include hazard identification, hazard characterization, exposure assessment, and risk characterization (WHO, 2010). Hazard identification is "*the process of determining whether an exposure to a contaminant can cause an increase in incidences of a particular health effect in humans*" (USEPA, 1989). *The h*azard identification process involves quantifying the nature and strength of the contaminant in the environment (USEPA, 2009). The concentration of the contaminant at the point of contact can be quantified using in-situ experimental measurements. Otherwise, if the receptor is far from the point of contamination, the quantity of the contaminant at the point of exposure could be determined using flow and transport mathematical models (Rivera-Velasquez *et al.*, 2013). Hazard characterization involves the evaluation of the toxicity of the contaminant and the relation between the dose received by a population and the incidence of adverse health effects.

The exposure assessment is used to estimate the magnitude of exposure, the frequency and duration of exposure, and the pathways by which a population gets exposed to the contaminant (USEPA, 2009). In exposure assessment, the contaminant released in the environment is analyzed, the exposed population and potential exposure pathways are identified, and the concentration of contaminant at the exposure point is estimated. Thus, exposure assessment begins when the contaminant is made available at the outer

boundary of the body during a specific period. Therefore, the degree of exposure is a function of concentration of the contaminant in the environmental media with time, and it is as shown in Eqn. 3.10

$$E = \int_{t_1}^{t_2} C(t)dt \qquad (3.10)$$

where C is the concentration of contaminant in mg/l for water, mg/kg for soil or food, or ug/m^3 for air, and $t_2 - t_1$ is the exposure duration. In either case, only part of the contaminant in the environmental matrices is inhaled, applied to the skin or ingested. This is known as the potential dose. The potential dose is usually normalized to time and body weight (USEPA, 1989). Only a fraction of the potential dose, i.e., the applied dose, encounters the absorption boundary (the skin, lungs, or gastrointestinal tract), which is then absorbed and made available for interaction with biological receptors, i.e., the internal dose. The dose transported to individual organs is known as the delivered dose, while the effective biological dose is the dose that reaches the cell, sites, or membrane where an adverse effect occurs (USEPA, 199s2).

The potential dose, D_{pot}, is evaluated using Eqn. 3.11, where IR represents the intake rates. The equation can be expressed in discrete form or as a summation of doses received during various events, as shown in Eqn. 3.12.

$$D_{pot} = \int_{t_1}^{t_2} C(t)IR(t) \, dt \qquad (3.11)$$

$$D_{pot} = \sum_i C_i . IR_i . ED_i \qquad (3.12)$$

ED_i is the exposure duration of an event. Given that the average values of C and IR are considered over a sum of the exposure durations for all events, then the average potential or applied dose is evaluated using Eqn. 3.13.

$$D_{pot} = C.\overline{IR}.ED \qquad (3.13)$$

However, for risk assessment, the biological response is considered, such that for non-cancer risks, the potential dose is averaged over the body weight (BW), and the period over which the exposure occurs, i.e., the averaging time (AT). Thus, the average daily dose (ADD) for non-cancer risk is calculated using Eqn. 3.14.

$$ADD_{pot} = \frac{C_i . IR_i . ED_i}{BW . AT} \qquad (3.14)$$

For cancer risk, the biological response is described in terms of exposure lifetime, LT. Thus, the average daily dose for cancer risk is given by Eqn. 3.15.

$$ADD_{pot} = \frac{C_i.IR_i.ED_i}{BW.LT} \qquad (3.15)$$

The internal dose depends on the contaminant uptake. However, for dermal exposure to contaminated water, the internal dose is calculated using Eqn. 3.16.

$$D_{int} = \int_{t_1}^{t_2} C(t).K_p.SA(t).dt \qquad (3.16)$$

where K_p is the permeation coefficient and is contaminant dependent, SA is the exposed surface area, and C is the concentration of the contaminant in the water. Since the concentration and surface area varies with time, the average internal dose over a given exposure duration from dermal exposure to a contaminant in water is evaluated using Eqn. 3.17.

$$D_{int} = \bar{C}.K_p.\overline{SA}.ED \qquad (3.17)$$

where $\overline{SA}$ is the average surface area exposed. Therefore, for the average non-cancer risk, the average daily internal dose, ADD_{Int} due to dermal contact with contaminant in water is given by Eqn. 3.18 (a), while Eqn. 3.18 (b) is used to evaluate the average daily internal dose for average cancer risk from dermal exposure to contaminated water.

$$ADD_{Int} = \frac{\bar{C}.K_p.\overline{SA}.ED}{BW.AT} \qquad 3.18(a)$$

$$ADD_{Int} = \frac{\bar{C}.K_p.\overline{SA}.ED}{BW.LT} \qquad 3.18(b)$$

Thus, potential dose from dermal exposure to contaminants in soil is estimated using Eqn. 3.19 (a) while the average daily dose internal dose from dermal exposure to contaminant in soil will be estimated using Eqn. 3.19 (b)

$$D_{pot} = C.F_{Adh}.\overline{SA}.ED \qquad 3.19\ (a)$$

$$ADD_{Int} = \frac{\bar{C}.F_{Adh}.S\bar{A}.ED}{BW.AT} \qquad 3.19\ (b)$$

where F_{Adh} is the soil adherence factor, defined as the amount of soil that adheres on a unit surface of skin per unit time. On the other hand, the internal average dose due to inhalation or ingestion of contaminant is evaluated using Eqn. 3.20. AF is the absorption factor of the contaminant through the gastrointestinal or respiratory track.

$$ADD_{Int} = \frac{\bar{C}.IR.AF.ED}{BW.AT} \qquad (3.20)$$

Deterministic and probabilistic approaches are usually used in exposure assessment. In the deterministic technique, reasonable maximum exposure (REM) values are used to quantify the doses. REM values are defined as the "*highest exposure that is reasonably expected to occur*" (USEPA, 1989). The input parameters' variability and uncertainty are not catered for while using the REM values. Thus, the deterministic model which is based on central tendency (Washburn *et al.,* 1998) provides limited information on the doses and, at the same time, could be an overestimate of the actual exposure values (Harris and Horn, 1996). In the probabilistic approach, statistical tools such as Monte Carlo simulation are used to quantify the input parameters' variability and uncertainty in exposure and risk assessment. Different probability distribution functions such as normal, lognormal, exponential, gamma, uniform, triangular among others are assigned to the input parameters. The input parameters are then sampled repeatedly and randomly, then used in the exposure model to provide a distributed output value (Harris and Horn, 1996). Thus, the output from the probabilistic model provides a range and the likelihood of a risk to human health from exposure to the contaminant. In this study, normal, lognormal, and triangular probability distribution functions were used to evaluate the exposure and human health risk.

Risk characterization involves the comparison of the estimated exposure value (ADD) to the threshold value of a particular contaminant, below which adverse effect may not occur (WHO, 2010). The risk is evaluated using Eqn. 3.24.

$$R = ADD \times T \qquad (3.24)$$

For carcinogens, the risk is evaluated as an incremental probability of a person developing cancer over a lifetime, referred to as incremental lifetime cancer risk (ILCR) (USEPA, 1989). The estimated daily intakes, which are averaged over a lifetime of 70 years are converted to incremental risk of an individual developing cancer. Thus, T in Eqn. 3.21 is a constant value called slope factor. The cancer risk relates directly with intake since ADD is averaged over 70 years. On the other hand, for non-cancer risk, T is the reciprocal of the maximum permissible value or dose (RfD) of a T. The ratio of exposure to toxicity is called hazard index, which assumes that there is a level of

exposure below which the population is unlikely to experience adverse health risk (USEPA, 1989).

Naturally occurring radioactive materials such as ^{232}Th and ^{238}U are chemo-toxic and radio-toxic. The chemo-toxicity health risk due to exposure to ^{232}Th and ^{238}U is like other heavy metals. However, radiotoxicity from exposure to these elements is evaluated by considering both external and internal doses. The external dose at the point of contact with the environmental radioactivity can is easily measured using dosimeters. However, doses from internal exposure can either be reconstructed using biomarkers such as fluid, tissue, and breath or be estimated by modeling exposure scenarios using codes (USEPA, 1992). Code such as RESRAD (RESidual RADioactive) OFF-SITE estimates radiation doses and cancer risk from exposure to radioactivity by an individual located within the boundary of the primary contamination, i.e., on-site, off-site, or both risks (Shhub, 2021). Different exposure scenarios (urban resident, rural farmer resident, worker, and recreational) are provided in the RESRAD OFF-SITE code for modeling internal and external doses and risks (Shhub, 2021).

RESRAD OFF-SITE calculates the radionuclide concentrations in different media as a function of time. Then it uses these concentrations for various environmental media to compute the intake, dose, and risk. The time integral dose or risk is calculated by performing a trapezoidal integration using dose or risk rates at the beginning and end of the time interval. All the dose and risk calculations fall within the time interval. The code assumes that the associated radionuclides are in secular equilibrium with the preceding principal radionuclide during transport and the point of exposure.

For external exposure to radiation, the dose and risk are a product of the radionuclide concentration in soil, the dose conversion factor, a cover and depth factor, the occupancy and indoor shielding factor, the source area, and the shape factor risks (Shhub, 2021). The ingestion of incidental soil is computed by summing the product of the dose conversion factor, the soil ingestion rate, the fraction of time spent on-site and off-site, and the radionuclide activity concentration in the soil at the on-site or off-site locations.

CHAPTER 4

Materials and Methods

4.1   Chapter Overview

In this chapter, detailed information on the study area, sampling and sample preparation techniques, water and soil pollution assessment methods and the human health risk techniques are presented and discussed.

4.2   Study Area

Water and soil samples were collected in March 2019 from the environs of the Kwale HMS deposit, where titanium ore mining and processing is ongoing, and around Mrima Hill, which has been earmarked for Nb ore and REE mining (Verplanck *et al*., 2014). Mrima Hill and the Kwale HMS deposits are both located in Kwale County, south coastal region of Kenya (Fig. 4.1).

Mrima Hill is a dome-shaped carbonatite alkaline intrusion with a northwesterly-southwesterly elongation bound by the latitudes of 4.47^o S and 4.49^o S and longitudes of 39.25^o E, and 39.27^o E. Its highest elevation is at Kichakasimba, 295 m above the sea level (Patel, 1991). It occupies an approximate area of 4 km^2. The central part of the hill is covered heavily with weathered manganiferous laterites whose thickness is over 100 m (Harmer and Nex, 2016). Fenitised sediments of sandstones and siltstones occur on the southwest and northeast edges of the hill. The western part of the hill is covered by dolomitic carbonatite, while calcite carbonatite covers the southeast and northwest (Harmer and Nex, 2016). Agglomeratic carbonatite occurs on the northern slope (JICA, 1991). This hill is part of the Jombo alkaline igneous complex, composed of barytes, pyroxene, nepheline, hornblende, pyrochlore, and ijolite ores (Caswell and Baker, 1953). JICA (1991) noted that traces of Pb and Zn accompany the manganiferous laterites and barytes.
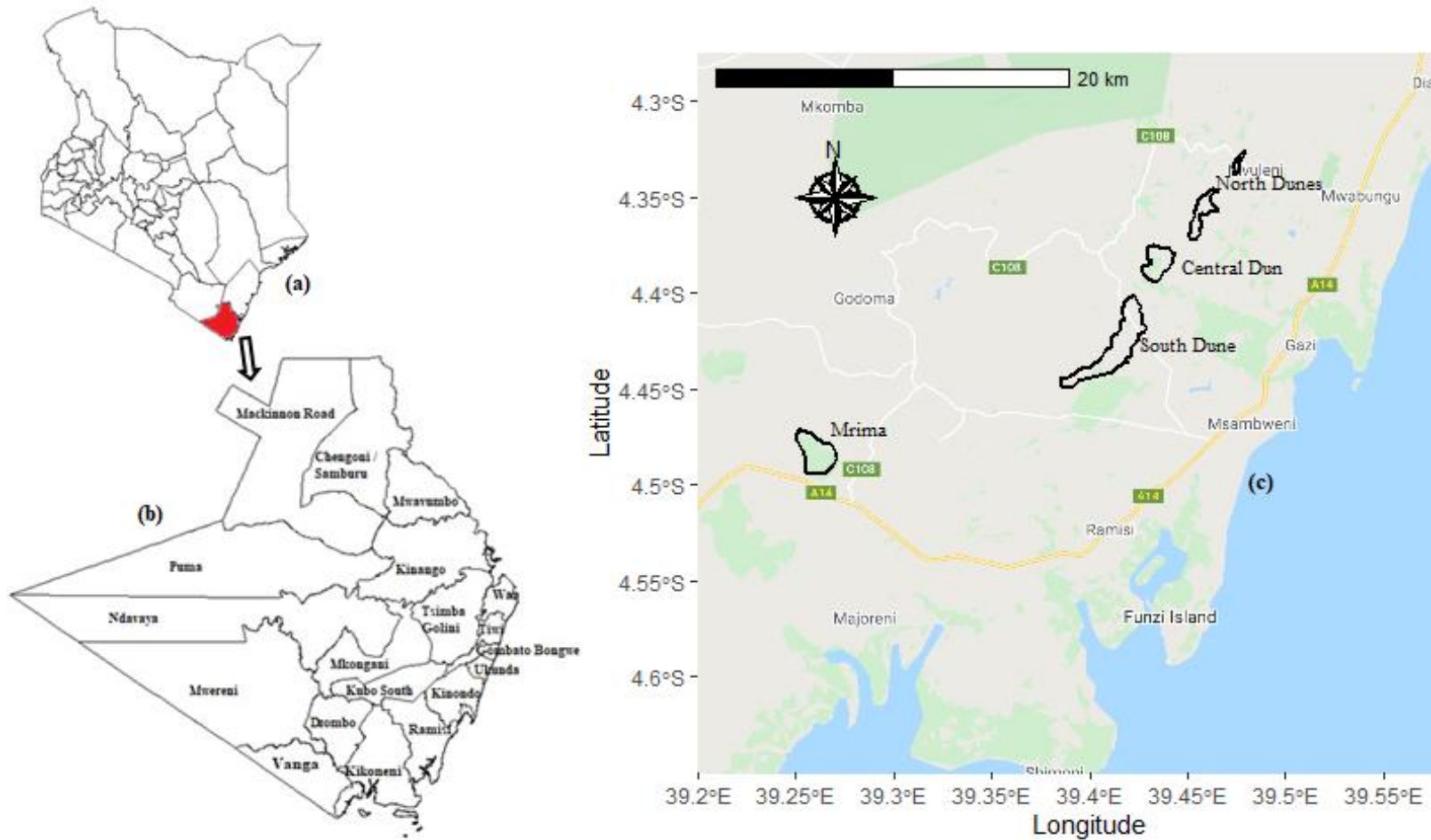
Fig. 4.1: (a) Map of Kenya (b) Administrative map of Kwale (c) Google Roadmap[TM] of Mrima Hill and approximate environs of the Kwale HMS Deposits
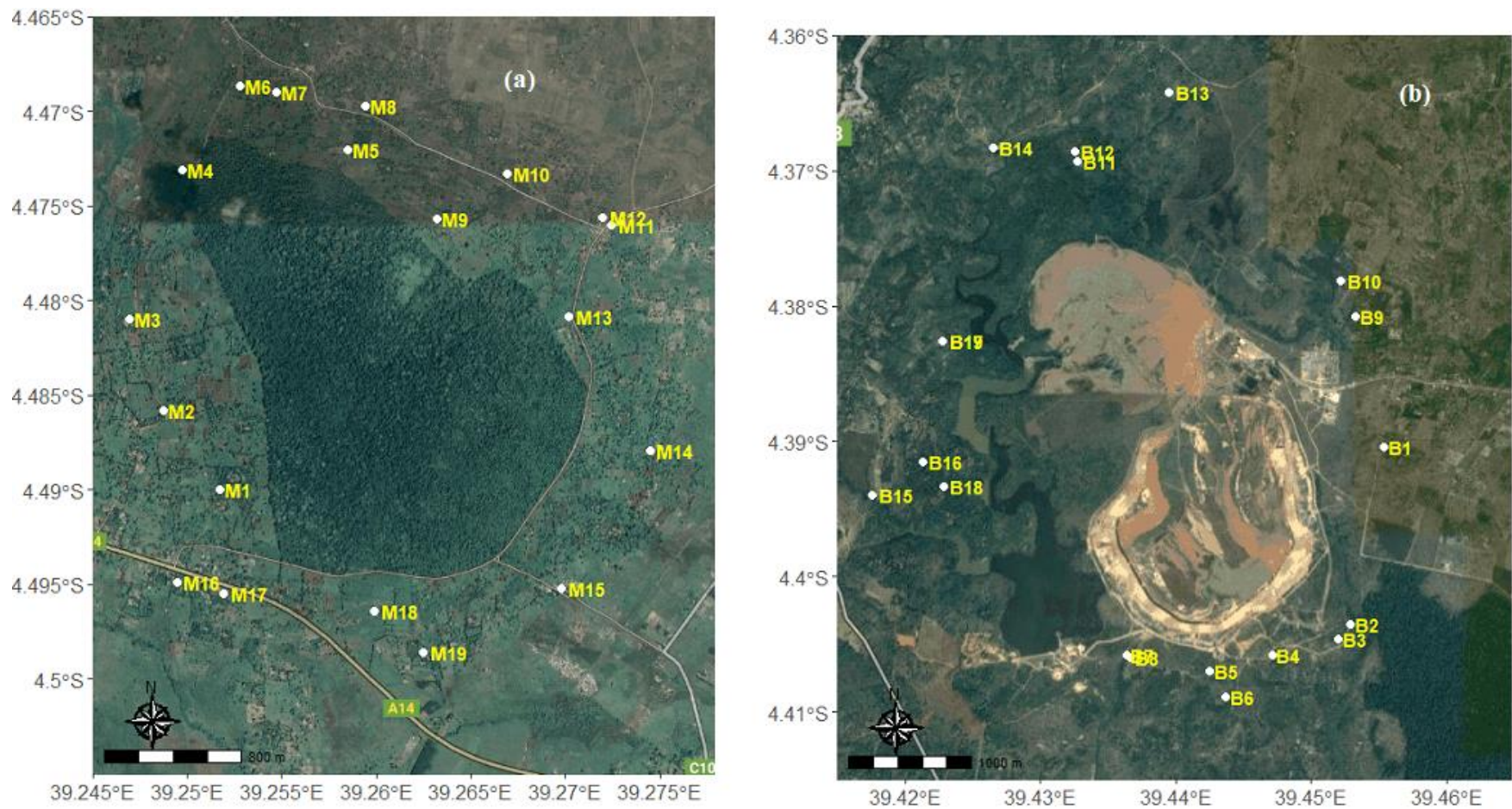
Fig. 4.2: Water sampling points at the environs of (a) Mrima Hill (b) Kwale HMS deposit overlaid on the Google Earth^{TM} map.
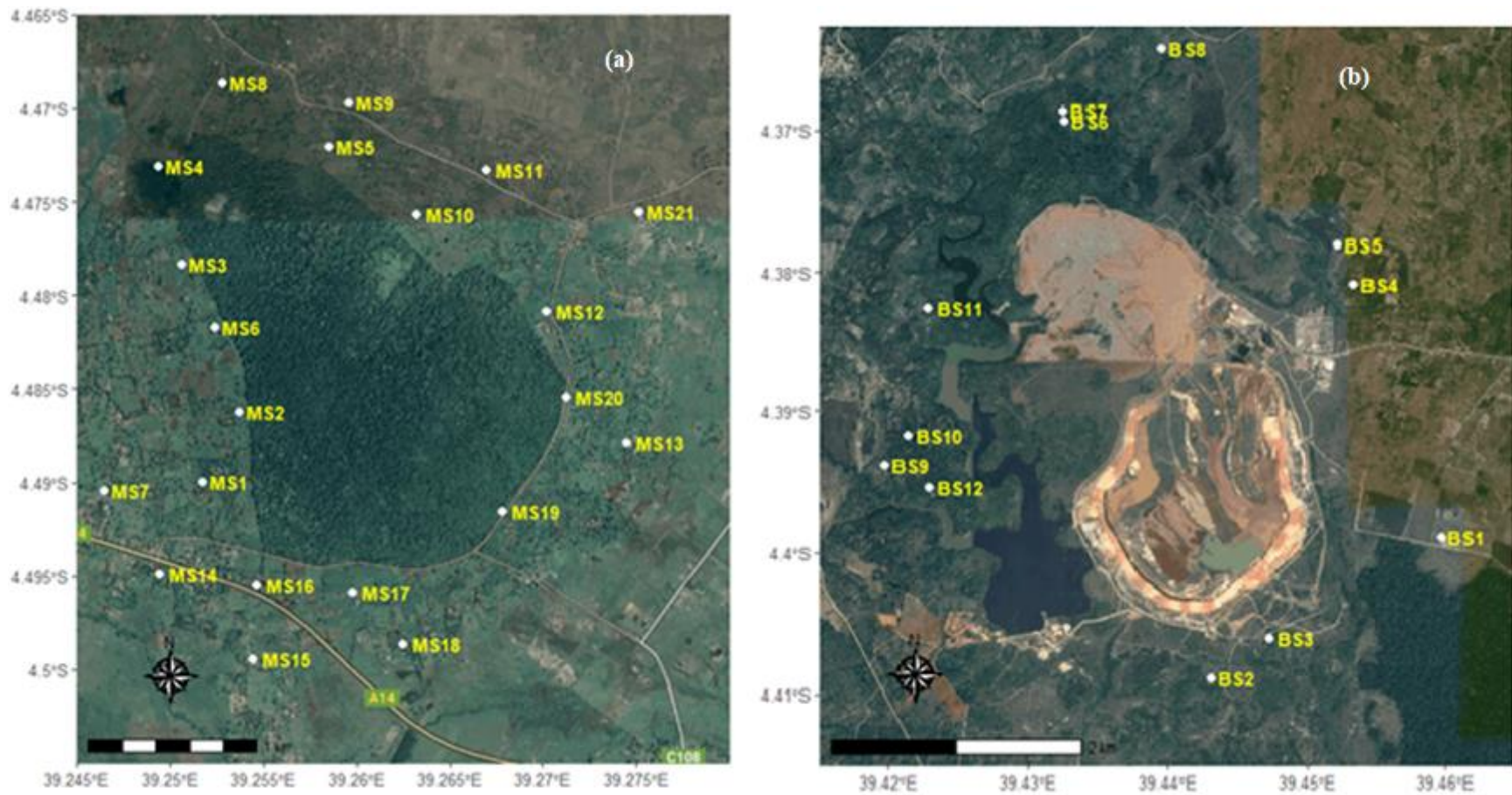
Fig. 4.3: Soil sampling points at environs of (a) Mrima Hill, (b) Kwale HMS deposit overlaid on Google Earth[TH] map

The Kwale heavy mineral sand was deposited within three aeolian dunes: south, central, and north, during the Pliocene age through intense erosion (Fernley and Drolia, 2011). The deposits lie within three administrative sub-counties of Kubo South, Kinondo, and Ramisi. The south dune deposit is 4.5 km long, 600 m to 800 m wide, and 19 m thick, separated from the central dune by the Mkurumudzi River. The central dune is 2 km long, 1.25 km wide, and on average 29 m thick, whereas the north dune extends 2 km long, 50 m to 1 km wide, and is approximately 66 m deep. The Kwale HMS deposit is currently under Tiomin Resources Kenya Inc. License No. PL/2018/CI19 (Fernley and Drolia, 2011), occupying an approximate area of 10 km^2, and its mining and mineral processing activities stretch from Maumba to Nguluku. The site lies between the latitudes of 4.41^o S and 4.47^o S and longitudes of 39.42^o E and 39.45^o E.

The monsoon winds, characterized by bimodal rainfall patterns, influence the tropical climatic condition of Kenya's coastal region (Ahmad, 2018). The long rains observed from April to July are due to the southeasterly monsoon winds, while the short rains occur from October through to December, corresponding to the northeasterly monsoon winds. The temperatures in this region range from 22.7oC to 33.1oC. The highest temperature is experienced in February, while July has the lowest temperature (Njuki *et al.*, 2014).

4.3 Sampling and Sample Preparation Procedures
4.3.1 Sampling and Pretreatment Techniques
A total of thirty-three (33) soil samples and thirty-eight (38) drinking water samples were collected around Mrima Hills and the Kwale HMS deposit in March 2019 using the random judgmental sampling technique (see Fig 4.2(a), (b) and 4.3 (a), (b)). This was to ensure coverage of the surrounding area encompassing the mine. A hand auger was used to drill the ground, and soil samples were scoped off to 0-20 cm according to ISO-18589-2 (ISO, 2007) procedures. The soil was collected at four nodes at each sampling point and mixed into a composite sample. The soil samples were air-dried at ambient temperature for approximately three (3) months and subsequently crushed into smaller sizes using a mortar and pestle. The samples were then auto-sieved to a particle size of 25

μm through a Retsch AS 200® 3-stage vibratory sieve shaker operating at 460 W and 100 Hz

Before water sample collection, we purged the borehole and flushed the tap water to remove any stagnant water in the plumbing system (Joint FAO/IAEA, 2018). The stagnant water could contain enhanced levels of lead and copper corroded from the plumbing system (WHO, 2011), mainly if the water flowing through it was acidic (Jurgens *et al*., 2019). For surface water, the samples were collected at the central part of the stream, canal, or well (Joint FAO/IAEA, 2018). Nitric acid was added to each water sample to stabilize the analytes and prevent microbial activities (Harb *et al.*, 2014). Before analysis, the water samples were filtered through a 0.22 μm Durapore® membrane and preserved at a temperature of 4°C.

4.3.2   Chemicals, Reagents, and Solution Preparation

Ultra-double de-ionized water and supra pure acid nitric acid (55%) obtained from ACT (Pty) Ltd® were used for cleaning and preparing all solutions. The 1000 μg /mL of Rh used as an internal standard, and multi-elemental aqueous CRM 50 MUL 14 -1000 Lot ME63 matrix in 5% HNO_3 and 3% HF, and 500 MUL 31-1000 Lot ME160 matrix in 5% HNO_3, and MULT31-1000 Lot ME160 matrix in 5% HNO_3 used for the calibration of the ICP-MS were purchased from De Bruyn Spectroscopic Solutions, South Africa. These CRM had all the elements of interest in this study. Furthermore, a multi-element tuning solution containing 1.0 μg/L of Li, Mg, Co, Tl, Y, and Ce, in 2% nitric acid obtained from Agilent Technologies was utilized to check the stability of the system (Crews *et al.*, 2007) and optimize the gas flow rates, torch position, and optical parameters so that the system gained maximum sensitivity (Roos, 2008). The tuning solution also limits oxides level and the doubly charged ions (Kadar *et al.*, 2011).

A 50 ug/L stock solution of Rh in a 2.5% nitric acid matrix was prepared and used as a procedural blank and an internal standard. The internal standard compensates for the instrument drift and matrix effect that could otherwise cause the enhancement or suppression of the signal (Vanhaecke *et al.*, 1992). In addition, calibration solutions in 5,

20, 50, 100, 500, and 1000 ug/L from the multi-element aqueous CRM solution were prepared and used to calibrate the ICP-MS.

4.3.3 Soil Sample Digestion and Preparation

A sub-sample of soil was weighed to the nearest 0.1 g and transferred to a high-pressure Teflon vessel, and a closed microwave-assisted wet digestion technique was used to extract the analytes from the soil samples (Falciani *et al.*, 2000). Each soil sample was treated with a mixture of nitric acid and hydrochloric acid (aqua regia) in a ratio of 3:1 (US-EPA Method 3051A, 2007). The aqua regia is a strong oxidizing agent, and it dissolves base elements of sulfates, oxides, carbonates, and sulfides (Lamble and Hill, 1998). It also aids in the recovery of Cu, Pb, and Zn (Gaudino *et al.*, 2007) and stabilizes analytes such as ^{238}U, which could otherwise accumulate in the ICP-MS introduction system (Pappas, 2012). In addition to the aqua regia, one mL of hydrofluoric acid and a few drops of hydrogen peroxide were added to the mixture. Hydrofluoric acid aids in the extraction of resistant metals such as Zr, Ni, and Cr (Gaudino *et al.*, 2007), while hydrogen peroxide enhances the destruction of organic matter (Enamorado-Báez *et al.*, 2013) The Teflon vessels were then tightly closed and placed in the Anton Paar Multiwave 3000$^{®}$ with an XF-100 rotor digestion, and the analytes were extracted from the soil using a stepwise digestion method as shown in Fig. 4.4. First, each aliquot was quantitatively transferred to vials and brought to a volume of 50 mL with double de-ionized water.

Each aliquot, for both water and soil samples, was filtered through a 0.22 µm Durapore® membrane filter to remove any residue and diluted by a factor of 5 for inductively coupled plasma mass spectroscopy (ICP-MS) analysis. The aliquots were diluted further by a factor of 50 for Ti, Cr, Mn, and Fe analysis since their concentrations were above the linear dynamic range of the initial dilution factor of 5 for ICP-MS analysis.
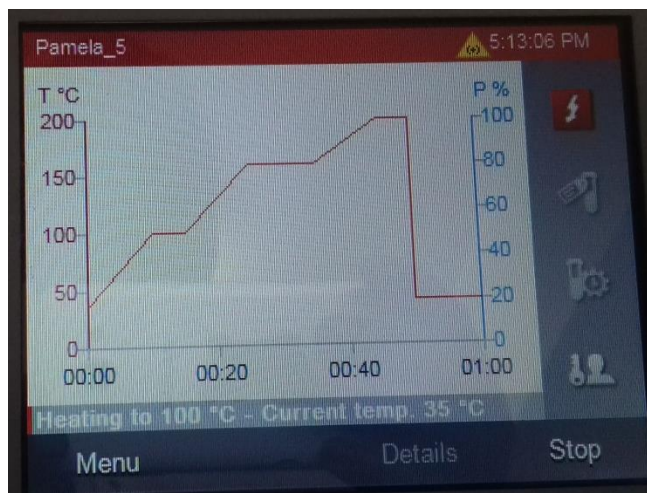
Fig. 4.4: Stepwise closed microwave digestion method

4.4   ICP-MS Analytical Technique

4.4.1   Experimental Set-up

Based on the versatility, extensive dynamic range, and very low detection limits at ppt level, an Agilent 7700s ICP-MS equipped with an octopole collision cell, pressurized with helium gas, was used to measure the mass fraction of ^{238}U, ^{232}Th, and other heavy metals in the soil and water samples. The cell provides a standard helium (He) mode and a high energy helium (HEHe) mode. The helium gas collides with the polyatomic ions, reducing their kinetic energy (Linge and Jarvis, 2009). Furthermore, a bias voltage placed at the exit of the collision cell prohibits the slow polyatomic ions from reaching the mass analyzer, only allowing the singly ionized charges to reach the mass analyzer. Each ion is then converted into a discrete electrical pulse and counted by the detector. Fig. 4.5 is a schematic representation of ICP-MS with the main parts indicated, i.e., the sample introduction system, ion extraction interface, mass analyzer, and detector.

The Agilent 7700s ICP-MS sample introduction system consists of an auto-sampler, a peristaltic pump operating at a speed of 0.1 rps, a micro-flow nebulizer supporting the uptake of 1.0 mL min^{-1}, and a Scott-type-Peltier cooled spray chamber operating at a temperature of 2° C, coupled with an extraction interface of a sampling depth of 8mm for He mode and HEHe mode. Table 4.1 shows some pre-set instrumental operating parameters.
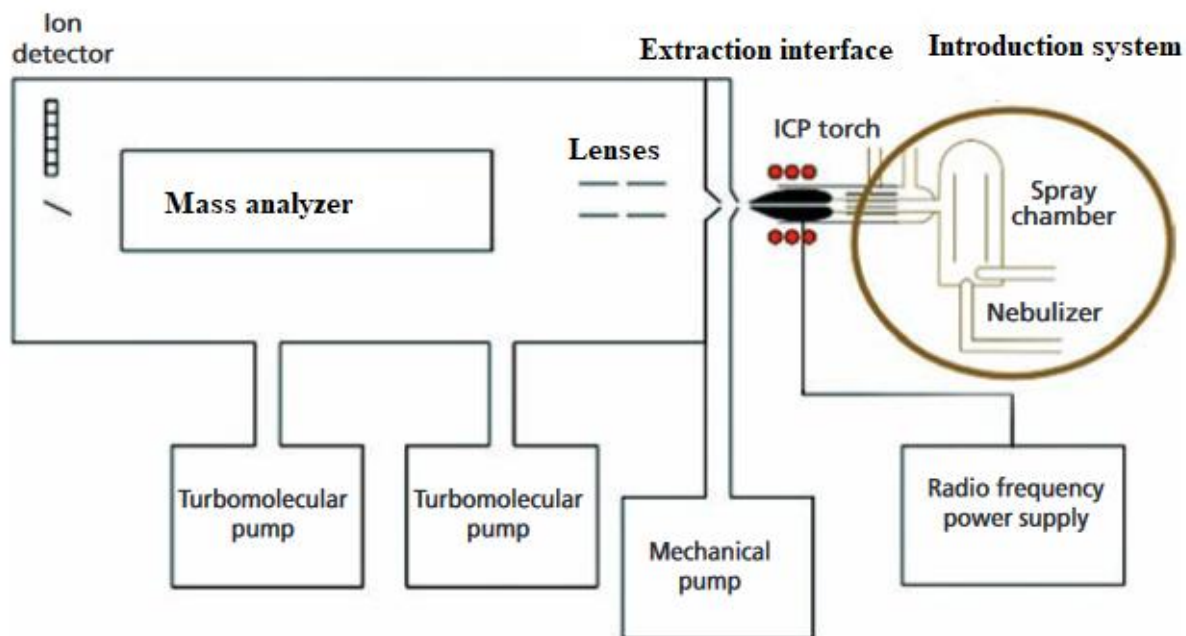
Fig. 4.4: A schematic representation of ICP-MS sample digestion method

(Adapted from: Brennan *et al.*, 2015)

The ICP-MS hardware accessories, setup, and operation were controlled by MassHunter software. A batch of tuning acquisition parameters, data analysis method, and sample list was developed, saved, and recalled during subsequent sample analysis. The ICP-MS was optimized daily using the multi-element tuning solution. The system was automated to use a 2% nitric acid solution to rinse the tubing and to remove any precipitates, such as the anionic complex $[ThF6]^{-2}$, formed during the sample digestion process with the hydrochloric acid (Pappas, 2012). If not rinsed from the ICP-MS tubing, the precipitates could cause memory interference. Multi-point calibration curves, with the relative response plotted against concentration, were obtained for each analyte of interest in the two collision modes.

Table 4.1: Agilent 7700 ICP-MS series instrumental operating parameters

Parameter	Gas mode	
	He	HEHe
Interface Pressure (Pa)	2.30×10^{2}	
Analyzer pressure	1.32×10^{-4}	
Cooling water minimum flow rate (L min^{-1})	5.0	
Forward RF power (W)	1549	
Reflected RF power (W)	12	
Plasma Frequency (MHz)	27.28	
Carrier gas (Lmin^{-1})	0.7	
Makeup gas (Lmin^{-1})	0.5	
ORS gas flow rate (mLmin^{-1})	3.6	10

4.4.2 Method Validation

External multi-elemental CRM and internal quality control samples were analyzed to validate the analytical method used in this research. Appendix B-2 and B-3 shows the set of percent recovery of the analytes in the external muti elemental CRM and the internal quality control samples respectively, analyzed in the helium, He, and the high energy helium, HEHe, collision modes. The data indicates that over 99% of the analytes in the external multi-elemental CRM and internal control samples in the HEHe collision mode were within the acceptable range of $\pm 10\%$ and $\pm 12\%$ (US DA, 2018), respectively, compared to analysis in the He collision mode. Selected samples were also analyzed in replicate using the same analytical procedure, and the relative percent difference (RPD) of elemental concentration evaluated using Eqn. 4.1. The RPD values of the analytes in the replicate samples are shown in Appendix B-4. The analysis of the soil and water samples was most appropriate in the HE-He collision mode, since the RPD of more than 90% of the analytes in the replicate samples was within the acceptable range of $\pm 20\%$ (US DA, 2018). In addition, the correlation coefficients of the calibration curves were evaluated. The correlation coefficient values, r values, obtained from the calibration curves from HE-He collision mode were more than 0.995, (see Appendix B-5). Thus, in

this research He-He collision mode was appropriate for ICP-MS analysis of the soil and water samples.

$$\text{RPD} = \frac{(C_1 - C_2) \times 200}{C_1 + C_2} \qquad (4.1)$$

where, C_1 is the elemental concentration of the first duplicate concentration and C_2 is the elemental concentration of the second duplicate concentration.

4.4.3 Quantification of Elements

The analyte concentration (C_E), in µg/L, was determined from the calibration curve by the Agilent MassHunter software such that,

$$C_E = \frac{(R - b)}{m}$$

where R is the correlation coefficient of the analyte, b is the relative response intercept, and m is the gradient of the curve. For digested samples, the mass concentration, C_m, was obtained using Eqn. 4.2.

$$C_m (\mu g/g) = \frac{C_E \times V_E \times D}{W} \qquad (4.2)$$

where C_E (µg/L) is the analyte concentration in the final extract, V_E (L) is the final extract volume of the sample, D (unitless) is the dilution factor, and W is the sample mass in grams. The activity concentration of ^{232}Th and ^{238}U was thereafter evaluated using Eqn. 4.3

$$C_{A.} (Bq/g) = \frac{0.6931 \times C_m \times N_A}{M \times t_{1/2}} \qquad (4.3)$$

where C_m is the mass concentration of the natural radionuclide in $\mu g/g$, N_A is the Avogadro's constant, M is the molar mass of the radionuclide (232 moles per gram for Th and 238 moles per gram for U), while $t_{1/2}$ is the half-life of radionuclides in seconds.

4.5 Statistical Analysis

A descriptive statistical method, including skewness and kurtosis, using the OriginPro® was applied to the concentration of Cr, Mn, Ni, Cu, Zn, As, Cd, Pb, Th, and U in water and soil samples and compared the national and international guidelines on maximum contaminant values in drinking water and soil samples. Besides descriptive statistics, the Shapiro-Wilk test (Reimann and Filzmoser, 1999) was conducted to determine the normality of data before hierarchical clustering analysis and use in ecological and human health risk assessment. The Shapiro-Wilk test showed a normal distribution of metals in the sample, except for Ni. Therefore, Spearman Correlation, a non-parametric correlation test, was performed to relate the elemental variables and assess the possible source of the heavy metals in the samples. Furthermore, a hierarchical cluster analysis technique was used to group the samples based on the similarity of the metal concentration (Ramasamy et al., 2014).

4.6 Water Quality Assessment Technique

The water quality index (WQI) was used to determine the influence of each of the observed selected heavy metal concentrations on the overall quality of water. WQI was based on the weighted arithmetic index method and the World Health Organization maximum heavy metal contamination levels in drinking water (WHO MCL) such that,

$$WQI = \frac{\sum_{i=1}^{n} Q_i W_i}{\sum_{i}^{n} W_i}$$

where Q_i is the quality rating scale of each metal, W_i is the weight unit of each metal and it is inversely proportional to the WHO recommended standard concentration of the heavy metal in drinking water, while n is the number of metals under consideration. The value of Q_i was evaluated using Eqn. 4.4 while W_i was evaluated using Eqn. 4.5

$$Q_i = \frac{(C_i - C_0)}{(S_i - C_0)} \times 100 \tag{4.4}$$

where C_i is the observed mean concentration of the ith parameter, C_0 is the actual value of pure water and it given as zero for heavy metals (Goher *et al.*, 2014), while S_i is the standard desirable value of the ith parameter.

$$W_i = \frac{K}{S_n} \qquad (4.5)$$

where S_n is the maximum contaminant level of the nth parameter and K is a proportionality constant of the 'Weights' of various water quality characteristics (Goher *et al.*, 2014) and it is given as

$$K = \frac{1}{^1/_{S_1} + ^1/_{S_2} + \cdots + ^1/_{S_n}} = \frac{1}{\Sigma^1/_{S_n}}$$

Goher *et al.* (2014) classified the WQI into five categories as shown in Table 4.2

Table 4.2: Water quality indices based on the weighted arithmetic index method.

WQI value	Rating	Grade
0 – 26	Excellent	A
27 – 50	Good	B
51 – 75	Poor	C
76 – 100	Very poor	D
> 100	Unsuitable for human consumption	E

4.7   Soil Pollution Assessment Technique

The soil pollution from Ti mining at the environs of the Kwale HMS deposit and prospecting Nb at Mrima hill was evaluated using the geo-accumulation index (I_{geo}), enrichment factor (EF), and pollution index (PI). The geo-accumulation index evaluates the degree of heavy metal contamination by comparing the concentration of the metals to the geochemical background levels provided by Chen *et al.* (1991), as shown in Eqn. 4.6.

$$I_{geo} = log_2 \left(\frac{C_i}{1.5 \, GB_i} \right) \qquad (4.6)$$

where C_i is the ith elemental concentration of the heavy metals in the soil samples, GB_i is the geochemical background of the ith element, while the constant 1.5 is the background correction value in the soil matrix due to the lithogenic differences in the earth crust (Kowalska *et al.*, 2018). Kowalska *et al.* (2018) further classified the degree of soil contamination into seven categories, as shown in Table 4.3.

The influence of anthropogenic activities on the concentration of U, Th, and other heavy metals in the soil was assessed using the enrichment factor, EF, defined by Eqn. 4.7.

$$EF = \frac{\left(^{C_E}/_{R_E}\right)_{sample}}{\left(^{B_i}/_{R_E}\right)_{Background}} \qquad (4.7)$$

where $(C_E/R_E)_{sample}$ is the ratio of the concentration of the analyzed element to the concentration of a reference element in the soil samples, while $(B_i/R_E)_{Background}$ is the ratio of the concentration of the element to the concentration of a reference element of the geochemical background. Sc was used as a reference element, a metal beside Ti, Mn, and Fe, which is assumed to be abundant in the earth's crust and they rarely enhanced by pedogenic weathering processes of the parent materials or anthropogenic activities (Maina *et al*., 2016). Ti, Mn, and Fe were not used in this research since Ti and Fe occurred substantially in ilmenite ore being mined at the Kwale HMS deposit (Abuodha and Hayombe, 2006). Furthermore, the carbonatites and laterites at Mrima Hill are rich in Fe and Mn (Horkel *et al*., 1984; Verplanck *et al*., 2014).

Table 4.3: Classification of the degree of contamination of soil using geoaccumulation index

Class	I_{geo} values	Quality of soil
0	$I_{geo} \leq 0$	unpolluted
1	$0 < I_{geo} \leq 1$	unpolluted to moderately polluted
2	$1 < I_{geo} \leq 2$	moderately polluted
3	$2 < I_{geo} \leq 3$	moderately to strongly polluted
4	$3 < I_{geo} \leq 4$	strongly polluted
5	$4 < I_{geo} \leq 5$	strongly to extremely polluted
6	$I_{geo} > 5$	extremely polluted

The pollution index, PI, was used to assess the heavy metal that was of the highest threat to the soils at the environs of Kwale HMS deposit and Mrima Hill. PI was evaluated using Eqn. 4.8. Kowalska *et al.* (2018) classified pollution threat into five distinct groups: Class 1, PI<1, threat absent; class 2, $1 < PI < 2$, threat is low; class 3, $2 < PI < 3$, threat is moderate; class 4, $3 < PI < 5$, threat is strong, and class 5, $PI > 5$, threat is very strong. Furthermore, the pollution load index, PLI, was used to assess the degree of

pollution due to accumulation of the heavy metals in soil at the two environs. The PLI was assessed using Eqn. 4.9

$$PI_i = \frac{C_{Ei}}{GB_i}$$ (4.8)

$$PLI = \sqrt[n]{PI_1 \times PI_2 \times PI_3 \dots \times PI_n}$$ (4.9)

where n is the number of metals analyzed and PI is the pollution index. PLI is classified into three distinct groups degree of pollution: $PLI < 1$, no pollution; $PLI = 1$ as the baseline level of pollution; and $PLI > 1$, which indicates deterioration of soil quality.

4.8 Human Health Risk Assessment

4.8.1 Chemotoxicity Human Health Risk Assessment

Deterministic and probabilistic techniques were used to evaluate non-carcinogenic and carcinogenic health risk of children and adults from exposure to heavy metal contaminated water and soil. In deterministic technique, the reasonable maximum exposure values (single values), defined as "*the highest exposure that is reasonably expected to occur*" (USEPA, 1989) were to evaluate the health risk. However, the probabilistic technique is based on Monte Carlo simulation. The Monte Carlo simulation is a statistical tool that quantifies the variation and uncertainty from input parameters in the health risk assessment.

In this study, we used both USEPA deterministic model and USEPA model embedded in the EnviroPRA Monte Carlo simulation package (Barrio-parra and Dominguez-Castillo, 2017) to evaluate the carcinogenic and non-carcinogenic health risk. A thousand (1,000) repetitively, randomly selected input parameters of different probability distribution functions (pdf) were used to estimate the carcinogenic and non-carcinogenic health risk. The 50th percentile from the probabilistic risk was identified as the median risk, while the 95th percentile represented the high-end risk. However, the point estimate represented the mean risk from the deterministic evaluation.

The non-carcinogenic health risk due to exposure to Cr, Mn, Ni, Cu, Zn, As, Pb, Cd and U was evaluated using Eqn. 4.10. The population could experience adverse non-carcinogenic health effect if the hazard index, $HI > 1$ (USEPA, 1989).

$$HI = \sum(THQ)_i \tag{4.10}$$

where THQ is the target hazard quotient of the ith metal and it is defined as the ratio of average daily dose, ADD, in mg/kg.day to the corresponding threshold concentration or reference doses, RfDs, in (mg/kg.day)$^{-1}$ of a specific contaminant. The RfDs values of the heavy metals are listed in Table 4.4. Although inhalation, ingestion, dermal route are the three mechanisms of exposure to contaminants we only considered that ingestion and dermal routes in this study, which are the main mechanism of exposure to heavy metals (Timofeev *et al*., 2019). THQ values were evaluated using Eqn. 4.11.

$$THQ = \left(\frac{ADD}{RfD}\right)_{ingest,soil} + \left(\frac{ADD}{RfD}\right)_{ingest,water} + \left(\frac{ADD}{RfD}\right)_{dermal,soil} \tag{4.11}$$

The ADD due to exposure to the metals via dermal contact with soil, and ingestion of water or soil are given in Eqn. 4.12 and 4.13, respectively,

$$ADD_{dermal,soil} = \frac{C_i \times SA \times AF \times ABS \times EF \times ED}{BW \times AT} \tag{4.12}$$

$$ADD_{ingest,(soil\ or\ water)} = \frac{C_i \times IR \times EF \times ED}{BW \times AT} \tag{4.13}$$

where C_i is the geometric mean of the metal concentration (in mg/kg for soil, mg/L for water), SA in cm^2 is the skin surface available for contact, AF is the soil adherence factor in mg/(cm^{-2}.day) of 0.07 for an adult and 0.2 for a child, ABS is the skin absorption factor and is contaminant specific. The ABS is greater in tropical regions where less clothing issue (USEPA, 1989). EF in day/year, is the exposure frequency of 350 days/year assuming that 15 days are spent away from the site (USEPA, 1989), ED is the exposure duration in years. The exposure duration is fixed at 70 when evaluating the carcinogenic human health risk. BW represents the average weight in kg, AT is the averaging period of 6 years for a child and 24 years for an adult (Smith, 1994) and IR is the intake rate. The input variables with their corresponding distribution parameter for children and adults are shown in Table 4.4.

Table 4.4: Input parameters used for probabilistic human health risk.

Parameter		Unit	Probabilistic input parameters		References
			Distribution	Distribution parameter	
Mass Concentration	Soil	mg/kg,	LN	GM; GSD (Metal specific)	
	Water	mg/L			
Activity concentration		pCi/kg	LN	GM, GSD (^{232}Th, ^{238}U)	This work
Ingestion rate (soil)	Adult		TR	Min = 0.1; Mode 25; Max= 50	
	Child	mg/day	LN	GM = In 24; GSD In 4	(Qu *et al.*, 2012)
Ingestion rate (water)	Adult		LN	GM= In 1.12; GSD = In 1.63	
	Child	L/day	LN	GM= In 0.619; GSD = In 1.65	
Exposure duration (non-carcinogenic)	Adult		N	M= 11.36; SD= 13.72	
	Child	Year	N	Same to adult but truncated at 6 years	(Smith, 1994)
Exposure Frequency		Day/year	TR	Min =240; Mode =345; Max =365	(Smith, 1994)
Body Weights (BW)	Adult		LN	GM =In 64.72; GSD =In 1.22	
	Child	kg	TR	Min=6.5; Mode=15; Max=26.1	(Smith, 1994)
Skin Surface area available for contact	Adult		TR	Min=760; mode=1530; max=4220	
	Child	cm^2	TR	Min=430; mode=860; max=2160	(Qu *et al.*, 2012)

*LN – lognormal distribution; TR – triangular distribution; N –normal distribution; GM –geometric mean; GSD – geometric standard deviation; Min – minimum; Max- maximum

Table 4.5: Reference dose (RfD) in $(mg/kg.day)^{-1}$, skin absorption factor (ABS), permeation coefficient (k_p) in cmh^{-1}, and cancer slope factors (SF) of various heavy metals

	Dermal			Ingestion	
	RfD	**SF**	**ABS**	**RfD**	**SF**
Cr	1.95E-02	n.a	4.00E-02	1.5E+00[*]	5.00E-01
Mn	9.60E-04	n.a	1.00E-03	1.40E-01	n.a
Ni	2.00E-02	n.a	3.50E-01	2.00E-02	n.a
Cd	1.25E-05	n.a	1.40E-01	1.0E-03*	8.50E-03
Cu	4.00E-02	n.a	1.00E-01	4.00E-02	n.a
Zn	3.00E-01	n.a	2.00E-02	3.00E-01	n.a
As	3.00E-04	3.66E+00	3.00E-02	3.00E-04	1.50E+00
Pb	4.00E-02	n.a	6.00E-03	3.50E-03	8.50E-03
U	n.a	n.a	n.a	3.00E-03[*]	n.a
Reference	(Chen *et al.*, 2016; Shomar and Rashkeev 2020)	(Chen *et al.*, 2016)	(HC, 2004; Timofeev *et al.*, 2019);	(Chen *et al.*, 2016; Shomar and Rashkeev 2020)	(H. Chen *et al.*, 2016)

RfD – Reference Dose; SF- Slope factor; ABS – Dermal absorption factor; n.a –not available; * reference dose for ingestion of water for Cr =3.00E-03; Cd = 5.00E-04; U = 6.0E-04 (USEPA, 2018)

The carcinogenic risk, also referred to as incremental lifetime cancer risk, ILCR, is defined as the incremental probability of an individual developing cancer over a lifetime due to exposure to carcinogen (Alidadi *et al*., 2019). ILCR values above 10^{-4} indicates that there is a high probability of one person in a population of 10,000 developing cancer in lifetime. Even though U and As have been identified as Group A carcinogen (USEPA, 2018), hexavalent Cr and Pb as probable carcinogen (US DOE, 2011), while Ni, Cu, and Cd as non-carcinogen via the ingestion route (USEPA, 2018), As has also been identified as a group A carcinogen via the dermal route (Surdu *et al*., 2013). However, the ILCR in either pathway was evaluated using Eqn. 4.14.

$$ILCR_{Cr,As,Pb} = (ADD \times SF)_{Cr,As,Pb} + (ADD \times SF)_{As} \qquad (4.14)$$

where ADD is the average daily intake while SF is the cancer slope factor, and it is metal specific as shown in Table 4.5. However, the averaging time, AT, in Eqns. 4.12 and 4.13 is equivalent to the average life expectancy of 70 years.

4.1.1 Radiogenic Human Health Risk Assessment

RESRAD OFF-SITE 4.0 code was used to estimate the total effective dose equivalent (TEDE) and the incremental lifetime morbidity cancer risk, ILCR, from exposure to ^{232}Th, ^{238}U, and their respective progenies by a rural resident farmer at the environs of Kwale HMS deposit and Mrima Hill. The rural resident farmer was assumed to be self-sufficient since most of the dietary needs were met at the site of residence (Shhub, 2021). The exposure pathways considered in this scenario were inhalation of soil particles, incidental ingestion of soil, and direct external exposure to the radionuclides for an exposure duration (ED) of 30 years. The assumption was that radionuclide was distributed uniformly in the layer of soil containing the naturally occurring radionuclide ^{232}Th and ^{238}U within it (Shhub, 2021).

During sample collection, we observed that the residents in both environs were peasant farmers, occupying an approximate area of 0.1 ha. Therefore, the soil thickness of 2.0 m was used to model the dose and risk. Incidental soil ingestion of 100 mg/day (Simon, 1998) and a default value of 8400 m^3/year for inhalation rate for an adult was used. Other input parameters include precipitation of 1025 mm per annum, an average temperature of

27° C, and wind speed in a north-westerly direction of 3.8 m/s (Njuki *et al.*, 2014). Given that the sandy loam soil at the titanium mine originated from sedimentary materials and was of loose texture, susceptible to erosion (Caswell and Baker, 1953), bulk density of 1.44 g/cm3, total porosity of 0.43, effective porosity of 0.4, run-off coefficient of 0.65, hydraulic conductivity of 1090 m/year and a b parameter of 4.38 (Yu *et al.*, 1993). On the other hand, a bulk density of 1.28 g/cm^3, total porosity of 0.43, effective porosity of 0.06, b parameter of 8.52, run-off coefficient of 0.2, and hydraulic conductivity of 773 m/year were used for the lateritic clay loam soil of Mrima Hill (Yu *et al.*, 1993, Kaniu *et al.*, 2019). Other default input parameters used in the RESRAD OFF-SITE code provided by Yu *et al.* (1993) are shown in Table 4.6.

Table 4.6: Input parameters used in the RESRAD OFFSITE Code

Input parameter	Value
Indoor to outdoor dust concentration	0.4
External gamma penetration factor	0.7
Fraction of time spent on primary contamination	
Indoor	0.4
Outdoor	0.2
Fraction of time spent offsite but outdoor	0.4
Depth of soil mixing layer, m	0.15
Mass of lading of particulate, g/cm^3	0.0001
Deposition velocity of respiratory particulates, m/s	0.001

The excess cancer risk from internal exposure to the ^{232}Th, ^{238}U, and their progenies were evaluated using Eqn.4.15, while Eqn. 4.16 was used to evaluate the excess cancer risk from external exposure to radionuclides (Eckerman *et al.*, 1999).

$$\text{Risk}_{\text{Int}} = \text{Intake (mBq/yr)} \times \text{ED (yr)} \times \text{CSF (risk/year per mBq/g)} \quad (4.15)$$

$$\text{Risk}_{\text{Ext}} = C_A \text{ (mBq/g)} \times \text{ED (yr)} \times \text{CSFs(risk/year per mBq/g)} \quad (4.16)$$

where ED is the exposure duration of 30 years, CSF is the morbidity cancer slope factor, indicated in Appendix F-3, and C_A is the soil activity concentration.

CHAPTER 5

Results and Discussion

5.1   Chapter Overview

In this chapter, the results on the concentration and distribution of Cr, Mn, Ni, Cu, Zn, As, Cd, Pb, Th and U in soil and water samples, quality of drinking water, and pollution indices of soil samples collected from the environs of the Kwale HMS deposit and Mrima Hill are presented and discussed. The results of carcinogenic and noncarcinogenic human health risk from exposure to U, Th and other heavy metals in water and soil are also presented and discussed. In addition, the total effective dose equivalent (TEDE) and the estimate values of the incremental lifetime cancer risk (ILCR) from exposure to ^{232}Th and its progenies (^{228}Th, ^{228}Ra), ^{238}U and its progenies (^{234}U, ^{230}Th, ^{226}Ra, ^{210}Pb, and ^{210}Pb) are presented and discussed.

5.2   Results of Concentration of Th, U, and other Heavy Metals

The results obtained from ICP-MS analysis of water and soil samples from the environs of Mrima Hill and the Kwale HMS deposit are shown in Appendix C-1, C-2, C-3, and C-4. The sampling points, the electrical conductivity (EC), and the potential hydrogen (pH) of water are also shown in Appendix C-5 and C-6.

5.2.1   Concentration of Th, U, and other heavy Metals in Water Samples

A statistical summary of the concentration of the metals in water samples with a comparison to the national and international guidelines on maximum contaminant values in drinking water is shown in Table 5.1.

A normality test performed on the data using the Shapiro-Wilk test (Reimann and Filzmoser, 1999) showed that the concentration of metals in the water samples at both study areas was distributed normally except for Ni, whose p-values were more than 0.05. Therefore, Spearman correlation, a non-parametric correlation test, was used to establish the interdependence of the variables in the samples and provide a possible source of the heavy metals in water and soil samples. Further statistical analysis showed that the skewness of all the metals of interest was higher than unity, indicating that the concentration of the metals was skewed towards the lower concentration (Lu *et al.*,

56

2010). Thus, median and median absolute deviation (MAD) were used for comparison (Reimann and Filzmoser, 1999). However, the geometric mean (GM) and the geometric standard deviation (GSD), which provide excellent median estimators, were used in risk assessment (National Research Council, 1994). WHO (2011) also indicated that the human health risk is directly proportional to the geometric mean of exposed dose.

The median metal concentration, in mg/L, in the water samples from the environs of Mrima Hill and Kwale HMS deposit followed a reducing order of $Cr > Mn > Cd > Zn > Ni > Pb > Cu > U > As > Th$ and $Cr > Zn > Mn > Cd > Ni > Pb > Cu > As > Th > U$ respectively. The median concentration of Cr, (0.569 ± 0.205) mg/L and (0.422 ± 0.393) mg/L, were observed in samples from the environs of Mrima Hill and the Kwale HMS deposit. These values were approximately 10-times higher than the national and WHO maximum contaminant value of 0.05 mg/L (WASREB, 2008; WHO, 2011) and approximately 5-times more than the USEPA maximum contaminant value of 0.1 mg/L (USEPA, 2018). Furthermore, the levels of Cr in all the samples from both study areas were above the national, WHO, and USEPA maximum contaminant value in drinking water. Sample BW7 had the highest Cr concentration of 6.778 mg/L. The sample was drawn from an abandoned shallow water pan beside a stream flowing from the tailing storage dam of the titanium mine at the Kwale HMS deposit. Sample B5, whose Cr concentration had the second highest value of 1.972 mg/L, was sampled along another stream flowing from the tailing storage dam. However, sample B9, which had the lowest concentration of Cr of 0.112 mg/L, was drawn from a water pan northeast of the mining site. Thus, a high variability of Cr with a relative standard deviation of 1.63 was observed among the water samples from the environs of the Kwale HMS deposit compared to Cr in water samples from Mrima Hill, whose relative standard deviation (RSD) was 0.32.

Table 5.1: Statistical summaries of the concentration, in mg/L (ppm) of U, Th, and other heavy metals in water samples from environs of Mrima Hill and Kwale HMS deposit, with a comparison to the national and international MCL in drinking water

	Mrima Hill							Kwale HMS deposit							Guideline values		
	Median	MAD	AM	SD	GM	GSD	RSD	Median	MAD	AM	SD	GM	GSD	RSD	WASREB	USEPA	WHO
Cr	0.569	0.205	0.578	0.188	0.552	1.35	0.32	0.422	0.393	0.933	1.52	0.488	2.91	1.63	0.05	0.1	0.05
Mn	0.043	0.063	0.109	0.147	0.001	26.8	1.35	0.099	0.102	0.169	9.17	0.096	3.34	1.02	0.1	NA	0.4
Ni	0.012	0.002	0.012	0.003	0.012	1.27	0.24	0.007	0.001	0.008	0.002	0.007	1.30	0.26	NA	NA	0.07
Zn	0.055	0.327	0.086	0.091	0.061	2.26	1.06	0.009	0.008	0.196	0.001	0.082	7.61	3.08	5	NA	3
Cu	0.003	0.002	0.006	0.012	0.002	3.70	2.10	0.002	0.001	0.002	0.002	0.002	1.66	0.71	0.1	1.3	2
As	0.001	0.002	0.002	0.003	0.001	2.79	1.18	0.001	0.001	0.001	0.001	0.001	1.24	0.85	0.05	0.01	0.01
Cd	0.019	0.025	0.026	0.028	0.007	5.94	1.09	0.083	0.223	0.086	0.012	0.084	1.24	0.23	0.005	0.005	0.003
Pb	0.006	0.002	0.007	0.003	0.006	1.60	0.53	0.002	0.001	0.003	0.003	0.003	1.73	0.75	0.05	0.015	0.01
Th	0.000	0.000	0.000	0.000	0.000	2.08	1.91	0.0005	0.0002	0.0005	0.0002	0.0004	1.74	0.53	NA	NA	NA
U	0.002	0.001	0.003	0.003	0.001	3.89	1.21	0.0002	0.0000	0.0003	0.0004	0.0002	2.31	1.19	NA	0.03	0.03

MAD -median absolute deviation, AM – arithmetic mean, SD -Standard deviation, GM- Geometric mean, GSD – Geometric mean deviation, RSD – relative standard deviation, NA – Not available

The median concentrations of Cd in water samples at both study areas were above the national and USEPA maximum contaminant value of 0.005 mg/L (WASREB, 2008; US EPA, 2018) and WHO maximum contaminant value of 0.003 mg/L (WASREB, 2008). The concentration of Cd in all the samples from the environs of the Kwale HMS deposit was above these guideline values, while 13 samples from Mrima Hill had Cd above these guideline values. The 6-samples (M14, M15, M16, M17, M18, and M19) whose Cd values were below these guideline values were collected from the southern edge of Mrima Hill. Sample M17, whose Cd concentration was below the detection limit of 0.4 ng/L, was drawn from a well that was 100 m deep, while sample M1, whose source was a diesel-generated community borehole, had the highest concentration of Cd (0.1146 mg/L). Other water samples from Mrima Hill whose Cd concentration were above the national and international permissible values in drinking water were collected from the western, southeast, and northwest edges of Mrima Hill. The high levels of Cd in these water samples could be attributed to the underlying carbonatite rocks and lateritic rocks enriched in phosphates (Harmer and Nex, 2016). However, the high concentration of Cd in water samples from the environs of Kwale HMS deposit may be solely be due to the use of phosphate farming, extensive abstraction of groundwater for farming that induces pyrite oxidation enhancing release of Cd from clay minerals (Kubier and Pichler, 2019), Cd pollution from heavy machinery that uses diesel fuels at the mining facility (Abuodha and Hayombe, 2006), and the sludge from the mineral mining activities (Kubier and Pichler, 2019).

The concentration of Pb in all the water samples from the environs of the Kwale HMS deposit were within the national (WASREB, 2008), WHO (WHO, 2011), and USEPA (USEPA, 2018) permissible values of 0.05 mg/L, 0.01 mg/L, and 0.015 mg/L respectively. The median concentration of Pb in samples from the Kwale HMS deposit was 0.002 ± 0.001 mg/L, varying between 0.0054 mg/L and 0.0115 mg/L with a relative standard deviation of 0.75. The concentration of Pb in all the samples from Mrima Hill were within the allowable value of 0.05 mg/L in drinking water. However, samples M1 (0.0156 mg/L) and M2 (0.0153 mg/L) were above the USEPA and WHO maximum contaminant values of 0.015 mg/L and 0.01 mg/L. The two samples were collected from the southwestern slope of Mrima Hill.

The concentration of Cu, Zn, Mn, As, Ni, Pb, and U in all the samples collected at both sampling sites were within the permissible guideline values of these metals in drinking water. The water samples from the environs of Mrima Hill had higher concentration of Cu, As, Ni, and U when compared to samples from the Kwale HMS deposit. This is contrary to the Th and Mn concentration in the samples from the two sampling sites. Samples from Kwale HMS deposit had higher Th and Mn concentration compared to samples from the environs of Mrima Hill. O'Neal and Zheng (2015) elucidated that surface water and water near mining operations had higher Mn compared to groundwater. However, the median concentration of U in samples obtained from Mrima Hill was 10-times more than in samples from Kwale HMS deposit. Similarly, the median concentration of Pb in water samples from Mrima Hill was twice compared to the median concentration of Pb in samples from Kwale HMS deposit.

A further statistical analysis using spearman correlation showed that at 95% significance level, samples from the Kwale HMS deposit showed a very strong positive correlation between Cr and Fe ($R^2 = 0.993$). A strong positive correlation was observed between the following pairs: Cr and Mn ($R^2 = 0.728$), Mn and Fe ($R^2 = 0.757$), Cd and Th ($R^2 = 0.620$). A moderate positive correlation was observed between Sc and Pb ($R^2 = 0.533$), Ti ($R^2 = 0.447$), As ($R^2 = 0.448$), and U ($R^2 = 0.471$); Ti and As ($R^2 = 0.448$), Th ($R^2 = 0.541$). However, a strong negative correlation was observed between Pb and Cd ($R^2 = -0.659$), Pb and Th ($R^2 = -0.572$), as shown in Table 5.2.

Despite the negative correlation observed between Cd and Pb in water samples from Kwale HMS deposit, a strong positive correlation was observed between Cd and Pb ($R^2 = 0.789$) in water samples from the environs of Mrima Hill as shown in Table 5.3. A strong positive correlation was also observed between Cr and Fe ($R^2 = 0.846$), Cu ($R^2 = 0.621$), and Mn ($R^2 = 0.545$); Fe and Cu ($R^2 = 0.638$), Mn ($R^2 = 0.565$), and Cd and Ti ($R^2 = 0.540$). However, a strong negative correlation was observed between U and Cr ($R^2 = -0.470$), Mn ($R^2 = -0.618$), and Fe ($R^2 = -0.604$); Cd and Cu ($R^2 = -0.474$).

Table 5.2: Spearman correlation at 95% confidence level of Th, U, and other heavy metals in water samples from the environs of Kwale HMS Deposit

	Sc	Ti	Cr	Mn	Fe	Ni	Cu	Zn	As	Cd	Pb	Th	U
Sc	1												
Ti	0.447	1											
Cr	0.140	0.146	1										
Mn	-0.111	0.105	0.728	1									
Fe	0.139	0.151	0.993	0.758	1								
Ni	0.118	0.268	0.140	0.079	0.153	1							
Cu	0.156	-0.170	0.333	0.051	0.305	0.161	1						
Zn	0.137	0.130	-0.405	-0.572	-0.416	0.237	-0.038	1					
As	0.448	0.448	0.281	0.382	0.289	0.111	0.235	-0.121	1				
Cd	-0.167	0.114	0.100	0.340	0.125	0.337	-0.153	-0.090	0.330	1			
Pb	0.533	0.093	-0.100	-0.401	-0.142	-0.123	0.442	0.337	0.043	-0.659	1		
Th	0.078	0.541	0.007	0.219	0.049	0.413	-0.376	0.012	0.237	0.620	-0.518	1	
U	0.471	0.176	-0.078	0.043	-0.025	0.048	0.238	-0.023	0.474	0.038	0.111	0.150	1

Table 5.3: Spearman correlation at 95% confidence level of Th, U, and other heavy metals in water samples from the environs of Mrima Hill

	Sc	Ti	Cr	Mn	Fe	Ni	Cu	Zn	As	Cd	Pb	Th	U
Sc	1												
Ti	-0.256	1											
Cr	0.181	-0.256	1										
Mn	0.103	-0.106	0.545	1									
Fe	-0.125	-0.096	0.846	0.565	1								
Ni	0.204	0.037	0.447	0.424	0.232	1							
Cu	0.047	-0.046	0.621	0.296	0.639	0.400	1						
Zn	-0.251	0.316	-0.042	0.012	0.249	-0.186	-0.056	1					
As	0.098	-0.088	-0.179	-0.002	-0.158	0.156	0.218	-0.123	1				
Cd	-0.133	0.540	-0.554	-0.283	-0.416	-0.133	-0.474	0.339	0.177	1			
Pb	-0.214	0.381	-0.268	-0.233	-0.058	-0.065	-0.184	0.505	0.189	0.789	1		
Th	-0.105	-0.072	0.286	0.358	0.434	0.105	0.398	0.013	0.135	-0.342	-0.191	1	
U	0.023	0.063	-0.470	-0.618	-0.604	0.067	-0.286	-0.063	0.235	0.386	0.167	-0.346	1

Izbicki et al. (2015) noted that the solubility of the toxic chromium species, Cr (VI), depended on the level of Cr (III) in the primary mineral ores such as mica, garnet, pyroxene, spinel, and amphiboles of carbonatites rocks (Caswell and Baker, 1953; (Kabata-Pendias, 2010; Van Gosen *et al.*, 2014). The presence of manganese (Mn) oxides in these underlying ores and the presence of alkaline or near-neutral groundwater, as observed in this study (see Table C5 and C6 in the Appendix), provided a conducive environment for the oxidation of the naturally occurring Cr (III) to Cr (VI) (Oze *et al.*, 2007; Tchounwou *et al*., 2012; Izbicki *et al*., 2015). Thus, the strong correlation between Mn and Cr, as observed in this study, could be due to geogenic processes. However, the negative correlation between Cd and Pb in water samples from the Kwale HMS deposit and the positive correlation between the two metals in samples from Mrima Hill show that the source of the two metals differs.

Cd is abundant in sulfides, carbonates, and phosphorite rocks (Kubier *et al*., 2019). The weathering of these rocks increases the concentration of Cd in surface and groundwater. The presence of clay minerals, hydrous oxides, and organic matter (Virakornphanich, *et al.*, 1991), as observed in Mrima Hill (Kaniu *et al*., 2019), enhances the sorption of Cd, but the redox state, pH, and ionic strength in the solution influences its mobility (Kubier et al., 2019; Hao et al. 2020). The alkaline carbonatite rocks at Mrima Hill are covered with lateritic manganiferous soils (Harmer and Nex, 2016) and have traces of Pb-Zn (JICA, 1991). Thus, geogenic activities may be the source of Pb and Cd in water samples from the environs of Mrima Hill. However, the extensive abstraction of water for mining and farming activities at the Kwale HMS deposit, the use of diesel-powered machinery (Abuodha and Hayombe, 2006), and sludge from the mineral activities (Kubier and Pichler, 2019) could be the source of Cd in samples from at the Kwale HMS deposit. In addition, the plumbing system may also elevate Pb and Cu in tap water (Swaran *et al.*, 2006; Harvey *et al*., 2016; Gibson *et al.*, 2020). Hence, the Pb in water samples from the Kwale HMS deposit and the Cu in water samples from Mrima Hill could be due to anthropogenic activities.

The water samples were clustered based on the concentration of the metals in the samples. The data was standardized using z-scores and the Euclidean distance based on similarities between the metal concentrations. The ward cluster analysis method was performed on the z-scored data, and the hierarchical cluster analysis results were displayed as dendrograms, as shown in Fig. 5.1 and 5.2.

Although one cluster was observed between samples from the two study areas, samples B5 and B14, B2 and B3, B17 and B18, and B4 and B10 from the environs of the Kwale HMS deposit were clustered at the same level, as shown in Fig. 5.1. Other samples clustered around these samples showed observable similarities. Samples B17 and B18 were collected from the Mkurumudzi River and Nora River. Samples B13, B19, and B15 were either sampled from a water pan beside a stream or a stream flowing into the Mkurumudzi River, as shown in Appendix B-3. Samples B4 and B10 were groundwater (a borehole and a well water). Sample B16, clustered alongside B4 and B10, was also drawn from a well. Sample B6 was supplied to the residents by the Base Titanium industry, while sample B12 was from a resident, and the water could have been from the same source as B6. The probable source of B12 could be B6. Sample B5, collected from a stream flowing from the tailing storage dam, had the same characteristics as B14, a water pan, upstream of Mkurumudzi River, which was used as a cattle watering point.

The sources of samples B2 and B3 were a stream flowing from the titanium mine and adjacent to the Kongoni forest. Sample B9, clustered with B2 and B3, was sourced from a water pan beside a stream. Samples B7 and B11 had unique characteristics, and they were clustered on their own. Sample B7, which had the highest concentration of Cr (6.778 mg/L) and Fe (10.79 mg/L), was a discarded shallow well beside a stream flowing from the tailing storage dam at the Kwale HMS deposit. Sample B11 was rainwater stored in a Jerican for more than six months. It had the highest concentration of Zn (2.646 mg/L).
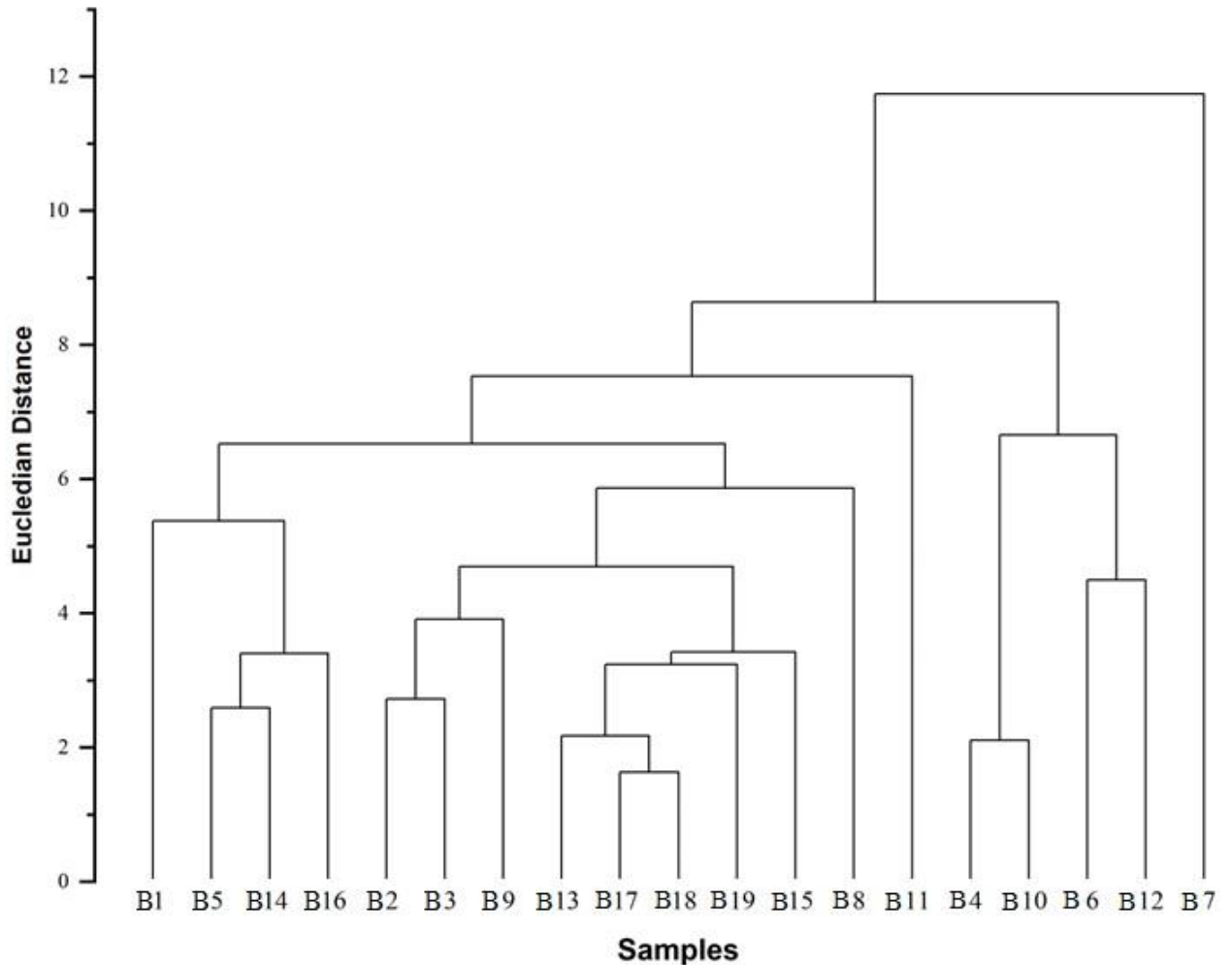
Fig. 5.1: Hierarchical clusters of water samples from the environs of the Kwale HMS deposit based on the concentration of metals in the samples.

On the other hand, all the samples from Mrima Hill were clustered around M2 and M3, M4 and M6, M8 and M19, M12 and M18, M14 and M15, as shown in Fig. 5.2, even though the samples were sourced from either boreholes or wells. The clustering of the samples was uniquely characterized. For instance, samples M4 and M7, which were stored in plastic Jerican were sampled from a borehole where sample M6 was collected, as shown in Appendix C-6. Sample M10, clustered with M4, M6, and M7, sampled at home, was sourced at M8, a community well, but it was also stored in a plastic Jerican. Sample M5, which was also stored in a plastic Jerican, was sourced at the M8, although it was grouped alongside samples M1, M2, and M3. Sample M9, which had the highest

concentration of Cr (1.111 mg/L), and Fe (1.250 mg/L) was also stored in a plastic Jerican. However, it was clustered uniquely as shown in Fig. 5.2.
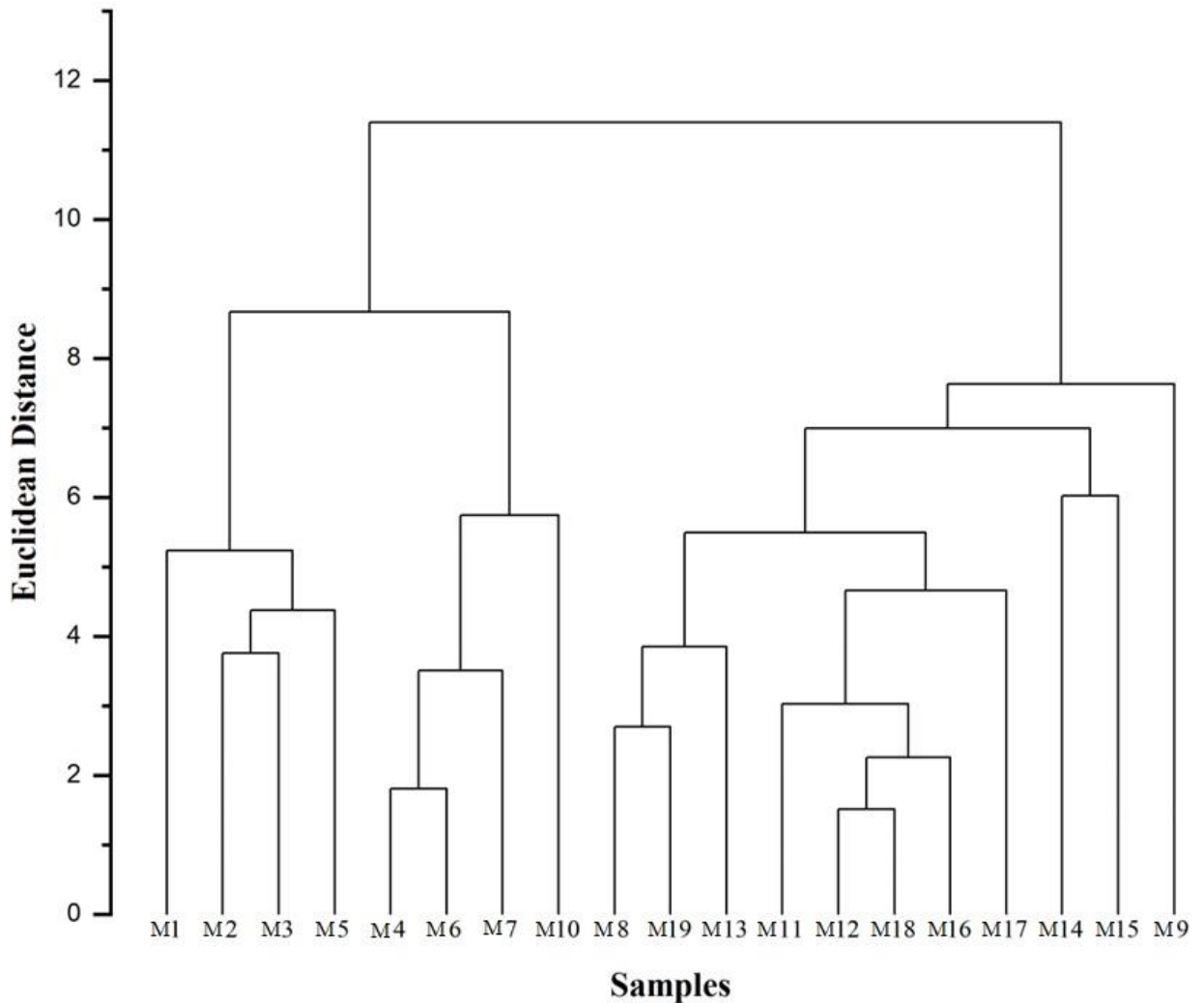
Fig. 5.2: Hierarchical clusters of water samples from environs of Mrima Hill based on the concentration of metals in the samples.

5.2.2 Concentration of Th, U and Heavy Metals in Soil Samples

A statistical summary of the concentration of the metals in comparison to the global average concentration (GAC) as provided by Kabata-pendias (2011) is shown in Table 5.4. A normality test using Shapiro-Wilk test showed a normal distribution of the concentration of the metals since the p-value of approximately 80% of the metals from both sampling sites was greater than 0.05. Thus, Spearman correlation, a non-parametric

correlation test, was used to establish the relationship between the analyzed heavy metals in the samples and provide a possible source of the metals.

The mean concentration, in mg/kg or stated otherwise, in the soil samples from the environs of Mrima Hill and Kwale HMS deposit followed a reducing order of $Fe > Cr > Ti > Mn > Zn > Zr > Nb > As > Pb > Ni > Th > Cu > Cd > Sc > U$ and $Fe > Cr > Ti > Mn > Zr > Zn > As > Nb > Sc > Cu > Th > Cd > U,$ respectively. The mean concentration of Cr in the soil samples from the Mrima Hill ranged between 26,939 mg/kg and 299,791 mg/kg, values that were $\cong$ 450 to $\cong$ 5000 times higher than the global average concentration of 59.5 mg/kg (Kabata-Pendias, 2010) and $\cong$ 2 to 7 times higher than the Cr value obtained at the Kwale HMS deposit in this study. The concentration of Cr in soil samples from the Kwale HMS deposit was $\cong$ 250 to 710 times higher than the global average concentration. Furthermore, the Cr values at Mrima Hill and Kwale HMS deposit were $\cong$ 135 to 1500 and $\cong$ 75 to $\cong$ 215 times respectively higher than the maximum allowable concentration (MAC) of 200 mg/kg (Kabata-Pendias, 2010) of Cr in topsoils and $\cong$ 60 to $\cong$ 660 times in Mrima Hill soil samples and $\cong$ 33 to $\cong$95 times for Kwale HMS deposit soil samples higher than the trigger value (TV) of 450 mg/kg (Kabata-Pendias, 2010) in topsoils.

Kabata-pendias (2011) noted that the concentration of Cr in soil was depended on the parent rock (Kabata-Pendias, 2010) and could be as high as 100,000 mg/kg, if the parent rock was serpentine (Izbicki *et al.*, 2015). Cr is also associated with pyroxene, amphibolite, chromates, and mica (Kabata-Pendias, 2010). The alkaline-carbonatite intrusion of Mrima Hill has considerable amount of pyroxene, amphiboles, and mica (Caswell and Baker, 1953). Likewise, heavy mineral sand deposit of Kwale are associated with gangue minerals of pyroxene and chrome-bearing spinel (Van Gosen *et al.*, 2014), which contain substantial naturally occurring trivalent chromium.

Table 5.4: Statistical summaries in mg/kg (ppm) of U, Th, and heavy metals in soils samples from the environs of Mrima Hill and Kwale HMS deposit with a comparison to global average concentration of the metals in topsoils

	Mrima Hill							Kwale HMS deposit							
	Median	MAD	AM	SD	GM	GSD	RSD	Median	MAD	AM	SD	GM	GSD	RSD	GAC
Sc	28.3	10.3	33.8	17.0	30.7	1.54	0.50	17.0	3.73	18.0	5.23	17.5	1.30	0.29	4.6
Ti (%)	3.44	0.96	3.59	1.01	3.43	1.40	0.28	2.09	0.40	2.17	0.51	2.12	1.25	0.24	0.7
Cr	127,046	54,441	128,748	30	107,834	1.93	0.00	25,375	8,006	27,580	9,093	26,241	1.39	0.33	59.5
Mn	11,193	6,824	11,947	6,779	9,803	2.04	0.57	1,706	731	3,460	3,804	2,336	2.32	1.10	488
Fe (%)	19.3	9.85	20.0	11.3	16.7	1.93	0.56	3.65	1.36	4.03	1.52	3.78	1.47	0.38	3.5
Ni	135	57.2	157	90	132	1.92	0.57	24.5	6.96	26.1	7.68	25.1	1.32	0.29	29
Cu	44.1	22.9	55.4	32.7	48.3	1.69	0.59	17.2	3.36	17.9	3.87	17.5	1.25	0.22	38.9
Zn	1564	1347	2329	2231	1637	2.35	0.96	155	72.2	159	55.5	150	1.43	0.35	70
As	156	64.9	167	88	149	1.60	0.53	152	38.8	156	36.0	152	1.25	0.23	6.83
Zr	289	108	330	174	292	1.68	0.53	180	38.6	199	74.8	189	1.35	0.38	267
Nb	238	137	291	269	196	2.77	0.92	38.9	9.7	47.8	23.6	43.6	1.53	0.49	12
Cd	43.7	13.4	47.2	15.2	44.8	1.41	0.32	4.73	1.22	4.83	2.80	3.99	2.10	0.58	0.41
Pb	159	96	159	109	124	2.18	0.69	19.6	4.35	20.9	6.33	20.1	1.32	0.30	27
Th	97.0	84.4	112	88.5	71.0	3.31	0.79	10.8	4.99	10.5	4.26	9.50	1.63	0.41	9.2
U	7.13	4.47	12.1	15.9	8.12	2.26	1.31	2.01	0.27	2.66	1.37	2.43	1.53	0.52	3.0

MAD - median absolute deviation; AM - arithmetic mean; SD – standard deviation; GM – geometric mean; GSD – geometric standard deviation, RSD – relative standard deviation; GAC – Global average mean

A further statistical analysis using correlation analysis showed a very strong relationship between Cr and Fe ($R^2 = 1.000$), Mn ($R^2 = 0.950$) and Zn ($R^2 = 0.918$) in soil samples from the environs of Mrima Hill. At 99% confidence level, a strong positive correlation between Cr and other metals; Ti ($R^2 = 0.711$), Ni (($R^2 = 0.767$), Cu ($R^2 = 0.758$), Zr ($R^2 = 0.738$), Nb ($R^2 = 0.877$), Pb ($R^2 = 0.765$), U ($R^2 = 0.749$), and Th ($R^2 = 0.681$), as shown in Table 5.5 was observed. Thus, the source of Cr and associated metals could be as a result of the weathering processes of the alkaline-carbonatite intrusion rocks at Mrima Hill, which is covered with lateritic manganiferous soils (Harmer and Nex, 2016) and has traces of Pb-Zn (JICA, 1991). However, a very strong correlation was only observed between Cr and Fe (($R^2 = 0.998$) in samples from the Kwale HMS deposit, with a strong correlation between Cr and Pb ($R^2 = 0.745$), Th ($R^2 = 0.731$), and Ni ($R^2 = 0.632$) with a mild co-occurrence with Mn ($R^2 = 0.490$) as postulated by (Abuodha and Hayombe, 2006). It is worth to note that high concentration of Cr was also observed in water samples from the two sampling sites (Kilavi *et al.*, 2021).

Despite the lower concentration of Cd in soils samples as compared to the rest of the metals, its mean concentration of 47.2 mg/kg and 4.73 mg/kg from the environs of Mrima Hill and Kwale HMS deposit was 110 and 10 times higher than the global mean concentration of 0.41 mg/kg (Kabata-Pendias, 2010). However, the mean concentration of Cd in soil samples from the environs of Kwale HMS deposit was below the MAC of 5 mg/kg and TAV of 20 mg/kg in topsoils (Kabata-Pendias, 2010), while in soils samples from environs of Mrima Hill, the mean Cd concentration was 9-times higher than the MAC, and 2-times higher than the TAV values in topsoils.

Table 5.5: Correlation analysis of Ti, Nb, Th, U, and other heavy metals in samples in collected at the environs of Mrima Hill

	Sc	Ti	Cr	Mn	Fe	Ni	Cu	Zn	As	Zr	Nb	Cd	Pb	Th	U
Sc	1														
Ti	0.607	1													
Cr	0.534	0.711	1												
Mn	0.501	0.669	0.946	1											
Fe	0.537	0.714	1.000	0.950	1										
Ni	0.833	0.714	0.767	0.796	0.772	1									
Cu	0.851	0.723	0.758	0.741	0.763	0.909	1								
Zn	0.394	0.695	0.918	0.853	0.920	0.631	0.714	1							
As	0.931	0.479	0.548	0.470	0.548	0.772	0.815	0.471	1						
Zr	0.860	0.791	0.738	0.727	0.742	0.947	0.956	0.663	0.805	1					
Nb	0.657	0.657	0.878	0.822	0.880	0.804	0.898	0.884	0.719	0.853	1				
Cd	0.356	0.333	0.441	0.363	0.433	0.314	0.324	0.284	0.208	0.265	0.272	1			
Pb	0.692	0.714	0.765	0.739	0.771	0.774	0.877	0.787	0.740	0.832	0.875	0.128	1		
Th	0.743	0.608	0.681	0.626	0.683	0.696	0.802	0.651	0.746	0.803	0.811	0.331	0.804	1	
U	0.650	0.645	0.749	0.678	0.752	0.746	0.904	0.822	0.715	0.832	0.952	0.167	0.845	0.732	1

Table 5.6: Correlation analysis of Ti, Nb, Th, U, and other metals in samples collected at the environs of the Kwale HMS deposit.

	Sc	Ti	Cr	Mn	Fe	Ni	Cu	Zn	As	Zr	Nb	Cd	Pb	Th	U
Sc	1														
Ti	0.607	1													
Cr	0.534	0.711	1												
Mn	0.501	0.669	0.946	1											
Fe	0.537	0.714	1.000	0.950	1										
Ni	0.833	0.714	0.767	0.796	0.772	1									
Cu	0.851	0.723	0.758	0.741	0.763	0.909	1								
Zn	0.394	0.695	0.918	0.853	0.920	0.631	0.714	1							
As	0.931	0.479	0.548	0.470	0.548	0.772	0.815	0.471	1						
Zr	0.860	0.791	0.738	0.727	0.742	0.947	0.956	0.663	0.805	1					
Nb	0.657	0.657	0.878	0.822	0.880	0.804	0.898	0.884	0.719	0.853	1				
Cd	0.356	0.333	0.441	0.363	0.433	0.314	0.324	0.284	0.208	0.265	0.272	1			
Pb	0.692	0.714	0.765	0.739	0.771	0.774	0.877	0.787	0.740	0.832	0.875	0.128	1		
Th	0.743	0.608	0.681	0.626	0.683	0.696	0.802	0.651	0.746	0.803	0.811	0.331	0.804	1	
U	0.650	0.645	0.749	0.678	0.752	0.746	0.904	0.822	0.715	0.832	0.952	0.167	0.845	0.732	1

Cd contamination of topsoils has been associated with both anthropogenic activities and geogenic processes. The anthropogenic activities include atmospheric deposition from metal smelters, use of phosphate fertilizer, Pb and Zn mining, extensive abstraction of groundwater which induces pyrite oxidation and enhances Cd-release from clay minerals (Kubier and Pichler, 2019), and pollution from diesel-powered machinery (Al-gizzi *et al.*, 2020), while the geogenic processes such as weathering of parent rocks with Cd levels. For instance, the high concentration of Cd in soils of 222 mg/kg in Slovakia was due to weathering of the pyritized quartz and 8.15 mg/kg in Jurassic rocks in France (Kabata-Pendias, 2010). A negative correlation observed between Cd and Cr- Fe in samples from the environs of Kwale HMS deposits points to an anthropogenic source of Cd in the soil samples. On the other hand, a weak positive correlation of 0.44057 and 0.43268 was observed between Cd with Cr and Fe. Thus, the weathering of the calcite and dolomitic carbonatites at Mrima Hill (Caswell and Baker, 1953), whose products includes lateritic soils enriched in phosphates (Harmer and Nex, 2016) coupled with the phosphate's fertilizers used in farming at Mrima Hill could be the source of Cd in the topsoils.

The mean concentrations of As of 156 mg/kg and 167 mg/kg in the soil from the environs of Kwale HMS deposit and Mrima Hill were $\cong$24 times higher than the global mean concentration of 6.83 mg/kg (Kabata-Pendias, 2010). Furthermore, the mean concentration of As in the soils from both sampling sites were $\cong$8 times higher than the MAC of 20 mg/kg (Kabata-Pendias, 2010) in topsoils and $\cong$ 2 times higher than the TV of 65 mg/kg (Kabata-Pendias, 2010) of As in topsoils. Although Tchounwou *et al.* (2012) noted that higher levels of As occurred in topsoils near mineral deposits or mining sites, a literature review of concentration of As in topsoils from European countries by Loukola-ruskeeniemi *et al.* (2021) showed that the concentration of As in topsoils from France was as high as 12,000 mg/kg against the geochemical background value of 18 mg/kg, while in Finland, the concentration of As in topsoils was 1050 mg/kg against a geochemical background value of 30 mg/kg.

The concentration of Ti in soil samples collected at the environs of Mrima Hill and the Kwale HMS deposit ranged from 1.20% to 5.76% and 1.40% to 3.44% respectively with a mean concentration of 3.59% and 2.17%. These values were $\cong$ 11 and $\cong$7 times higher than the global average mean of 0.33% in topsoils (Kabata-Pendias, 2010). The values of Ti in soils samples from the environs of Mrima Hill were within the range observed earlier by Patel and Mangala (1994), while the Ti values in the soil samples at the Kwale HMS sand was approximately twice the value obtained by Maina *et al.* (2016) at the same site before the start of mining activities. A further statistical analysis among metals in soil samples at Mrima Hill showed a strong correlation between Ti with Cr ($R^2 =$ 0.711), Mn ($R^2 = 0.670$), Fe ($R^2 = 0.715$), Ni ($R^2 = 0.723$), Zn ($R^2 = 0.695$), Zr ($R^2 = 0.790$), Nb ($R^2 = 0.657$), Pb ($R^2 = 0.714$), Th ($R^2 = 0.608$), and ($R^2 =$ 0.645), as indicated Table 5.5.

Similarly, the mean concentrations of Fe and Mn in soil samples from the Kwale HMS deposit were $\cong$ 2 and $\cong$ 3 times respectively higher than the mean concentration of Fe and Mn observed by Maina *et al.* (2016), contrary to the values of Fe and Mn in soil samples collected at the environs Mrima Hill which strongly correlated ($R^2 = 0.950$), as shown in Table 5.5, and were within the range of values observed by Patel and Mangala (1994). A weak positive correlation of $R^2 = 0.486$ was observed between the two metals in soils samples from the environs of Kwale HMS deposit, as shown in Table 5.6. This shows that the mining activities enhanced the concentration of Mn and Ti in topsoils at the environs of the Kwale HMS deposit.

Other than Cr, Cd, As, Ti, Fe, and Mn, whose mean concentrations in samples from the environs of Kwale HMS deposit were higher than their respective global mean values, the mean concentration of Nb in the soil samples from this area was $\cong$ 5 times higher than the global mean concentration of 12 mg/kg Nb in topsoils (Kabata-Pendias, 2010). A further statistical analysis showed co-occurrence of Nb with Th and Pb, which in turn correlated strongly with Cr and Fe, as shown in Table 5.6, contrary to the negative correlation observed between Nb and Zr. However, Zr was strongly correlated with U ($R^2 = 0.930$). On the other hand, Nb in soil samples from Mrima Hill were $\cong$ 24 times higher than the global average mean of 12 mg/kg, and it strongly correlated with Pb

($R^2 = 0.875$), Th ($R^2 = 0.811$), U ($R^2 = 0.952$), Zr ($R^2 = 0.853$), and other metals as shown in Table 5.6. Other metals such as Ni, Zr, Pb, Th, and U, which also strongly corelated, as shown in Table 5.6, were higher than the global mean concentration by 29, 267, 27, 9.2, and 3.0, respectively, in topsoil. However, the mean concentration in mg/kg of Ni (17.9), Zr (199), Pb (20.9), Th (10.5), and U (2.6) in soil samples from the environs of Kwale HMS deposits were approximately equal to the global mean concentration of respective metals in topsoil. Mrima Hill which has been earmarked for Nb ore and REE mining (Verplanck *et al.*, 2014), been associated with monazite and pyrochlore ores which have high Th and U concentrations (Verplanck *et al.*, 2014), with traces of Pb-Zn (Horkel *et al.*, 1984).

Other than Cr, Cd, As, Ti, Fe, and Mn, whose mean concentrations in samples from the environs of Kwale HMS deposit were higher than their respective global mean values, the mean concentration of Nb in the soil samples from this area was $\cong$ 5 times higher than the global mean concentration of 12 mg/kg Nb in topsoils (Kabata-Pendias, 2010). A further statistical analysis showed co-occurrence of Nb with Th and Pb, which in turn correlated strongly with Cr and Fe, as shown in Table 5.6, contrary to the negative correlation observed between Nb and Zr. However, Zr was strongly correlated with U ($R^2 = 0.930$).

Nb in soil samples from Mrima Hill were $\cong$ 24 times higher than the global average mean of 12 mg/kg, and it strongly correlated with Pb ($R^2 = 0.875$), Th ($R^2 = 0.811$), U ($R^2 = 0.952$), Zr ($R^2 = 0.853$), and other metals as shown in Table 5.6. Other metals such as Ni, Zr, Pb, Th, and U, which also strongly corelated, as shown in Table 5.6, were higher than the global mean concentration by 29, 267, 27, 9.2, and 3.0, respectively, in topsoil. However, the mean concentration in mg/kg of Ni (17.9), Zr (199), Pb (20.9), Th (10.5), and U (2.6) in soil samples from the environs of Kwale HMS deposits were approximately equal to the global mean concentration of respective metals in topsoil. Mrima Hill which has been earmarked for Nb ore and REE mining (Verplanck *et al.*, 2014), been associated with monazite and pyrochlore ores which have high Th and U concentrations (Verplanck *et al.*, 2014), with traces of Pb-Zn (Horkel *et al.*, 1984).

5.3 Results of Water Quality and Soil Pollution Assessment

In this section, the assessment of quality of drinking water and the soil pollution level from the environs of Mrima Hill and the Kwale HMS deposit water are presented and discussed.

5.3.1 Water Quality Assessment Results

Despite the high concentrations of Cr in the water samples from the two study areas, the contribution of Cd to the water quality index, WQI, was highest, as shown in Tables 5.7 and 5.8. Due to its toxicological effects, Cd, a non-essential element, has been listed as a priority hazardous substance by several organizations, including the WHO and USEPA (Kubier *et al*., 2019). Therefore, WASREB and USEPA have set the threshold value of Cd in drinking water at 0.005 mg/L (WASREB, 2008; US EPA, 2018), while WHO has set it at 0.003 mg/L (WHO, 2011). Since the evaluation of the quality rating of heavy metals is an inverse of the WHO value and a multiple of other parameters as described in the methodology section, it was observed that the contribution of Cd to the quality rating was higher than Cr, whose WHO threshold value in drinking water is 0.05 mg/L. Thus, the quality rating values of Cd in all the water samples obtained from the environs of the Kwale HMS deposit were higher than 100, as shown in Table 5.3.1, making it unsuitable for human consumption. However, the quality rating value of Cr varied, with the highest value of 451, observed in sample B7 (collected at a discarded water pan) and the lowest in B9 (7.48).

Table 5.7: The contribution of each of the metals in water samples from the environs of Kwale HMS deposit the WQI

	B1	B2	B3	B4	B5	B6	B7	B8	B9	B10	B11	B12	B13	B14	B15	B16	B17	B18	B19	Median
Cr	10.4	51.9	47.5	**121**	**131**	11.6	**451**	47.9	7.48	22.4	10.4	13.2	41.5	39.5	9.92	86.0	22.03	25.4	28.1	28.07
Ni	0.24	0.15	0.24	0.24	0.30	0.22	0.39	0.36	0.15	0.23	0.33	0.31	0.21	0.23	0.37	0.25	0.22	0.22	0.26	0.24
Cu	0.00	0.00	0.00	0.00	0.00	0.00	0.00	0.00	0.00	0.00	0.00	0.00	0.00	0.00	0.00	0.00	0.00	0.00	0.00	0.00
As	0.99	0.71	1.43	1.11	0.61	4.85	5.25	2.09	0.42	1.39	0.21	1.52	0.28	2.05	0.37	1.65	2.05	1.74	2.04	1.43
Cd	1393	1249	1429	1248	1400	1188	1528	2233	1216	1173	1631	1825	1532	1574	1496	1754	1832	2142	2452	1528
Pb	6.13	4.85	4.85	13	4.32	11.3	3.74	3.65	5.53	19.1	3.20	4.08	2.56	4.03	3.23	2.85	3.08	3.08	5.94	4.08
U	0.02	0.02	0.13	0.02	0.03	0.21	0.03	0.03	0.02	0.04	0.01	0.23	0.02	0.04	0.06	0.02	0.04	0.04	0.03	0.03
WQI	1411	1307	1483	1384	1536	1216	1988	2287	1230	1216	1645	1844	1577	1620	1510	1845	1859	21723	2488	1578

Table 5.8: The contribution of each of the metals in water samples from the environs of Mrima Hill to the water quality index, WQI

	M1	M2	M3	M4	M5	M6	M7	M8	M9	M10	M11	M12	M13	M14	M15	M16	M17	M18	M19	Median
Cr	27.6	28.0	25.8	25.0	28.6	32.1	35.7	43.6	73.9	28.8	25.1	39.2	54.0	41.9	48.2	37.8	44.9	38.8	50.8	37.8
Ni	0.48	0.33	0.39	0.36	0.28	0.42	0.56	0.41	0.33	0.36	0.22	0.42	0.60	0.39	0.45	0.41	0.41	0.36	0.58	0.41
Cu	0.00	0.00	0.00	0.00	0.00	0.00	0.00	0.00	0.00	0.00	0.00	0.00	0.00	0.00	0.00	0.00	0.00	0.00	0.00	0.00
As	0.44	3.73	5.23	11.9	0.29	13.2	16.1	0.42	1.06	2.35	1.28	1.39	4.13	1.82	4.89	0.20	3.41	3.21	0.33	2.35
Cd	2118	895	744	651	1018	1051	345.5	273	389	336	316	512	375	26.5	38.9	46.7	0.00	19.1	8.22	346
Pb	40.2	38.4	24.6	24.4	17.9	22.5	27.9	20.5	69.5	14.9	48.2	18.6	17.0	18.2	14.9	14.8	11.7	12.7	12.5	18.6
U	0.72	0.47	0.74	0.97	0.01	0.98	0.27	0.02	0.31	3.02	0.38	0.42	0.39	0.25	0.13	0.59	0.11	0.37	0.54	0.39
WQI	2187	966	801	714	1065	1120	426	338	534	385	391	572	451	89.1	107	101	60.5	74.5	73.0	426

Similarly, the high concentration of Cd in some of water samples from the environs of Mrima Hill made the water unsuitable for human consumption. For instance, the Cd levels of 0.115 mg/L in sample M1 contributed 2118 to the sum of 2187 of the WQI. M1 was sampled at a community diesel-pumped borehole. Other samples with Cd concentration above the WHO permissible value of 0.003 mg/L included M2 through to M13. The quality rating values of Cd in these samples were more than 300, contrary to the samples M14, M15, M16, M17, M18, and M19, whose Cd quality ratings were less than 50. The quality rating of Cr in 16 of the samples from environs of Mrima Hill ranged between 25.0 and 44.9, with a mean of 37.8, therefore they were of good quality for human consumption as classified by Goher *et al.* (2014) . However, the quality rating of Cr in M19, M13, and M9 were 50.8, 54.0, and 73.9, and therefore they were of poor quality for human consumption according to *Goher et al.* (2014).

The contribution of As and Pb to WQI in samples from Mrima Hill was higher than those observed in samples from the environs of the Kwale HMS deposit. The median rating value of As in water samples from Mrima Hill was 2.35 and ranged between 0.20 and 16.7, while the median quality rating value in water samples from the Kwale HMS deposit was 1.43 and ranged between 0.21 and 5.25. The contribution of Pb to WQI in the samples from Mrima Hill ranged between 11.7 and 69.5, with a median of 18.6, while the contribution of Pb to WQI in samples from the Kwale HMS deposit ranged from 2.56 to 19.6. The contributions of Ni, Cu, and U to WQI were negligible.

5.3.2   Soil Pollution Assessment Results

Pollution of soil by each of the heavy metals in soils sampled at the environs of Kwale HMS deposit and Mrima Hill was evaluated using the geo-accumulation (I_{geo}) index, pollution index (PI), and enrichment factor (EF). The I_{geo} of individual metals from the environs of Kwale HMS deposit and Mrima Hill are shown in Figs. 5.3 and 5.4 and in Appendix D-1 and D-2, respectively. Although the I_{geo} of Ti, Fe, Cr, Mn, As, Nb, and Cd in all the soil samples from the two sampling sites were above zero, different sources could account for the high I_{geo} values of these metals. For instance, the high I_{geo} values of Ti, Fe, Cr, Mn, and Nb in soil samples from Mrima Hill are due to the alkaline carbonatite parent rocks (Harmer and Nex, 2016) which has a substantial amount of

pyroxene, amphiboles, mica, phosphates and Nb ores (Caswell and Baker, 1953) rich in Ti, Nb, Fe, Mn, Cr, and Cd, while the heavy mineral sand deposit of Kwale are associated with the rutile, ilmenite and the gauge minerals of pyroxene and chrome rich in Ti, Cr and Mn (Abuodha and Hayombe, 2006; Van Gosen et $al.$, 2014).

High I_{geo} values of Cr and Cd observed in soil samples from the environs of Mrima Hill and Kwale HMS deposit were more than 5, as shown in Table 5.9. The I_{geo} mean value of Cr in the soil samples from the environs of Mrima Hill and Kwale HMS deposit were 10.38 and 7, respectively, while the I_{geo} mean value of Cd were 8.856 and 5.144 respectively, an indication of extreme pollution of soils by Cr and Cd. The pollution of the soil could be due to both geogenic and anthropogenic activities at the sampling sites, including presence of phosphates in the alkaline-carbonatite parent rocks at Mrima Hill (Verplanck et $al.$, 2014), use of phosphorous fertilizers, heavy machinery that uses diesel at the Kwale HMS mining facility (Abuodha and Hayombe, 2006; Al-gizzi et $al.$, 2020), sludge from the mineral processing activities, and extensive groundwater abstraction (Kubier and Pichler, 2019).

Despite Abuodha and Hayombe (2006) theorizing an increase in Th and U from heavy mineral sand mining activities at the Kwale deposit, the I_{geo} values of Th and U in all the soils samples from the Kwale HMS deposit were below zero, with a mean of -1.0373 and -0.7907. This demonstrates that the soil samples in the environs of the Kwale HMS deposit were unpolluted with Th and U from the mining and mineral processing activities of the heavy mineral sands. Nevertheless, the I_{geo} values of Th and U in most of the soil samples from the environs of Mrima Hill were more than 1, with a mean of 1.864 and 0.951, as shown in Table 5.9. The I_{geo} values of Th varied from -3.148 to 4.050, as shown in Appendix D-2, with sample MS19 (I_{geo} = -3.148) being the least unpolluted, while MS3 (I_{geo} = 4.050), thus classified as strongly polluted. The I_{geo} values of U varied from -0.671 to 4.184.

Table 5.9: Mean I_{geo} values and the respective soil quality due to specific heavy metal in soil samples collected at the environs of Kwale HMS deposit and Mrima Hill

	Kwale HMS deposit		Mrima Hill	
	I_{geo}	Soil Quality	I_{geo}	Soil Quality
Ti	1.286	Moderately polluted	1.980	Moderately polluted
Cr	7.870	Extremely polluted	10.38	Extremely polluted
Mn	1.850	Moderately polluted	3.919	Strongly polluted
Fe	-0.154	Unpolluted	1.992	Moderately polluted
Ni	-0.457	Unpolluted	1.934	Moderately polluted
Cu	-0.778	Unpolluted	0.687	Unpolluted to moderately polluted
Zn	0.575	Unpolluted to moderately polluted	4.025	Strongly polluted
As	3.464	Strongly polluted	3.436	Strongly polluted
Zr	-0.908	Unpolluted	-0.285	Unpolluted
Nb	1.645	Moderately polluted	3.809	Strongly polluted
Cd	5.144	Extremely polluted	8.656	Extremely polluted
Pb	-0.840	Unpolluted	1.787	Moderately polluted
Th	-1.037	Unpolluted	1.864	Moderately polluted
U	-0.791	Unpolluted	0.951	unpolluted to moderately polluted

Sample MS20 was the least unpolluted (I_{geo} = -0.671), while sample MS3 (I_{geo} = 4.188) was strongly polluted. Similarly, the Igeo mean value of Pb in soils samples from the environs of Mrima Hill was above zero (1.587), while the Igeo in soil samples from the Kwale HMS deposits was below zero (-0.8404). The high values of I_{geo} is associated with the weathering processes of the carbonatite alkaline intrusion U and Th-bearing ores of pyrochlore and monazite (Verplanck *et al.*, 2014). Earlier studies done at the same site had shown a radioactive anomaly, with an activity concentration of Th and U exceeding the global mean concentration of 42 Bq/kg Th and 30 Bq/kg U in soils (Patel, 1991; Kebwaro *et al.*, 2011; Kaniu *et al.*, 2018). Patel and Mangala (1994) observed uneven distribution of Th in carbonatite samples from Mrima Hill ranging between 95 mg/kg and 3341 mg/kg.
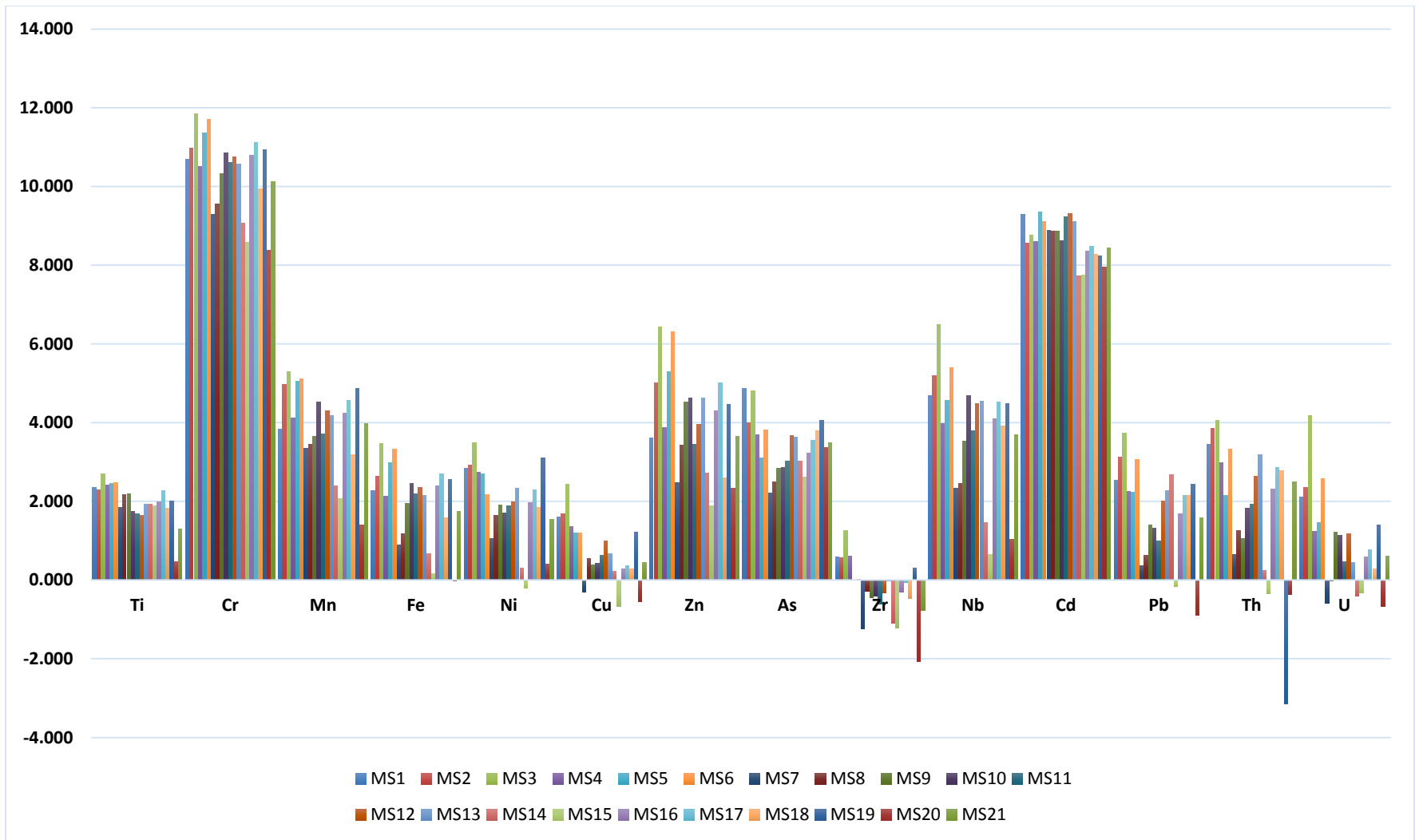
Fig. 5.3: Comparison of I$_{geo}$ values of U, Th and other heavy metals in soil samples from environs of Mrima Hill
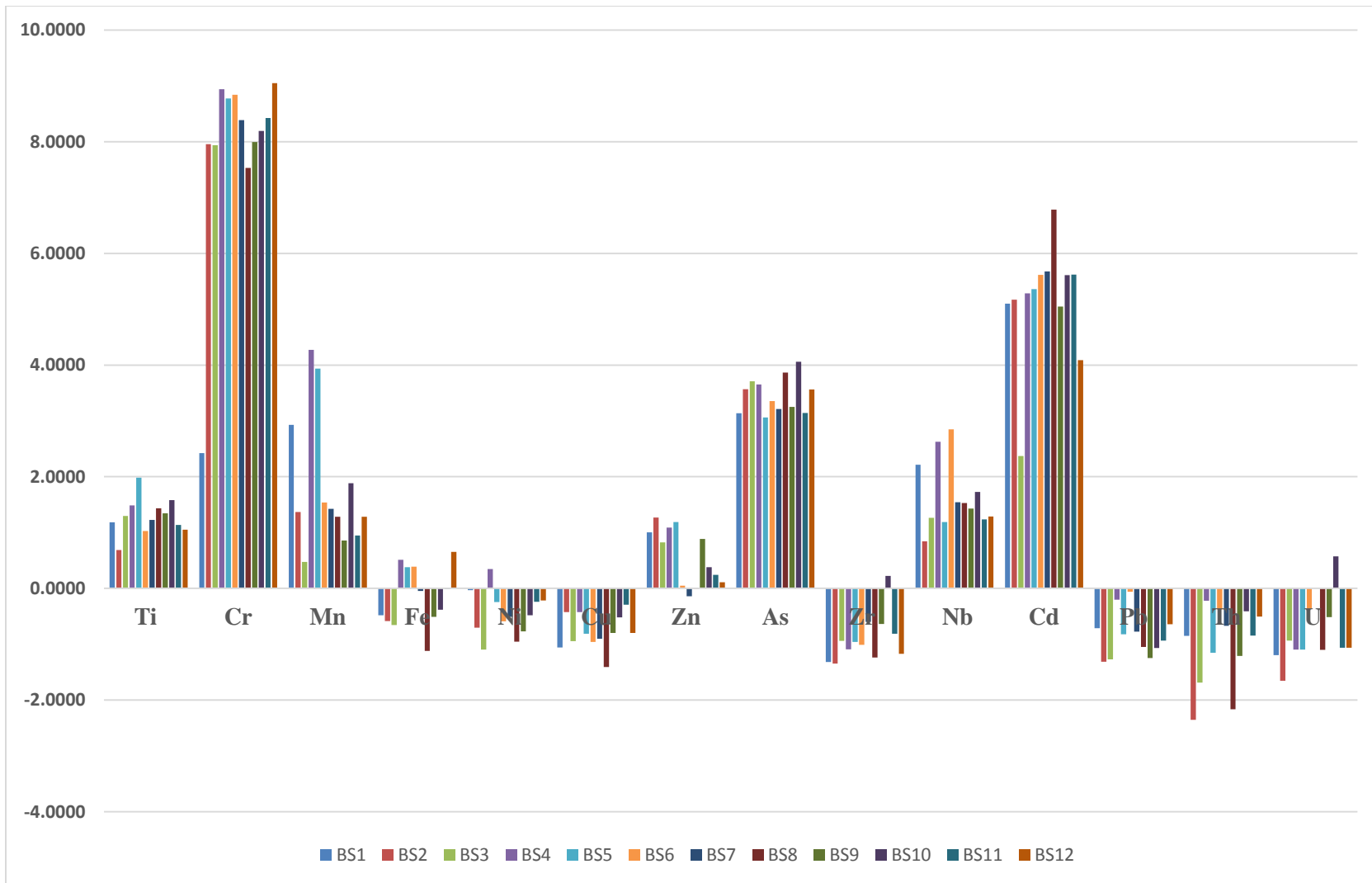
Fig. 5.4: Comparison of Igeo of U, Th and other heavy metals in soil samples from the environs of Kwale HMS deposit.

The mean I_{geo} values of As in soil samples from the environs of Kwale HMS deposit and Mrima Hill were 3.464 and 3.43, respectively. The I_{geo} values of As in soil samples from the Kwale HMS deposit ranged from 3.0599 to 4.0606, showing that all the soil samples were strongly polluted by arsenic. On the other hand, the I_{geo} values of As in soil samples from the environs of Mrima Hill ranged from 2.220 to 4.867, with varying pollution levels, from moderately polluted to strongly polluted. Both geogenic and anthropogenic activities are the probable contributors to the high level of As in soil at the environs of Mrima Hill and Kwale HMS deposit. For instance, shale and sandstone rocks have a high concentration of As (Alarcón-Herrera *et al.*, 2013).

The Kwale heavy mineral sand deposited within the aeolian dunes is derived from the Duruma Sandstone series consists of shales, grits, and sandstones (Caswell and Baker, 1953). This, coupled with the mining activities at the Kwale HMS deposit, could have exacerbated the level of As in topsoils. On the other hand, the Duruma Sandstone series underlain the alkaline igneous rocks of Mrima Hill (Caswell and Baker, 1953). Harmer and Nex (2016) noted fenitised sediments of sandstones and siltstones on the southwest and northeast edges of Mrima Hill. Thus, pollution of As in the soil around Mrima Hill could be due to the weathering processes of the parent rock.

It is worth noting that the soil samples from the environs of the Kwale HMS deposit were unpolluted by Fe, Ni, Cu, Zr, and Zn and moderately polluted by Mn. However, the samples collected from the environs of Mrima Hill showed that the soil from this area was unpolluted by Zr and Cu, moderately polluted by Ni and Fe, and strongly polluted by Zn and Mn. The Zn and Mn pollution observed in soil samples from the environs of Mrima Hill could be due to the weathering processes of the parent alkaline-carbonatite rocks, covered with lateritic manganiferous soils (Harmer and Nex, 2016) with traces of Pb-Zn in their vents (JICA, 1991).

The mean pollution indices, PI, of the heavy metals in soils from the environs of Kwale HMS deposit and Mrima Hill varied and followed a decreasing order of $Cr > Cd > As > Mn > Nb > Ti > Zn > Fe > Ni > U > Cu > Pb > Zr > Th$ and $Cr > Cd > Zn > Nb > Mn > As > Fe > Ni > Pb > Ti > U > Cu > Zr$, as shown in Table 5.10. The PI of Cr in soil samples from the Kwale HMS deposit ranged between 278 and 798, with a

mean of 511, as shown in Appendix D-3, alluding to a higher pollution threat, as classified by Kowalska *et al.* (2018) from Cr in soils from the environs of the Kwale HMS deposit. Similarly, the pollution threat from Cr from the environs of Mrima Hill was the highest (PI = 2384), as shown in Table 5.10. The mean PI of Cr in soil samples from Mrima Hill was ~4 times more than that of the Kwale HMS deposit. The PI of Cr in the soil samples from environs of Mrima Hill deposit ranged between 499 and 5552, as shown in Appendix D-4.

Cd, Mn, and As were also of greatest (very strong) pollution threat to the soils around the Kwale HMS deposit but at a lower scale. The PI of Cd ranged from 7.8 to 76.7 with a mean of 65.2, while that of As ranged from 12.5 to 25.0, with a mean of 16.9. The PI of Mn was lower, ranging from 2.72 to 29.0, with a mean of 8.01. The soil pollution threat due to Ti (PI =3.75) and Nb (PI =5.14) was high. The pollution threat of soils from Zn was moderate (PI =2.37), while that of Fe (PI = 1.44) and Ni (PI = 1.13) were low. The pollution threat due to other metals: Cu, Zr, Pb, Th, and U, was inconsequential since their PI values were below unity, which contrasts with the PI of the heavy metals from Mrima Hill. The pollution threat from 11 of the heavy metals (Ti, Cr, Mn, Fe, Ni, Zn, As, Nb, Cd, Pb, and Th was very high (very strong) whose PI values were greater than mean of 5, as shown in Table 5.10. The pollution threat from U in soil samples from Mrima Hill was high (strong), while the pollution threat from Cu and Zr was moderate.

Following the high PI values of Cr, Cd, and Mn in soils samples from the Kwale HMS deposit, the pollution load index, PLI, was higher than 1 (PLI = 3.87), showing that the soil quality was deteriorating due to pollution of the soil with these metals. Similarly, the high PI values of all the heavy metals at Mrima Hill showed a deterioration of soil quality. The PLI due to these metals in soil samples from the environs of Mrima Hill was ~ 17 times higher than the expected for soil quality on 1 (Kowalska *et al.*, 2018).

Table 5.10: The mean pollution index. PI, of heavy metals in soils samples from environs of Kwale HMS deposit and Mrima Hill

	Kwale HMS Deposit		Mrima Hill	
	PI	Threat	PI	Threat
Ti	3.75	Moderate	6.20	Very strong
Cr	511	Very strong	2384	Very strong
Mn	8.01	Very strong	27.7	Very strong
Fe	1.44	Low	7.13	Very strong
Ni	1.13	Low	6.84	Very strong
Cu	0.89	Absent	2.77	Moderate
Zn	2.37	Moderate	34.8	Very strong
As	16.9	Very strong	18.1	Very strong
Zr	0.84	Absent	1.39	Moderate
Nb	5.14	Very strong	31.3	Very strong
Cd	65.2	Very strong	638	Very strong
Pb	0.87	Absent	6.62	Very strong
Th	0.80	Absent	8.61	Very strong
U	0.95	Absent	4.33	Strong

A further evaluation of the pollution level of the soil using enrichment factors, EF, showed that the mean EF values of Cr, Cd, As, Mn, Nb, and Ti in topsoils from the environs of Kwale HMS deposit 303, 37.8, 9.81, 4.04, 2.80, and 2.27, as shown in Table 5.11, values that were above the threshold EF of 1.5 in topsoils (Kowalska *et al.*, 2018). These EF values were approximately 200, 25, 6, 2.5, 2, 1.5 times higher than the threshold value of 1.5 in topsoils. The enrichment factors of some of the metals (Mn, Nb, Ti) obtained by Maina *et al.* (2016) before the mining and mineral processing activities at the Kwale HMS deposit were below the EF threshold value of 1.5. Thus, the mining and mineral activities enhanced the concentration of Cr, Cd, As, Mn, and Ti in soils at this site. The enrichment factors of other metals, Fe, Ni, Cu, Zn, Zr, Pb, Th, and U, were below the threshold value, indicating that these metals in the soil could be due to natural processes (Kowalska *et al.*, 2018).

Table 5.11: Enrichment factors, EF, of heavy metals in soil samples from the environs of Kwale HMS deposit and Mrima Hill

	Ti	Cr	Mn	Fe	Ni	Cu	Zn	As	Zr	Nb	Cd	Pb	Th	U
Kwale HMS	2.27	303	4.04	0.76	0.59	0.48	1.34	9.81	0.46	2.80	37.8	0.47	0.42	0.54
Mrima Hill	2.14	764	8.85	2.28	2.08	0.85	10.8	5.71	0.43	9.05	224	2.03	2.51	1.17

The enrichment factors of most metals in soils samples from Mrima Hill were higher than the threshold value of 1.5 in topsoils. Cr had the highest mean EF value 764, a value that was approximately 500 times higher than the threshold value. The EF values of Cr in the soil samples ranged from 310 to 1653, as shown in Appendix D-6. Other metals whose mean EF was higher than the threshold value of 1.5 include: Cd, Zn, Mn, and As, as shown in Table 5.11. The values of enrichment factors of Cd, Zn, Mn, and As in all the samples at the environs of Mrima Hill were more than 1.5, as shown in Appendix D-6. The high EF values as discussed earlier are due to the weathering processes of the parent rocks at Mrima Hill, coupled with the agricultural activities taking place at this hill. The EF of Ti, Fe, Ni, Pb, and Th were approximately equal to the threshold value of 1.5, while the EF values of Cu, Zr, and U were below the threshold value of 1. Thus, Ti, Fe, Pb, Th, Ni, Cu, U, Zr were not enhanced by the geogenic and anthropogenic activities.

5.4 Results of Non-carcinogenic and Carcinogenic Risk Assessment

In this section, the results from evaluation of average daily dose (ADD), the target health quotient (THQ), hazard indices (HI), and the incremental lifetime cancer risk (ILCR) are presented and discussed. The HI value is the sum of the THQ from exposure to the heavy metals via ingestion and dermal contact to the heavy metals. If the values of THQ or the HI are greater than 1, then the population was prone to non-carcinogenic health risks such as spinal and renal tabular dysfunction (Aoshima, 2016), genito-urinary diseases (Banning and Benfer, 2017), and irreversible cognitive impairment (Gibson *et al.*, 2020). On the other hand, the carcinogenic health risk is characterized by the ILCR values. The population is at susceptible to cancer risk if ILCR $> 1.0E - 04$.

5.4.1 Non-Carcinogenic Risk Assessment Results

The average daily doses (ADD) from exposure to Cr, Mn, Ni, Zn, Cu, As, Cd, Pb, and U in soil and water via ingestion and Cr, Mn, Ni, Zn, Cu, As, Cd, and Pb via dermal contact to soils were evaluated. Two population groups: adults and children, were considered in this assessment. Both deterministic and probabilistic models were used in assessing ADD of heavy metals in soil and water. The point estimates from the deterministic human health risk assessment were used to represent the mean values of ADD, while the 50th percentile of the probabilistic health risk assessment represented the median values of ADD. However, the 95th percentile represented the high-end estimates values of the ADD.

The ADD point estimates values for a child and adult from the ingestion pathway of soil particles from the environs of Kwale HMS deposit followed a decreasing order of $Cr > Mn > As > Zn > Ni > Pb > Cd > U$, as shown in Appendix E-1 and Fig. 5.5, with Cr and Mn contributing ~ 91 % and ~8 % respectively to the ADD of 0.37 mg/kg per day for a child, and 0.0397 mg/kg per day for an adult. However, from the probabilistic evaluation, the high-end ADD of a child from exposure to the soil particles via ingestion pathway followed a decreasing order of $Cr > Mn > As > Zn > Pb > Cd > Ni > Cu > U$, with Cr and Mn contributing 87% and 10% to the total ADD of 0.889 mg/kg-day. The high-end ADD of an adult from this exposure followed the same a decreasing order $Cr > Mn > Zn > As > Pb > Cd > Ni > Cu > U$ with Cr and Mn contributed 90% and 8% to a total of 0.0915 mg/kg-day ADD. The ADD point estimates values of the metals for a child were ~9 times higher than the equivalent adult ADD. However, the child's high-end ADD values of the metals varied from ~6 (Zn) to ~38 (Cd) times higher than the corresponding high-end ADD values of the metals for an adult.

Fig. 5.5: Deterministic and probabilistic average daily dose in mg/kg-day for a child and adult from ingestion of heavy metals in soil from the environs of Kwale HMS deposit and Mrima Hill

On the other hand, the point estimates ADD values for a child and adult from ingestion of soil samples from the environs of Mrima Hill followed a decreasing order of $Cr > Mn > Zn > As > Ni > Pb > Cu > Cd > U$, with Cr, Mn, and Zn contributing 90%, 8%, and 1%, respectively, to the total ADD of 1.53 mg/kg-day for a child and 0.164 mg/kg-day for an adult. The contribution of the other metals to the ADD was below 1%. The high-end probabilistic assessment showed that the ADD values for a child followed a decreasing order of $Cr > Mn > Zn > As > Pb > Ni > Cd > Cu > U$, with Cr and Mn contributing 91% and 7%, respectively, to the total ADD of 4.88 mg/kg-day. The ADD for an adult decreased following an order of $Cr > Mn > Zn > Pb > Ni > As > Cu > Cd > U$. Cr, Mn, and Zn contributed 92%, 6% and 1.6% to the total ADD of 0.486 mg/kg-day. It is worth to note that the ADD point estimate values for a child was also ~9 times higher than that of an adult, like observation made for the point estimate values for child and adult from ingestion of soil particles sampled in the environs of Kwale HMS deposit. However, the ratio of child to adult 95th percentile ADD values was ~2 (Cu) to 34 (As), accounting for the variability and uncertainty in the input parameters.

Following the high concentration of the heavy metals in soil samples from Mrima Hill compared to the Kwale HMS deposit, the point estimates values of the ADD from ingestion of Cr, Mn, Ni, Zn, Cd, Pb, and U in soils from the environs of Mrima Hill were higher than the ADD values of equivalent heavy metals from Kwale HMS deposit, as shown in Fig. 5.5 and Appendix E-1. The point estimates ADD values of Zn and Cd for adults and children from the environs of Mrima Hill were ~ 11 times more than the ADD values of the same population living around the Kwale HMS deposit. The concentrations of Cd and Zn in soil sampled from the environs of Mrima Hill were ~11 times higher than the metals in soil samples from the Kwale HMS deposit. The ADD point estimates of Pb and Ni from ingestion of soils from Mrima Hill were ~6 and 5 times higher than ADD point estimates of Pb and Ni from Kwale HMS deposit, while the ADD point estimates Cr and Mn were ~4 times higher compared to the ADD from ingestion of soil from the Kwale HMS deposit.

Due to the variability and uncertainty in the input parameter, the ratio of the probabilistic assessment of the average daily dose from Mrima Hill to that of Kwale HMS deposit for the population varied. The high-end ADD value of Pb for a child from the environs of Mrima Hill was ~11 times higher than the corresponding ADD of Pb from the Kwale HMS deposit. The high-end ADD of Cr, Ni, and Pb from ingestion of soils by a child from Mrima Hill were ~5 times more than the respective ADD of the metals from the Kwale HMS deposit. The high-end ADD value of Mn and Cr from ingestion of soil from Mrima Hill were ~ 3 times higher than their corresponding ADD values of these metals from ingestion of the soil particles from the Kwale HMS deposit. However, high-end ADD values of Cu and As from the ingestion of soil from Mrima Hill were equal to those from the Kwale HMS deposit. On the other hand, the high-end ADD of Zn from the ingestion of soil particles by an adult living around Mrima Hill was ~13 times higher than those living around the Kwale HMS deposit. The high-end ADD values of Cr and Pb were ~5 times higher than the corresponding value from the environs of the Kwale HMS deposit, while Cr and U were ~5 times higher, as shown in Fig. 5.5.

Further health risk assessment showed that the sum of the point estimate values of the ADD from the ingestion of heavy metals in soil particles for a child and an adult living around Kwale HMS deposit and Mrima Hill were ~300 and ~200 times higher than the respective sum of the point estimate ADD values from dermal exposure to the metals in the soil. However, the sum of high-end probabilistic ADD values for a child from the ingestion pathway was ~25, for Kwale HMS deposit, and ~35, for Mrima Hill, times higher than that of the dermal exposure of a child to the soil particles, but ~80, for Kwale HMS deposit, and ~100, for Mrima Hill, times higher than that of dermal exposure of an adult to the soil particles.

The point estimates of the ADD for both child and adult from dermal exposure to soil particles from the environs of Kwale HMS deposit followed a decreasing order of $Cr > As > Mn > Cu > Ni > Pb > Zn > Cd$, with Cr, As, and Mn contributing ~78%, ~13%, and ~7%, respectively, to the total ADD of (1.19E-03) mg/kg-day for a child and (1.83E-04) mg/kg-day for an adult, as shown in Appendix E-2. However, high-end probabilistic ADD for a child followed a decreasing order of $Cr > As > Mn > Zn >$

$Ni > Pb > Cu > Cd,$ with Cr, As, and Mn contributing ~77%, ~14%, and ~7% to a total ADD of 0.0355 mg/kg per day, while that of an adult followed a decreasing order of $Cr > As > Mn > Zn > Pb > Ni > Cu > Cd,$ with Cr, As, and Mn, in either case, contributing ~78%, ~11%, and ~9% to a total ADD of ~0.001 mg/kg- day for an adult, and as shown in Fig. 5.6.

Thus, the sum of high-end probabilistic ADD values from dermal exposure to soils particles by children and adults living around the Kwale HMS deposit were ~30 and ~6 times, respectively higher than the corresponding sum of the point estimate values. Similarly, the sum of the high-end probabilistic ADD values from dermal exposure to the soil particles by the children and adults living around Mrima Hill were ~30 and ~6 times higher than the respective sum of the point estimate values. However, the ADD point estimate values for children and adults followed a decreasing order of $Cr > Mn > As > Zn > Ni > Pb > Cu > Cd$, with Cr, Mn, As, and Cu contributing ~87%, 8%,3%, and 1% to the total ADD of (4.44E-03) mg/kg per day for a child, and (4.678E-04) mg/kg per day for an adult as shown in Fig. 5.6 and Appendix E-2. The high-end ADD values for a child and an adult followed the same reducing order of $Cr > Mn > As > Zn > Pb > Ni > Cu > Cd$ with a contribution of 87%, 8%, 4%, and 1% from Cr, Mn, As, and Zn, respectively to the total ADD of (1.31E-01) mg/kg per day for a child and 89%, 7%, 3%, and 1% to the total of (4.37E-03) mg/kg-day for an adult.

Contrary to observations relating to the sum of the point estimate ADD values and the sum of the 95th ADD values from dermal exposure to and ingestion of heavy metals in soil particles at the study areas, the sum of point estimate ADD values from ingestion of heavy metals in water for children in the environs of Mrima Hill were higher than the corresponding sum of the 95th percentile ADD at the same environment as shown in Fig 5.7 and Appendix E-3.
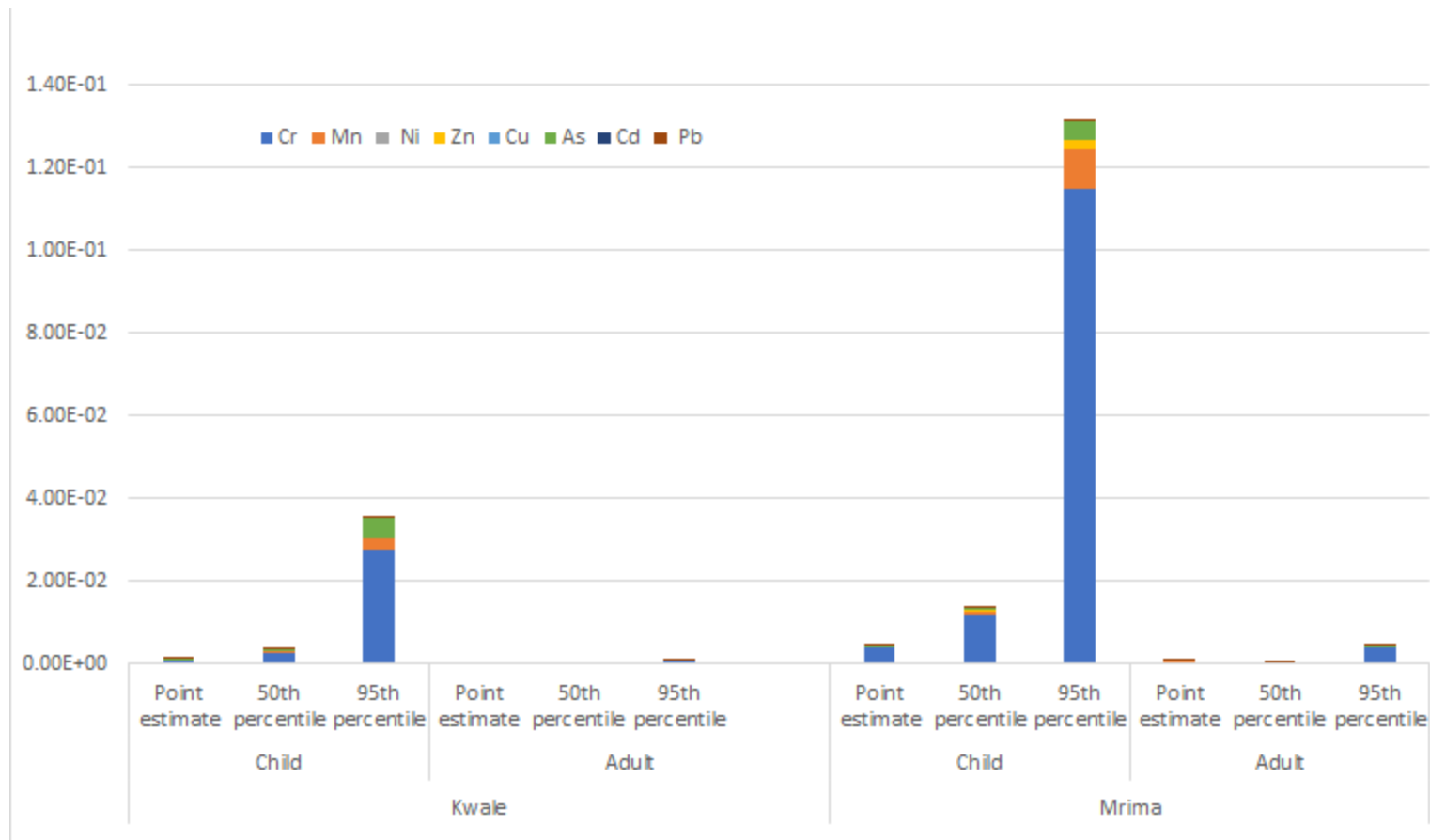
Fig. 5.6: Deterministic and probabilistic average daily dose in mg/kg-day for a child and adult from dermal exposure of heavy metals in soil from the environs of Kwale HMS deposit and Mrima Hill

91

The sum of the ADD point estimate value of metals for a child in the environs of Kwale HMS was approximately five times higher than the 95th ADD value. The total ADD point estimate value of the metals for a child from the environs of Mrima Hill was approximately ten times higher than the sum of the 95th ADD value. However, the sum of the point estimates ADD values of the metals from the ingestion of water by adults from areas around the Kwale HMS deposit was approximately equal to that of the 95th probabilistic value. However, the sum of the point estimate ADD values of the metals for adults in the environs of Mrima Hill were approximately two times higher than the sum of the 95th percentile ADD value, as shown in Fig. 5.7 and Appendix E-3.

Despite the low deterministic and probabilistic ADD values from the ingestion of heavy metals in drinking water compared to soil particles, Cr contributed the highest ADD values to the total ADD of metals in water in both study areas. For instance, Cr contributed ~70% to the point estimates ADD values of 0.0447 mg/L-day for a child and 0.0192 mg/L-day for an adult from ingesting metals in water from the environs of Kwale HMS deposit. The other metals followed a reducing order of $Mn > Cd > Zn > Ni > Pb > Cu > As > U$, with Mn, Cd, Zn, and Ni contributing ~13%, ~12%, ~2%, and ~1%, respectively, to the total ADD of a child and adult. Even although the 95th percentile ADD values for a child followed the same order as point estimate values, Cr, Mn, Cd, and Zn contributed ~72%, 19%, 5%, and 2% to the total ADD value of 0.0196 mg/L-day. However, the 95th percentile values of the metals for an adult followed a reducing order of $Cr > Mn > Zn > Cd > Ni > Pb > Cu > As > U$, with a contribution of 70%, 14%, 9%, and 5% from Cr, Mn, Zn, Cd, respectively to a sum of 0.0211 mg/L-day, as shown in Appendix E-3 and Fig. 5.7.
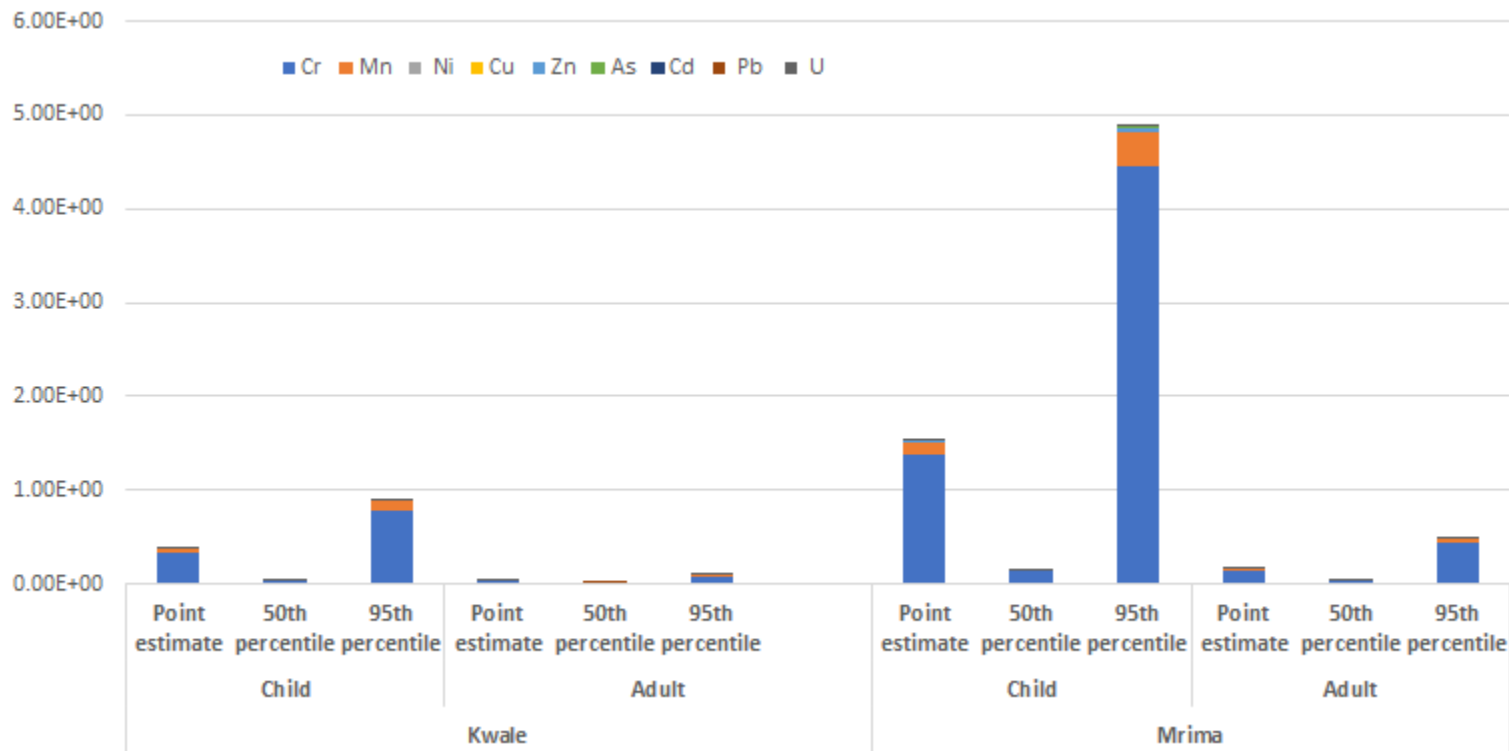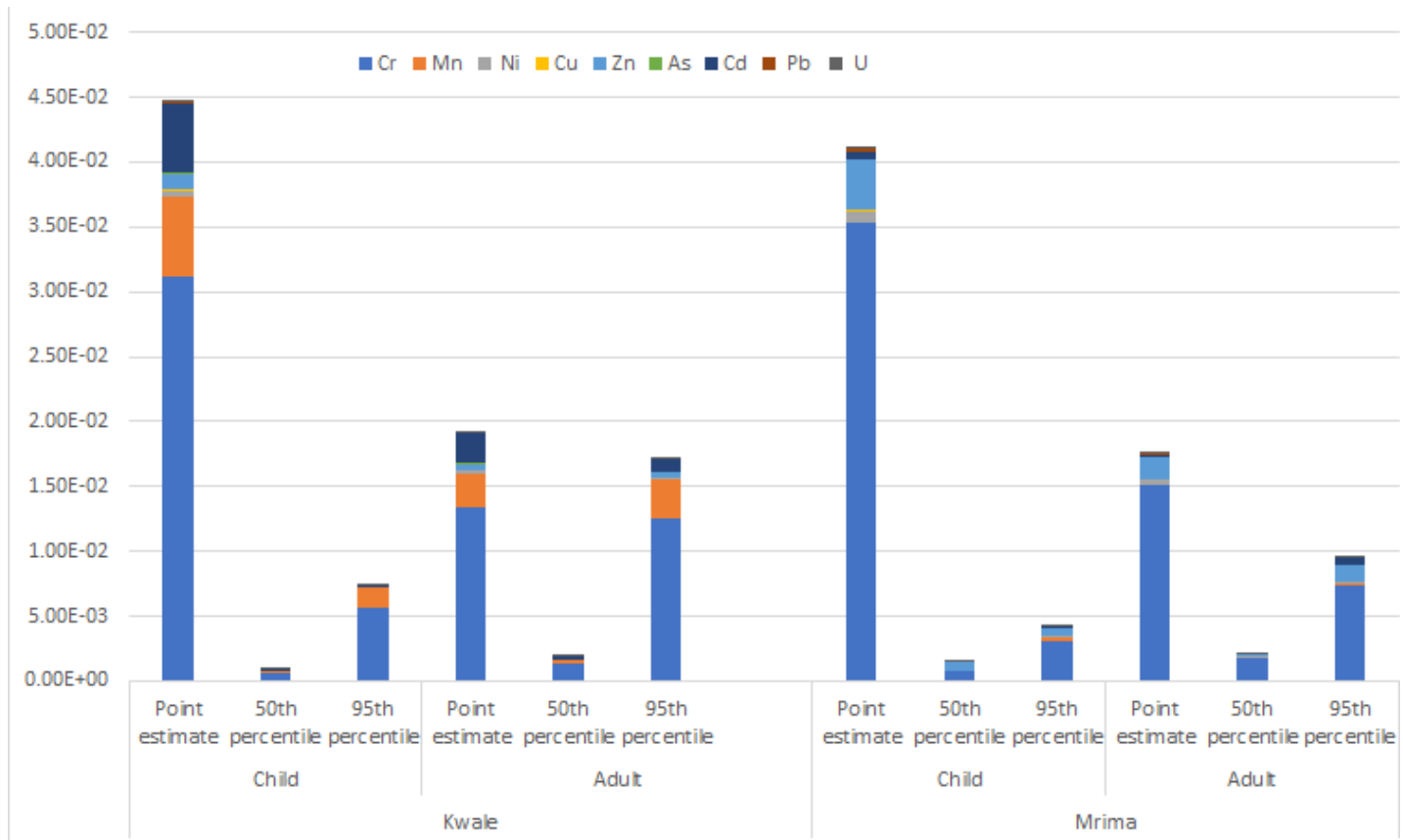
Fig. 5.7: Deterministic and probabilistic average daily dose in mg/kg-day for a child and adult from ingestion of heavy metals in drinking water from the environs of Kwale HMS deposit and Mrima Hill

Both deterministic and probabilistic ADD values from ingestion of heavy metals in water by a child and adult living around the Kwale HMS deposit followed a reducing order of $Cr > Mn > Cd > Zn > Ni > Pb > Cu > As > U$, with Cr contributing the highest percentage of ~69% to the total ADD. The contribution of Mn, Cd, Zn, and Ni to the point estimate ADD values of 0.0447 mg/L-day and 0.0192 mg/L-day for a child and an adult was 13%, 12%, 2%, and 1%, respectively. Cr, Mn, and Cd contributed 77%, 20% and 1% to the sum of the high-end ADD value of 0.00739 mg/L-day for a child, while the contribution of the metals to the high-end ADD value for an adult of 0.0172 mg/L-day was ~72%, ~17% and ~6%, respectively. However, the point estimate ADD values of children and adults from the Mrima followed a decreasing order of $Cd > Zn > Ni > Cd > Pb > Cu > U > Mn > As$, with Cr, Zn, Ni, and Cd contributing ~85%, ~9%, ~2%, and ~1% respectively to ADD sum of 0.0412 mg/L-day for a child and 0.0177 mg/L-day for an adult.

The high-end probabilistic ADD for a child from ingestion of the metals in water sampled at the environs of Mrima Hill followed a reducing order of $Cr > Zn > Mn > Cd > Ni > U > U > Pb > As$, with Cr, Zn, Mn, Cd, Ni, and U contributing ~71%, ~12%, ~7%, 3%, ~1%, and ~1% respectively, to the total ADD of 0.00430 mg/L-day. The high-end probabilistic ADD for an adult followed a reducing order of $Cr > Zn > Cd > Ni > Mn > Pb > U > Cu > As,$ with a contribution of ~76%, 12%, 5%, 1% and 1% from Cr, Zn, Cd, Ni, and Mn to a sum of 0.00964 mg/L-day. The total point estimate ADD values of a child from ingestion of metals in drinking water sampled from environs of Mrima Hill was ~2 higher than the average daily dose ingested by an adult.

The results of the non-carcinogenic heath risk assessment show that the point estimate and the high-end probabilistic values of As for a child from ingestion of soil particles from the environs of Kwale HMS deposit were high and above the threshold value of 1, as shown in appendix E-4 and Fig 5.7, contrary to the low As ADD values as presented earlier, where ADD values of Cr were the highest. Arsenic has been classified as a priority hazardous substance (Belluck *et al.* 2003) and its reference dose of 3.00E-04 (mg/kg-day)[^-1], which is much lower than that of Cr (RfD_{Cr} = 1.5 (mg/kg-day)[^-1]). Thus, As contributed ~90% of 7.09 of the child's point estimate HI and 15.9 to child's high-end

probabilistic HI value. Although the point estimate THQ value of As for an adult living around the Kwale HMS deposit contributed ~90% to the HI, its value of 0.76 was below the threshold value of 1 (USEPA, 1989). However, the high-end HI value for an adult value 1.83, with As contributing a THQ value of 1.62 to the HI, as shown in Fig. 5.8 and appendix E-4.

The point estimate THQ values for a child and an adult from ingestion of other metals in soil particles from the environs of Kwale HMS deposit followed a reducing order of $Cr > Mn > Pb > Cd > Ni > U > Zn > Cu$, with Cr and Mn contributing 3% each to the HI. The THQ high-end values of the other metals for a child and the adult followed a decreasing order of $Mn > Cr > Pb > Cd > Ni > U > Zn > Cu$ and $Mn > Cd > Cr > Pb > Ni > U > Zn > Cu$, with Cd contributing ~3% to the total HI of an adult as compared to that child's HI. It was further observed that the HI high-end probabilistic values for both child and adult were ~2 times higher than the corresponding point estimate values. However, the ratios of the high-end THQ to point estimate THQ values of individual metals varied. For example, the high-end THQ from exposure to Mn, Cd, and Pb for a child was ~3 times higher than the corresponding points estimate THQ values, while the rest of the metals were ~2 times higher. The high-end THQ from exposure to Pb for an adult was ~ 10 times higher than the corresponding point estimate, while the high-end THQ from exposure to the other metals were approximately 2 times higher than the corresponding point estimate values. In addition, the high-end HI values of a child were ~10 times higher than that of an adult.

The point estimate THQ values of metals from ingestion of soil particles by a child and an adult residing in the environs of Mrima Hill followed a reducing order of $As > Cr > Mn > Pb > Cd > Ni > U > Zn$, with As, Cr, Mn, Pb, and Cd contributing ~67%, 10%, 9%, 6%, and 5%, respectively, to the child's HI of 9.40, and 1.01 of an adult's HI. The adult's THQ point estimate values of all the metals were below 1. However, the child's THQ point estimate value of As was 6.36, as shown in Appendix E-4, while the THQ point estimate values of the rest of the metals were below 1. Thus, the deterministic point estimate values indicate that the child was susceptible to the non-carcinogenic health risk effects from ingestion of As in soil particles in the environs of Mrima Hill. However, the

probabilistic estimation of the THQ showed that the 95th percentile values of As, Mn, Cr, Cd, and Pb were 14.3, 2.55, 2.45, 1.76, and 1.29, respectively, as shown in Appendix E-4, values which were much higher than the threshold value of THQ. The HI value from ingestion of soil particles was therefore ~22 times higher than the threshold value. On the other hand, the THQ value of As for an adult was above the threshold value of 1.

Despite very low probabilistic ADD values from dermal exposure to Cr, Mn, and Cd in soil by a child living at environs of Mrima Hill and Kwale HMS deposit, their respective THQ values were ~3, ~4, and ~2 times higher than the corresponding THQ values from exposure to the metals via ingestion of the soil. The high THQ values from dermal exposure to Cr, Mn, and Cd can be attributed to range of input parameters as shown in Eqn. 4.4, coupled with the high skin adherence factor of 0.2 mg/(cm^{-2}.day) and the low dermal exposure reference doses of 1.95E-02 mg/kg-day for Cr, 9.6E-04 mg/kg-day for Mn, and 1.25E-05 mg/kg-day for Cd, compared to the oral reference doses 1.5E+00 mg/kg-day for Cr, 1.40E-01 mg/kg-day for Mn, and 1.00E-03 mg/kg-day for Cd. However, the high-end THQ value of Mn from dermal exposure by an adult at the two study areas were approximately equal to the corresponding high-end THQ value from ingestion of the Mn by an adult. The skin adherence factor for an adult is 0.07 mg/(cm^{-2}.day). The point estimate THQ values from dermal exposure to all the metals by both child and adult at the two study sites were much less than the point estimate THQ values from ingestion of the metals. Nevertheless, the THQ point estimate values from dermal exposure to the metals in soils from the two study areas were much lower than the respective THQ point estimate values from exposure to the metals via ingestion pathway.
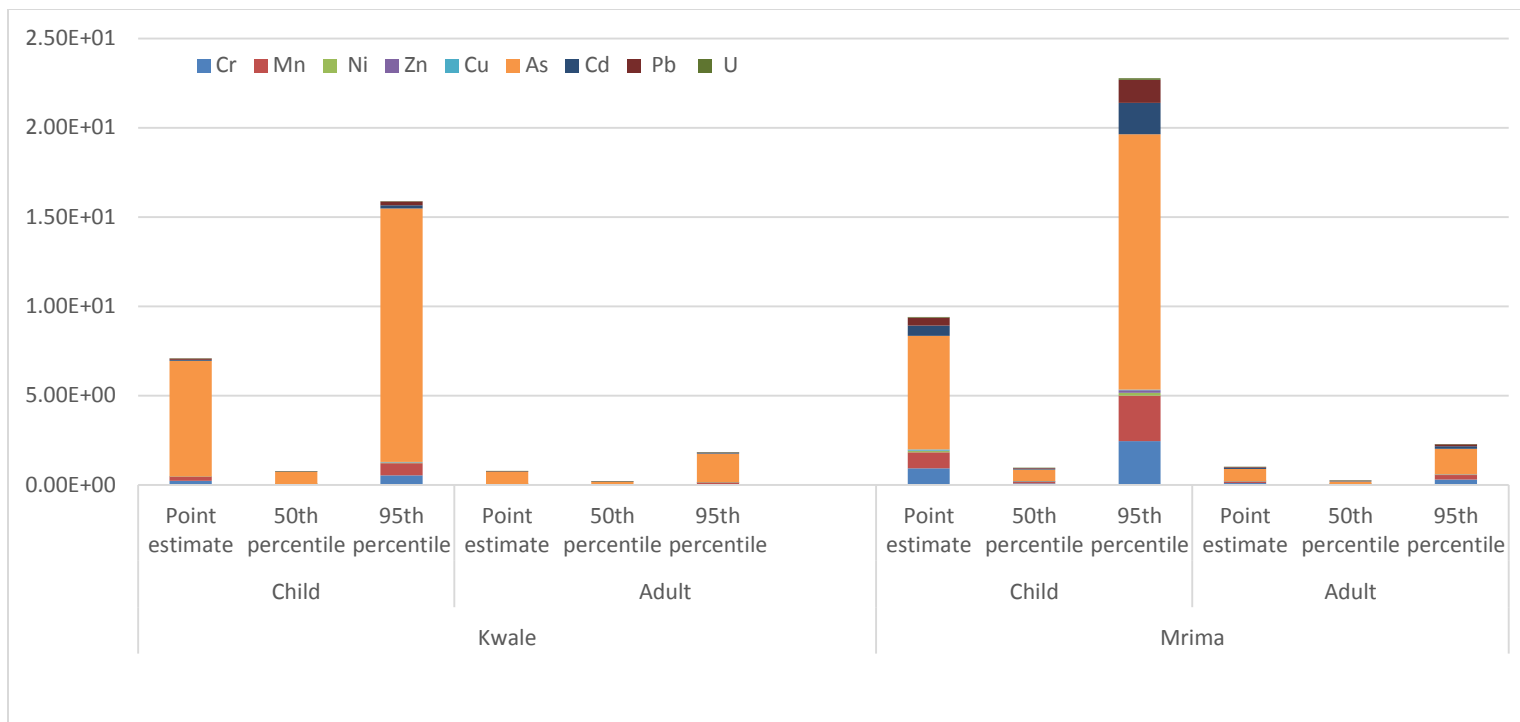
Fig. 5.8: Deterministic and probabilistic target health quotient (THQ) and hazard indices (HI) due to exposure to heavy metals via ingestion of soil particles by a child and an adult living around Kwale HMS deposit and Mrima Hill

The point estimate and the high-end THQ values for adults and children from dermal exposure to metals in soil sampled from the environs of Kwale HMS deposit followed a decreasing order of $As > Mn > Cr > Cd > Ni > Pb > Zn > Cu$ as shown in Appendix E-5 and Fig. 5.9. However, the percentage contribution of the metals to the sum of the point estimate and high-end THQ values varied. The percentage contribution of As, Mn, Cr, and Cd to the point THQ estimate value was 78%, 12%, 7%, and 2% to 0.692 of the child's HI and adult's HI of 0.106. Although the HI values were below the threshold value of 1 for non-carcinogenic human health risk, the HI value for a child was ~6 times higher than that of an adult. The HI value for a child from high-end probabilistic estimation was 15.3, while that of an adult was 0.551, with As, Mn, Cr, and Cd contributing ~70%, ~18%, ~8%, and ~2% respectively to the HI. The high-end HI value for a child was ~28 times higher than the corresponding point estimate values.

On the other hand, the point estimate THQ values from dermal exposure to metals for both adult and child living around Mrima Hill followed a decreasing order of $As > Mn > Cr > Cd > Ni > Cu > Pb > Zn$, with As, Mn, Cr, and Cd contributing ~43%, ~29%, ~17%, and 11%, respectively to the child's HI of 1.23 and adult's HI of 0.187 as shown in Appendix E-5. The high-end estimate THQ values for a child and adult followed a decreasing order of $As > Mn > Cr > Cd > Zn > Ni > Pb > Cu$. Although As contributed ~42% to the high-end probabilistic HI, the child's HI was 33.8, while that of an adult was only 1.02, a value that was equal to the threshold value for non-carcinogenic health risk. The THQ value of each metal for an adult was below 1. However, the high-end THQ values of As, Mn, Cr, and Cd for children were 14.1, 9.77, 5.91, and 4.02, respectively, as shown in Appendix E-5 values that were way above the threshold value for non-carcinogenic health risk.
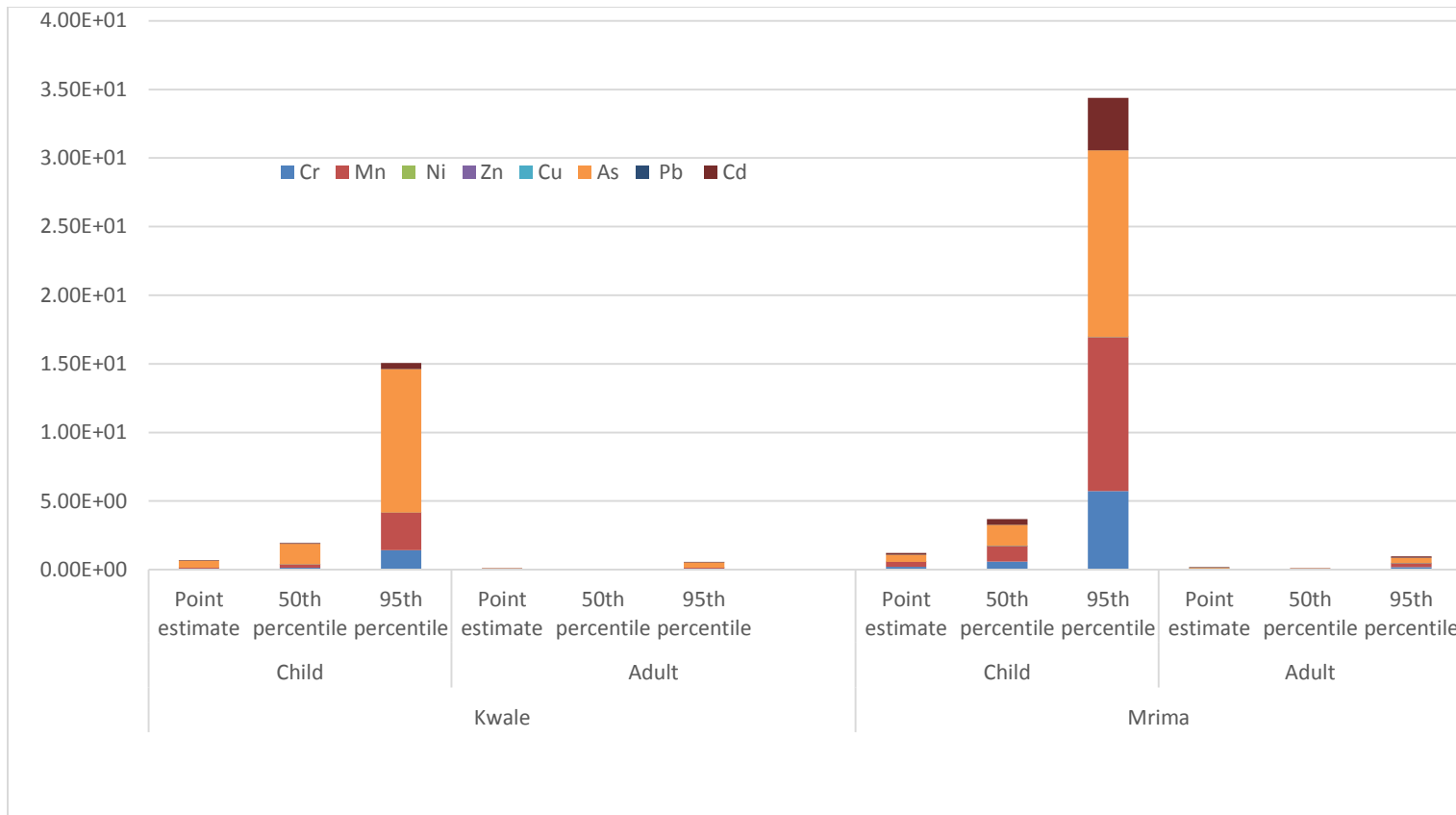
Fig. 5.9: Deterministic and probabilistic target health quotient (THQ) and hazard indices (HI) from dermal exposure to heavy metals in soil particles by a child and an adult living around Kwale HMS deposit and Mrima Hill

Even though the concentration of Cr and Cd in water samples was lower than the concentration of the metals in soil samples from the environs of Mrima Hill and the Kwale HMS deposit, the THQ values from exposure to the metals in drinking water via ingestion pathways were higher than from exposure to the metals via ingestion of soil particles. The difference in THQ was due to the low oral reference dose values of Cr (3.00E-03) and Cd (5.00E-04) of drinking water compared to oral reference dose values of the metals of soil (RfD_{Cr} =1.5 and RfD_{Cd}=1.0E-03). Thus, the point estimate HI values from ingestion of the metals in drinking water were high compared to the point estimate values of HI from ingestion of the metals in soil particles.

Regardless of the ADD values, the point estimate THQ values for both adult and child living around Mrima Hill from dermal exposure to heavy metals in soil followed a decreasing order of $As > Mn > Cr > Cd > Ni > Cu > Pb > Zn$, with As, Mn, Cr, and Cd contributing ~43%, ~29%, ~17%, and 11%, respectively to the child's HI of 1.23 and adult's HI of 0.187 as shown in Appendix E-5. The high-end estimate THQ values for a child and adult followed a decreasing order of $As > Mn > Cr > Cd > Zn > Ni > Pb > Cu$. Although the As contributed ~42% to the high-end probabilistic HI, the child's HI was 33.8, while that of an adult was only 1.02, a value that was equal to the threshold value for non-carcinogenic health risk. Each of the THQ value of each metal for an adult was below 1. However, the high-end THQ values of As, Mn, Cr, and Cd for children were 14.1, 9.77, 5.91, and 4.02, respectively, values that were way above the threshold value for non-carcinogenic health risk.

The point estimate THQ values from exposure to the metals in drinking water from the environs of Kwale HMS deposit followed a reducing order of $Cd > Cr > As > Pb > Mn > Ni > Zn > Cu > U$, with Cd and Cr contributing 50% and 48%, respectively to the child's HI of 21.5 and adult's HI of 9.23. However, the 95th percentile THQ values of the metals for both adults and children followed a reducing order of $Cr > Cd > As > Pb > Mn > U > Ni > Zn > Cu$, with Cr contributing the highest percentage of 69 followed by Cd with 28% contribution to the child's HI of 2.78 and adult's HI of 7.06, as shown in Appendix E-6. The contributions of the other metals in deterministic and probabilistic assessments to HI were below 1%.
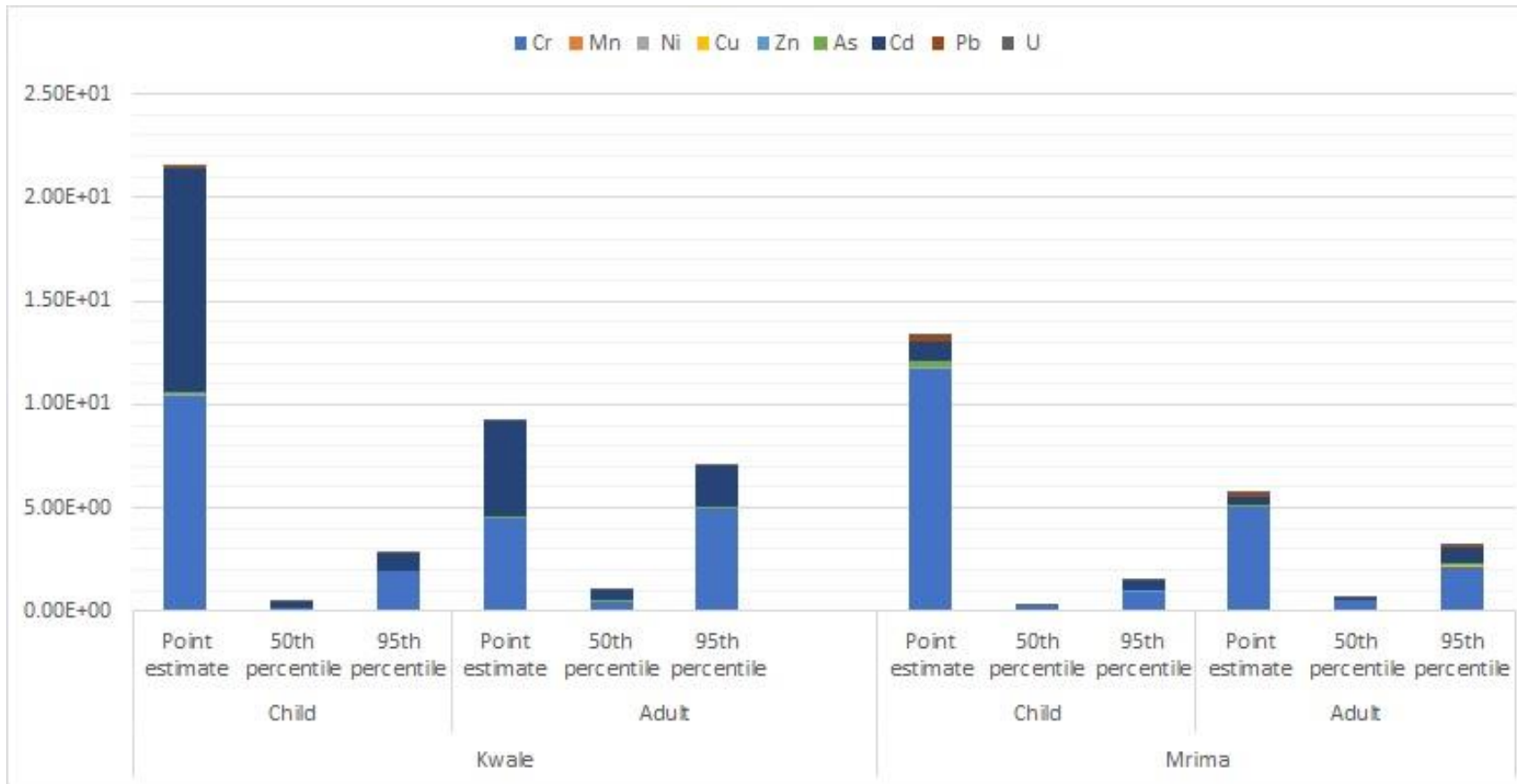
Fig. 5.10: Deterministic and probabilistic target health quotient (THQ) and hazard indices (HI) from ingestion of to heavy metals in drinking by a child and an adult living around Kwale HMS deposit and Mrima Hill

On the other hand, the point estimate THQ values of the metals in drinking water from the environs of Mrima Hill followed a decreasing order of $Cr > Cd > Pb > As > Ni > U > Zn > Cu > Mn$. Cr, Cd, Pb, and As contributed ~88%, ~7%, 2%, and 1%, respectively, to the child's HI of 13.3 and the adult's HI of 5.70. The high-end HI values for children and adults from exposure to the metals in water via ingestion were lower than the corresponding point estimate values, as shown in Fig. 5.10. The adults THQ values followed a reducing order of $Cr > Cd > As > U > Pb > Mn > Ni > Zn > Cu$, with Cr, Cd As, U, and Pb contributing ~66%, ~21%, ~5%, ~4%, AND ~2% to HI of 3.30. The child's THQ values followed a decreasing order of $Cr > Cd > As > U > Pb > Zn > Mn > Ni > Cu$, with Cr, Cd, As, U, and Pb contributing ~60%, ~27%, ~4%, ~4%, and 2%, respectively, to HI of 1.58. Thus, the HI values of adults were much higher than children's HI, similar to the observation made Saha *et al.* (2017) on health risk assessment of heavy metals in surface and groundwater around the Dhaka Export processing zone in Bangladesh.

It is worth noting that the child's and adult's HI point estimate values from exposure to the metals in water from the two study areas via ingestion pathway were higher than the corresponding high-end probabilistic HI values. The residents in both study areas were exposed more to Cr, contrary to the WQI values, which were influenced more by Cd contamination.

In summary, the sum point estimate ADD values for non-carcinogenic health risk from exposure to heavy metals via ingestion and dermal contact for children and adults living around Mrima Hill was ~4 times and ~3 times, respectively, higher than the sum of the point estimate ADD values for a child living around Kwale HMS deposit as shown in Table 5.12. However, the sum of high-end ADD values from exposure to the metals for children and adults residing in Mrima Hill was ~5 times higher than the sum of the equivalent ADD values for the population living around the Kwale HMS deposit. Furthermore, the sum of the high-end values from probabilistic estimation for both adult and child in the two study areas were higher than the point estimate values from the deterministic evaluation. The sum of median ADD values for children and adults from the two study areas was the least.

Table 5.12: A summary of non-carcinogenic values of ADD from ingestion and dermal exposure to heavy metals in soil and water samples in the environs of Kwale HMS deposit and Mrima Hill.

| | Kwale HMS deposit | | | | | | Mrima Hill | | | | | |
| | Child | | | Adult | | | Child | | | Adult | | |
	Point estimate	50th percentile	95th percentile	Point estimate	50th percentile	95th percentile	Point estimate	50th percentile	95th percentile	Point estimate	50th percentile	95th percentile
$Ingest_{Soil}$	3.70E-01	3.71E-02	8.89E-01	3.97E-02	8.54E-03	9.15E-02	1.53E+00	1.48E-01	4.88E+00	1.64E-01	3.69E-02	4.86E-01
$Dermal_{Soil}$	1.19E-03	3.59E-03	3.55E-02	1.82E-04	1.15E-04	1.05E-03	4.44E-03	1.35E-02	1.31E-01	6.78E-04	4.20E-04	4.37E-03
$Ingest_{Water}$	4.47E-02	9.20E-04	7.39E-03	1.92E-02	1.90E-03	1.72E-02	4.12E-02	1.52E-03	4.30E-03	1.77E-02	2.09E-03	9.64E-03
Total	**4.16E-01**	**4.16E-02**	**9.32E-01**	**5.90E-02**	**1.06E-02**	**1.10E-01**	**1.58E+00**	**1.63E-01**	**5.01E+00**	**1.82E-01**	**3.94E-02**	**5.00E-01**

Table 5.13: A summary of deterministic and probabilistic hazard indices from exposure to soil and water samples at the environs of Kwale HMS deposit and Mrima Hill via ingestion and dermal pathway.

| | Kwale HMS deposit | | | | | | Mrima Hill | | | | | |
| | Child | | | Adult | | | Child | | | Adult | | |
	Point estimate	50th percentile	95th percentile	Point estimate	50th percentile	95th percentile	Point estimate	50th percentile	95th percentile	Point estimate	50th percentile	95th percentile
$Ingest_{Soil}$	7.09E+00	7.46E-01	1.59E+01	7.60E-01	1.77E-01	1.83E+00	9.40E+00	9.51E-01	2.28E+01	1.01E+00	2.32E-01	2.28E+00
$Dermal_{Soil}$	6.92E-01	1.90E+00	1.53E+01	1.06E-01	6.13E-02	5.51E-01	1.23E+00	3.68E+00	3.38E+01	1.87E-01	1.12E-01	1.02E+00
$Ingest_{Water}$	2.15E+01	4.50E-01	2.78E+00	9.23E+00	1.04E+00	7.06E+00	1.33E+01	2.70E-01	1.58E+00	5.70E+00	6.37E-01	3.30E+00
Total	**2.93E+01**	**3.10E+00**	**3.40E+01**	**1.01E+01**	**1.28E+00**	**9.44E+00**	**2.39E+01**	**4.90E+00**	**5.82E+01**	**6.89E+00**	**9.81E-01**	**6.60E+00**

Table 5.13 shows a summary of the HI values from the exposure assessment. The sum of the point estimate HI values from exposure to the metals in soil and water samples from the environs of the Kwale HMS deposit was higher than the corresponding sum of the HI values from the Mrima Hill. This is contrary to the sum of the point estimate ADD values as earlier presented and discussed. However, the sum of probabilistic HI values for children from the environs of Mrima Hill was ~2 times higher than the equivalent HI values for the children living around the Kwale HMS deposit. The high values of HI from deterministic and probabilistic evaluation, which are above the threshold, show that the population in the two study areas remain susceptible to non-cancer risk due to exposure to the heavy metals in soil and water.

5.4.2 Carcinogenic Risk Assessment Results

The incremental lifetime cancer risk, ILCR, from exposure to As, Cr, and Pb via ingestion pathway and As via dermal route evaluated using the USEPA model is presented and discussed. The ILCR is a product of the average daily dose, ADD, and slope factor, SF, of a specific metal discussed in section 4.6.1. However, the average life expectancy fixed at 70 years for a child and adult was used in evaluating the carcinogenic ADD. The point estimate and probabilistic ADD values from exposure to heavy metals in water and soil sampled from the environs of Kwale HMS deposit and Mrima Hill via ingestion route are presented in Appendix E-7 and E-8.

The sum of the point estimate ADD values for children and adults from non-carcinogenic health risk assessment of the metals was ~10 times and ~2 times, respectively, more than the corresponding point estimate values from carcinogenic health risk assessment, as shown in Fig. 5.11 and 5.12. The non-carcinogenic high-end ADD values for both children and adults from ingestion of metals in water were approximately equal to the corresponding carcinogenic high-end ADD values. However, the ratio of the high-end ADD of non-carcinogenic to carcinogenic values from ingestion of the metals in soil varied, as shown in Fig. 5.12. This was due to additional input parameters, i.e., the adherence factor of soil particles to the skin and surface area of skin exposed to the soil particles, coupled with a high concentration of the metals in soil, whose probability distribution values varied. It was further noted that the sum of ADD values from

exposure to the carcinogen in the soil particles was higher than the corresponding ADD values from exposure to the carcinogen in water, as shown in Appendices E-7 and E-8. However, Cr contributed the highest percentage of ~99% to the total carcinogenic ADD values from exposure to the three carcinogens in water and soil samples from the environs of the Kwale HMS deposit and Mrima Hill. Arsenic contributed the lowest percentage to the total carcinogenic ADD from exposure to metals in water samples, as shown in Appendix C-7, while Pb contributed the lowest value to the carcinogenic ADD from exposure to the metals in soil samples. Similar observations were made while evaluating the non-carcinogenic ADD.

Due to the high ADD values of Cr and the cancer slope factor of 5.0E-01, the ILCR from exposure to Cr in water sampled from the environs of Mrima Hill and Kwale HMS deposit exceeded the recommended USEPA highest acceptable limit of 10^{-4}, as shown in Table 5.14. The ILCR values of As were within the tolerable USEPA limit of 10^{-4} to 10^{-6}, while the ILCR values of Pb were below the USEPA limit of 10^{-6}. The sum of the point estimate ILCR values for the children and adults from exposure to the carcinogens in water samples from the Kwale HMS deposit was approximately equal to the corresponding ILCR values exposure to the carcinogens in water samples from the environs of Mrima Hill. However, the high-end ILCR values of the carcinogens from Mrima Hill were ~2 times higher than equivalent values from the Kwale HMS deposit.

The ILCR from exposure to Cr and As in soil sampled from the environs of Mrima Hill and Kwale HMS deposit exceeded the recommended USEPA highest acceptable limit of 10^{-4}, as shown in Tables 5.15. The ILCR from exposure to Pb in soil samples from Mrima Hill was within the recommended acceptable limits of 10^{-4} and 10^{-6}. However, the ILCR from exposure to Pb in soil samples from the Kwale HMS deposit was below the recommended acceptable limit of 10^{-6}. The summation of ILCR shows that the population residing around Mrima Hill and Kwale HMS was prone to carcinogenic human health risks from exposure to carcinogens in soil and water samples. Children were more susceptible to carcinogenic health risks.
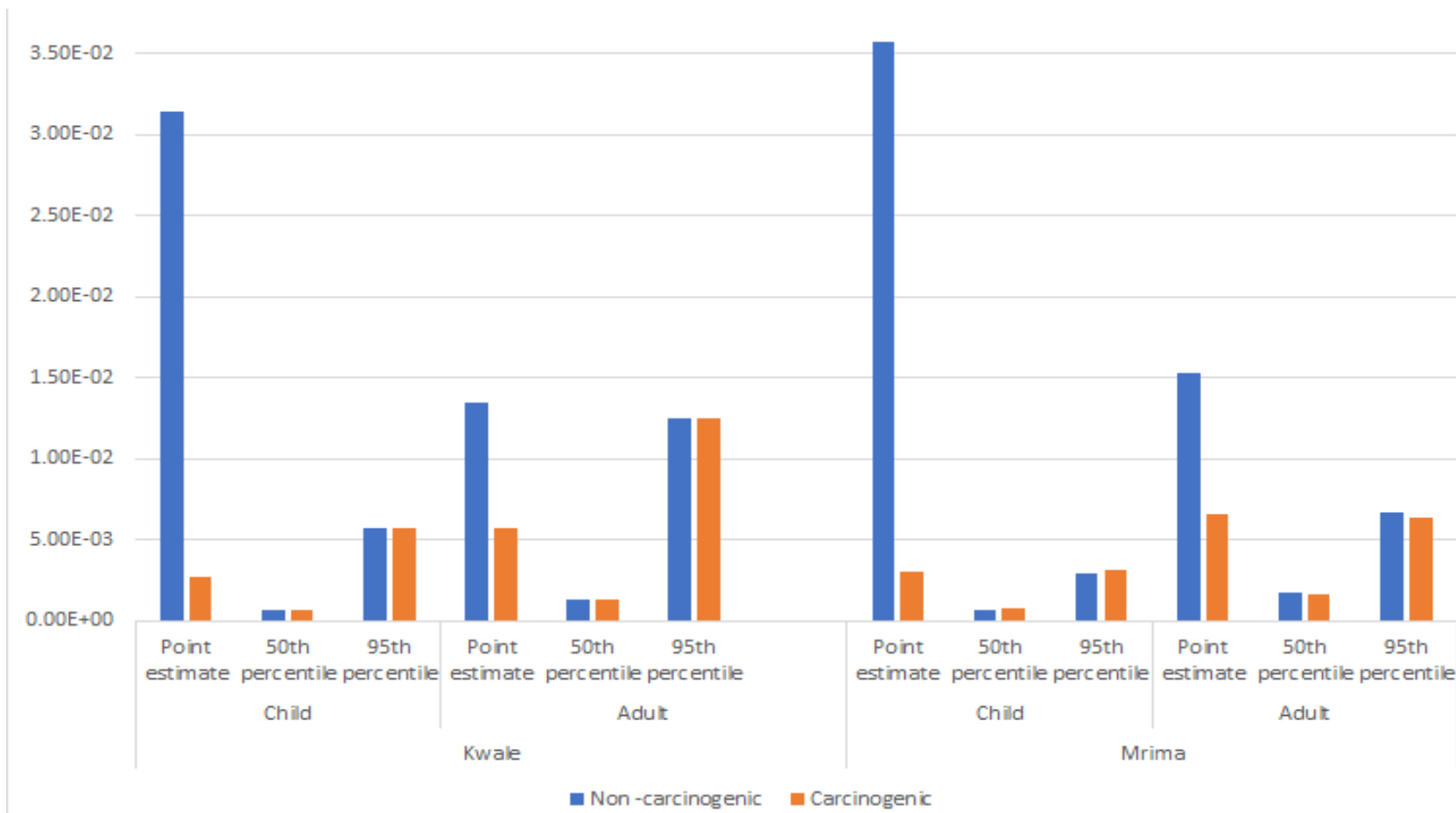
Fig. 5.11: Comparison of the sum of non-carcinogenic and carcinogenic average daily dose, ADD, from exposure to Cr, As, and Pb via ingestion pathways in water samples from environs of Kwale HMS deposit and Mrima.
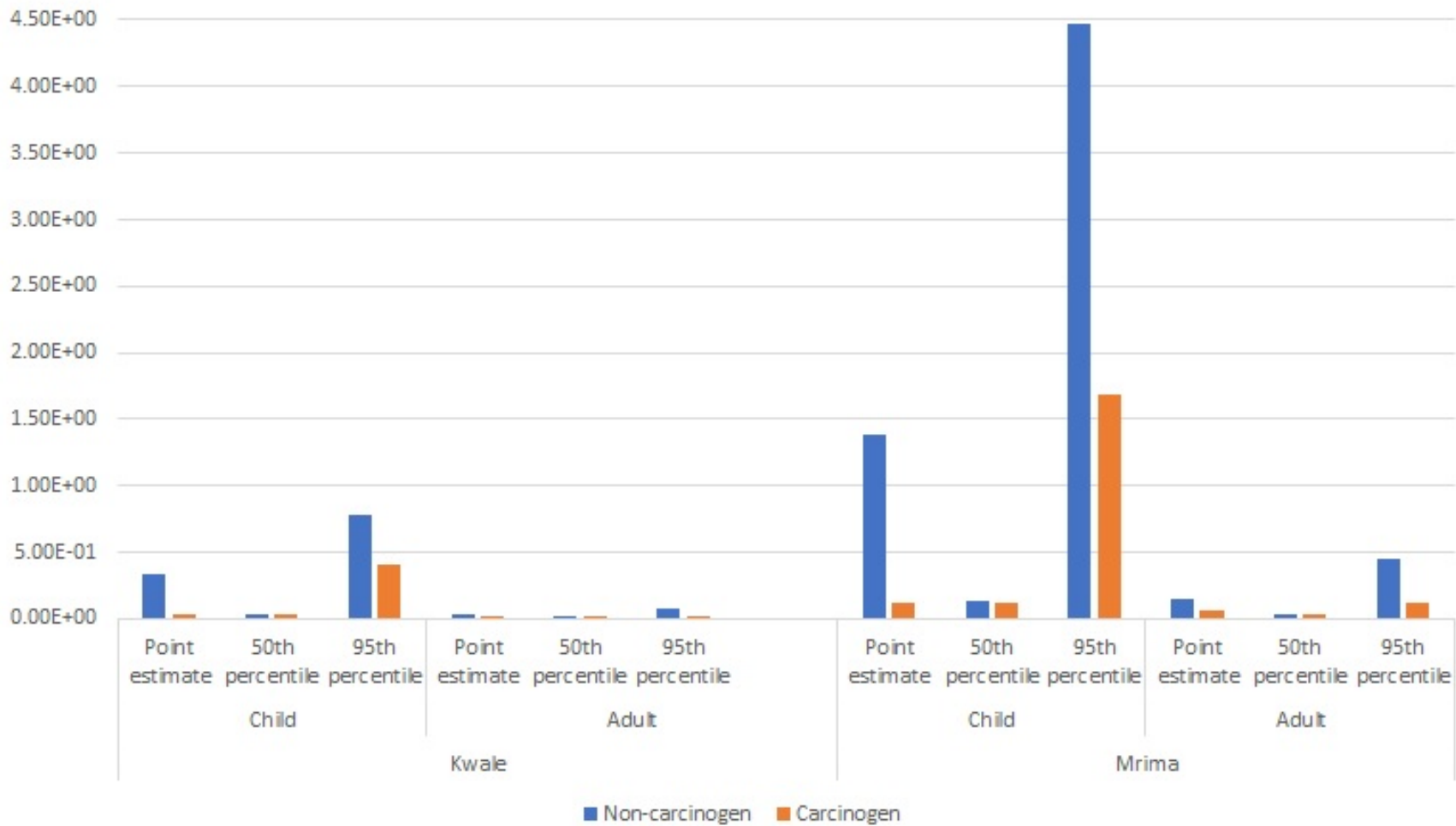
Fig. 5.12: Comparison of the sum of non-carcinogenic and carcinogenic average daily dose, ADD, from ingestion of Cr, As, and Pb in soil samples from environs of Kwale HMS deposit and Mrima

Table 5.14: Incremental lifetime cancer risk, ILCR, due to exposure to Cr, As, Pb via ingestion pathways in water samples from environs of Kwale HMS deposit and Mrima Hill

	Kwale HMS deposit						Mrima Hill					
	Child			Adult			Child			Adult		
	Point estimate	50th percentile	95th percentile	Point estimate	50th percentile	95th percentile	Point estimate	50th percentile	95th percentile	Point estimate	50th percentile	95th percentile
Cr	1.34E-03	3.15E-04	2.86E-03	2.86E-03	6.46E-04	6.25E-03	1.51E-03	4.10E-04	1.54E-03	3.24E-03	8.13E-04	3.16E-03
As	5.77E-06	1.29E-06	1.11E-05	1.24E-05	2.89E-06	2.14E-05	9.68E-06	2.18E-06	2.81E-05	2.07E-05	2.89E-06	2.14E-05
Pb	1.35E-07	3.53E-08	1.64E-07	2.90E-07	7.68E-08	3.68E-07	2.80E-07	7.22E-08	3.21E-07	6.00E-07	7.68E-08	3.68E-07
Total	**1.34E-03**	**3.16E-04**	**2.87E-03**	**2.88E-03**	**6.49E-04**	**6.27E-03**	**1.52E-03**	**4.12E-04**	**1.57E-03**	**3.26E-03**	**8.16E-04**	**3.18E-03**

Table 5.15: Incremental lifetime cancer risk, ILCR, from ingestion of Cr, As, Pb in soil particles from the environs of Kwale HMS deposit and Mrima Hill

	Kwale HMS deposit						Mrima Hill					
	Child			Adult			Child			Adult		
	Point estimate	50th percentile	95th percentile	Point estimate	50th percentile	95th percentile	Point estimate	50th percentile	95th percentile	Point estimate	50th percentile	95th percentile
Cr	1.44E-02	1.52E-02	1.99E-01	7.70E-03	4.29E-03	9.82E-03	5.91E-02	5.92E-02	8.42E-01	3.17E-02	1.62E-02	5.95E-02
As	2.50E-04	2.73E-04	4.17E-03	1.34E-04	7.21E-05	1.53E-04	2.45E-04	2.58E-04	3.90E-03	1.32E-04	6.74E-05	1.99E-04
Pb	1.87E-07	2.10E-07	2.03E-06	1.00E-07	5.39E-08	1.18E-07	1.16E-06	1.33E-06	1.54E-05	6.20E-07	3.16E-07	1.34E-06
Total	**1.46E-02**	**1.55E-02**	**2.03E-01**	**7.84E-03**	**4.36E-03**	**9.97E-03**	**5.93E-02**	**5.95E-02**	**8.46E-01**	**3.18E-02**	**1.63E-02**	**5.97E-02**

Incremental lifetime cancer risk, ILCR, analysis due to dermal exposure to As in soil samples showed that the point estimate ILCR values for children and adults living around Mrima Hill and Kwale HMS were below the highest USEPA acceptable limit of 10^{-4}. However, the high-end ILCR values for children exceeded the limit of 10^{-4}, as shown in Table 5.16. The deterministic and probabilistic ILCR values for children and from both environments were approximately six times higher than high-end ILCR values for adults. Thus, children were more susceptible to the carcinogenic effects of dermal exposure to As in soil.

Table 5.16: The incremental lifetime cancer risk from dermal exposure to As in soil sampled from the environs of Kwale HMS deposit and Mrima Hill

	Child			Adult		
	Point estimate	50th percentile	95th percentile	Point estimate	50th percentile	95th percentile
Kwale	5.99E-04	6.91E-05	1.56E-04	9.14E-05	1.11E-05	2.33E-05
Mrima	5.87E-04	6.63E-05	2.00E-04	8.96E-05	1.08E-05	2.87E-05

A summary of the carcinogenic human health, as shown in Table 5.17, shows that the population living around Mrima Hill was more prone to the carcinogenic effects from dermal and ingestion of heavy metals in soil and water sampled from this environment. The summation of incremental lifetime cancer risk of metal in the samples from Mrima hill was ~3 times higher than the equivalent values from the Kwale HMS deposit. The high ILCR values from Mrima Hill were due to the ingestion of soil.

Table 5.17: A summary of carcinogenic human health risk from dermal exposure to As in soil samples and ingestion of Cr, As, and Pb in water and soil samples from the environs of Mrima Hill and Kwale HMS deposit

| | **Kwale** | | | | | | **Mrima** | | | | | |
| | **Child** | | | **Adult** | | | **Child** | | | **Adult** | | |
	Point estimate	50th percentile	95th percentile	Point estimate	50th percentile	95th percentile	Point estimate	50th percentile	95th percentile	Point estimate	50th percentile	95th percentile
Ingest$_{Soil}$	1.46E-02	1.55E-02	2.03E-01	7.84E-03	4.36E-03	9.97E-03	5.93E-02	5.95E-02	8.46E-01	3.18E-02	1.63E-02	5.97E-02
Dermal$_{Soil}$	5.99E-04	6.91E-05	1.56E-04	9.14E-05	1.11E-05	2.33E-05	5.87E-04	6.63E-05	2.00E-04	8.96E-05	1.08E-05	2.87E-05
Ingest$_{Water}$	1.34E-03	3.16E-04	2.87E-03	2.88E-03	6.49E-04	6.27E-03	1.52E-03	4.12E-04	1.57E-03	3.26E-03	8.16E-04	3.18E-03
$\sum ILCR$	**1.65E-02**	**1.59E-02**	**2.06E-01**	**1.08E-02**	**5.02E-03**	**1.63E-02**	**6.14E-02**	**6.00E-02**	**8.48E-01**	**3.51E-02**	**1.71E-02**	**6.29E-02**

5.5 Results of the TEDE and ILCR from Exposure to ^{232}Th, ^{238}U, and their progenies

The total effective dose equivalent (TEDE) and the excess lifetime cancer morbidity risk (ILCR) from exposure to ^{232}Th, ^{238}U, and their respective progenies with half-lives more than 30 days in soils were evaluated using RESRAD-OFFSITE 4.0 code. The TEDE and ILCR for a rural resident farmer living around Kwale HMS deposit and Mrima Hill, who is assumed to be self-reliant (Shhub, 2021), were assessed. The exposure pathways considered in this scenario were inhalation of soil particles, incident ingestion of soil, and direct external exposure pathways considered for 30 years, as discussed in the methodology section.

5.5.1 Activity concentration of ^{232}Th and ^{238}U is soil samples

Using the mass fractions of ^{232}Th and 238U obtained from the ICP-MS measurements, the activity concentrations of ^{232}Th and ^{238}U in soil samples from the environs of Mrima Hill and the Kwale HMS deposit were evaluated using Eqn. 4.4. The activity concentration of these NORMs in the soil samples are provided in Appendix F-1 and F-2. The activity concentration of ^{232}Th in soil samples from areas around the Kwale HMS deposit ranged from 15.60 Bq/kg to 68.30 Bq/kg with a mean of 38.77 ± 1.63 Bq/kg, while that of ^{238}U ranged between 16.59 Bq/Kg and 77.59 Bq/Kg with a mean of 30.11 ± 1.53 Bq/kg. Although the mean activity values of ^{232}Th and ^{238}U were below the global average values of 45 Bq/Kg and 33 Bq/Kg (UNSCEAR, 2000), the mean concentration of ^{232}Th was twice the value obtained by Osoro *et al.* (2011) at the same site before mining and mineral processing activities of the heavy mineral sand had commenced. Abuodha and Hayombe (2006) postulated a remarkably high activity concentration of radionuclides from heavy mineral sand mining and processing activities. However, the activity concentration was not enhanced above the global average values and was thus inconsequential.

On the other hand, the activity concentration of ^{232}Th in soil samples from the environs of Mrima Hill ranged from 61.8 Bq/kg to 1318 Bq/kg with a mean of 294 ± 3.36 Bq/kg, while that of ^{238}U ranged between 32.7 Bq/kg and 946 Bq/kg with a mean of 101 ± 2.26 Bq/kg. The mean activity concentrations of ^{232}Th and ^{23}8U were approximately 7 and 3 times higher than the values obtained at the environs of Kwale HMS deposit and ~6 and ~3 times higher than the global average values of 45 Bq/Kg and 33 Bq/Kg (UNSCEAR, 2000) in soils. Nevertheless, the mean activity concentrations of the radionuclides were ~2 times lower than the values obtained by Kaniu *et al.* (2018) in the same study area. It is worth to note that soil samples collected in open field with visible intensive anthropogenic activities around the Kwale HMS deposit and Mrima Hill had higher activity concentration of ^{232}Th and ^{238}U compared to those samples in areas covered with vegetation. These soil samples include BS6, BS7, BS10. MS1, MS2, and MS3.

5.5.2   Total Effective Dose Equivalent (TEDE)

The total effective dose equivalent (TEDE) received by a rural resident living around the Kwale HMS deposit and from Mrima Hill is shown in Table 5.18. The rural resident farmer in the environs of Kwale HMS deposit received the highest TEDE of 67.72 µSv in the 74th year, while a farmer living around Mrima Hill received the highest TEDE of 504.71 µSv in the 80th year. The maximum TEDE values received by the residents from the areas around the Kwale HMS deposit were $\cong$ 15 times less than the public exposure limit of 1000 µSv /yr (Lecomte *et al.*, 2019), while the values from areas around Mrima Hill were $\cong$ 2 times less than this public exposure limit. However, in either case, the external exposure to radiation from the soils contributed the highest TEDE, which increased gradually from 68% to 98% of the total TEDE by the 10th year, as shown in Table 5.18. The high values of external dose could be due to an outdoor occupancy factor of 0.6 for a rural resident farmer (Ziajahromi *et al.*, 2015).

A further investigation of the contribution of ^{232}Th, ^{238}U, and its progenies to the TEDE showed that ^{228}Ra contributed the highest value to the TEDE ~1.41 µSv/year out of ~2.66 µSv/year at the initial contact with the radionuclide-contaminated soils from the environs of Kwale HMS deposit, and ~10.7 µSv/year out of ~17.4 µSv/year with radionuclide-contaminated soils from the environs of Mrima Hill, as shown in Fig 5.13, Fig. 5.14,

Appendix F-4 and Appendix F-5. The contribution of ^{238}U, ^{232}Th, and ^{228}Th to TEDE at the initial contact with soils from the environs of Kwale HMS deposit were ~0.635, ~0.280, and ~0.330 µSv/year. On the other hand, ^{238}U, ^{232}Th, and ^{228}Th in soils around Mrima Hill contribution to the TEDE was ~2.12, ~2.50, and ~2.13 µSv/year respectively. However, from the 5th year, the TEDE of the ^{228}Th was higher than that of ^{228}Ra and a gradual increase of their TEDE was observed while that of ^{232}Th and ^{238}U decreased in subsequent years. It is worth noting that the contribution of progenies of ^{238}U to the TEDE was insignificant.

The maximum dose of ^{228}Ra in soils from the environs of Kwale HMS deposit was ~24.06 µSv at the 86.78th year, while that of ^{228}Th was ~42.78 µSv at the 92.34th year. Likewise, the maximum dose of ^{228}Ra in soils from the environs of Mrima Hill was ~180.3 µSv at the 82.995th year, while that of ^{228Th} was ~ 320.4 µSv at the 86.01st year. The ingrowth of ^{228}Th and ^{228}Ra is related to their half-lives of 1.91 years and 5.75 years, half-lives which are shorter than that of the parent radionuclide ^{232}Th. Although the parent and daughter nuclides remain in secular equilibrium as atoms, Lee *et al.* (1997) noted that the activity concentration of daughters increases steadily. In this study, the activity concentrations of ^{228}Th and ^{228}Ra increased steadily (see Fig. 5.13 and 5.14). Furthermore, ^{228}Ra decays 100% through beta minus emission to an excited state of ^{228}Ac, whose half-life is 6.5 hours. ^{228}Ac then disintegrates to ^{228}Th through internal conversion and gamma emission processes. Even though ^{232}Th decays 100% through alpha-particle emission to various excited states of ^{224}Ra (with a half-life of 3.6 days), ^{224}Ra emits gamma photons to gain stability. Thus, the high external dose observed in this study was due to gamma and beta emission (Shhub, 2021) from the decay of ^{228}Ra and ^{228}Th.

Table 5.18: The total effective dose equivalent, TEDE, in μSv/year from exposure to ^{232}Th, ^{238}U, and their progenies

	Kwale HMS Deposit				Mrima Hill			
Year	External	Inhalation	Soil ingestion	TEDE	External	Inhalation	Soil ingestion	TEDE
0	2.2518	0.140	0.263	2.655	14.540	1.032	1.856	17.427
5	24.938	0.164	0.551	25.652	185.13	1.206	4.018	190.36
10	42.820	0.183	0.721	43.724	320.54	1.351	5.303	327.19
20	59.498	0.201	0.869	60.568	400.51	1.438	6.015	407.97
25	62.745	0.205	0.897	63.847	444.72	1.486	6.400	452.61
30	64.516	0.206	0.912	65.634	468.47	1.512	6.606	476.59
35	65.486	0.207	0.921	66.614	481.50	1.526	6.717	489.74
40	66.004	0.208	0.925	67.137	488.50	1.533	6.777	496.81
45	66.284	0.208	0.927	67.419	492.25	1.536	6.808	500.60
50	66.435	0.208	0.928	67.571	494.24	1.538	6.823	502.60
55	66.513	0.208	0.929	67.650	495.30	1.539	6.831	503.67
60	66.553	0.208	0.929	67.690	495.86	1.539	6.835	504.23
65	66.573	0.208	0.929	67.710	496.14	1.539	6.836	504.52
70	66.581	0.208	0.929	67.717	496.27	1.539	6.835	504.65
75	66.582	0.208	0.928	67.719	496.33	1.539	6.834	504.70
80	66.581	0.208	0.928	67.717	496.34	1.538	6.833	504.71
85	66.577	0.208	0.928	67.713	496.33	1.538	6.832	504.70
90	66.573	0.208	0.928	67.709	496.31	1.538	6.830	504.67
95	66.568	0.208	0.927	67.703	496.28	1.537	6.829	504.64
100	66.563	0.208	0.927	67.698	496.24	1.537	6.827	504.61
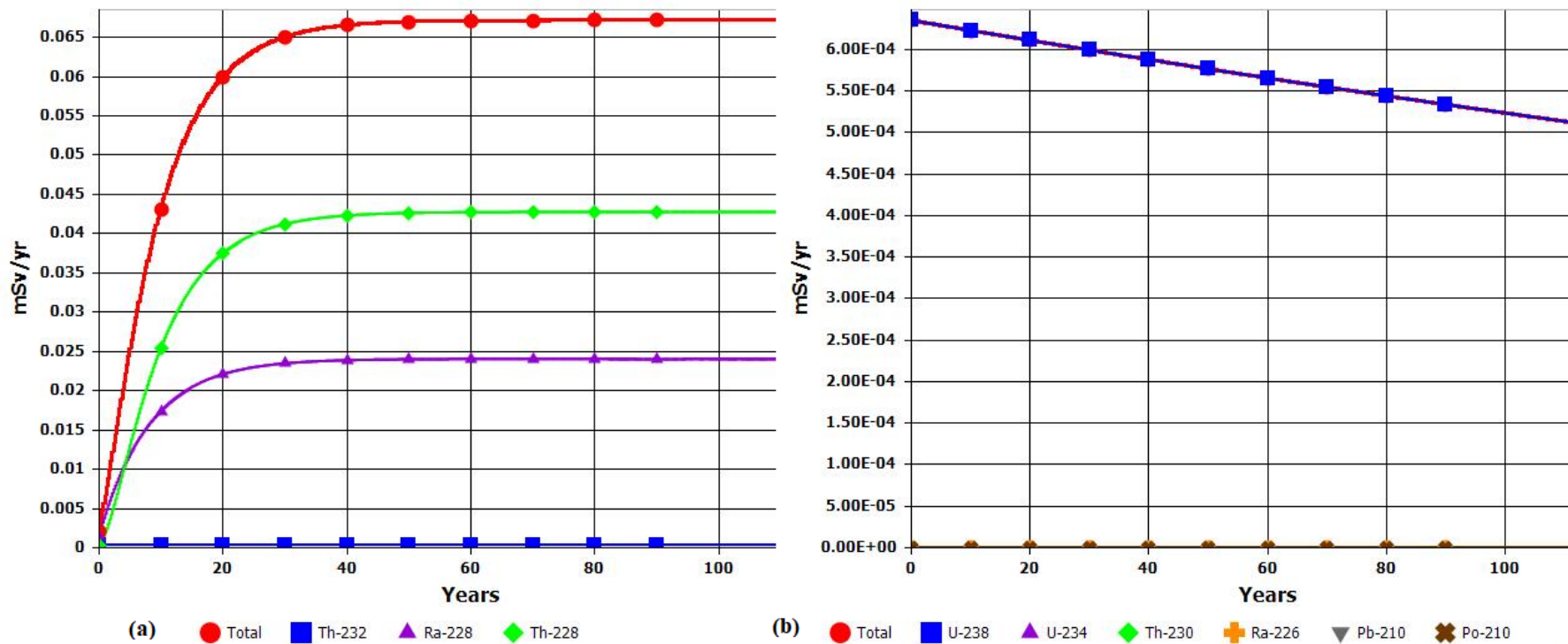
Fig. 5.13: The contribution of the parent nuclides ^{232}Th and ^{238}U and their progenies in soil samples from environs of Kwale HMS deposit to the total effective dose equivalent in mSv/year

115
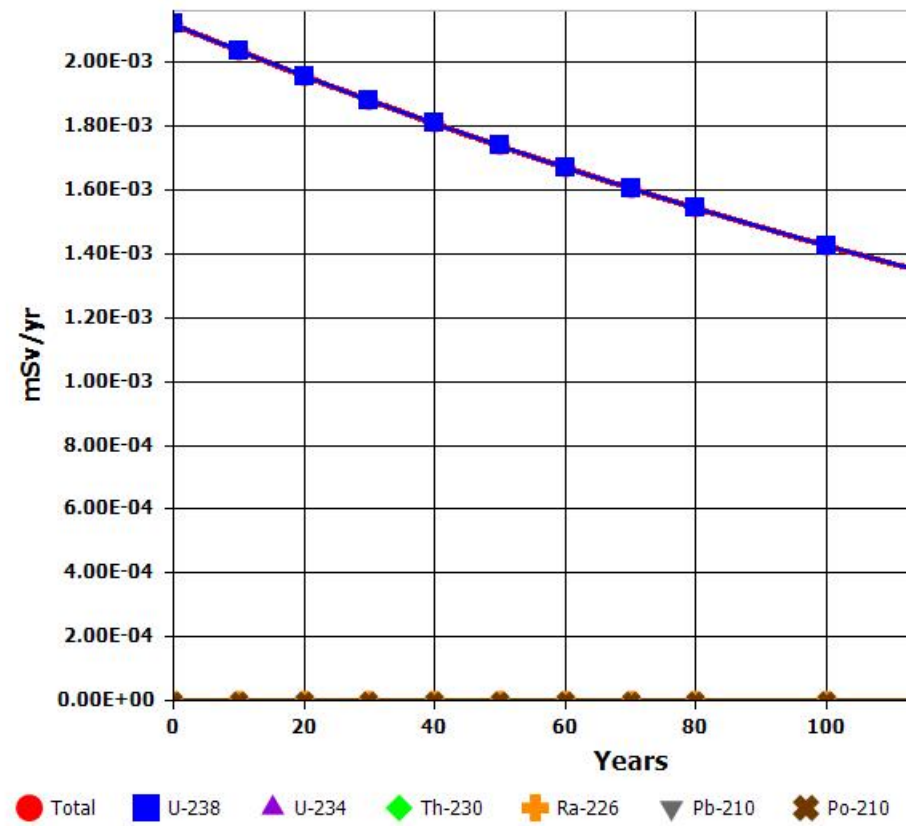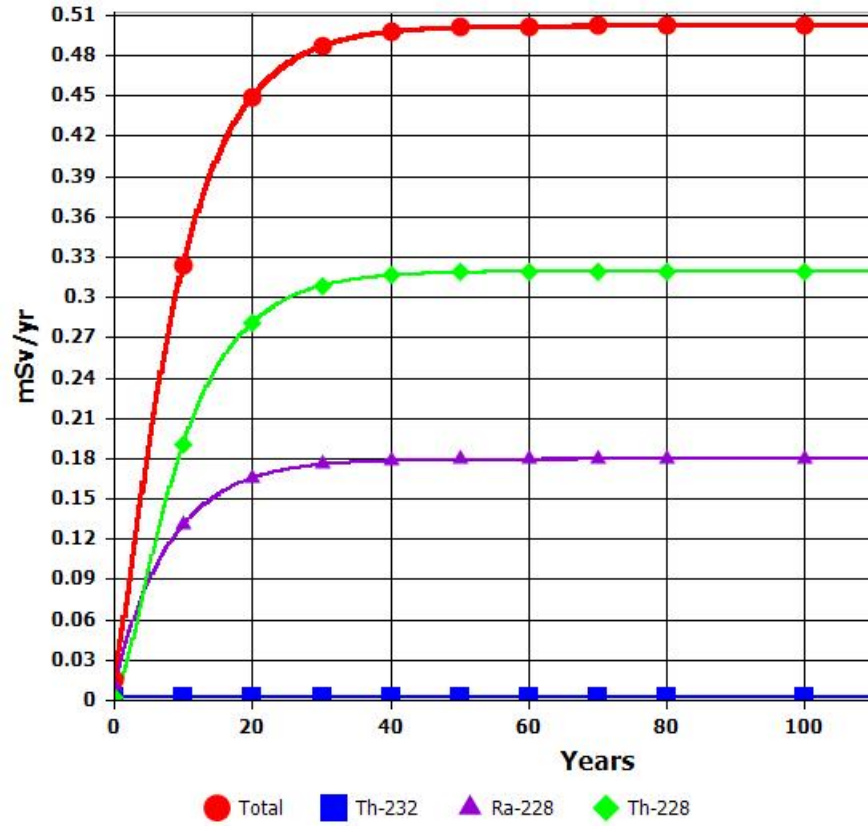
Fig. 5.14: Contribution of the parent nuclides, ^{232}Th and ^{238}U, and their progenies to the total effective dose equivalent in mSv/year
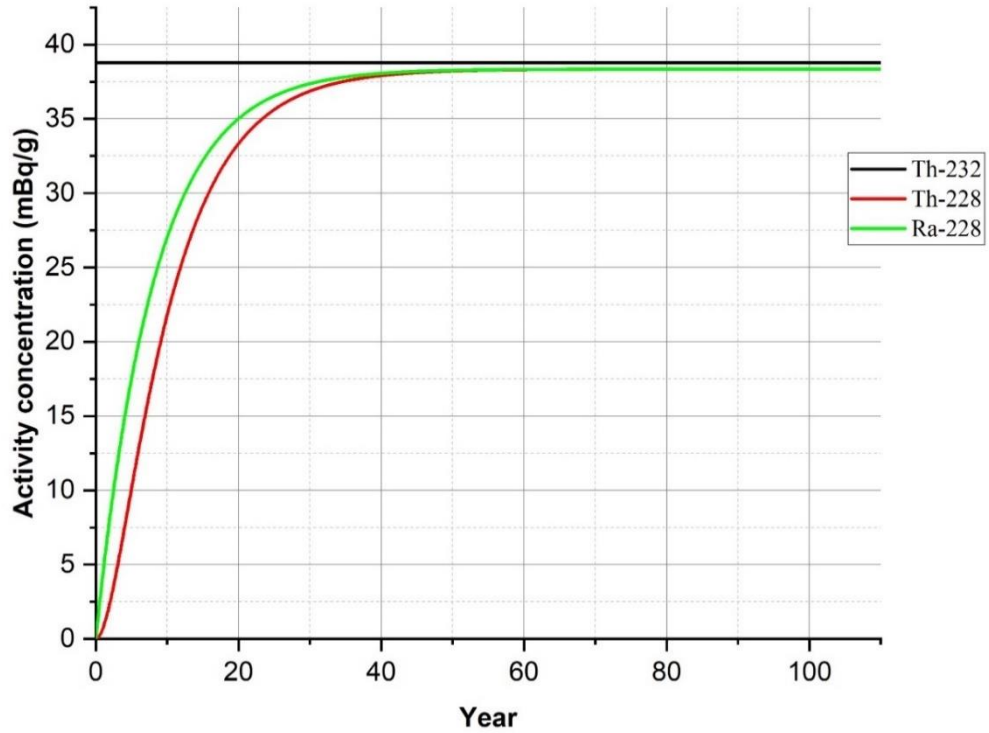
Fig. 5.15: Ingrowth of ^{232}Th progenies in soil samples from the environs Kwale HMS deposit
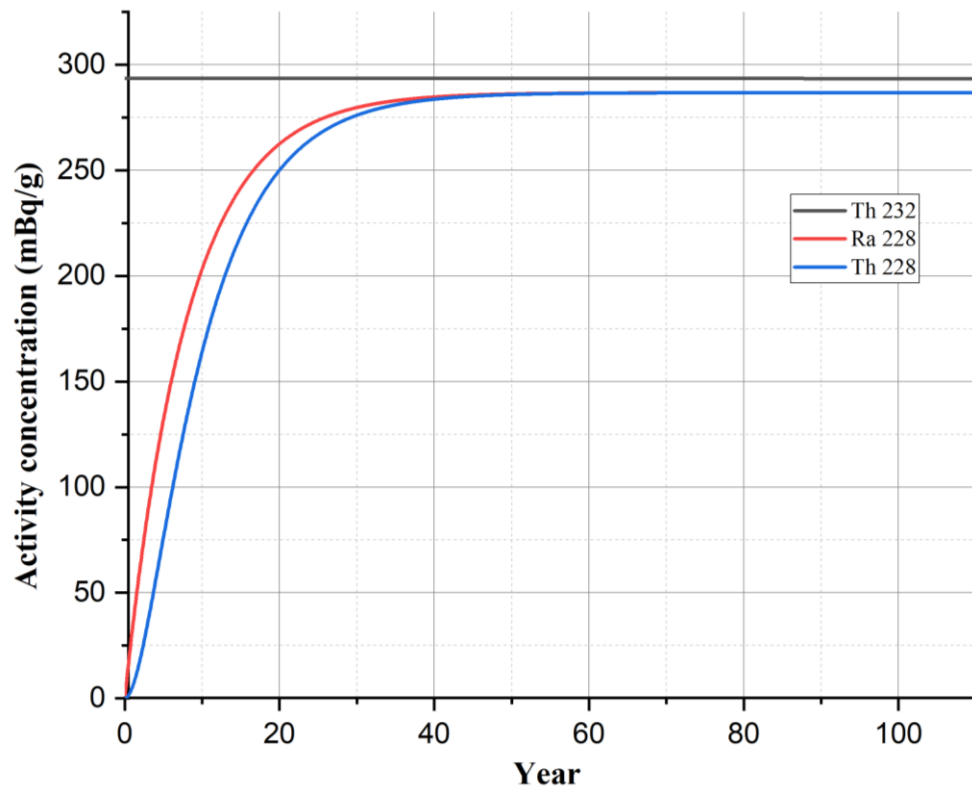
Fig. 5.16: Ingrowth of ^{232}Th progenies in soil samples from the environs of Mrima Hill

5.5.3 Incremental Lifetime Cancer Risks

The incremental lifetime morbidity cancer risks (ILCR) from exposure to ^{232}Th, ^{238}U, and their progenies in soil samples from the environs of Kwale HMS deposit and Mrima Hill, are shown in Table 5.19. Although the total ILCR was above the acceptable regulatory limit of 10E-04 (USEPA, 1989), approximately 90% of the total ILCR was from external exposure to ^{228}Ra and ^{228}Th. The cancer slope factors of the two progenies and their daughter nuclides,1.07E-07, for 228Ra+D, and 1.98E-07, for 228Th+D (Eckerman *et al.*, 1999), combined with the ingrowth of the progenies were higher compared to the ^{238}U progenies. The ILCR from inhalation and incidental ingestion of soil and dust particles from both study areas was below the recommended acceptable regulatory limit of 1.0E-04. It is worth noting that the ILCR from the ingestion of soil and dust particles was high compared to the inhalation of dust particles. There was a probability of one person living around Mrima Hill in a population of 100,000 in the 20th year developing cancer in a lifetime from ingestion of soils as compared to one person in a million living in the same environment developing cancer in a lifetime from inhalation of dust particles loaded with radionuclides. However, the total ILCR shows a higher probability of one person living in the environs of Mrima Hill in a population of 10,000 developing cancer in a lifetime at the point of contact with the radionuclide compared with 8 persons in the same population of 10,000 from the environs of Mrima Hill, as shown in Table 5.19. The probability increased to one person in every one thousand persons in the 10th year of living around Mrima Hill developing cancer in a lifetime.

It is worth to note the percentage risk contribution of ^{228}Th to the health risk at the initial contact with the NORMs was 60.5%, which increased steadily to 63.2% in the 15th year (Appendices F-6 and F-7). ^{228}Ra contributed 38.1% to the health risk at the initial contact with the contaminated soil but decreased to 35.6% in the 15th year. The contribution of ^{238}U and ^{232}Th to ILCR at the initial contact was 1.23% and 0.13% but decreased steadily in subsequent years. Even though the ILCR from the progenies of ^{238}U increased with time, the ILCR values were way below the regulatory limit of 10^{-6}, hence inconsequential to human health.

Table 5.19: Incremental lifetime cancer morbidity risk from exposure to ^{232}Th, ^{238}U, and their progenies

	Kwale HMS Deposit				Mrima Hill			
Year	External	Inhalation	Ingestion	Total	External	Inhalation	Ingestion	Total
0	1.0909E-04	1.7942E-07	1.0532E-06	1.1032E-04	8.1503E-04	1.2758E-06	7.6455E-06	8.2395E-04
5	1.3070E-04	2.0424E-07	1.2118E-06	1.3212E-04	9.7777E-04	1.4625E-06	8.8362E-06	9.8806E-04
10	1.4412E-04	2.1987E-07	1.3030E-06	1.4564E-04	1.0769E-03	1.5780E-06	9.5079E-06	1.0880E-03
15	1.5156E-04	2.2852E-07	1.3524E-06	1.5314E-04	1.1619E-03	1.6765E-06	1.0067E-05	1.1736E-03
20	1.5564E-04	2.3321E-07	1.3791E-06	1.5725E-04	1.1781E-03	1.6948E-06	1.0172E-05	1.1900E-03
25	1.5789E-04	2.3573E-07	1.3935E-06	1.5952E-04	1.1869E-03	1.7043E-06	1.0226E-05	1.1988E-03
30	1.5909E-04	2.3701E-07	1.4010E-06	1.6073E-04	1.1940E-03	1.7109E-06	1.0267E-05	1.2060E-03
35	1.5974E-04	2.3763E-07	1.4048E-06	1.6138E-04	1.1953E-03	1.7116E-06	1.0273E-05	1.2073E-03
40	1.6009E-04	2.3790E-07	1.4067E-06	1.6173E-04	1.1960E-03	1.7115E-06	1.0275E-05	1.2079E-03
45	1.6027E-04	2.3798E-07	1.4074E-06	1.6191E-04	1.1963E-03	1.7111E-06	1.0274E-05	1.2083E-03
50	1.6036E-04	2.3795E-07	1.4075E-06	1.6201E-04	1.1964E-03	1.7104E-06	1.0272E-05	1.2084E-03
55	1.6041E-04	2.3787E-07	1.4074E-06	1.6205E-04	1.1964E-03	1.7097E-06	1.0269E-05	1.2084E-03
60	1.6043E-04	2.3775E-07	1.4070E-06	1.6207E-04	1.1964E-03	1.7089E-06	1.0266E-05	1.2084E-03
65	1.6043E-04	2.3762E-07	1.4066E-06	1.6207E-04	1.1964E-03	1.7081E-06	1.0263E-05	1.2083E-03
70	1.6043E-04	2.3749E-07	1.4061E-06	1.6207E-04	1.1963E-03	1.7072E-06	1.0260E-05	1.2083E-03
75	1.6042E-04	2.3735E-07	1.4056E-06	1.6206E-04	1.1962E-03	1.7064E-06	1.0257E-05	1.2082E-03
80	1.6041E-04	2.3720E-07	1.4051E-06	1.6205E-04	1.1961E-03	1.7056E-06	1.0254E-05	1.2081E-03
85	1.6040E-04	2.3706E-07	1.4046E-06	1.6204E-04	1.1961E-03	1.7048E-06	1.0251E-05	1.2080E-03
90	1.6039E-04	2.3692E-07	1.4040E-06	1.6203E-04	1.1960E-03	1.7040E-06	1.0248E-05	1.2079E-03
95	1.6038E-04	2.3679E-07	1.4036E-06	1.6202E-04	1.1961E-03	1.7048E-06	1.0251E-05	1.2080E-03
100	1.6037E-04	2.3668E-07	1.4032E-06	1.6201E-04	1.1960E-03	1.7040E-06	1.0248E-05	1.2079E-03

CHAPTER 6

Conclusion and Recommendations

6.1   Conclusion

The results showed that the median concentrations of Cr in water samples from the environs of Mrima Hill and Kwale HMS deposits were (0.569 ± 0.205) mg/L and (0.422 ± 0.393) mg/L, respectively. These values exceeded the WASREB, WHO of 0.05 mg/l, and USEPA of 0.1 mg/L in drinking water. Although the median concentrations of Mn and Zn in water samples were higher than Cd, the concentration of Cd in all samples from the environs of the Kwale HMS deposit were above the WASREB, USEPA values of 0.005 mg/L and WHO value of 0.003 mg/L, while 13 water samples from Mrima Hill had Cd above these permissible values. However, Cu, Zn, Mn, As, Ni, Pb, and U in all the water samples were within the guideline values of metals in drinking water. Similarly, the mean concentration of Cr in soil samples from Mrima Hill was $\cong$2000 and $\cong$450 times higher than the global average concentration (GAC) and trigger values (TV) of Cr in topsoils but $\cong$5 times higher than the Cr value obtained at the Kwale HMS deposit. Despite the lower levels of Cd in soil samples compared to other metals, its mean concentration in the samples from the environs of Mrima Hill and Kwale HMS deposit was $\cong$110 and $\cong$10 times higher than the GAC. However, the mean concentration of Cd in soil samples from the environs of Kwale HMS deposit was below the maximum acceptable concentration (MAC) and TV in topsoils, while in soils samples from the environs of Mrima Hill, the mean Cd concentration was $\cong$9 times higher than the MAC, and $\cong$2 times higher than the TV in topsoils. In addition, the arsenic concentration in soil samples from the study areas was $\cong$24 times higher than the GAC, $\cong$ 8 times higher than the MAC, and $\cong$ 2 times higher than the TV. However, the concentrations of Pb, Th, U, Zn, and Mn, which are metals of health concern were below the GAC, MAC, and TV of the respective metals in topsoils.

Despite the high concentration of Cr in water samples from the two study areas, Cd contributed the highest percentages of 97 and 81 to the water quality index (WQI) of 1598 and 426, respectively, for samples from the Kwale HMS deposit and Mrima

Hill. Cr contributed 1.7% and 8.9% to the WQI of samples from the Kwale HMS deposit and Mrima Hill. All the water samples from the Kwale HMS deposit were unsuitable for human consumption due to Cd contamination, while 13 out of the 19 from Mrima Hill were unsuitable for consumption due to Cd contamination. However, the soil pollution assessment showed that the soils from the two study areas were extremely polluted by Cd and Cr, whose Igeo values were above 5. In addition, the soil samples from the two study areas were strongly polluted by arsenic. The soil Igeo value of As was 3.4. The enrichment factor showed that the enhancement of these three metals could be due to both pedogenic and anthropogenic processes.

The health risk assessment results showed that the children living near Kwale HMS deposit and Mrima Hill were more prone to the effects of exposure to metals in soil samples than the adults. Arsenic contributed $\cong$90% and $\cong$67% of the child's high end probabilistic hazard indices (HI) of 22.8 and 15.9 and deterministic HI of 9.40 and 7.09 from ingestion of soil sampled in the environs of Mrima Hill and the Kwale HMS deposit, respectively. However, the deterministic HI of As for adults living in these environments was less than 1, while the high-end probabilistic values were 2.28 and 1.83. Arsenic also contributed $\cong$42% and $\cong$70% of 33.8 and 15.3, respectively, to the child's high-end probabilistic HI from dermal exposure to the soil sampled around Mrima Hill and the Kwale HMS deposit. The assessment is in contrast with the ingestion of metals in drinking water. The deterministic values were higher than the probabilistic values. In addition, the Cr contributed $\cong$88% of the child's and adult's deterministic HI of 13.3 and 5.70 and probabilistic HI of 2.65 and 3.30, respectively, living around Mrima Hill. However, Cd and Cr contributed $\cong$50% and $\cong$48%, respectively, to the child's and adult's deterministic HI of 21.5 and 9.3 for the population living around the Kwale HMS deposit, with Cr contributing 60% of the child's and adult's probabilistic values of 2.78 and 7.06, respectively. The carcinogenic health risk evaluation from ingestion of Cr, As, and Pb in drinking water and soil particles also showed the population was prone to cancer risks from ingestion of Cr in water and As in soil, whose incremental lifetime cancer risk (ILRC) exceeded the USEPA acceptable limit of 10^{-4}. The children were also prone to dermal exposure to As whose ILCR values exceeded the USEPA acceptable limit of 10^{-4}. The ILCR values from ingestion of Pb in soil was below the permissible limit of 10^{-4}, while the

ILCR values of Pb exposure to As in drinking water was within the permissible limit of 10^{-6} to 10^{-4}. Thus, the sum of ILCR was greater than 10^{-4}.

Although the external dose from exposure to gamma and beta emission from ^{228}Ra and ^{228}Th, progenies of ^{232}Th was higher than the internal exposure from incidental ingestion of soil and inhalation of dust contaminated with the radionuclides, the maximum TEDE values for a rural resident farmer from the environs of Kwale HMS deposit and Mrima Hill were highest (67.72 μSv and 504.7 μSv, respectively) in the 74th year of exposure. Furthermore, ILCR was slightly above the recommended regulatory limit of 10^{-4} due to external exposure, thus having a negligible effect on human health.

6.2   Recommendations

Even though the internal dose due to exposure to NORMs at the environs of Mrima Hill and Kwale HMS deposit was low, a prolonged exposure to such low radiation may lead to radiation induced bystander effect. Thus, assessment of the activity concentration, radiological dose, and human health risk during mining activities should be monitored frequently to protect the public from radiation exposure This research further showed that the population living around Kwale HMS deposit, an on ongoing titanium mining site, and Mrima Hill, a prospecting Nb and REE mining site were prone to non-cancer and cancer effects due to exposure to the As, Cd, Cr, and to some extent Pb and Mn. Therefore, there is a need for government of Kenya to put in place mechanisms to monitor, control, and mitigate heavy metal pollution of water and soil due to mining and mineral processing activities. Epidemiological studies of health risks from exposure to heavy metals in soil and drinking water from the environs of Mrima Hill and Kwale HMS deposit could be carried out to assess the occurrence and distribution of carcinogenic and non-carcinogenic risks.

References

Abuodha, J. O. Z., & Hayombe, P. O. (2006). Protracted environmental issues on a proposed titanium minerals development in Kenya's south coast. *Marine Georesources and Geotechnology*, *24*(2), 63–75. https://doi.org/10.1080/10641190600704251

Adamu, C. I., Nganje, T. N., & Edet, A. (2015). Environmental Nanotechnology , Monitoring & Management Heavy metal contamination and health risk assessment associated with abandoned barite mines in Cross River State , southeastern Nigeria. *Environmental Nanotechnology, Monitoring & Management*, *3*, 10–21. https://doi.org/10.1016/j.enmm.2014.11.001

Ahmad, R. (2018). Tropical Environments. In P. Bobrowsky & B. Marker (Eds.), *Encyclopedia of Engineering Geology. Encyclopedia of Earth Sciences Series* (pp. 1–5). Springer. https://doi.org/10.1007/978-3-319-12127-7_285-1

Ahmad, S. A., Sayed, M. H. S. U., Barua, S., Khan, M. H., Faruquee, M. H., Jalil, A., … Talukder, H. K. (2001). Arsenic in Drinking Water and Pregnancy Outcomes. *Environmental Health Perspectives*, *109*(6), 2000–2002.

Åkesson, A., Bjellerup, P., Lundh, T., Lidfeldt, J., Nerbrand, C., Samsioe, G., … Vahter, M. (2006). Cadmium-induced effects on bone in a population-based study of women. *Environmental Health Perspectives*, *114*(6), 830–834. https://doi.org/10.1289/ehp.8763

Al-gizzi, I. A., Al-hejuje, M. M., & Nema, J. D. (2020). Concentration of some Heavy Metals Emissions from Electrical Generators in Air and Green Plants in Basrah City , Iraq Concentration of some Heavy Metals Emissions from Electrical Generators in Air and Green Plants in Basrah City , Iraq. *Biological and Applied Environmental Research*, *4*(2), 90–101.

Alarcón-Herrera, M. T., Bundschuh, J., Nath, B., Nicolli, H. B., Gutierrez, M., Reyes-Gomez, V. M., … Sracek, O. (2013). Co-occurrence of arsenic and fluoride in groundwater of semi-arid regions in Latin America: Genesis, mobility and remediation. *Journal of Hazardous Materials*, *262*, 960–969. https://doi.org/10.1016/j.jhazmat.2012.08.005

Alidadi, H., Belin, S., Sany, T., Zarif, B., Oftadeh, G., & Mohamad, T. (2019). Health risk assessments of arsenic and toxic heavy metal exposure in drinking water in northeast Iran. *Environmental Health and Preventive Medicine*, *24*(59), 1–17.

Alves, A. R., & Coutinho, R. (2019). Life cycle assessment of niobium : A mining and production case study in. *Minerals Engineering*, *132*, 275–283. https://doi.org/10.1016/j.mineng.2018.11.041

Anitha, J. K., J, S., Rejith, R. G., & Sundararajan, M. (2020). Monazite chemistry and its distribution along the coast of Neendakara – Kayamkulam belt , Kerala , India. *SN Applied Sciences*, *2*(5), 1–18. https://doi.org/10.1007/s42452-020-2594-6

Aoshima, K. (2016). Itai-itai disease: Renal tubular osteomalacia induced by environmental exposure to cadmium—historical review and perspectives. *Soil Science and Plant Nutrition*, *62*(4), 319–326. https://doi.org/10.1080/00380768.2016.1159116

Aoshima, K., Fan, J., Cai, Y., Katoh, T., Teranishi, H., & Kasuya, M. (2003). Assessment of bone metabolism in cadmium-induced renal tubular dysfunction by measurements of biochemical markers. *Toxicology Letters*, *136*(3), 183–192. https://doi.org/10.1016/S0378-4274(02)00356-9

Asic, A., Kurtovic-Kozaric, A., Besic, L., Mehinovic, L., Hasic, A., Kozaric, M., … Marjanovic, D. (2017). Chemical toxicity and radioactivity of depleted uranium: The evidence from in vivo and in vitro studies. *Environmental Research*, *156*(December 2016), 665–673. https://doi.org/10.1016/j.envres.2017.04.032

ATSDR. (2012). *Toxicological Profile for Chromium. ATSDR's Toxicological Profiles*. Atlanta, Georgia. https://doi.org/10.1201/9781420061888_ch63

ATSDR. (2022). *Toxicological Profile for Copper*. Atlanta, Georgia.

Bagdon, R. E., & Hazen, R. E. (1991). Skin permeation and cutaneous hypersensitivity as a basis for making risk assessments of chromium as a soil contaminant. *Environmental Health Perspectives*, *92*, 111–119. https://doi.org/10.2307/3431146

Banning, A., & Benfer, M. (2017). Drinking water uranium and potential health effects in the german federal state of Bavaria. *International Journal of Environmental Research and Public Health*, *14*(8). https://doi.org/10.3390/ijerph14080927

Barrio-parra, F., & Dominguez-Castillo, A. (2017). *EniroPRA:Envirommental Probabilisitc Risk Assessment Tools*. Retrieved from https://cran.r-project.org/package=%0AEnviroPRA

Bello, S., Nasiru, R., Garba, N. N., & Adeyemo, D. J. (2019). Carcinogenic and non-

carcinogenic health risk assessment of heavy metals exposure from Shanono and Bagwai artisanal gold mines, Kano state, Nigeria. *Scientific African*, *6*, 4–9. https://doi.org/10.1016/j.sciaf.2019.e00197

Belluck, D. A., Benjamin, S. L., Baveye, P., Sampson, J., & Johnson, B. (2003). Widespread Arsenic Contamination of Soils in Residential Areas and Public Spaces : An Emerging Regulatory or Medical Crisis ? *International Journal of Toxicology*, *22*, 109–128. https://doi.org/10.1080/10915810390198311

Bilčíková, J., Fialková, V., Kováčiková, E., Miškeje, M., Tombarkiewicz, B., & Kňažická, Z. (2018). Influence of Transition Metals on Animal and Human Health: A Review. *Contemporary Agriculture*, *67*(3–4), 187–195. https://doi.org/10.1515/contagri-2018-0027

Bjørklund, G., Semenova, Y., Pivina, L., Dadar, M., & Rahman, M. (2020). Uranium in drinking water : a public health threat. *Archives of Toxicology*, *94*, 1551–1560.

Bortey-Sam, N., Nakayama, S. M. M., Ikenaka, Y., Akoto, O., Baidoo, E., Mizukawa, H., & Ishizuka, M. (2015). Health risk assessment of heavy metals and metalloid in drinking water from communities near gold mines in Tarkwa, Ghana. *Environmental Monitoring and Assessment*, *187*(7), 1–12. https://doi.org/10.1007/s10661-015-4630-3

Borzsonyi, M., Bereczky, A., Rudnail, P., Csanady, M., & Horvathl, A. (1992). Epidemiological studies on human subjects exposed to arsenic in drinking water in Southeast Hungary. *Archives of Environmental Health: An International Journal*, *66*, 77–78.

Bouabid, S., Tinakoua, A., Lakhdar-Ghazal, N., & Benazzouz, A. (2016). Manganese neurotoxicity: behavioral disorders associated with dysfunctions in the basal ganglia and neurochemical transmission. *Journal of Neurochemistry*, *136*(4), 677–691. https://doi.org/10.1111/jnc.13442

Brennan, R., Dulude, J., & Thomas, R. (2015). Approaches to Maximize Performance and Reduce the Frequency of Routine Maintenance in ICP-MS. *Spectroscopy*, *30*(10), 12–25.

Bressler, J. P., & Goldstein, G. W. (1991). Mechanisms of lead neurotoxicity. *Biochemical Pharmacology*, *41*(4), 479–484. https://doi.org/10.1016/0006-2952(91)90617-E

Briffa, J., Sinagra, E., & Blundell, R. (2020). Heavy metal pollution in the environment and their toxicological effects on humans. *Heliyon*, *6*(9), e04691.

https://doi.org/10.1016/j.heliyon.2020.e04691

Carvalho, F. P., Matine, O. F., Taímo, S., Oliveira, J. M., Silva, L., & Malta, M. (2014). Radionuclides and radiation doses in heavy mineral sands and other mining operations inmozambique. *Radiation Protection Dosimetry*, *158*(2), 181–186. https://doi.org/10.1093/rpd/nct202

Caswell, P. V., & Baker, B. H. (1953). *Geology of Mombasa-Kwale area*. Report No.24, Ministry of Environment and Natural Resources, Mines and Geological department, Nairobi, Kenya.

Cember, H. and, & Johnson, T. E. (2012). *Introduction to Health physics. Health physics* (4 ed., Vol. 102). Mc Graw Hill Companies. https://doi.org/10.1097/01.HP.0000410056.48665.

Chen, J., Wei, F., Zheng, C., Wu, Y., & Adriano, D. C. (1991). Background concentrations of elements in soils of China. *Water, Air, and Soil Pollution*, 699–712.

Chen, L., Wang, J., Beiyuan, J., Guo, X., Wu, H., & Fang, L. (2022). Environmental and health risk assessment of potentially toxic trace elements in soils near uranium (U) mines: A global meta-analysis. *Science of the Total Environment*, *816*, 151556. https://doi.org/10.1016/j.scitotenv.2021.151556

Choudhari, R., Sathwara, N. G., Shivgotra, V. K., Patel, S., Rathod, R. A., Shagufta, S., … Saiyed, H. N. (2010). Study of lead exposure to children residing near a lead – zinc mine. *Indian Journal of Occupational and Environmental Medicine*, *14*(2), 58–62. https://doi.org/10.4103/0019-5278.72243

Collin, M. S., Venkatraman, S. K., Vijayakumar, N., Kanimozhi, V., Arbaaz, S. M., Stacey, R. G. S., … Swamiappan, S. (2022). Bioaccumulation of lead (Pb) and its effects on human: A review. *Journal of Hazardous Materials Advances*, *7*(March), 100094. https://doi.org/10.1016/j.hazadv.2022.100094

Crews, H. M., Robb, P., Baxter, M., J. (2007). Application of Plasma Spectrometry in Food Science. In J. Hill, S. (Ed.), *Inductively Coupled Plasma Spectrometry and its Applications* (2 ed., p. 403). Oxford: bLACKWELL.

Dastgiri, S., Mosaferi, M., Fizi, M. A. H., Olfati, N., Zolali, S., Pouladi, N., & Azarfam, P. (2010). Arsenic exposure, dermatological lesions, hypertension, and chromosomal abnormalities among people in a rural community of northwest Iran. *Journal of Health, Population and Nutrition*, *28*(1), 14–22. https://doi.org/10.3329/jhpn.v28i1.4519

Desouky, O., Ding, N., & Zhou, G. (2015). Targeted and non-targeted effects of ionizing radiation. *Journal of Radiation Research and Applied Sciences*, *8*(2), 247–254. https://doi.org/10.1016/j.jrras.2015.03.003

Eckerman, K. F., Leggett, R. W., Nelson, C. B., Puskin, J. S., & Richardson, C. B. (1999). *Cancer risk coefficients for environmental exposure to radionuclides* (EPA 402-R-99-001 No. Federal Guidance Report No. 13). Washington, DC.

El-Jaoual, T., & Cox, D. A. (1998). Manganese toxicity in plants. *Journal of Plant Nutrition*, *21*(2), 353–386. https://doi.org/10.1080/01904169809365409

Enamorado-Báez, S. M., Abril, J. M., & Gómez-Guzmán, J. M. (2013). Determination of 25 Trace Element Concentrations in Biological Reference Materials by ICP-MS following Different Microwave-Assisted Acid Digestion Methods Based on Scaling Masses of Digested Samples. *ISRN Analytical Chemistry*, *2013*, 1–14. https://doi.org/10.1155/2013/851713

Erlangung, O. Zur. (2014). *Re-scanning in scanned ion beam therapy in the presence of organ motion*. PhD Theis: Technical University of Darmstadt.

Falciani, R., Novaro, E., Marchesini, M., & Gucciardi, M. (2000). Multi-elemental analysis of soil and sediment by ICP-MS after a microwave assisted digestion method. *J. Anal. At. Spectrom*, *15*, 561–565. https://doi.org/10.1039/b000742k

Fernley, M., & Drolia, V. (2011). *African Mineral: Metals and Minerals*. GMP Securities Europe LLP.

Finnegan, P. M., & Chen, W. (2012). Arsenic toxicity: The effects on plant metabolism. *Frontiers in Physiology*, *3 JUN*(June), 1–18. https://doi.org/10.3389/fphys.2012.00182

Gaudino, S., Galas, C., Belli, M., Barbizzi, S., De Zorzi, P., Jaćimović, R., … Sansone, U. (2007). The role of different soil sample digestion methods on trace elements analysis: A comparison of ICP-MS and INAA measurement results. *Accreditation and Quality Assurance*, *12*(2), 84–93. https://doi.org/10.1007/s00769-006-0238-1

Genchi, G., Carocci, A., Lauria, G., & Sinicropi, M. S. (2020). Nickel : Human Health and Environmental Toxicology. *International Journal of Environmental Research and Public Health*, *17*(679), 1–21.

Gibson, J. M., Fisher, M., Clonch, A., Macdonald, J. M., & Cook, P. J. (2020). Children drinking private well water have higher blood lead than those with city water. *PNAS*, 1–10. https://doi.org/10.1073/pnas.2002729117

Giri, S., Singh, A. K., & Mahato, M. K. (2020). Monte Carlo simulation-based probabilistic health risk assessment of metals in groundwater via ingestion pathway in the mining areas of Singhbhum copper belt , India. *International Journal of Environmental Health Research*, *30*(4), 447–460. https://doi.org/10.1080/09603123.2019.1599101

Goher, M. E., Hassan, A. M., Abdel-moniem, I. A., Fahmy, A. H., & El-sayed, S. M. (2014). Evaluation of surface water quality and heavy metal indices of Ismailia Canal , Nile River , Egypt. *The Egyptian Journal of Aquatic Research*, *40*(3), 225–233. https://doi.org/10.1016/j.ejar.2014.09.001

Guo, H., Aleyasin, H., Dickinson, B. C., Haskew-layton, R. E., & Ratan, R. R. (2014). Recent advances in hydrogen peroxide imaging for biological applications. *Cell and Bioscience*, *4*(64), 1–10.

Guo, H. R., Yu, H. S., Hu, H., & Monson, R. R. (2001). Arsenic in drinking water and skin cancers: Cell-type specificity (Taiwan, ROC). *Cancer Causes and Control*, *12*(10), 909–916. https://doi.org/10.1023/A:1013712203455

Haakonde, T., Yabe, J., Choongo, K., Chongwe, G., & Islam, M. S. (2020). Preliminary Assessment of Uranium Contamination in Drinking Water Sources Near a Uranium Mine in the Siavonga District, Zambia, and Associated Health Risks. *Mine Water and the Environment*, *39*(4), 735–745. https://doi.org/10.1007/s10230-020-00731-5

Hao, W., Kashiwabara, T., Jin, R., Takahashi, Y., Gingras, M., Alessi, D. S., & Konhauser, K. O. (2020). Clay minerals as a source of cadmium to estuaries. *Scientific Reports*, *10*(1), 1–11. https://doi.org/10.1038/s41598-020-67279-w

Harb, S., Zahran, A. M., Abbady, A., & Ahmed, F. A. (2014). Assessment of Natural Radioactivity in Soil and Water Samples from Aden Governorate South Of Yemen Region. *International Journal of Recent Research in Physics and Chemical Sciences*, *1*(1), 1–7.

Haribala, Hu, B., Wang, C., Gerilemandahu, Xu, X., Zhang, S., … Li, Y. (2016). Assessment of radioactive materials and heavy metals in the surface soil around uranium mining area of Tongliao, China. *Ecotoxicology and Environmental Safety*, *130*, 185–192. https://doi.org/10.1016/j.ecoenv.2016.04.002

Harmer, R. E., & Nex, P. A. M. (2016). Rare Earth Deposits of Africa. *Episodes*, *39*(2), 381–406. https://doi.org/10.18814/epiiugs/2016/v39i2/95784

Harris, G., & Horn, R. Van. (1996). *Use of Monte Carlo Methods in Environmental*

Risk Assessment at the INEL: Applications and Issures. Idaho.

Harvey, P. J., Handley, H. K., & Taylor, M. P. (2016). Widespread copper and lead contamination of household drinking water, New South Wales, Australia. *Environmental Research*, *151*, 275–285. https://doi.org/10.1016/j.envres.2016.07.041

Henriques, V. A. R. (2009). Titanium production for aerospace applications. *Journal of Aerospace Technology and Management*, *1*(1), 7–17. https://doi.org/10.5028/jatm.2009.01010717

Holmes, A. L., Wise, S. S., Sandwick, S. J., & Wise, J. P. (2006). The clastogenic effects of chronic exposure to particulate and soluble Cr(VI) in human lung cells. *Mutation Research - Genetic Toxicology and Environmental Mutagenesis*, *610*(1–2), 8–13. https://doi.org/10.1016/j.mrgentox.2006.06.006

Horkel, A. D., Neubauer, W., Niedermayer, G., Okelo, R. E., Wachira, J. K., & Werneck, W. (1984). Notes on the Geology and Mineral Resources of the Southern Kenyan Coast. *Mitteilungen Der Österreichischen Geologischen Gesellschaft*, *77*, 151–159. Retrieved from http://www2.uibk.ac.at/downloads/oegg/Band_77_151_159.pdf

Horta, A., Malone, B., Stockmann, U., Minasny, B., Bishop, T. F. A., McBratney, A. B., … Pozza, L. (2015). Potential of integrated field spectroscopy and spatial analysis for enhanced assessment of soil contamination: A prospective review. *Geoderma*, *241–242*, 180–209. https://doi.org/10.1016/j.geoderma.2014.11.024

Hou, X., & Roos, P. (2008). Critical comparison of radiometric and mass spectrometric methods for the determination of radionuclides in environmental, biological and nuclear waste samples. *Analytica Chimica Acta*, *608*(2), 105–139. https://doi.org/10.1016/j.aca.2007.12.012

Houk, R. S. (1986). Mass Spectrometry of Inductively Coupled Plasmas. *Analytical Chemistry*, *58*(1), 97A-105A. https://doi.org/10.1021/ac00292a003

Hu, K., Clemons, P. S., & Houk, R. S. (1993). Inductively coupled plasma mass spectrometry with an enlarged sampling orifice and offset ion lens. II. Polyatomic Ion interferences and matrix effects. *Journal of the American Society for Mass Spectrometry*, *4*(1), 28–37. https://doi.org/10.1016/1044-0305(93)85039-Z

Hu, G., Bakhtavar, E., Hewage, K., Mohseni, M., & Sadiq, R. (2019). Heavy metals risk assessment in drinking water: An integrated probabilistic-fuzzy approach.

Journal of Environmental Management, *250*(July), 109514.
https://doi.org/10.1016/j.jenvman.2019.109514

Huang, S., Peng, B., Yang, Z., Chai, L., Xu, Y., & Su, C. (2009). Spatial distribution
of chromium in soils contaminated by chromium-containing slag. *Transactions
of Nonferrous Metals Society of China (English Edition)*, *19*(3), 756–764.
https://doi.org/10.1016/S1003-6326(08)60346-5

Humsa, T. Z., & Srivastava, R. K. (2015). Impact of Rare Earth Mining and
Processing on Soil and Water Environment at Chavara, Kollam, Kerala: A Case
Study. *Procedia Earth and Planetary Science*, *11*, 566–581.
https://doi.org/10.1016/j.proeps.2015.06.059

ISO. (2007). *Measurement of radioactivity in te environment -Soils, Part 2: Guidance
for the selection of the sampling strategy, sampling and pre-treatment of
samples.* (No. 18589–2). *ISO 18589-2:2007(E)*. Geneva.

Izbicki, J. A., Wright, M. T., Seymour, W. A., McCleskey, R. B., Fram, M. S., Belitz,
K., & Esser, B. K. (2015). Cr(VI) occurrence and geochemistry in water from
public-supply wells in California. *Applied Geochemistry*, *63*, 203–217.
https://doi.org/10.1016/j.apgeochem.2015.08.007

Järup, L., Elinder, C. G., Hellström, L., Alfvén, T., Carlsson, M. D., Grubb, A., …
Schütz, A. (2000). Low level exposure to cadmium and early kidney damage:
The OSCAR study. *Occupational and Environmental Medicine*, *57*(10), 668–
672. https://doi.org/10.1136/oem.57.10.668

JICA. (1991). *Report on the mineral exploration in Mombasa Area Republic of Kenya
(Phase I).*

Jiménez-Oyola, S., Chavez, E., García-Martínez, M. J., Ortega, M. F., Bolonio, D.,
Guzmán-Martínez, F., … Romero, P. (2021). Probabilistic multi-pathway human
health risk assessment due to heavy metal(loid)s in a traditional gold mining area
in Ecuador. *Ecotoxicology and Environmental Safety*, *224*.
https://doi.org/10.1016/j.ecoenv.2021.112629

Johansson, L. Y. (2008). *Determination of Pb-210 and Po-210 in aqueous
environmental samples*. PhD Thesis: University of Hannover.

Joint FAO/IAEA. (2018). *Sampling and Isotope analysis of agricultural pollutants in
water* (No. IAEA-TECDOC-1850). Vienna, Austria.

Jurgens, B. C., Parkhurst, D. L., & Belitz, K. (2019). Assessing the Lead Solubility
Potential of Untreated Groundwater of the United States. *Environmental Science*

and *Technology*, *53*, 3095–3103. https://doi.org/10.1021/acs.est.8b04475

Kabata-Pendias, A. (2010). *Trace elements in soils and plants: Fourth edition. Trace Elements in Soils and Plants, Fourth Edition* (4th ed.). Boca Raton, USA: Taylor & Francis Group, LLC. https://doi.org/10.1201/b10158

Kabata-Pendias, A., & Mukherjee, A. B. (2007). *Trace Elements from Soil to Human*. Springer.

Kadar, A., Noël, L., Chekri, R., Vastel, C., Millour, S., & Guérin, T. (2011). Optimisation of ICP-MS collision/reaction cell conditions for the determination of elements likely to be interfered (V, Cr, Fe, Co, Ni, As and Se) in foodstuffs. *Talanta*, *85*(5), 2605–2613. https://doi.org/10.1016/j.talanta.2011.08.027

Kamachi, M. U., Sridhar, T. M., & Baldev, R. A. J. (2003). Corrosion of bio implants. *Sadhana - Academy Proceedings in Engineering Sciences*, *28*(3–4), 601–637. https://doi.org/10.1007/BF02706450

Kamunda, C., Mathuthu, M., & Madhuku, M. (2016). Health risk assessment of heavy metals in soils from witwatersrand gold mining basin, South Africa. *International Journal of Environmental Research and Public Health*, *13*(7). https://doi.org/10.3390/ijerph13070663

Kaniu, M. I., Angeyo, H. K., Darby, I. G., & Muia, L. M. (2018). Rapid in-situ radiometric assessment of the Mrima-Kiruku high background radiation anomaly complex of Kenya. *Journal of Environmental Radioactivity*, *188*, 47–57. https://doi.org/10.1016/j.jenvrad.2017.10.014

Kaniu, M. I., Angeyo, K. H., & Darby, I. G. (2018). Occurrence and multivariate exploratory analysis of the natural radioactivity anomaly in the south coastal region of Kenya. *Radiation Physics and Chemistry*. https://doi.org/10.1016/j.radphyschem.2018.01.009

Kaniu, M. I., Darby, I. G., & Angeyo, H. K. (2019). Assessment and mapping of the high background radiation anomaly associated with laterite utilization in the south coastal region of Kenya. *Journal of African Earth Sciences*, *160*(May), 103606. https://doi.org/10.1016/j.jafrearsci.2019.103606

Kazapoe, R. W., Amuah, E. E. Y., & Dankwa, P. (2022). Sources and pollution assessment of trace elements in soils of some selected mining areas of southwestern Ghana. *Environmental Technology and Innovation*, *26*, 102329. https://doi.org/10.1016/j.eti.2022.102329

Kebwaro, J. M., Rathore, I. V. S., Hashim, N. O., & Mustapha A. O. (2011).

Radiometric assessment of natural radioactivity levels around Mrima Hill , Kenya. *International Journal of Physical Sciences*, *6*(13), 3105–3110. https://doi.org/10.5897/IJPS11.052

Kilavi, P. K., Kaniu, M. I., Patel, J. P., & Usman, I. T. (2021). Quality and human health risk assessment of uranium and other heavy metals in drinking water from Kwale County, Kenya. *Environmental Monitoring and Assessment*, *193*(11), 1–20. https://doi.org/10.1007/s10661-021-09466-4

Koppenaal, D. W., Eiden, G. C., & Barinaga, C. J. (2004). Collision and reaction cells in atomic mass spectrometry : development , status , and applications. *J. Anal. At. Spectrom*, 561–570.

Kowalska, J. B., Mazurek, R., Gąsiorek, M., & Zaleski, T. (2018). Pollution indices as useful tools for the comprehensive evaluation of the degree of soil contamination–A review. *Environmental Geochemistry and Health*, *40*(6), 2395–2420. https://doi.org/10.1007/s10653-018-0106-z

Kubier, A., & Pichler, T. (2019). Cadmium in groundwater − A synopsis based on a large hydrogeochemical data set. *Science of the Total Environment*, *689*, 831–842. https://doi.org/10.1016/j.scitotenv.2019.06.499

Kubier, A., Wilkin, R. T., & Pichler, T. (2019). Cadmium in soils and groundwater: A review. *Applied Geochemistry*, *108*(February). https://doi.org/10.1016/j.apgeochem.2019.104388

Kurttio, Paivi, Auvinen, A., Salonen, L., Saha, H., Pekkanen, J., & Komulainen, H. (2002). Renal Effects of Uranium in Drinking Water. *Environmental Health Perspectives*, *110*(4), 337–342.

Kurttio, Päivi, Komulainen, H., Leino, A., Salonen, L., Auvinen, A., & Saha, H. (2005). Bone as a possible target of chemical toxicity of natural uranium in drinking water. *Environmental Health Perspectives*, *113*(1), 68–72. https://doi.org/10.1289/ehp.7475

Lamble, J. K., & Hill, J. S. (1998). Critical Review Microwave digestion procedures for environmental matrices, *123*(July).

Lariviere, D., Taylor, V. F., Evans, R. D., & Cornett, R. J. (2006). Radionuclide determination in environmental samples by inductively coupled plasma mass spectrometry. *Spectrochimica Acta - Part B*, *61*(8), 877–904. https://doi.org/10.1016/j.sab.2006.07.004

Lecomte, J. F., Shaw, P., Liland, A., Markkanen, M., Egidi, P., Andresz, S., …

Mundigl, S. (2019). *ICRP Publication 142: Radiological Protection from Naturally Occurring Radioactive Material (NORM) in Industrial Processes*. *Annals of the ICRP* (Vol. 48). https://doi.org/10.1177/0146645319874589

Lee, D., Skrable, K. W., & French, C. S. (1997). Reevaluation of the committed dose equivalent from Th-232 and its radioactive progeny. *Health Physics*, *72*(4), 579–593. https://doi.org/10.1097/00004032-199704000-00010

Lee, M., Lee, H., Robert, J., & Herd, P. (2022). Effect of childhood proximity to lead mining on late life cognition. *SSM - Population Health*, *17*, 1–9. https://doi.org/10.1016/j.ssmph.2022.101037

Li, Y., Wang, H., Yu, J., Yan, Q., Hu, H., Zhang, L., … Ke, S. (2020). An assessment of sensitivity biomarkers for urinary cadmium burden. *BMC Nephrology*, *21*(1), 1–8. https://doi.org/10.1186/s12882-020-02036-9

Li, Z., Ma, Z., van der Kuijp, T. J., Yuan, Z., & Huang, L. (2014). A review of soil heavy metal pollution from mines in China: Pollution and health risk assessment. *Science of the Total Environment*, *468–469*, 843–853. https://doi.org/10.1016/j.scitotenv.2013.08.090

Linge, K. L. and, & Kym, E. J. (2009). Quadrupole ICP-MS: Introduction to instrumentation, measurement techniques and analytical capabilities. *Geostandards and Geoanalytical Research*, *33*(4), 445–467. https://doi.org/10.1111/j.1751-908X.2009.00039.x

Linge, K. L., & Jarvis, K. E. (2009). Quadrupole ICP-MS : Introduction to Instrumentation , Measurement Techniques and Analytical Capabilities. *Geostandards and Geoanalytical Research*, *33*(4), 445–467.

Linos, A., Petralias, A., Christophi, C. A., Christoforidou, E., Kouroutou, P., Stoltidis, M., … Karagas, M. R. (2011). Oral ingestion of hexavalent chromium through drinking water and cancer mortality in an industrial area of Greece - An ecological study. *Environmental Health*, *10*(1), 50. https://doi.org/10.1186/1476-069X-10-50

Lottermoser, B. G. (2010). *Mine Wastes: Characterization, treatment and environmental impacts* (3 ed.). Heidelberg: Springer-Verlag Berlin. https://doi.org/10.1007/978-3-642-12419-8

Loukola-Ruskeeniemi, K., Müller, I., Reichel, S., Jones, C., Battaglia-Brunet, F., Elert, M., … Valkama, H. (2022). Risk management for arsenic in agricultural soil – water systems : lessons learned from case studies in Europe. *Journal of*

Hazardous Materials, *15*(424(Pt D)). https://doi.org/10.1016/j.jhazmat.2021.127677

Lu, X., Wang, L., Li, L. Y., Lei, K., Huang, L., & Kang, D. (2010). Multivariate statistical analysis of heavy metals in street dust of Baoji, NW China. *Journal of Hazardous Materials*, *173*(1–3), 744–749. https://doi.org/10.1016/j.jhazmat.2009.09.001

Lyu, S., Wei, X., Chen, J., Wang, C., Wang, X., & Pan, D. (2017). Titanium as a beneficial element for crop production. *Frontiers in Plant Science*, *8*, 1–19. https://doi.org/10.3389/fpls.2017.00597

Ma, M., Wang, R., Xu, L., Xu, M., & Liu, S. (2020). Emerging health risks and underlying toxicological mechanisms of uranium contamination: Lessons from the past two decades. *Environment International*, *145*, 106107. https://doi.org/10.1016/j.envint.2020.106107

Ma, Minghao, Wang, R., Xu, L., Xu, M., & Liu, S. (2020). Emerging health risks and underlying toxicological mechanisms of uranium contamination : Lessons from the past two decades. *Environment International*, *145*, 106107. https://doi.org/10.1016/j.envint.2020.106107

Magill, J., & Galy, J. (2005). *Radioactivity, Radionuclides, Radiation*. Springer Berlin Heidelberg and European Communities.

Maina, D. M., Ndirangu, D. M., Mangala, M. M., Boman, J., Shepherd, K., & Gatari, M. J. (2016). Environmental implications of high metal content in soils of a titanium mining zone in Kenya. *Environmental Science and Pollution Research*, *23*(21), 21431–21440. https://doi.org/10.1007/s11356-016-7249-1

Manna, A., & Maiti, R. (2017). Geochemical contamination in the mine affected soil of Raniganj Coalfield – A river basin scale assessment Geoscience Frontiers Geochemical contamination in the mine affected soil of Raniganj Coal fi eld e A river basin scale assessment. *Geoscience Frontiers*, *9*(5), 1577–1590. https://doi.org/10.1016/j.gsf.2017.10.011

Martin, J. E. (2006). *Physics for Radiation Protection*. Wiley-VCH.

Martin, R., Dowling, K., Pearce, D., Sillitoe, J., & Florentine, S. (2014). Health Effects Associated with Inhalation of Airborne Arsenic Arising from Mining Operations. *Geosciences*, *4*, 128–175. https://doi.org/10.3390/geosciences4030128

Mathuthu, M., Kamunda, C., & Madhuku, M. (2016). Modelling of radiological

health risks from gold mine tailings in wonderfonteinspruit catchment area, South Africa. *International Journal of Environmental Research and Public Health*, *13*(6). https://doi.org/10.3390/ijerph13060570

McNulty, G. S. (2007). Production of titanium dioxide. *Proc. Conf. Seville, Spain*, 1–16. https://doi.org/US 2559638 A

Milton, H. A., Smith, W., Rahman, B., Hasan, Z., Dear, K., Rakibuddin, M., … Keith, K. I. (2005). Linked references are available on JSTOR for this article : Chronic Arsenic Exposure and Adverse Pregnancy Outcomes in Bangladesh. *Epidemiology*, *16*(1), 82–86. https://doi.org/10.1097/01.ede.0000147105.94041.e6

Ministry of Energy and Petroleum. (2015). *National Energy and Petroleum Policy*. *Government of the Republic of Kenya*.

Ministry of Mining. (2013). *Sector Plan for Oil and other minerls 2013-2017*. *Government of the Republic of Kenya*.

Mwashinga, E., Ojwang, L., & Mwaguni, S. (2019). Land-Based Activities as Pollution Sources on Fresh Water Resources: A Case Study of Selected Heavy Metal Contamination in River Mukurumudzi, Kwale County. *Kenya Acquatica Journal*, *5*(01), 19–27. Retrieved from http://41.89.141.8/kmfri/handle/123456789/1428

Mwesigye, A. R., & Tumwebaze, S. B. (2017). Water contamination with heavy metals and trace elements from Kilembe copper mine and tailing sites in Western Uganda; implications for domestic water quality. *Chemosphere*, *169*, 281–287. https://doi.org/10.1016/j.chemosphere.2016.11.077

Nabhani, K. A. L., Khan, F., & Yang, M. (2016). Technologically Enhanced Naturally Occuring Radioactive Materials in oil and gas production : A silet killer. *Process Safety and Environmental Protection*, *99*, 237–247. https://doi.org/10.1016/j.psep.2015.09.014

Nandutu, M., & Kim, J. (2021). Radiological dose assessment of the landfill disposal of consumer products containing naturally occurring radioactive materials in south korea. *Applied Sciences*, *11*(7172), 1–16. https://doi.org/10.3390/app11157172

National Research Council. (1994). *Science and judgment in risk assessment*. *Environmental Health Perspectives* (Vol. 102). Washington, DC: National Academies Press. https://doi.org/10.1289/ehp.94102908

National Research Council. (2000). *Copper in Drinking Water*. *Copper in Drinking Water*. Washington, DC: The National Acedemies Press. https://doi.org/10.17226/9782

Niu, H. (1994). *Fundamental studies of the plasma extraction and ion beam formation processes in inductively coupled plasma mass spectrometry*. Iowa State University.

Niu, H. S., & Houk, R. S. (1996). Fundamental aspects of ion extraction in ICP-MS. *Spectrochimica Acta*, *51*(B), 779–815.

Njuki, H. M., Okoth, O. N., Kinyanjui, S. N., Macharia, J. M., & Wandera, J. O. (2014). Socio – Economic Baseline Survey For Proposed Mining Of Niobium And Rare Earth Elements At Mrima Hill, Kwale. *Journal of Economics and Sustainable Development*, *5*(12), 176–185.

O'Connor, G., & Evans, E. H. (2007). Fundamental Aspects of Inductively Coupled Plasma-Mass Spectrometry (ICP-MS). In J. S. Hill (Ed.), *Inductively Coupled Plasma Spectrometry and its Applications* (Second, pp. 134–157). Oxford: Blackwell Publishing.

O'Neal, S. L., & Zheng, W. (2015). Manganese toxicity upon overexposure: A decade in Review. *Curr Envion Health Rep*, *2*(3), 1–24. https://doi.org/10.1007/s40572-015-0056-x.Manganese

O'Regan, B., & Gratzel, M. (1991). A low-cost, high-efficiency solar cell based on dye-sensitized colloidal TiO2 films. *Nature*, *354*, 737–740.

Odongo, W. O. G., Hashim, N., & Chege, M. W. (2021). Gamma Ray Spectrometric Analysis of Sand Samples from Selected Beaches along Kenyan Coastline. *Scientific World Journal*, *2021*, 1–8. https://doi.org/10.1155/2021/6621645

Osoro, M. K., Rathore, I. V., S, Mangala, M. J., & Mustapha, A., O. (2011). Radioactivity in Surface Soils Around the Proposed Sites for Titanium Mining Project in Kenya. *Journal of Environmental Protection*, *02*(04), 460–464. https://doi.org/10.4236/jep.2011.24053

Oulhote, Y., Mergler, D., Bellinger, D. C., Bouffard, T., Brodeur, M.-È. B., Saint-Amour, D., … Bouchard, M. F. (2016). Effects of manganese exposure on visuoperception and visual memory in schoolchildren. *NeuroToxicology*, *57*(12), 230–240. https://doi.org/10.1016/j.neuro.2016.10.006

Oze, C., Bird, D. K., & Fendorf, S. (2007). Genesis of hexavalent chromium from natural sources in soil and groundwater. *Environmental Science*, *104*(16), 6544–

6549.

Pappas, S. R. (2012). Sample preparation problem solving for inductively coupled plasma-mass spectrometrywith liquid introduction system I. solubility, chelation, and memory effects. *Spectroscopy(Springf)*, *176*(5), 20–31. https://doi.org/10.1016/j.physbeh.2017.03.040

Patel, J. P. (1991). Environmental Radiation Survey of the Area of High Natural Radioactivity of Mrima Hill of Kenya. *Discovery and Innovation*, *3*(3), 31–35.

Patel, J. P., & Mangala, M. J. (1994). Elemental analysis of carbonatite samples from Mrima Hill, Kenya, by energy dispersive x-ray fluorescence (EDXRF). *Nuclear Geophysics*, *8*(4), 389–393.

Phaniendra, A., Jestadi, D. B., & Periyasamy, L. (2015). Free Radicals: Properties, Sources, Targets, and Their Implication in Various Diseases. *Indian Journal of Clinical Biochemistry*, *30*(1), 11–26. https://doi.org/10.1007/s12291-014-0446-0

Pietrini, F., Carnevale, M., Beni, C., Zacchini, M., Gallucci, F., & Santangelo, E. (2019). Effect of different copper levels on growth and morpho-physiological parameters in giant reed (Arundo donax L.) in semi-hydroponic mesocosm experiment. *Water*, *11*(9), 1–19. https://doi.org/10.3390/w11091837

Pinkerton, L. E., Bloom, T. F., Hein, M. J., & Ward, E. M. (2004). Mortality among a cohort of uranium mill workers: an update. *Occupational and Environmental Medicine*, (2), 57–64.

Pokhrel, L. R., & Dubey, B. (2013). Global scenarios of metal mining, environmental repercussions, public policies, and sustainability: A review. *Critical Reviews in Environmental Science and Technology*, *43*(21), 2352–2388. https://doi.org/10.1080/10643389.2012.672086

Pourrut, B., Shahid, M., Dumat, C., Winterton, P., & Pinelli, E. (2011). Lead Uptake, Toxicity, and Detoxification in Plants. *Reviews of Environmental Contamination and Toxicology*, *213*, 113–136. https://doi.org/10.1007/978-1-4419-9860-6

Prise, K. M., & O'Sullivan, J. M. (2009). Radiation-induced bystander signalling in cancer therapy. *Nature Reviews Cancer*, *9*(5), 351–360. https://doi.org/10.1038/nrc2603

Prousek, J. (2007). Fenton chemistry in biology and medicine. *Pure and Applied Chemistry*, *79*(12), 2325–2338. https://doi.org/10.1351/pac200779122325

Qu, C., Sun, K., Wang, S., Huang, L., & Bi, J. (2012). Monte Carlo Simulation-Based Health Risk Assessment of Heavy Metal Soil Pollution: A Case Study in the

Qixia Mining Area, China. *Human and Ecological Risk Assessment*, *18*(4), 733–750. https://doi.org/10.1080/10807039.2012.688697

Raghavendra, T., Ramakrishna, S. U. B., Srinivasulu, D., Vijayalakshmi, T., Himabindu, V., & Arunachalam, J. (2020). Risk assessment due to intake of trace metals through the ingestion of groundwater around proposed uranium mining areas of Nalgonda district, Telangana, India. *Applied Water Science*, *10*(1), 1–6. https://doi.org/10.1007/s13201-019-1089-3

Ramasamy, V., Sundarrajan, M., Suresh, G., Paramasivam, K., & Meenakshisundaram, V. (2014). Role of light and heavy minerals on natural radioactivity level of high background radiation area, Kerala, India. *Applied Radiation and Isotopes*, *85*, 1–10. https://doi.org/10.1016/j.apradiso.2013.11.119

Rashed, M. N. (2010). Monitoring of contaminated toxic and heavy metals, from mine tailings through age accumulation, in soil and some wild plants at Southeast Egypt. *Journal of Hazardous Materials*, *178*(1–3), 739–746. https://doi.org/10.1016/j.jhazmat.2010.01.147

Rehman, I. ur, Ishaq, M., Ali, L., Khan, S., Ahmad, I., Din, I. U., & Ullah, H. (2018). Enrichment, spatial distribution of potential ecological and human health risk assessment via toxic metals in soil and surface water ingestion in the vicinity of Sewakht mines, district Chitral, Northern Pakistan. *Ecotoxicology and Environmental Safety*, *154*, 127–136. https://doi.org/10.1016/j.ecoenv.2018.02.033

Reimann, P., & Filzmoser, C. (1999). Normal and lognormal data distribution in geochemistry : death of a myth . Consequences for the statistical treatment of geochemical and environmental data. *Enviromental Geology*, *39*(9), 1001–1014.

Rivera-Velasquez, M. F., Fallico, C., Guerra, I., & Straface, S. (2013). A Comparison of deterministic and probabilistic approaches for assessing risks from contaminated aquifers: An Italian case study. *Waste Management and Research*, *31*(12), 1245–1254. https://doi.org/10.1177/0734242X13507305

Roos, P. (2008). Analysis of radionuclides using ICP-MS. *Radioactivity in the Environment*, *11*(07), 295–330. https://doi.org/10.1016/S1569-4860(07)11009-3

Rump, A., Eder, S., Lamkowski, A., Hermann, C., Abend, M., & Port, M. (2019). A quantitative comparison of the chemo- and radiotoxicity of uranium at different enrichment grades. *Toxicology Letters*, *313*(June), 159–168. https://doi.org/10.1016/j.toxlet.2019.07.004

Saha, N., Rahman, M. S., Ahmed, M. B., Zhou, J. L., Ngo, H. H., & Guo, W. (2017). Industrial metal pollution in water and probabilistic assessment of human health risk. *Journal of Environmental Management*, *185*, 70–78. https://doi.org/10.1016/j.jenvman.2016.10.023

Searle, A. K., Baghurst, P. A., Hooff, M. Van, Sawyer, M. G., Sim, M. R., Galletly, C., … Mcfarlane, A. C. (2014). Tracing the long-term legacy of childhood lead exposure : A review of three decades of the Port Pirie Cohort study. *Neurotoxicology*, *43*, 46–56. https://doi.org/10.1016/j.neuro.2014.04.004

Shabaan, D. (2018). *Natural Radioactivity Studies , Uranium source Depth , Radon Diffusion*. PhD Thesis: Ain Shams University.

Shahid, M., Ferrand, E., Schreck, E., & Dumat, C. (2013). Behavior and impact of zirconium in the soil-plant system: Plant uptake and phytotoxicity. *Reviews of Environmental Contamination and Toxicology*, *221*, 107–127. https://doi.org/10.1007/978-1-4614-4448-0_2

Sharma, A., Kapoor, D., Wang, J., Shahzad, B., Kumar, V., Bali, A. S., … Yan, D. (2020). Chromium bioaccumulation and its impacts on plants: An overview. *Plants*, *9*(1), 1–17. https://doi.org/10.3390/plants9010100

Sharma, P., Bihari, V., Agarwal, S. K., Verma, V., Kesavachandran, C. N., Pangtey, B. S., … Goel, S. K. (2012). Groundwater Contaminated with Hexavalent Chromium [Cr (VI)]: A Health Survey and Clinical Examination of Community Inhabitants (Kanpur, India). *PLoS ONE*, *7*(10), 3–9. https://doi.org/10.1371/journal.pone.0047877

Shhub, A. N. (2021). Assessment of Cs-137, Am-241, and Cf-252 in Well Logging. *Health Physics*, *121*(1), 7–17. https://doi.org/10.1097/HP.0000000000001404

Shtangeeva, I., Lin, X., Tuerler, A., Rudneva, E., Surin, V., & Henkelmann, R. (2006). Thorium and uranium uptake and bioaccumulation by wheat-grass and plantain. *Forest Snow and Landscape Research*, *80*(2), 181–190.

Simon, S. L. (1998). Soil ingestion by humans: A review of history, data, and etiology with application to risk assessment of radioactively contaminated soil. *Health Physics*, *74*(6), 647–672. https://doi.org/10.1097/00004032-199806000-00003

Smith, A. H., Marshall, G., Roh, T., Ferreccio, C., Liaw, J., & Steinmaus, C. (2018). Lung , Bladder , and Kidney Cancer Mortality 40 Years After Arsenic Exposure Reduction. *JNCI J Natl Cancer Inst*, *110*(3), 241–249. https://doi.org/10.1093/jnci/djx201

Smith, R. L. (1994). Use of Monte Carlo Simulation for Human Exposure Assessment at a Superfund Site. *Risk Analysis*, *14*(4), 433–439. https://doi.org/10.1111/j.1539-6924.1994.tb00261.x

Surdu, S., Fitzgerald, E. F., Bloom, M. S., Boscoe, F. P., Carpenter, D. O., Goessler, W., … Fletcher, T. (2013). Occupational exposure to arsenic and risk of nonmelanoma skin cancer in a multinational European study. *International Journal of Cancer*, *2191*, 2182–2191. https://doi.org/10.1002/ijc.28216

Sutliff-Johansson, S., Pontér, S., Engström, E., Rodushkin, I., Peltola, P., & Widerlund, A. (2021). Tracing anthropogenic sources of Tantalum and Niobium in Bothnian Bay sediments , Sweden. *Journal of Soils and Sediments*, *21*, 1488–1503.

Swaran, J. S. F., Govinder, F., & Geetu, S. (2006). Environmental occurrence, health effects and management of lead poisoning. In S. C. Jose & S. Jose (Eds.), *Lead: Chemistry, Analytical Aspects, Environmental Impact and Health Effects* (1st ed., pp. 158–228). Elsevier.

Takeda, A. (2003). Manganese action in brain function. *Brain Research Reviews*, *41*(1), 79–87. https://doi.org/10.1016/S0165-0173(02)00234-5

Taylor, A. A., Tsuji, J. S., Garry, M. R., Mcardle, M. E., Goodfellow, W. L., Adams, W. J., & Menzie, C. A. (2020). Critical Review of Exposure and Effects : Implications for Setting Regulatory Health Criteria for Ingested Copper. *Environmental Management*, *65*, 131–159. https://doi.org/10.1007/s00267-019-01234-y

Taylor, H. E. (2001). Inductively coupled plasma-mass spectrometry: Practices and Techniques. *Journal of Chemical Education*. Academic Press. https://doi.org/10.1021/ed078p1465

Tchounwou, P. B., Yedjou, C. G., Patlolla, A. K., & Sutton, D. J. (2012). Heavy Metals Toxicity and the Environment. *EXS*, *101*, 133–164. https://doi.org/10.1007/978-3-7643-8340-4

Timofeev, I., Kosheleva, N., & Kasimov, N. (2019). Health risk assessment based on the contents of potentially toxic elements in urban soils of Darkhan, Mongolia. *Journal of Environmental Management*, *242*(December 2018), 279–289. https://doi.org/10.1016/j.jenvman.2019.04.090

Tolins, M., Ruchirawat, M., & Landrigan, P. (2014). The Developmental Neurotoxicity of Arsenic : Cognitive and Behavioral Consequences of Early Life

Exposure. *Annals of Global Health*, *80*(4), 303–314.
https://doi.org/10.1016/j.aogh.2014.09.005

Tsai, S., Chou, H., The, H., Chen, C., & Chen, C. (2003). The Effects of Chronic
Arsenic Exposure from Drinking Water on the Neurobehavioral Development in
Adolescence. *Neurotoxicology*, *24*, 747–753. https://doi.org/10.1016/S0161-
813X(03)00029-9

UNSCEAR. (2000). *Sources and Effects of Ionizing Radiation. Report to the General
Assembly with Scientific Annexes* (Vol. I). New York: United Nations.

US-EPA Method 3051A. (2007). Microwave assisted acid digestion of sediments,
sludges, soils and oils. In *Test Methods for Evaluating Solid wastes* (3rd Ed., pp.
1–30). US Environmenta Protection Agency, Washington USA.

US DA. (2018). *Determination of Metals by ICP-MS and ICP-OES (Optical Emission
Spectrometry)* (No. CLG-TM3. 06).

US DOE. (2011). *The risk assessment information system (RAIS)*.
https://doi.org/10.1007/s12665-019-8198-z

USEPA. (1989). *Risk Assessment Guidance for Superfund Volume I Human Health
Evaluation Manual (Part A)* (Vol. I). Washington, DC.

USEPA. (1992). *Guidelines for Exposure Assessment* (57(104):22888-22938 No.
EPA/600/Z-92/001) (Vol. 57). Washington, DC.

USEPA. (2009). *Risk Assessment Guidance for Superfund Volume I: Human Health
Evaluation Manual (Part A). US.EPA* (Vol. I). https://doi.org/EPA-540-R-070-
002

USEPA. (2018). *2018 Edition of the Drinking Water Standards and Health Advisories
Tables* (No. EPA 822-F-18-001). Washington, DC.

Valko, M., Morris, H., & Cronin, M. T. D. (2005). Metals, Toxicity and Oxidate
Stress. *Science of the Total Environment*, *12*, 1161–1208. Retrieved from
http://dx.doi.org/10.1016/j.scitotenv.2013.11.032%0Ahttps://doi.org/10.1016/j.e
nvres.2019.108854%0Ahttp://dx.doi.org/10.1016/j.placenta.2009.02.007%0Ahtt
ps://doi.org/10.1016/j.envint.2020.105518%0Ahttps://doi.org/10.1016/j.scitotenv
.2019.134798%0Ahttp://d

Van Gosen, B. S., Fey, D. L., A.K., S., Verplanck, P. L., & Hoefen, T. M. (2014).
*Deposit Model for Heavy-Mineral Sands in Coastal Environments: U.S.
Geological Survey Investigations Report 2000-5070-L. Mineral Deposit Models
for Resource Assessment*. Reston, Virginia. https://doi.org/10.3133/sir20105070L

Vanhaeck, F., Balcaen, L., & Taylor, P. (2007). Use of ICP-MS for Isotope Ratio Measurements. In S. J. Hill (Ed.), *Inductively Coupled Plasma Spectrometry and its Applications* (2 nd, pp. 160–215). Blackwell Publishing.

Vanhaecke, F., Vanhoe, H., Dams, R., & Vandecasteele, C. (1992). The use of internal standards in ICP-MS. *Talanta*. https://doi.org/10.1016/0039-9140(92)80088-U

Verplanck, P. L., Van Gosen, B. S., Seal, R. P., & McCaffery, A. E. (2014). A Deposit Model for Carbonatite and Peralkaline Intrusion-Related Rare Earth Element Deposits. In *Mineral Deposit Models for Resource Assessment* (p. 25). Virginia: U.S. Geological Survey Scientific Investigations Report 2010-5070. https://doi.org/10.3133/sir29195979J

Virakornphanich, P., Matsue, N., & Yoshinaga, N. (1991). Clay mineralogy of a Reddish Brown Lateritic soil from Thailand Clay Mineralogy of a Reddish Brown Lateritic Soil from Thailand. *Soil Science and Plant Nutrition*, *37*(1), 175–178. https://doi.org/10.1080/00380768.1991.10415025

von Ehrenstein, O. S., Poddar, S., Yuan, Y., Mazumder, D. G., Eskenazi, B., Basu, A., … Smith, A. H. (2007). Children ' s Intellectual Function in Relation to Arsenic Exposure. *Epidemiology*, *18*(1), 44–51. https://doi.org/10.1097/01.ede.0000248900.65613.a9

Wang, Z., Qin, H., & Liu, X. (2019). Health risk assessment of heavy metals in the soil-water-rice system around the Xiazhuang uranium mine, China. *Environmental Science and Pollution Research*, *26*(6), 5904–5912. https://doi.org/10.1007/s11356-018-3955-1

Wardman, P., & Candeias, L. P. (1996). Fenton Chemistry : An Fenton Chemistry : An Introduction '. *Radiation Research*, *145*(5), 523–531.

Washburn, S., Arsnow, D., & Harris, R. (1998). Quantifying uncertainty in huma health risk assessment using probabilistic techniques. *Transactions on Ecology and the Environment*, *24*.

WASREB. (2008). *Guidelines on drinking water quality and effluent monitoring*. Nairobi, Kenya.

Wasserman, G. A., Liu, X., Parvez, F., Ahsan, H., Factor-litvak, P., Geen, A. Van, … Graziano, J. H. (2004). Children ' s Health Article Water Arsenic Exposure and Children ' s Intellectual Function in Araihazar ,. *Environmental Health Perspectives*, *112*(13), 1329–1333. https://doi.org/10.1289/ehp.6964

Wasserman, G. A., Liu, X., Parvez, F., Ahsan, H., Levy, D., Factor-Litvak, P., … Graziano, J. H. (2006). Water manganese exposure and children's intellectual function in Araihazar, Bangladesh. *Environmental Health Perspectives*, *114*(1), 124–129. https://doi.org/10.1289/ehp.8030

WHO. (2010). *Harmonization Project Document No. 8. WHO Human Health Risk Assessment TOOLKIT: chemical hazards. IPCS harmonization process*. Retrieved from https://www.who.int/ipcs/methods/harmonization/areas/ra_toolkit/en/

WHO. (2011). *Guidelines for Drinking-water Quality* (4ed.). Geneva, Switzerland: World Health Organization.

Woodruff, L. G., Bedinger, G. M., & Piatak, N. M. (2017). Titanium. In K. J. Schulz, J. H. DeYoung, R. R. Seal II, & D. C. Bradley (Eds.), *Critical Mineral Resources of the United States- Economic and Environmental Geology and Prospects for Future Supply* (pp. 3–36). U.S. Geological Survey, Reston, Virginia.

Wuana, R. A., & Okieimen, F. E. (2011). Heavy Metals in Contaminated Soils: A Review of Sources, Chemistry, Risks and Best Available Strategies for Remediation. *ISRN Ecology*, *2011*, 1–20. https://doi.org/10.5402/2011/402647

Xiao, R., Wang, S., Li, R., Wang, J. J., & Zhang, Z. (2017). Soil heavy metal contamination and health risks associated with artisanal gold mining in Tongguan, Shaanxi, China. *Ecotoxicology and Environmental Safety*, *141*(October 2016), 17–24. https://doi.org/10.1016/j.ecoenv.2017.03.002

Xu, D. M., Zhan, C. L., Liu, H. X., & Lin, H. Z. (2019). A critical review on environmental implications, recycling strategies, and ecological remediation for mine tailings. *Environmental Science and Pollution Research*, *26*(35), 35657–35669. https://doi.org/10.1007/s11356-019-06555-3

Yu, C., Gnanapragasam, E., Biwer, B., Cheng, J. J., Kamboj, S., Klett, T., … Wallo, A. (2009). RESRAD-OFFSITE - A new member of the RESRAD family of codes. *Radioprotection*, *44*(5), 659–664. https://doi.org/10.1051/radiopro/20095121

Yu, C., Loureiro, C., Cheng, J. J., Jones, L. G., Wang, Y. Y., Chia, Y. P., & Faillace, E. (1993). *Data Collection Handbook to Support Modeling Impacts of Radioactive Material In Soil* (No. ANL/EAIS-8). Argonne, IL, USA. Retrieved from https://web.evs.anl.gov/resrad/documents/data_collection_1993.pdf

Yusuf, M., Fariduddin, Q., Hayat, S., & Ahmad, A. (2011). Nickel: An overview of uptake, essentiality and toxicity in plants. *Bulletin of Environmental Contamination and Toxicology*, *86*(1), 1–17. https://doi.org/10.1007/s00128-010-0171-1

Zacharski, L. R., Ornstein, D. L., Woloshin, S., & Schwartz, L. M. (2000). Association of age, sex, and race with body iron stores in adults: Analysis of NHANES III data. *American Heart Journal*, *140*(1), 98–104. https://doi.org/10.1067/mhj.2000.106646

Zack, T., Kronz, A., Foley, S. F., & Rivers, T. (2002). Trace element abundances in rutiles from eclogites and associated garnet mica schists. *Chemical Geology*, *184*(1–2), 97–122. https://doi.org/10.1016/S0009-2541(01)00357-6

Zaman, M., Schubert, M., & Antao, S. (2012). Elevated radionuclide concentrations in heavy mineral-rich beach sands in the Cox's Bazar region, Bangladesh and related possible radiological effects. *Isotopes in Environmental and Health Studies*, *48*(4), 512–525. https://doi.org/10.1080/10256016.2012.696542

Zhang, H., Huang, G. he, & Zeng, G. ming. (2009). Health risks from arsenic-contaminated soil in Flin Flon-Creighton, Canada: Integrating geostatistical simulation and dose-response model. *Environmental Pollution*, *157*(8–9), 2413–2420. https://doi.org/10.1016/j.envpol.2009.03.014

Zhang, X., Yang, H., & Cui, Z. (2018). Evaluation and analysis of soil migration and distribution characteristics of heavy metals in iron tailings. *Journal of Cleaner Production*, *172*, 475–480. https://doi.org/10.1016/j.jclepro.2017.09.277

Zhuang, P., McBride, M. B., Xia, H., Li, N., & Li, Z. (2009). Health risk from heavy metals via consumption of food crops in the vicinity of Dabaoshan mine, South China. *Science of the Total Environment*, *407*(5), 1551–1561. https://doi.org/10.1016/j.scitotenv.2008.10.061

Ziajahromi, S., Khanizadeh, M., & Nejadkoorki, F. (2015). Using the RESRAD Code to Assess Human Exposure Risk to Ra-226, Th-232, and K-40 in Soil. *Human and Ecological Risk Assessment*, *21*(1), 250–264. https://doi.org/10.1080/10807039.2014.909194

Appendices

Appendix A: Radioactive decay processes

Appendix A-1: ^{232}Th decay series
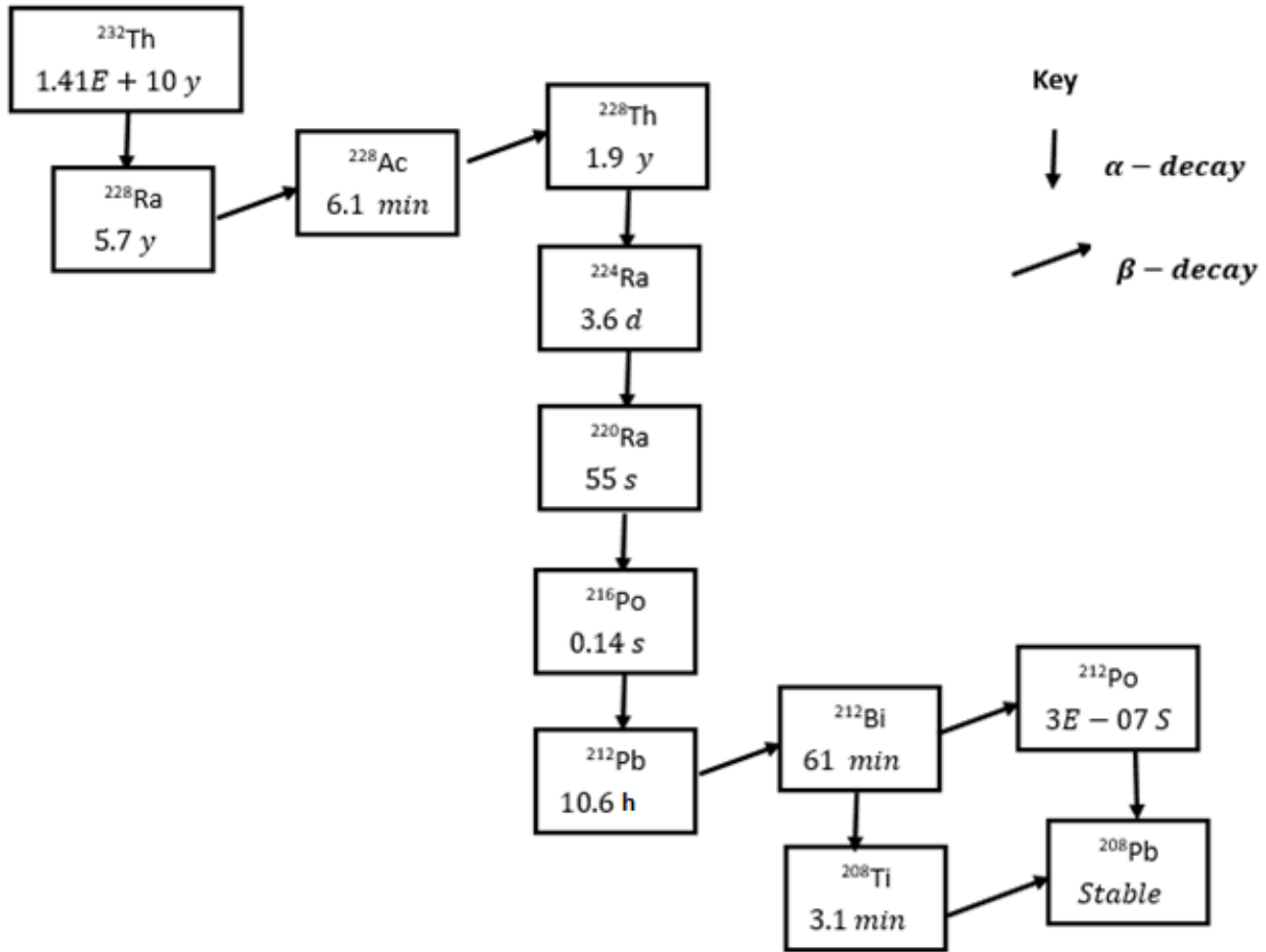
Appendix A-2: 238U decay series

238U
1.45E + 09 y

234tH
24.1 y

234Pa
1.7 min

234U
2.4E + 05 y

230Th
7.7E + 04 y

226Ra
1600 y

222Rn
3.82 d

218Po
3.05 min

214Pb
138.4 d

214Bi
19.9 min

214Po
1.64E − 04 s

210Pb
22.3 y

210Bi
5.0 d

210Po
138.4 d

206Pb
138.4 d

Key

$\alpha - decay$

$\beta - decay$
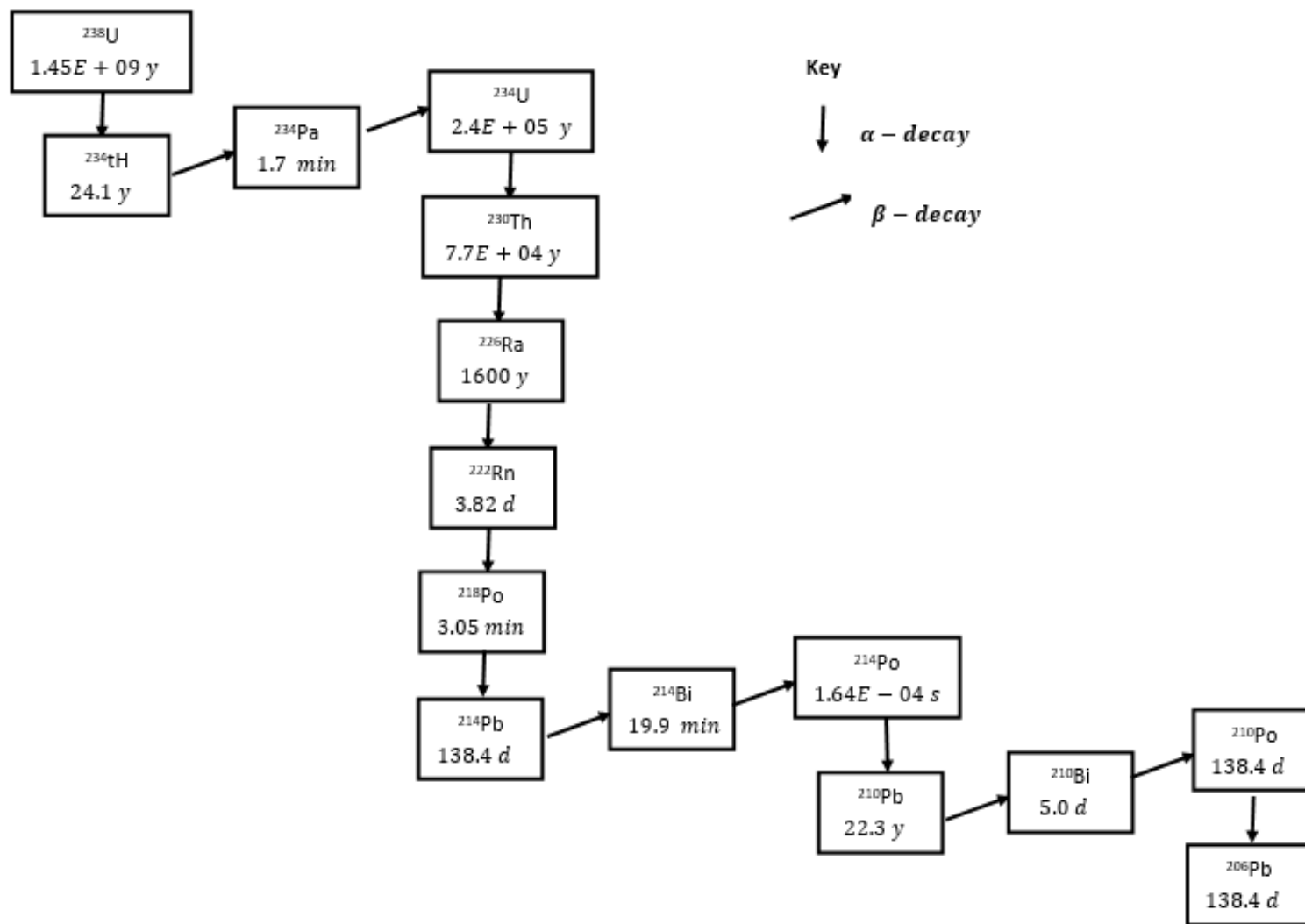
Appendix B: Validation of the analytical method

B-1: Instrumental detection limits of ICP-MS, in ng/kg

Sc	Ti	Cr	Mn	Ni	Cu	Zn	As	Cd	Pb	Th	U
3	4	2	0.2	0.1	0.02	5	2	0.4	0.3	0.03	0.03

B-2: Recovery of analytes in external certified reference materials, CRM

	He collision mode						HEHe collision mode					
	5	**20**	**50**	**100**	**500**	**1000**	**5**	**20**	**50**	**100**	**500**	**1000**
Cr	24029	-4.4	13.2	1233	-54.5	0.7	-2.4	-2.0	-2.1	-0.9	-1.0	1.9
Mn	9456	20.3	22.7	466	2.7	-5.6	2.6	-5.0	-0.7	-1.1	-1.6	2.0
Fe	26480	-0.5	18.0	1391	-65.6	1.8	16.0	-2.8	-0.7	-1.3	-2.4	1.4
Ni	6303	31.1	29.5	272	17.0	-7.2	3.7	-1.2	-0.9	-1.4	-2.6	1.8
Cu	8572	22.9	29.2	394	8.5	-6.4	4.7	-5.2	-1.0	-0.9	-3.0	0.8
As	2836	24.5	35.1	130	33.4	-9.8	-1.7	-4.1	-2.0	-0.5	-1.5	1.7
Cd	3380	171	85.1	141	33.8	-10.2	10.3	0.0	0.6	0.0	-3.7	0.8
Pb	3232	27.1	29.6	136	34.8	-10.2	-1.6	-4.0	-1.3	-0.8	-2.7	0.8
Th	1513	8.9	9.1	193	23.5	-7.9	-2.5	-3.6	-2.0	-1.6	-3.2	1.0
U	2753	25.0	27.4	102	34.3	-9.7	-2.0	-5.4	-1.5	-0.9	-2.4	0.7

B-3: Recovery of analytes in quality control samples

	He collision Mode								HEHe collision mode							
	500	**100**	**50**	**20**	**500**	**100**	**50**	**20**	**500**	**100**	**50**	**20**	**500**	**100**	**50**	**20**
Cr	5.0	-89	17	69	98	91	56	98	0.3	-0.8	1.0	-4.8	1.2	1.0	1.2	-4.4
Mn	1.9	5.1	8.0	48	63	81	2.5	96	0.3	-0.9	2.1	-5.3	1.3	-1.0	2.3	-5.0
Fe	4.0	-141	24	70	99	92	64	99	0.5	-1.3	1.3	-4.2	1.7	-1.4	1.9	-4.9
Ni	1.9	13	1.5	37	93	68	25	93	0.1	-1.0	1.7	-4.6	1.8	-1.0	3.7	-4.9
Cu	1.2	10	7.6	48	80	76	11	95	0.3	-0.6	1.9	-3.6	0.8	-0.8	0.9	-3.0
As	2.1	21	7.3	42	5.1	59	10	88	2.2	-0.8	1.7	-2.9	1.9	-0.8	3.1	-2.5
Cd	3.0	27	29	67	59	48	18	90	3.4	-0.8	1.3	-0.1	0.9	-0.8	3.5	-4.2
Pb	2.6	23	1.7	37	-2.8	56	-1.0	90	5.6	-0.8	21	-5.3	-27	-1.0	-59	-3.8
Th	1.8	10	1.3	17	2.8	64	3.3	90	4.3	-1.2	24	-5.3	-39	-1.1	-70	-4.2
U	1.7	23	1.4	37	-2.1	49	-2.4	87	6.3	-0.7	24	-3.6	-42	-0.8	-75	-5.5

B-4: Absolute relative percent deviation, RPD, of analytes in the selected duplicate samples

	MS1	MS6	MS11	MS16	BS1	BS6	BS12	BW1	BW7	BW14	MW1	MW11	MW19
Cr	0.07	2.49	14.5	3.56	10.9	1.89	6.27	22.9	1.9	-0.40	-10.4	-19.8	-1.96
Mn	5.25	2.14	13.6	5.67	-12.2	-9.27	-9.87	17.0	2.4	2.49	11.3	-6.48	BDL
Fe	0.20	-1.95	12.2	6.39	6.98	3.03	3.38	22.9	-2.36	1.81	-8.66	-20.9	16.8
Ni	-12.2	-11.9	32.2	-3.42	-6.83	-15.4	-10.9	8.41	1.66	-2.84	3.06	12.0	-8.58
Cu	-14.4	-13.6	36.5	-1.93	-11.6	-9.50	-11.9	-13.2	-13.1	-25.7	5.00	-3.25	-1.60
Zn	-10.1	5.17	33.7	-4.24	-11.0	-57.4	-25.1	BDL	BDL	BDL	-62.2	-28.5	16.2
As	-32.1	-9.55	30.0	-28.3	0.04	-7.69	-3.83	23.5	-4.12	-50.7	25.4	27.7	44.2
Cd	5.76	-11.5	6.57	49.4	BDL	BDL	BDL	17.7	-14.3	-5.94	0.45	6.03	72.9
Pb	-7.71	-9.32	31.8	1.58	-16.7	-7.12	-9.10	12.6	9.56	6.17	24.8	5.26	4.87
Th	50.1	-7.47	36.0	0.63	61.4	-13.3	-16.0	51.8	55.0	13.1	BDL	BDL	BDL
U	-9.98	-8.21	-31.4	2.27	BDL	BDL	BDL	23.5	26.8	27.3	12.3	28.5	15.5

B-5: Correlation coefficient, R, values from the calibration curves

Collision Mode	Cr	Mn	Fe	Ni	Cu	As	Cd	Pb	Th	U
He	0.96736	0.98795	0.9862	0.98666	0.98805	0.98965	0.9893	0.98372	0.98883	0.99104
HEHe	0.99992	0.99996	0.99975	0.99979	0.99952	0.99973	0.99919	0.99929	0.99939	0.99921

Appendix C: Distribution of Th, U, and related heavy metals in water and soil samples

C-1: Concentration of Th, U, and other heavy metals, in mg/L, in water samples from the environs of Kwale HMS deposit

	Sc	Ti	Cr	Mn	Fe	Ni	Cu	Zn	As	Cd	Pb	Th	U
BW1	0.00113	0.00071	0.15663	0.01470	0.13996	0.00714	0.00832	0.00744	0.00060	0.07539	0.00369	0.00014	0.00009
BW2	0.00132	0.00093	0.78103	0.24815	1.15789	0.00434	0.00207	0.00335	0.00043	0.06764	0.00292	0.00023	0.00013
BW3	0.00180	0.00225	0.71505	0.06988	1.02288	0.00703	0.00296	0.12685	0.00086	0.07733	0.00292	0.00033	0.00069
BW4	0.00133	0.00194	1.82523	0.06820	2.83946	0.00705	0.00237	0.10111	0.00067	0.06754	0.00808	0.00023	0.00012
BW5	0.00058	0.00262	1.97223	0.53198	3.03758	0.00887	0.00396	0.00335	0.00037	0.07581	0.00260	0.00022	0.00015
BW6	0.00187	0.00490	0.17397	0.03925	0.20142	0.00644	0.00168	0.03836	0.00292	0.06431	0.00677	0.00017	0.00116
BW7	0.00137	0.01415	6.77830	0.27856	10.79162	0.01140	0.00218	0.00335	0.00316	0.08269	0.00225	0.00069	0.00017
BW8	0.00128	0.00588	0.72072	0.35528	1.02546	0.01068	0.00199	0.48141	0.00126	0.12085	0.00220	0.00114	0.00014
BW9	0.00064	0.00841	0.11251	0.01798	0.12672	0.00453	0.00125	0.22532	0.00026	0.06582	0.00333	0.00052	0.00011
BW10	0.00139	0.00258	0.33624	0.08902	0.48128	0.00680	0.00176	0.00336	0.00084	0.06350	0.01152	0.00038	0.00022
BW11	0.00150	0.00125	0.15714	0.00850	0.16133	0.00983	0.00134	2.64618	0.00013	0.08830	0.00193	0.00037	0.00006
BW12	0.00206	0.00495	0.19814	0.03058	0.24616	0.00912	0.00208	0.00981	0.00092	0.09880	0.00246	0.00079	0.00127
BW13	0.00061	0.00142	0.62426	0.12441	0.94950	0.00616	0.00121	0.00335	0.00017	0.08292	0.00154	0.00050	0.00011
BW14	0.00057	0.00027	0.59349	0.31495	0.87107	0.00668	0.00478	0.00910	0.00123	0.08521	0.00243	0.00031	0.00024
BW15	0.00093	0.00162	0.14923	0.08315	0.19680	0.01077	0.00151	0.03404	0.00022	0.08100	0.00195	0.00059	0.00032
BW16	0.00126	0.00319	1.29350	0.58870	2.02754	0.00732	0.00114	0.00335	0.00100	0.09497	0.00172	0.00055	0.00011
BW17	0.00120	0.00176	0.33130	0.14629	0.48451	0.00660	0.00157	0.00335	0.00123	0.09916	0.00186	0.00047	0.00023
BW18	0.00054	0.00260	0.38126	0.09938	0.58722	0.00638	0.00188	0.00335	0.00105	0.11596	0.00185	0.00058	0.00020
BW19	0.00165	0.00356	0.42211	0.10942	0.63342	0.00779	0.00169	0.01684	0.00123	0.13272	0.00358	0.00055	0.00015

C-2: Concentration of Th, U, and other heavy metals, in mg/L, in water samples from the environs of Mrima Hill

	Sc	Ti	Cr	Mn	Fe	Ni	Cu	Zn	As	Cd	Pb	Th	U
MW1	0.00267	0.00618	0.41468	0.19504	0.12602	0.01421	0.00052	0.08822	0.00027	0.11465	0.01530	0.00000	0.00359
MW2	0.00141	0.01408	0.42036	0.00000	0.16230	0.00968	0.00292	0.32353	0.00225	0.04848	0.01562	0.00000	0.00213
MW3	0.00250	0.00527	0.38854	0.00000	0.11099	0.01163	0.00118	0.34237	0.00315	0.04028	0.00822	0.00000	0.00386
MW4	0.00188	0.00113	0.37634	0.00000	0.09784	0.01066	0.00116	0.07695	0.00718	0.03526	0.00719	0.00000	0.00525
MW5	0.00104	0.00815	0.43004	0.07588	0.17285	0.00830	0.00012	0.08829	0.00018	0.05511	0.00645	0.00000	0.00005
MW6	0.00189	0.00561	0.48225	0.01066	0.16958	0.01231	0.00320	0.03232	0.00795	0.05690	0.00737	0.00000	0.00533
MW7	0.00289	0.00212	0.53674	0.05566	0.14921	0.01653	0.00552	0.03395	0.00966	0.01871	0.00704	0.00000	0.00135
MW8	0.00134	0.00376	0.65573	0.04250	0.21745	0.01208	0.00278	0.04423	0.00026	0.01476	0.00750	0.00000	0.00009
MW9	0.00318	0.00115	1.11083	0.04152	1.24962	0.00983	0.00338	0.10713	0.00064	0.02108	0.00899	0.00000	0.00172
MW10	0.00173	0.00084	0.43238	0.00000	0.09639	0.01056	0.00050	0.01045	0.00142	0.01818	0.00517	0.00000	0.01608
MW11	0.00289	0.00296	0.37805	0.00000	0.08735	0.00655	0.00205	0.02119	0.00077	0.01712	0.00356	0.00000	0.00208
MW12	0.00267	0.00234	0.58949	0.23207	0.15556	0.01236	0.00257	0.06692	0.00084	0.02773	0.00609	0.00000	0.00203
MW13	0.00270	0.00976	0.81232	0.19158	0.19245	0.01777	0.00494	0.05486	0.00249	0.02033	0.00573	0.00000	0.00211
MW14	0.00117	0.00418	0.62947	0.14382	0.34910	0.01146	0.05632	0.09071	0.00110	0.00144	0.00525	0.00009	0.00116
MW15	0.00280	0.00181	0.72491	0.24988	0.30706	0.01334	0.00453	0.04344	0.00294	0.00211	0.00464	0.00038	0.00065
MW16	0.00294	0.00443	0.56854	0.00000	0.11360	0.01211	0.00125	0.04580	0.00012	0.00253	0.00318	0.00000	0.00306
MW17	0.00286	0.00000	0.67560	0.58312	0.28070	0.01208	0.00185	0.04858	0.00205	0.00000	0.00342	0.00000	0.00055
MW18	0.00244	0.00286	0.58340	0.21831	0.17528	0.01075	0.00551	0.04773	0.00193	0.00104	0.00314	0.00000	0.00178
MW19	0.00168	0.00123	0.76425	0.02409	0.33041	0.01724	0.01324	0.06405	0.00020	0.00045	0.00370	0.00000	0.00274

C-3: Concentration of Th, U, and other heavy metals, in mg/kg, unless stated otherwise, in soil samples from the environs of Kwale HMS deposit

	Sc	Ti (%)	Cr	Mn	Fe (%)	Ni	Cu	Zn	As	Zr	Nb	Cd	Pb	Th	U
BS1	22.64	1.98	21567	4939	3.01	33.78	14.41	201.3	121.3	142.6	64.810	3.800	22.00	10.82	1.834
BS2	13.10	1.40	20093	1672	2.80	21.17	22.38	242.4	163.6	139.7	25.025	4.900	14.48	3.82	1.338
BS3	14.33	2.14	19858	901	2.67	16.14	15.59	178.1	180.2	185.7	33.513	0.575	14.91	6.06	2.200
BS4	31.45	2.44	39808	12513	5.99	43.91	22.38	214.2	173.6	166.8	86.028	4.325	31.27	16.74	1.968
BS5	20.73	3.44	35500	9905	5.47	29.12	17.11	229.3	115.1	182.9	31.815	4.550	20.40	8.78	1.968
BS6	16.32	1.77	37146	1881	5.51	22.97	15.43	103.9	141.3	176.8	100.635	5.438	34.57	14.95	3.266
BS7	18.41	2.04	27078	1740	4.07	24.27	16.06	91.2	127.9	234.8	40.673	5.675	21.06	12.24	4.215
BS8	12.48	2.35	14989	1576	1.93	17.83	11.31	100.4	201.3	150.8	40.200	12.22	17.44	4.35	1.958
BS9	15.15	2.21	20665	1176	2.95	20.25	17.25	186.0	131.4	228.7	37.570	3.675	15.19	8.43	2.938
BS10	19.37	2.60	23672	2393	3.23	24.70	20.95	131.0	230.3	414.9	46.165	5.425	17.21	14.69	6.258
BS11	14.90	1.91	27770	1250	4.17	29.24	24.48	118.8	121.8	202.9	32.825	5.450	18.82	10.87	2.013
BS12	17.67	1.80	42811	1579	6.62	29.70	17.26	108.4	163.0	157.6	34.018	1.888	23.08	13.73	2.014

C-4: Concentration of Th, U, and other heavy metals, in mg/kg, unless stated otherwise, in soil samples from the environs of Mrima Hill

	Sc	Ti	Cr	Mn	Fe	Ni	Cu	Zn	As	Zr	Nb	Cd	Pb	Th	U
MS1	83.26	4.43	132958	9282	20.32	245.7	90.83	1221	402.7	533.62	360.5	69.51	208.0	213.9	18.05
MS2	54.15	4.25	163766	20406	26.09	259.7	96.03	3234	220.0	525.9	506.8	42.09	314.3	280.0	21.53
MS3	68.30	5.67	299791	25602	46.67	388.0	162.8	8680	385.0	850.1	1262	48.05	481.5	323.0	76.33
MS4	43.98	4.62	117898	11193	18.41	231.0	76.65	1471	178.4	542.1	218.8	43.22	170.3	154.0	9.925
MS5	35.90	4.74	213672	21411	33.33	223.7	68.69	3938	118.5	355.8	330.7	72.43	170.2	86.07	11.53
MS6	31.75	4.86	269792	22534	41.99	155.9	68.95	7984	194.4	361.4	588.6	60.84	299.3	196.2	24.93
MS7	18.46	3.14	50662	6590	7.778	71.23	24.32	557.0	64.29	150.5	70.77	52.16	46.36	30.40	2.808
MS8	24.38	3.92	60877	7107	9.531	107.0	44.07	1074	78.22	291.3	76.95	52.04	55.38	46.57	4.115
MS9	22.14	3.97	104019	8146	16.26	129.9	39.33	2302	99.46	259.6	161.8	51.99	94.33	40.54	9.703
MS10	21.72	2.91	148819	14928	22.98	113.0	40.41	2489	100.4	269.2	358.2	43.66	89.90	68.75	9.270
MS11	27.64	2.79	127046	8479	19.29	127.0	46.58	1096	111.9	233.2	193.4	66.20	71.63	73.80	5.840
MS12	35.23	2.73	140026	12836	21.47	136.5	59.51	1564	176.6	282.4	313.3	70.13	144.7	121.0	9.555
MS13	31.05	3.32	122267	11733	18.69	173.9	47.92	2473	170.9	348.4	327.1	61.68	172.8	178.5	5.708
MS14	19.27	3.32	43407	3393	6.662	42.87	34.80	662.9	111.6	166.7	38.43	23.68	230.0	23.18	3.150
MS15	19.33	3.21	30814	2729	4.713	30.05	18.85	370.6	84.30	153.3	21.80	23.92	32.38	15.39	3.348
MS16	25.29	3.44	143511	12254	22.21	135.3	36.41	1983	129.5	288.8	238.5	36.23	115.6	97.03	6.284
MS17	28.27	4.21	179090	15384	27.26	169.8	38.56	3223	162.0	338.5	321.1	39.48	159.3	141.1	7.130
MS18	33.61	3.10	80061	5913	12.65	123.2	36.68	606.1	190.7	257.8	209.3	34.59	159.3	133.3	5.105
MS19	43.91	3.52	157956	18984	24.85	294.7	69.28	2216	229.0	437.1	310.0	33.42	195.7	2.20	11.03
MS20	16.91	1.20	26939	1717	4.150	45.48	20.62	506.2	142.4	84.78	28.57	27.55	19.34	15.15	2.638
MS21	24.61	2.14	90343	10264	14.07	100.2	41.13	1264	155.7	209.2	179.4	38.46	108.2	109.3	6.363

C-5: Sample location, electrical conductivity, pH, and source of water samples from the environs of Kwale HMS deposit

	Lat.	Lon.	EC	pH	Source
BW1	-4.3904	39.45539	113	4.345	Diesel powered Borehole
BW2	-4.40356	39.4529	137	6.4	Stream
BW3	-4.40462	39.45201	227	7.832	Stream
BW4	-4.40577	39.44712	208	4.55	Borehole
BW5	-4.407	39.44254	114	5.991	Stream
BW6	-4.40886	39.44368	495	7.38	Water supplied Titanium Base industry and stored in tanks
BW7	-4.4058	39.43634	189	5.446	A discarded shallow well beside a stream
BW8	-4.40599	39.43666	120	5.664	Stream
BW9	-4.38079	39.45331	59.4	4.671	Water pan beside a stream
BW10	-4.37814	39.45221	180	5.97	Deep well
BW11	-4.3693	39.43269	10.6	5.8	Rainwater stored for over 6months in a Jerican
BW12	-4.36858	39.43254	98	4.971	Water pan beside a stream
BW13	-4.36422	39.43953	98.2	4.934	Water pan beside a stream
BW14	-4.3683	39.42648	139	6.38	Water pan beside Mkurumudzi river, used as cattle watering point
BW15	-4.39396	39.41761	261	4.981	Water pan beside a stream
BW16	-4.39153	39.4213	763	6.617	Solar powered Borehole
BW17	-4.38262	39.42281	150	7.3	Mkurumudzi river near the dam
BW18	-4.3933	39.42287	148	7.15	Nora river, a tributary of Mkurumudzi rover
BW19	-4.38262	39.42281	139	5.866	Water pan beside a stream

C-6: Sample location, electrical conductivity, pH, and source of water samples from the environs of Mrima Hill

	Lat.	Lon.	EC	pH	Source
MW1	-4.48997	39.25173	1745	6.93	Community Diesel pumped borehole
MW2	-4.48577	39.24871	1136	6.58	Hand pumped borehole
MW3	-4.481	39.24695	1121	6.68	Hand pumped borehole
MW4	-4.47307	39.24972	1047	6.93	Water stored in plastic
MW5	-4.47203	39.25849	604	6.1	Stored in a jug claim to have fetched at the community well
MW6	-4.46863	39.25277	915	7.74	Hand pumped borehole
MW7	-4.46896	39.25473	1064	6.53	Sampled at home water stored in plastic
MW8	-4.46969	39.25943	595	5.91	Community well
MW9	-4.47567	39.26318	603	6.06	Sampled at home water stored in plastic claims to be from the community well
MW10	-4.47329	39.26691	1679	6.89	Sampled at home, stored in plastic, and claim to be from the community well
MW11	-4.47598	39.27247	1578	7.31	Solar powered borehole
MW12	-4.47559	39.272	1454	6.62	Hand pumped borehole
MW13	-4.48082	39.27018	1442	7.06	Sampled at home but from the solar powered borehole
MW14	-4.48789	39.27448	905	7.23	Hand pumped borehole
MW15	-4.49519	39.26981	1163	6.92	Hand pumped borehole
MW16	-4.49489	39.24944	1687	7.39	Tapped from MW1
MW17	-4.49545	39.25194	1060	6.72	Deep well
MW18	-4.49639	39.25989	1237	6.57	Petrol pumped borehole
MW19	-4.49861	39.26247	1431	6.41	Hand pumped borehole

Appendix D: Water quality and soil pollution assessment

D-1 Geochemical accumulation index, I_{geo}, of Th, U, and related heavy metals in soil samples from the environs of Kwale HMS deposit

	Ti	Cr	Mn	Fe	Ni	Cu	Zn	As	Zr	Nb	Cd	Pb	Th	U
BS1	1.1831	2.4253	2.9301	-0.4795	-0.0305	-1.0583	1.0022	3.1356	-1.3178	2.216	5.0974	-0.7108	-0.8498	-1.1956
BS2	0.6864	7.9545	1.3674	-0.5859	-0.7049	-0.4228	1.2701	3.5673	-1.3471	0.8431	5.1714	-1.3142	-2.3509	-1.6509
BS3	1.2955	7.9376	0.475	-0.6555	-1.096	-0.9448	0.8255	3.707	-0.9368	1.2644	2.373	-1.2715	-1.6855	-0.9329
BS4	1.485	8.9409	4.2713	0.5124	0.348	-0.4229	1.0916	3.6533	-1.0916	2.6245	5.2841	-0.2032	-0.2202	-1.094
BS5	1.9838	8.7757	3.9341	0.3812	-0.2446	-0.8101	1.19	3.0599	-0.9587	1.1894	5.3572	-0.8193	-1.152	-1.094
BS6	1.0278	8.8411	1.5378	0.3916	-0.5871	-0.9597	0.0473	3.3559	-1.008	2.8508	5.6144	-0.0585	-0.3833	-0.3628
BS7	1.2279	8.385	1.4254	-0.0461	-0.5073	-0.9017	-0.1407	3.212	-0.5987	1.5438	5.676	-0.7735	-0.6719	0.0051
BS8	1.4336	7.5318	1.2819	-1.121	-0.9523	-1.4077	-0.002	3.8665	-1.2375	1.5269	6.7831	-1.046	-2.1652	-1.1014
BS9	1.3438	7.995	0.8598	-0.5098	-0.7689	-0.7982	0.8879	3.251	-0.6364	1.4293	5.0491	-1.2449	-1.2099	-0.5158
BS10	1.5799	8.191	1.8848	-0.3796	-0.4819	-0.5178	0.3819	4.0606	0.2229	1.7265	5.611	-1.065	-0.4086	0.5752
BS11	1.1358	8.4214	0.9478	-0.0099	-0.2387	-0.2935	0.2416	3.1418	-0.8094	1.2345	5.6176	-0.9361	-0.8438	-1.0614
BS12	1.0526	9.0459	1.2851	0.6557	-0.2164	-0.7972	0.1087	3.562	-1.1732	1.286	4.0882	-0.6417	-0.5063	-1.0605

D-2 Geochemical accumulation index, I_{geo}, of Th, U, and other related heavy metals in soil samples from the environs of Mrima Hill

	Ti	Cr	Mn	Fe	Ni	Cu	Zn	As	Zr	Nb	Cd	Pb	Th	U
MS1	2.348	10.68	3.84	2.275	2.832	1.598	3.603	4.867	0.586	4.692	9.29	2.53	3.455	2.103
MS2	2.289	10.98	4.977	2.635	2.912	1.679	5.008	3.995	0.565	5.183	8.567	3.126	3.844	2.358
MS3	2.705	11.85	5.304	3.474	3.491	2.44	6.432	4.802	1.258	6.499	8.758	3.742	4.05	4.184
MS4	2.41	10.51	4.11	2.132	2.744	1.353	3.872	3.693	0.609	3.971	8.605	2.242	2.981	1.241
MS5	2.445	11.37	5.046	2.989	2.697	1.195	5.292	3.102	0.001	4.567	9.35	2.241	2.142	1.457
MS6	2.481	11.7	5.12	3.322	2.176	1.201	6.312	3.816	0.024	5.399	9.098	3.056	3.331	2.569
MS7	1.853	9.289	3.346	0.889	1.046	-0.303	2.47	2.22	-1.24	2.343	8.876	0.365	0.64	-0.581
MS8	2.173	9.554	3.455	1.182	1.633	0.555	3.418	2.503	-0.287	2.464	8.873	0.621	1.256	-0.029
MS9	2.189	10.327	3.652	1.953	1.913	0.391	4.517	2.849	-0.454	3.536	8.871	1.39	1.056	1.208
MS10	1.741	10.843	4.526	2.452	1.712	0.43	4.631	2.863	-0.401	4.683	8.619	1.32	1.818	1.142
MS11	1.68	10.62	3.71	2.2	1.88	0.635	3.447	3.02	-0.608	3.793	9.22	0.992	1.92	0.476
MS12	1.648	10.76	4.308	2.354	1.984	0.988	3.96	3.677	-0.332	4.489	9.303	2.007	2.634	1.186
MS13	1.932	10.56	4.178	2.154	2.333	0.676	4.621	3.63	-0.029	4.552	9.118	2.263	3.194	0.442
MS14	1.933	9.066	2.389	0.666	0.313	0.214	2.722	3.015	-1.093	1.462	7.737	2.676	0.249	-0.415
MS15	1.884	8.571	2.074	0.166	-0.199	-0.671	1.883	2.611	-1.213	0.644	7.751	-0.153	-0.342	-0.327
MS16	1.983	10.79	4.241	2.403	1.972	0.279	4.302	3.23	-0.3	4.096	8.35	1.683	2.315	0.581
MS17	2.274	11.11	4.569	2.698	2.299	0.362	5.003	3.553	-0.071	4.525	8.475	2.146	2.855	0.764
MS18	1.831	9.949	3.19	1.591	1.836	0.29	2.592	3.789	-0.464	3.907	8.284	2.145	2.773	0.282
MS19	2.018	10.93	4.873	2.565	3.095	1.207	4.462	4.053	0.298	4.474	8.234	2.442	-3.148	1.393
MS20	0.468	8.378	1.406	-0.017	0.399	-0.541	2.333	3.367	-2.068	1.034	7.955	-0.897	-0.365	-0.671
MS21	1.296	10.12	3.985	1.744	1.538	0.455	3.652	3.496	-0.765	3.685	8.437	1.587	2.487	0.599

D-3: Pollution index, PI, of heavy metals in soils from the Kwale HMS deposit

	BS1	BS2	BS3	BS4	BS5	BS6	BS7	BS8	BS9	BS10	BS11	BS12	Mean
Cr	399	372	368	737	657	688	501	278	383	438	514	793	511
Cd	51.4	66.2	7.8	58.4	61.5	73.5	76.7	165	49.7	73.3	73.6	25.5	65.2
As	13.2	17.8	19.6	18.9	12.5	15.4	13.9	21.9	14.3	25.0	13.2	17.7	16.9
Mn	11.4	3.87	2.08	29.0	22.9	4.36	4.03	3.65	2.72	5.54	2.89	3.66	8.01
Nb	6.97	2.69	3.60	9.25	3.42	10.82	4.37	4.32	4.04	4.96	3.53	3.66	5.14
Ti	3.41	2.41	3.68	4.20	5.93	3.06	3.51	4.05	3.81	4.48	3.30	3.11	3.75
Zn	3.00	3.62	2.66	3.20	3.42	1.55	1.36	1.50	2.78	1.95	1.77	1.62	2.37
Fe	1.08	1.00	0.95	2.14	1.95	1.97	1.45	0.69	1.05	1.15	1.49	2.36	1.44
Ni	1.47	0.92	0.70	1.91	1.27	1.00	1.06	0.78	0.88	1.07	1.27	1.29	1.13
U	0.65	0.48	0.79	0.70	0.70	1.17	1.51	0.70	1.05	2.23	0.72	0.72	0.95
Cu	0.72	1.12	0.78	1.12	0.86	0.77	0.80	0.57	0.86	1.05	1.22	0.86	0.89
Pb	0.92	0.60	0.62	1.30	0.85	1.44	0.88	0.73	0.63	0.72	0.78	0.96	0.87
Zr	0.60	0.59	0.78	0.70	0.77	0.75	0.99	0.64	0.96	1.75	0.86	0.67	0.84
Th	0.83	0.29	0.47	1.29	0.68	1.15	0.94	0.33	0.65	1.13	0.84	1.06	0.80

D-4: Pollution index, PI, of heavy metals in soils from the environs of Mrima Hill

	Ti	Cr	Mn	Fe	Ni	Cu	Zn	As	Zr	Nb	Cd	Pb	Th	U
MS1	7.64	2462	21.5	7.26	10.7	4.54	18.2	43.8	2.25	38.8	939	8.67	16.5	6.45
MS2	7.33	3033	47.2	9.32	11.3	4.8	48.3	23.9	2.22	54.5	569	13.1	21.5	7.69
MS3	9.78	5552	59.3	16.7	16.9	8.14	130	41.8	3.59	136	649	20.1	24.8	27.3
MS4	7.97	2183	25.9	6.57	10	3.83	22	19.4	2.29	23.5	584	7.09	11.8	3.54
MS5	8.17	3957	49.6	11.9	9.73	3.43	58.8	12.9	1.5	35.6	979	7.09	6.62	4.12
MS6	8.37	4996	52.2	15	6.78	3.45	119	21.1	1.52	63.3	822	12.5	15.1	8.9
MS7	5.42	938	15.3	2.78	3.1	1.22	8.31	6.99	0.64	7.61	705	1.93	2.34	1
MS8	6.76	1127	16.5	3.4	4.65	2.2	16	8.5	1.23	8.27	703	2.31	3.58	1.47
MS9	6.84	1926	18.9	5.81	5.65	1.97	34.4	10.8	1.1	17.4	703	3.93	3.12	3.47
MS10	5.01	2756	34.6	8.21	4.91	2.02	37.2	10.9	1.14	38.5	590	3.75	5.29	3.31
MS11	4.81	2353	19.6	6.89	5.52	2.33	16.4	12.2	0.98	20.8	895	2.98	5.68	2.09
MS12	4.7	2593	29.7	7.67	5.93	2.98	23.3	19.2	1.19	33.7	948	6.03	9.31	3.41
MS13	5.72	2264	27.2	6.68	7.56	2.4	36.9	18.6	1.47	35.2	833	7.2	13.7	2.04
MS14	5.73	804	7.9	2.38	1.86	1.74	9.89	12.1	0.7	4.13	320	9.58	1.78	1.13
MS15	5.54	571	6.32	1.68	1.31	0.94	5.53	9.16	0.65	2.34	323	1.35	1.18	1.2
MS16	5.93	2658	28.4	7.93	5.88	1.82	29.6	14.1	1.22	25.6	490	4.82	7.46	2.24
MS17	7.26	3316	35.6	9.74	7.38	1.93	48.1	17.6	1.43	34.5	534	6.64	10.9	2.55
MS18	5.34	1483	13.7	4.52	5.36	1.83	9.05	20.7	1.09	22.5	467	6.64	10.3	1.82
MS19	6.07	2925	43.9	8.88	12.82	3.46	33.1	24.9	1.84	33.3	452	8.15	0.2	3.94
MS20	2.07	499	3.98	1.48	1.98	1.03	7.56	15.5	0.36	3.1	372	0.81	1.17	0.94
MS21	3.68	1673	23.8	5.02	4.36	2.06	18.9	16.9	0.88	19.3	520	4.51	8.41	2.27
PI	**6.2**	**2384**	**27.7**	**7.13**	**6.84**	**2.77**	**34.8**	**18.1**	**1.39**	**31.3**	**638**	**6.62**	**8.61**	**4.33**

D-5: Enrichment factors of heavy metals in soil samples from the environs of Kwale HMS deposit and Mrima Hill

	BS1	BS2	BS3	BS4	BS5	BS6	BS7	BS8	BS9	BS10	BS11	BS12	Mean
Ti	1.58	1.93	2.70	1.40	3.00	1.97	2.00	3.41	2.64	2.43	2.32	1.85	2.27
Cr	185	298	269	246	333	443	286	233	265	238	363	471	303
Mn	5.30	3.10	1.53	9.67	11.61	2.80	2.30	3.07	1.89	3.00	2.04	2.17	4.04
Fe	0.499	0.801	0.698	0.714	0.989	1.266	0.829	0.580	0.730	0.625	0.013	1.405	0.762
Ni	0.681	0.738	0.514	0.637	0.641	0.642	0.602	0.652	0.610	0.582	0.011	0.767	0.590
Cu	0.334	0.897	0.571	0.374	0.433	0.496	0.458	0.476	0.598	0.568	0.010	0.513	0.477
Zn	1.39	2.90	1.95	1.07	1.73	0.997	0.776	1.26	1.92	1.06	0.015	0.961	1.34
As	6.11	14.3	14.4	6.30	6.33	9.88	7.93	18.4	9.90	13.6	0.111	10.5	9.81
Zr	0.279	0.473	0.574	0.235	0.391	0.480	0.565	0.535	0.669	0.949	0.007	0.395	0.463
Nb	3.23	2.16	2.64	3.09	1.73	6.96	2.49	3.64	2.80	2.69	0.030	2.17	2.80
Cd	23.8	53.1	5.69	19.5	31.1	47.3	43.7	139	34.4	39.7	0.619	15.2	37.8
Pb	0.425	0.484	0.455	0.435	0.431	0.927	0.500	0.611	0.439	0.389	0.007	0.571	0.473
Th	0.386	0.236	0.342	0.430	0.342	0.740	0.537	0.281	0.449	0.613	0.007	0.628	0.416
U	0.304	0.383	0.576	0.235	0.356	0.751	0.858	0.588	0.727	1.21	0.006	0.427	0.535

D-6: Enrichment factor, EF, of heavy metals in soil samples from the environs of Mrima Hill

	Ti	Cr	Mn	Fe	Ni	Cu	Zn	As	Zr	Nb	Cd	Pb	Th	U
MS1	0.96	311	2.71	0.92	1.35	0.57	2.3	5.52	0.28	4.89	118	1.09	2.08	0.81
MS2	1.42	588	9.16	1.81	2.19	0.93	9.36	4.64	0.43	10.6	110	2.54	4.18	1.49
MS3	1.5	854	9.11	2.56	2.59	1.25	19.9	6.43	0.55	20.9	100	3.08	3.82	4.19
MS4	1.9	521	6.19	1.57	2.4	0.91	5.24	4.63	0.55	5.62	139	1.69	2.83	0.85
MS5	2.39	1157	14.5	3.48	2.85	1	17.2	3.77	0.44	10.4	286	2.07	1.94	1.2
MS6	2.77	1653	17.3	4.96	2.24	1.14	39.4	6.99	0.5	20.9	272	4.13	4.99	2.94
MS7	3.08	534	8.68	1.58	1.76	0.69	4.73	3.97	0.36	4.33	401	1.1	1.33	0.57
MS8	2.91	485	7.08	1.47	2	0.95	6.91	3.66	0.53	3.56	303	0.99	1.54	0.63
MS9	3.24	913	8.94	2.75	2.68	0.93	16.3	5.13	0.52	8.25	333	1.86	1.48	1.64
MS10	2.42	1332	16.7	3.97	2.38	0.98	18	5.27	0.55	18.6	285	1.81	2.56	1.6
MS11	1.83	894	7.46	2.62	2.1	0.88	6.21	4.62	0.37	7.9	340	1.13	2.16	0.79
MS12	1.4	773	8.86	2.28	1.77	0.89	6.96	5.72	0.36	10	282	1.8	2.77	1.02
MS13	1.94	766	9.19	2.26	2.56	0.81	12.5	6.28	0.5	11.9	282	2.44	4.64	0.69
MS14	3.12	438	4.28	1.3	1.02	0.95	5.39	6.61	0.38	2.25	174	5.22	0.97	0.61
MS15	3.01	310	3.43	0.91	0.71	0.51	3	4.98	0.35	1.27	176	0.73	0.64	0.65
MS16	2.46	1103	11.8	3.29	2.44	0.76	12.3	5.84	0.51	10.6	203	2	3.1	0.93
MS17	2.7	1232	13.2	3.62	2.74	0.72	17.9	6.54	0.53	12.8	198	2.47	4.03	0.95
MS18	1.67	463	4.28	1.41	1.67	0.57	2.83	6.48	0.34	7.03	146	2.07	3.2	0.57
MS19	1.45	700	10.51	2.12	3.06	0.83	7.91	5.95	0.44	7.97	108	1.95	0.04	0.94
MS20	1.29	310	2.47	0.92	1.23	0.64	4.69	9.61	0.22	1.91	231	0.5	0.72	0.58
MS21	1.57	714	10	2.14	1.86	0.88	8.05	7.22	0.38	8.23	222	1.92	3.59	0.97
Mean EF	**2.14**	**764**	**8.85**	**2.28**	**2.08**	**0.85**	**10.8**	**5.71**	**0.43**	**9.05**	**224**	**2.03**	**2.51**	**1.17**

Appendix E: Carcinogenic and non-carcinogenic human health risk assessment

E-1: Non-carcinogenic point and probabilistic average daily dose, ADD, in mg/kg per day of heavy metals in soil via ingestion pathway.

	Kwale						Mrima					
	Child			**Adult**			**Child**			**Adult**		
	Point estimate	50th percentile	95th percentile	Point estimate	50th percentile	95th percentile	Point estimate	50th percentile	95th percentile	Point estimate	50th percentile	95th percentile
Cr	3.36E-01	3.38E-02	7.82E-01	3.59E-02	7.74E-03	8.24E-02	1.38E+00	1.32E-01	4.46E+00	1.48E-01	3.31E-02	4.47E-01
Mn	2.99E-02	2.78E-03	9.58E-02	3.20E-03	6.82E-04	7.73E-03	1.25E-01	1.30E-02	3.57E-01	1.34E-02	3.14E-03	2.94E-02
Ni	3.21E-04	3.08E-05	5.47E-04	3.44E-05	7.17E-06	6.79E-05	1.69E-03	1.45E-04	3.00E-03	1.81E-04	4.10E-05	4.60E-04
Cu	2.24E-04	2.24E-05	4.37E-04	2.40E-05	5.27E-06	5.14E-05	6.18E-04	2.24E-05	4.37E-04	6.62E-05	1.40E-05	1.75E-04
Zn	1.91E-03	1.85E-04	3.91E-03	2.05E-04	4.47E-05	6.16E-04	2.09E-02	2.07E-03	4.65E-02	2.24E-03	5.10E-04	8.12E-03
As	1.95E-03	2.04E-04	4.55E-03	2.09E-04	4.74E-05	5.67E-04	1.91E-03	2.01E-04	5.98E-03	2.05E-04	4.07E-05	1.75E-04
Cd	5.10E-05	2.48E-05	5.51E-04	5.47E-06	1.73E-06	1.42E-05	5.72E-04	5.69E-05	1.68E-03	6.13E-05	1.32E-05	1.32E-04
Pb	2.57E-04	2.54E-05	7.78E-04	2.75E-05	6.40E-06	5.85E-05	1.59E-03	1.53E-04	4.34E-03	1.70E-04	3.65E-05	5.01E-04
U	3.10E-05	3.23E-06	8.02E-05	3.33E-06	7.62E-07	7.34E-06	1.04E-04	1.08E-05	2.87E-04	1.11E-05	2.53E-06	3.48E-05
Sum	**3.70E-01**	**3.71E-02**	**8.89E-01**	**3.97E-02**	**8.54E-03**	**9.15E-02**	**1.53E+00**	**1.48E-01**	**4.88E+00**	**1.64E-01**	**3.69E-02**	**4.86E-01**

E-2: Non-carcinogenic point and probabilistic average daily dose, ADD, in mg/kg per day from dermal contact to heavy metal contaminated soils.

	Kwale						Mrima					
	Child			**Adult**			**Child**			**Adult**		
	Point estimate	50th percentile	95th percentile	Point estimate	50th percentile	95th percentile	Point estimate	50th percentile	95th percentile	Point estimate	50th percentile	95th percentile
Cr	9.39E-04	2.85E-03	2.75E-02	1.43E-04	9.22E-05	8.25E-04	3.86E-03	1.18E-02	1.15E-01	5.89E-04	3.66E-04	3.88E-03
Mn	8.36E-05	2.67E-04	2.73E-03	1.28E-05	8.70E-06	9.76E-05	3.51E-04	1.02E-03	9.38E-03	5.36E-05	3.35E-05	3.02E-04
Ni	9.00E-07	2.51E-06	2.05E-05	1.37E-07	7.84E-08	6.14E-07	4.72E-06	1.37E-05	1.26E-04	7.20E-07	4.15E-07	3.85E-06
Zn	6.26E-07	1.45E-05	1.30E-04	9.56E-08	4.81E-07	4.45E-06	5.86E-05	1.81E-04	2.28E-03	8.95E-06	5.12E-06	5.17E-05
Cu	5.36E-06	1.80E-06	1.92E-05	8.18E-07	5.06E-08	4.96E-07	1.73E-06	4.84E-06	5.54E-05	2.64E-07	1.65E-07	1.54E-06
As	1.64E-04	4.56E-04	5.12E-03	2.50E-05	1.39E-05	1.20E-04	1.60E-04	4.82E-04	4.30E-03	2.45E-05	1.41E-05	1.26E-04
Cd	1.43E-07	4.76E-07	5.47E-06	2.18E-08	1.47E-08	1.12E-07	1.60E-06	4.97E-06	5.02E-05	2.45E-07	1.48E-07	1.05E-06
Pb	7.20E-07	2.03E-06	1.95E-05	1.10E-07	6.43E-08	6.37E-07	4.45E-06	1.37E-05	1.52E-04	6.79E-07	4.19E-07	4.07E-06
Sum	**1.19E-03**	**3.59E-03**	**3.55E-02**	**1.82E-04**	**1.15E-04**	**1.05E-03**	**4.44E-03**	**1.35E-02**	**1.31E-01**	**6.78E-04**	**4.20E-04**	**4.37E-03**

E-3: Non-carcinogenic point and probabilistic average daily dose, ADD, in mg/L-day from ingestion of heavy metals in water.

	Kwale						Mrima					
	Child			**Adult**			**Child**			**Adult**		
	Point estimate	50th percentile	95th percentile	Point estimate	50th percentile	95th percentile	Point estimate	50th percentile	95th percentile	Point estimate	50th percentile	95th percentile
Cr	3.12E-02	6.29E-04	5.71E-03	1.34E-02	1.29E-03	1.25E-02	3.53E-02	7.12E-04	2.88E-03	1.51E-02	1.71E-03	6.59E-03
Mn	6.13E-03	1.23E-04	1.48E-03	2.63E-03	2.72E-04	3.03E-03	8.81E-05	1.66E-06	4.11E-04	3.77E-05	4.43E-06	9.84E-04
Ni	4.72E-04	1.04E-05	4.34E-05	2.02E-04	2.32E-05	9.30E-05	7.51E-04	1.58E-05	6.21E-05	3.22E-04	3.57E-05	1.44E-04
Cu	1.33E-04	3.00E-06	1.42E-05	5.69E-05	5.87E-06	2.87E-05	1.56E-04	3.15E-06	3.92E-05	6.69E-05	6.25E-06	9.08E-05
Zn	1.16E-03	2.49E-05	2.34E-05	4.98E-04	4.70E-05	4.00E-04	3.88E-03	7.65E-05	4.79E-04	1.66E-03	1.80E-04	1.13E-03
As	4.49E-05	9.19E-07	8.84E-07	1.93E-05	1.89E-06	1.61E-05	7.53E-05	1.55E-06	2.35E-05	3.23E-05	3.10E-06	3.56E-05
Cd	5.39E-03	1.24E-04	1.12E-04	2.31E-03	2.55E-04	1.06E-03	4.66E-04	6.70E-06	1.50E-04	2.00E-04	1.58E-05	3.54E-04
Pb	1.86E-04	4.01E-06	4.16E-06	7.95E-05	8.45E-06	4.24E-05	3.84E-04	8.10E-06	3.83E-05	1.65E-04	1.93E-05	8.35E-05
U	1.27E-05	2.71E-07	2.98E-07	5.45E-06	5.82E-07	5.28E-06	1.02E-04	2.09E-06	2.23E-05	4.39E-05	5.24E-06	6.43E-05
Sum	**4.47E-02**	**9.20E-04**	**7.39E-03**	**1.92E-02**	**1.90E-03**	**1.72E-02**	**4.12E-02**	**8.28E-04**	**4.11E-03**	**1.77E-02**	**1.98E-03**	**9.48E-03**

E-4: Deterministic and probabilistic target health quotient (THQ) and hazard indices (HI) due to exposure to heavy metals via ingestion of soil particles

	Kwale						Mrima					
	Child			**Adult**			**Child**			**Adult**		
	Point estimate	50th percentile	95th percentile	Point estimate	50th percentile	95th percentile	Point estimate	50th percentile	95th percentile	Point estimate	50th percentile	95th percentile
Cr	2.24E-01	2.26E-02	5.30E-01	2.40E-02	5.16E-03	4.17E-02	9.19E-01	9.16E-02	2.45E+00	9.85E-02	2.24E-02	3.00E-01
Mn	2.13E-01	2.44E-02	6.85E-01	2.29E-02	5.22E-03	8.99E-02	8.95E-01	9.33E-02	2.55E+00	9.59E-02	2.24E-02	2.50E-01
Ni	1.61E-02	1.54E-03	3.25E-02	1.72E-03	3.59E-04	3.39E-03	8.43E-02	7.23E-03	1.50E-01	9.03E-03	1.89E-03	1.96E-02
Zn	6.38E-03	6.18E-04	1.41E-02	6.84E-04	1.49E-04	1.77E-03	1.54E-02	6.91E-03	1.55E-01	1.65E-03	1.63E-03	1.82E-02
Cu	5.59E-03	5.59E-04	1.36E-02	5.99E-04	1.32E-04	1.28E-03	6.97E-02	1.55E-03	3.56E-02	7.47E-03	3.50E-04	3.56E-03
As	6.49E+00	6.83E-01	1.42E+01	6.96E-01	1.58E-01	1.61E+00	6.36E+00	6.45E-01	1.43E+01	6.82E-01	1.36E-01	1.42E+00
Cd	5.10E-02	5.18E-03	1.73E-01	5.47E-03	5.99E-03	6.13E-02	5.72E-01	5.83E-02	1.76E+00	6.13E-02	3.60E-02	1.43E-01
Pb	7.34E-02	7.10E-03	2.22E-01	7.87E-03	1.83E-03	1.88E-02	4.54E-01	4.38E-02	1.29E+00	4.86E-02	1.01E-02	1.11E-01
U	1.03E-02	1.08E-03	2.27E-02	1.11E-03	2.40E-04	2.43E-03	3.46E-02	3.71E-03	8.83E-02	3.71E-03	8.45E-04	1.16E-02
HI	**7.09E+00**	**7.46E-01**	**1.59E+01**	**7.60E-01**	**1.77E-01**	**1.83E+00**	**9.40E+00**	**9.51E-01**	**2.28E+01**	**1.01E+00**	**2.32E-01**	**2.28E+00**

E-5: Deterministic and probabilistic target health quotient (THQ) and hazard indices (HI) from exposure to heavy metals via dermal contact to soil particles

	Kwale						Mrima					
	Child			**Adult**			**Child**			**Adult**		
	Point estimate	50th percentile	95th percentile	Point estimate	50th percentile	95th percentile	Point estimate	50th percentile	95th percentile	Point estimate	50th percentile	95th percentile
Cr	4.82E-02	1.46E-01	1.41E+00	7.36E-03	4.72E-03	4.23E-02	1.98E-01	6.06E-01	5.91E+00	3.02E-02	1.88E-02	1.99E-01
Mn	8.71E-02	2.36E-01	2.74E+00	1.33E-02	9.07E-03	1.02E-01	3.66E-01	1.06E+00	9.77E+00	5.58E-02	3.49E-02	3.15E-01
Ni	4.50E-05	1.25E-04	2.03E-03	6.87E-06	3.92E-06	3.07E-05	2.36E-04	6.85E-04	6.30E-03	3.60E-05	2.08E-05	1.92E-04
Zn	1.57E-05	4.84E-05	4.33E-04	2.39E-06	1.61E-06	1.48E-05	4.32E-05	6.03E-04	8.61E-03	6.60E-06	1.84E-05	1.72E-04
Cu	1.79E-05	4.50E-05	4.79E-04	2.73E-06	1.40E-06	1.24E-05	1.95E-04	1.21E-04	1.38E-03	2.98E-05	4.13E-06	3.84E-05
As	5.45E-01	1.48E+00	1.07E+01	8.33E-02	4.64E-02	3.98E-01	5.35E-01	1.61E+00	1.41E+01	8.16E-02	4.69E-02	4.23E-01
Pb	1.80E-05	5.06E-05	4.88E-04	2.75E-06	1.61E-06	1.59E-05	1.11E-04	3.43E-04	3.80E-03	1.70E-05	1.04E-05	1.02E-04
Cd	1.14E-02	3.81E-02	4.38E-01	1.74E-03	1.12E-03	9.02E-03	1.28E-01	3.98E-01	4.02E+00	1.96E-02	1.18E-02	8.38E-02
HI	**6.92E-01**	**1.90E+00**	**1.53E+01**	**1.06E-01**	**6.13E-02**	**5.51E-01**	**1.23E+00**	**3.68E+00**	**3.38E+01**	**1.87E-01**	**1.12E-01**	**1.02E+00**

E-6: Deterministic and probabilistic target health quotient (THQ) and hazard indices (HI) of heavy metals in water via ingestion route

	Kwale						Mrima					
	Child			**Adult**			**Child**			**Adult**		
	Point estimate	50th percentile	95th percentile	Point estimate	50th percentile	95th percentile	Point estimate	50th percentile	95th percentile	Point estimate	50th percentile	95th percentile
Cr	1.04E+01	2.14E-01	1.94E+00	4.46E+00	5.01E-01	4.93E+00	1.18E+01	2.37E-01	9.60E-01	5.04E+00	5.71E-01	2.18E+00
Mn	4.38E-02	8.90E-04	9.80E-03	1.88E-02	2.01E-03	2.23E-02	6.29E-04	1.18E-05	9.18E-01	2.70E-04	3.03E-05	8.84E-03
Ni	2.36E-02	4.70E-04	1.86E-03	1.01E-02	1.17E-03	4.66E-03	3.76E-02	7.89E-04	3.11E-03	1.61E-02	1.78E-03	7.24E-03
Cu	3.32E-03	6.47E-05	2.97E-04	1.42E-03	1.46E-04	7.45E-04	3.90E-03	7.88E-05	9.80E-04	1.67E-03	1.56E-04	2.27E-03
Zn	3.87E-03	7.34E-05	7.83E-04	5.84E-04	1.76E-04	1.74E-03	1.29E-02	2.54E-03	2.28E-02	5.54E-03	6.01E-04	4.00E-03
As	1.50E-01	3.19E-03	2.71E-02	6.42E-02	6.86E-03	5.50E-02	2.51E-01	5.18E-03	7.84E-02	1.08E-01	1.03E-02	1.68E-01
Cd	1.08E+01	2.28E-01	7.84E-01	4.62E+00	5.18E-01	2.01E+00	9.32E-01	2.86E-02	5.75E-01	3.99E-01	3.17E-02	7.05E-01
Pb	1.33E-01	2.67E-03	1.22E-02	5.68E-02	6.16E-03	2.95E-02	2.74E-01	1.21E-02	5.05E-02	1.18E-01	1.37E-02	6.51E-02
U	2.12E-03	4.66E-04	3.08E-03	9.08E-04	1.08E-03	7.40E-03	1.71E-02	3.49E-03	3.71E-02	7.31E-03	7.98E-03	1.57E-01
HI	**2.15E+01**	**4.50E-01**	**2.78E+00**	**9.23E+00**	**1.04E+00**	**7.06E+00**	**1.33E+01**	**2.90E-01**	**2.65E+00**	**5.70E+00**	**6.37E-01**	**3.30E+00**

E-7: Carcinogenic point and probabilistic average daily dose, ADD, in mg/L-day from exposure to heavy metals in water via ingestion pathway.

	Kwale						Mrima					
	Child			Adult			Child			Adult		
	Point estimate	50th percentile	95th percentile	Point estimate	50th percentile	95th percentile	Point estimate	50th percentile	95th percentile	Point estimate	50th percentile	95th percentile
Cr	2.67E-03	6.30E-04	5.72E-03	5.73E-03	1.29E-03	1.25E-02	3.03E-03	8.19E-04	3.08E-03	6.49E-03	1.63E-03	6.31E-03
As	3.85E-06	8.57E-07	7.42E-06	8.25E-06	1.93E-06	1.43E-05	6.45E-06	1.46E-06	1.88E-05	1.38E-05	1.93E-06	1.43E-05
Pb	1.59E-05	4.15E-06	1.93E-05	3.41E-05	9.03E-06	4.33E-05	3.29E-05	8.50E-06	3.78E-05	7.06E-05	9.03E-06	4.33E-05
Sum	**2.69E-03**	**6.35E-04**	**5.74E-03**	**5.77E-03**	**1.30E-03**	**1.26E-02**	**3.07E-03**	**8.29E-04**	**3.13E-03**	**6.57E-03**	**1.64E-03**	**6.37E-03**

E-8: Carcinogenic point and probabilistic average daily dose, ADD, in mg/L-day from exposure to heavy metals in soil via ingestion pathway.

	Kwale						Mrima					
	Child			Adult			Child			Adult		
	Point estimate	50th percentile	95th percentile	Point estimate	50th percentile	95th percentile	Point estimate	50th percentile	95th percentile	Point estimate	50th percentile	95th percentile
Cr	2.88E-02	3.05E-02	3.98E-01	1.54E-02	8.58E-03	1.96E-02	1.18E-01	1.18E-01	1.68E+00	6.33E-02	3.25E-02	1.19E-01
As	1.67E-04	1.82E-04	2.78E-03	8.94E-05	4.81E-05	1.02E-04	1.64E-04	1.72E-04	2.60E-03	8.77E-05	4.49E-05	1.33E-04
Pb	2.20E-05	2.47E-05	2.39E-04	1.18E-05	6.34E-06	1.39E-05	1.36E-04	1.56E-04	1.81E-03	7.29E-05	3.72E-05	1.58E-04
Sum	**2.89E-02**	**3.07E-02**	**4.01E-01**	**1.55E-02**	**8.63E-03**	**1.98E-02**	**1.18E-01**	**1.19E-01**	**1.69E+00**	**6.35E-02**	**3.26E-02**	**1.19E-01**

Appendix F: Radiotoxicity human health risk assessment

F-1: Activity concentration of ^{232}Th and ^{238}U in soil samples from environs of Kwale HMS deposit

	BS1	BS2	BS3	BS4	BS5	BS6	BS7	BS8	BS9	BS10	BS11	BS12
Th	44.2	15.6	24.7	68.3	35.8	61.0	49.9	17.7	34.4	59.9	44.3	56.0
U	22.7	16.6	27.3	24.4	24.4	40.5	52.3	24.3	36.4	77.6	25.0	25.0

F-2: Activity concentration of ^{232}Th and ^{238}U in soil samples from environs of Mrima Hill

	MS1	MS2	MS3	MS4	MS5	MS6	MS7	MS8	MS9	MS10	MS11	MS12	MS13	MS14	MS15	MS16	MS17	MS18	MS19	MS20	MS21
Th	1164	1143	1318	628	351	800	124	190	165	280	301	494	728	94.6	62.8	396	576	544	8.98	61.8	446
U	224	267	946	123	143	309	34.8	51.0	120	115	72.4	118	70.8	39.1	41.5	77.9	88.4	63.3	137	32.7	78.9

169

F-3: Cancer Slope factors

Nuclide	Soil Ingestion	Inhalation	External
Pb-210	3.12E-11	4.41E-10	1.15E-10
Pb-210 +D	3.12E-11	4.41E-10	4.64E-10
Po-210	6.09E-10	3.92E-10	1.22E-12
Ra-226+D	1.39E-11	7.63E-10	2.26E-07
Ra-228+D	3.86E-11	1.18E-09	1.09E-07
Th-228+D	1.14E-11	3.90E-09	1.98E-07
Th-230	3.22E-12	9.21E-10	2.28E-11
Th-232	3.60E-12	1.17E-09	9.69E-12
U-234	2.58E-12	7.52E-10	6.85E-12
U-238	3.34E-12	6.39E-10	3.35E-12
U-238+D	3.26E-12	6.40E-10	3.22E-09

F-4: Contribution of ^{232}Th, ^{238}U, and their progenies, in µSv/yr, in soils samples from environs of Kwale HMS deposit to the TEDE

Year	Th-232	Ra-228	Th-228	U-238	U-234	Th-230	Ra-226	Pb-210	Po-210	TEDE
0	0.330274	1.4094	0.2803	0.6351	6.02E-08	1.04E-12	1.83E-14	5.33E-18	5.55E-18	2.6552
5	0.330271	11.8114	12.881	0.6290	6.61E-07	9.5E-11	1.23E-11	6.65E-15	7.61E-15	25.652
10	0.330268	17.3908	25.380	0.6229	1.24E-06	3.4E-10	8.30E-11	8.21E-14	1.10E-13	43.724
15	0.330265	20.4305	33.120	0.6170	1.81E-06	7.32E-10	2.63E-10	3.72E-13	5.28E-13	54.497
20	0.330262	22.1007	37.527	0.6110	2.38E-06	1.28E-09	6.08E-10	1.11E-12	1.62E-12	60.569
25	0.330259	22.9965	39.915	0.6052	2.93E-06	1.96E-09	1.16E-09	2.55E-12	3.8E-12	63.847
30	0.330256	23.4845	41.220	0.5994	3.47E-06	2.78E-09	1.96E-09	5.02E-12	7.59E-12	65.634
35	0.330254	23.7525	41.938	0.5936	4.00E-06	3.75E-09	3.08E-09	8.93E-12	1.36E-11	66.614
40	0.330251	23.8961	42.323	0.5879	4.52E-06	4.84E-09	4.53E-09	1.46E-11	2.25E-11	67.137
45	0.330248	23.9743	42.533	0.5822	5.02E-06	6.07E-09	6.38E-09	2.25E-11	3.48E-11	67.419
50	0.330245	24.0171	42.647	0.5766	5.53E-06	7.44E-09	8.67E-09	3.31E-11	5.14E-11	67.571
55	0.330242	24.0400	42.709	0.5711	6.01E-06	8.92E-09	1.14E-08	4.67E-11	7.28E-11	67.650
60	0.330239	24.0524	42.742	0.5656	6.49E-06	1.05E-08	1.47E-08	6.38E-11	9.98E-11	67.690
65	0.330236	24.0590	42.760	0.5601	6.96E-06	1.23E-08	1.85E-08	8.51E-11	1.34E-10	67.710
70	0.330234	24.0625	42.770	0.5548	7.42E-06	1.41E-08	2.29E-08	1.11E-10	1.74E-10	67.717
75	0.330231	24.0643	42.775	0.5495	7.87E-06	1.61E-08	2.79E-08	1.41E-10	2.22E-10	67.719
80	0.330228	24.0652	42.777	0.5441	8.31E-06	1.82E-08	3.36E-08	1.77E-10	2.80E-10	67.717
85	0.330225	24.0655	42.779	0.5389	8.74E-06	2.04E-08	4.00E-08	2.19E-10	3.46E-10	67.713
90	0.330222	24.0656	42.779	0.5338	9.16E-06	2.27E-08	4.71E-08	2.67E-10	4.22E-10	67.709
95	0.330219	24.0656	42.779	0.5286	9.58E-06	2.51E-08	5.50E-08	3.22E-10	5.10E-10	67.703
100	0.330216	24.0654	42.779	0.5235	9.98E-06	2.76E-08	6.36E-08	3.83E-10	6.08E-10	67.698

F-5: Contribution of ^{232}Th, ^{238}U, and their progenies, in µSv/yr, in soil samples from Environs of Mrima Hill to the TEDE

Year	Th-232	Ra-228	Th-228	U-238	U-234	Th-230	Ra-226	Pb-210	Po-210	TEDE
0	2.499	10.68	2.125	2.1237	2.010E-07	3.464E-12	6.044E-14	4.623E-18	1.621E-18	17.427
5	2.499	88.94	96.83	2.0819	2.174E-06	3.123E-10	4.024E-11	2.159E-14	2.454E-14	190.36
10	2.499	131.10	191.55	2.0410	4.070E-06	1.121E-09	2.745E-10	2.716E-13	3.610E-13	327.19
15	2.499	153.59	249.12	2.0013	5.868E-06	2.391E-09	8.595E-10	1.213E-12	1.712E-12	407.21
20	2.499	165.92	281.82	1.9619	7.616E-06	4.136E-09	1.966E-09	3.570E-12	5.202E-12	452.19
25	2.499	172.55	299.62	1.9233	9.292E-06	6.323E-09	3.737E-09	8.214E-12	1.221E-11	476.59
30	2.499	176.13	309.23	1.8854	1.090E-05	8.934E-09	6.313E-09	1.615E-11	2.433E-11	489.74
35	2.499	178.05	314.41	1.8483	1.244E-05	1.195E-08	9.825E-09	2.850E-11	4.334E-11	496.81
40	2.499	179.07	317.18	1.8124	1.390E-05	1.532E-08	1.433E-08	4.614E-11	7.068E-11	500.56
45	2.499	179.63	318.69	1.7767	1.531E-05	1.909E-08	2.006E-08	7.073E-11	1.090E-10	502.60
50	2.499	179.93	319.50	1.7418	1.667E-05	2.323E-08	2.707E-08	1.033E-10	1.599E-10	503.67
55	2.499	180.09	319.93	1.7075	1.796E-05	2.770E-08	3.546E-08	1.451E-10	2.255E-10	504.23
60	2.499	180.18	320.16	1.6743	1.918E-05	3.244E-08	4.519E-08	1.967E-10	3.065E-10	504.51
65	2.499	180.22	320.29	1.6413	2.036E-05	3.755E-08	5.660E-08	2.604E-10	4.069E-10	504.65
70	2.499	180.24	320.35	1.6090	2.149E-05	4.296E-08	6.964E-08	3.369E-10	5.277E-10	504.70
75	2.499	180.26	320.38	1.5774	2.256E-05	4.865E-08	8.440E-08	4.274E-10	6.707E-10	504.71
80	2.498	180.26	320.39	1.5467	2.357E-05	5.454E-08	1.007E-07	5.315E-10	8.354E-10	504.70
85	2.498	180.26	320.40	1.5163	2.455E-05	6.076E-08	1.191E-07	6.528E-10	1.028E-09	504.67
90	2.498	180.26	320.40	1.4572	2.636E-05	7.392E-08	1.616E-07	9.477E-10	1.496E-09	504.61
95	2.498	180.25	320.39	1.4310	2.713E-05	8.022E-08	1.836E-07	1.107E-09	1.748E-09	504.57
100	2.498	180.25	320.39	1.4285	2.720E-05	8.084E-08	1.858E-07	1.123E-09	1.774E-09	504.57

F-6: Contribution of 232Th, 238U, and their progenies in soil samples from the environs of Mrima Hill to the incremental lifetime cancer risk, ILCR

Year	Th-232	Ra-228	Th-228	U-238	U-234	Th-230	Ra-226	Pb-210	Po-210	Total
0	1.0530E-06	3.1668E-04	5.0181E-04	4.4048E-06	9.7987E-12	1.2122E-15	3.6652E-15	4.4514E-18	7.0728E-18	8.2395E-04
5	1.0530E-06	3.6895E-04	6.1374E-04	4.3182E-06	1.2882E-11	1.9026E-15	6.7231E-15	9.3165E-18	1.4986E-17	9.8806E-04
10	1.0530E-06	3.9710E-04	6.8560E-04	4.2332E-06	1.5840E-11	2.7766E-15	1.1314E-14	1.7568E-17	2.8527E-17	1.0880E-03
15	1.0530E-06	4.1212E-04	7.2580E-04	4.1509E-06	1.8642E-11	3.8124E-15	1.7681E-14	3.0337E-17	4.9630E-17	1.1431E-03
20	1.0530E-06	4.2035E-04	7.4813E-04	4.0692E-06	2.1362E-11	5.0294E-15	2.6303E-14	4.9415E-17	8.1345E-17	1.1736E-03
25	1.0529E-06	4.2477E-04	7.6020E-04	3.9891E-06	2.3968E-11	6.4082E-15	3.7409E-14	7.6260E-17	1.2618E-16	1.1900E-03
30	1.0529E-06	4.2715E-04	7.6670E-04	3.9106E-06	2.6463E-11	7.9421E-15	5.1279E-14	1.1253E-16	1.8699E-16	1.1988E-03
35	1.0529E-06	4.2843E-04	7.7020E-04	3.8336E-06	2.8850E-11	9.6243E-15	6.8175E-14	1.5991E-16	2.6671E-16	1.2035E-03
40	1.0529E-06	4.2911E-04	7.7206E-04	3.7591E-06	3.1105E-11	1.1425E-14	8.8064E-14	2.1927E-16	3.6684E-16	1.2060E-03
45	1.0529E-06	4.2948E-04	7.7307E-04	3.6851E-06	3.3289E-11	1.3383E-14	1.1168E-13	2.9381E-16	4.9286E-16	1.2073E-03
50	1.0528E-06	4.2967E-04	7.7361E-04	3.6126E-06	3.5374E-11	1.5471E-14	1.3900E-13	3.8453E-16	6.4655E-16	1.2079E-03
55	1.0528E-06	4.2977E-04	7.7389E-04	3.5415E-06	3.7364E-11	1.7682E-14	1.7023E-13	4.9307E-16	8.3075E-16	1.2083E-03
60	1.0528E-06	4.2982E-04	7.7403E-04	3.4726E-06	3.9239E-11	1.9982E-14	2.0506E-13	6.1928E-16	1.0452E-15	1.2084E-03
65	1.0528E-06	4.2985E-04	7.7411E-04	3.4043E-06	4.1049E-11	2.2423E-14	2.4456E-13	7.6792E-16	1.2982E-15	1.2084E-03
70	1.0528E-06	4.2986E-04	7.7414E-04	3.3373E-06	4.2773E-11	2.4971E-14	2.8846E-13	9.3896E-16	1.5896E-15	1.2084E-03
75	1.0527E-06	4.2986E-04	7.7415E-04	3.2716E-06	4.4413E-11	2.7621E-14	3.3690E-13	1.1338E-15	1.9219E-15	1.2083E-03
80	1.0527E-06	4.2986E-04	7.7415E-04	3.2080E-06	4.5952E-11	3.0334E-14	3.8931E-13	1.3509E-15	2.2924E-15	1.2083E-03
85	1.0527E-06	4.2985E-04	7.7414E-04	3.1449E-06	4.7433E-11	3.3172E-14	4.4714E-13	1.5969E-15	2.7127E-15	1.2082E-03
90	1.0527E-06	4.2984E-04	7.7413E-04	3.0830E-06	4.8838E-11	3.6098E-14	5.0985E-13	1.8706E-15	3.1806E-15	1.2081E-03
95	1.0527E-06	4.2984E-04	7.7412E-04	3.0223E-06	5.0169E-11	3.9107E-14	5.7755E-13	2.1729E-15	3.6979E-15	1.2080E-03
100	1.0527E-06	4.2983E-04	7.7410E-04	2.9628E-06	5.1429E-11	4.2195E-14	6.5030E-13	2.5050E-15	4.2665E-15	1.2079E-03

F-7: Contribution of ^{232}Th, ^{238}U, and their progenies in soil samples from environs of Kwale HMS deposit to the incremental lifetime cancer risk, ILCR

| Year	Th-232	Ra-228	Th-228	U-238	U-234	Th-230	Ra-226	Pb-210	Po-210	Total
0	1.3916E-07	4.2110E-05	6.6712E-05	1.3561E-06	3.0525E-12	3.7377E-16	1.1314E-15	1.3761E-18	2.1962E-18	1.1032E-04
5	1.3916E-07	4.9068E-05	8.1570E-05	1.3431E-06	4.0369E-12	5.8796E-16	2.0788E-15	2.8820E-18	4.6566E-18	1.3212E-04
10	1.3916E-07	5.2891E-05	9.1280E-05	1.3301E-06	5.0133E-12	8.6456E-16	3.5279E-15	5.4835E-18	8.9446E-18	1.4564E-04
15	1.3916E-07	5.4941E-05	9.6738E-05	1.3174E-06	5.9595E-12	1.1960E-15	5.5593E-15	9.5514E-18	1.5698E-17	1.5314E-04
20	1.3916E-07	5.6068E-05	9.9778E-05	1.3046E-06	6.8978E-12	1.5889E-15	8.3330E-15	1.5678E-17	2.5929E-17	1.5729E-04
25	1.3916E-07	5.6671E-05	1.0141E-04	1.2921E-06	7.8068E-12	2.0330E-15	1.1892E-14	2.4256E-17	4.0320E-17	1.5952E-04
30	1.3916E-07	5.7000E-05	1.0231E-04	1.2797E-06	8.6977E-12	2.5314E-15	1.6367E-14	3.5907E-17	5.9945E-17	1.6073E-04
35	1.3916E-07	5.7179E-05	1.0279E-04	1.2675E-06	9.5709E-12	3.0831E-15	2.1857E-14	5.1222E-17	8.5825E-17	1.6138E-04
40	1.3915E-07	5.7263E-05	1.0302E-04	1.2575E-06	1.0277E-11	3.5767E-15	2.7211E-14	6.7016E-17	1.1258E-16	1.6168E-04
45	1.3915E-07	5.7330E-05	1.0320E-04	1.2432E-06	1.1275E-11	4.3500E-15	3.6371E-14	9.5613E-17	1.6114E-16	1.6191E-04
50	1.3915E-07	5.7358E-05	1.0328E-04	1.2313E-06	1.2096E-11	5.0556E-15	4.5495E-14	1.2569E-16	2.1232E-16	1.6201E-04
55	1.3915E-07	5.7373E-05	1.0332E-04	1.2193E-06	1.2909E-11	5.8195E-15	5.6138E-14	1.6240E-16	2.7488E-16	1.6205E-04
60	1.3915E-07	5.7381E-05	1.0334E-04	1.2077E-06	1.3697E-11	6.6228E-15	6.8139E-14	2.0552E-16	3.4850E-16	1.6207E-04
65	1.3915E-07	5.7385E-05	1.0335E-04	1.1961E-06	1.4468E-11	7.4732E-15	8.1694E-14	2.5607E-16	4.3491E-16	1.6207E-04
75	1.3915E-07	5.7388E-05	1.0336E-04	1.1732E-06	1.5972E-11	9.3224E-15	1.1400E-13	3.8282E-16	6.5192E-16	1.6206E-04
80	1.3914E-07	5.7388E-05	1.0336E-04	1.1619E-06	1.6695E-11	1.0309E-14	1.3271E-13	4.5950E-16	7.8340E-16	1.6205E-04
85	1.3914E-07	5.7388E-05	1.0336E-04	1.1507E-06	1.7412E-11	1.1350E-14	1.5353E-13	5.4714E-16	9.3378E-16	1.6204E-04
90	1.3914E-07	5.7387E-05	1.0336E-04	1.1397E-06	1.8105E-11	1.2422E-14	1.7605E-13	6.4430E-16	1.1006E-15	1.6203E-04
95	1.3914E-07	5.7387E-05	1.0336E-04	1.1295E-06	1.8737E-11	1.3445E-14	1.9828E-13	7.4178E-16	1.2681E-15	1.6202E-04
100	1.3914E-07	5.7387E-05	1.0336E-04	1.1214E-06	1.9242E-11	1.4287E-14	2.1698E-13	8.2464E-16	1.4105E-15	1.6201E-04

Appendix G: Activities in pictorial form

Appendix G-1: Sample collection

Appendix G-2: Sample preparation and analysis
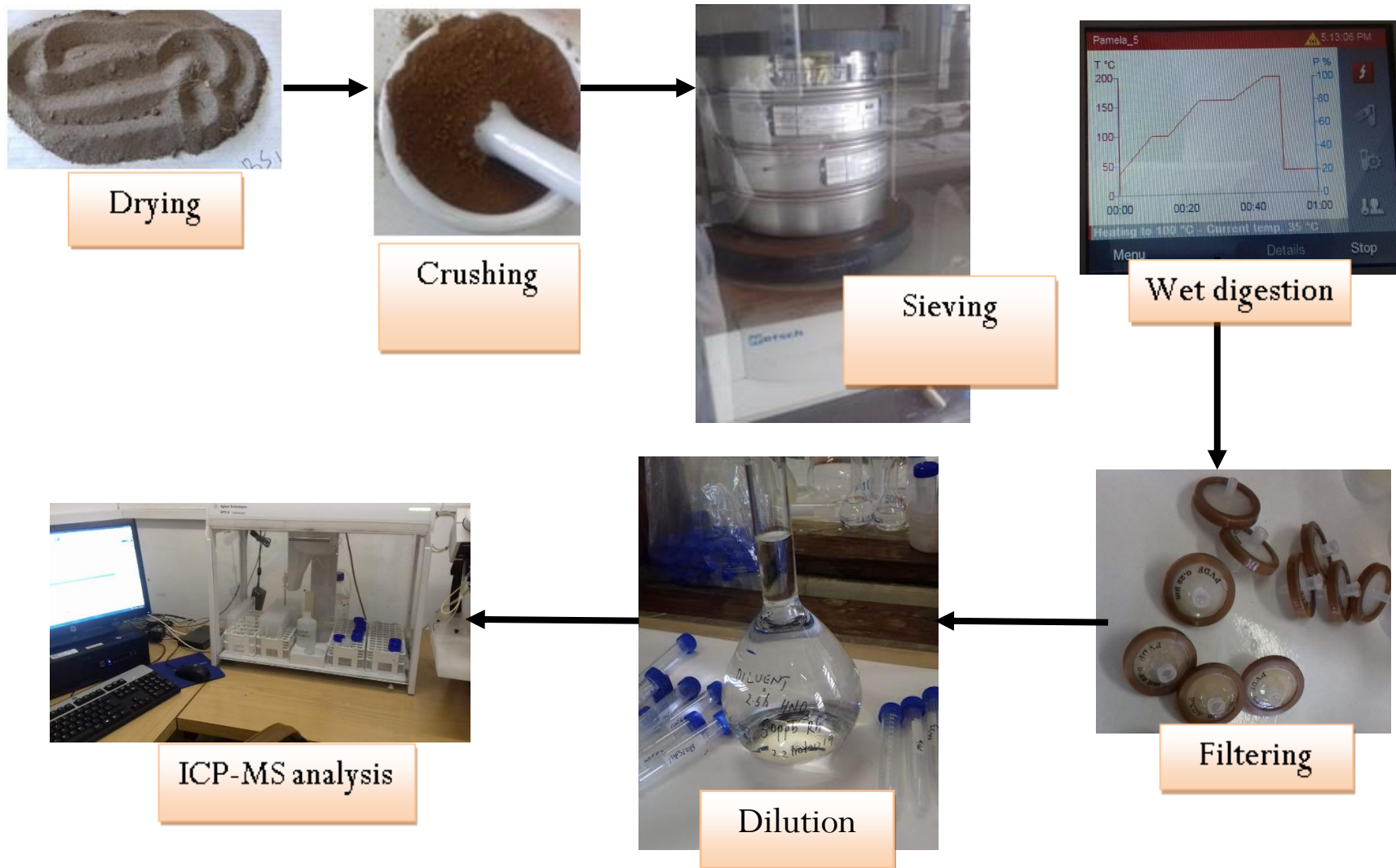
Appendix H: Research Permit

Ref. No. **NACOSTI/P/18/31747/25610**   Date: **18th October, 2018**

Pamella Kageliza Kilavi
The Technical University of Kenya
P.O. Box 52428 - 00200
NAIROBI.

Kindly assist the bearer of this note for her research work.
7-2-2019

07 FEB 2019

RE: RESEARCH AUTHORIZATION

Following your application for authority to carry out research on *"Radiological dose and risk assessment of enhanced naturally occurring radioactive materials from selected high background radiation areas of Kenya"* I am pleased to inform you that you have been authorized to undertake research in **Elgeyo Marakwet and Kwale Counties** for the period ending **17th October, 2019.**

You are advised to report to **the County Commissioners and the County Directors of Education, Elgeyo Marakwet and Kwale Counties** before embarking on the research project.

BONIFACE WANYAMA
FOR: DIRECTOR-GENERAL/CEO

Copy to:

The County Commissioner
Elgeyo Marakwet County.

The County Director of Education
Elgeyo Marakwet County.

8/2/18

SNR. CHIEF
KINONDO LOCATION
Date: 08/02/2019

The County Commissioner
Kwale County.

Telegrams: "EDUCATION", Kwale
Telephone: Kwale 040-2104010
Email Address: kwalecde@gmail.com
Please when replying quote

REF: KWL/CDE/A/VOL1./128

THE COUNTY DIRECTOR OF EDUCATION
P.O BOX 20 – 80403
KWALE

DATE: 07/02/2019

Pamella Kageliza Kilavi
Technical University of Kenya
P O Box 52428 - 00200
NAIROBI

RE: RESEARCH AUTHORIZATION

Following your request to conduct a study on **"Radiological dose and risk assessment of enhanced naturally occurring radioactive materials from selected high background radiation areas of Kenya"** in Kwale County. You have been granted permission to conduct the research for the duration scheduled.

You are advised that this program should not interfere with normal School learning activities.

A report on the Exercise will be required as feedback.

A report on the Exercise will be required as feedback.

Thank you,

7/2/2019

ZILLAH MWAGHOGHO
FOR: COUNTY DIRECTOR OF EDUCATION
KWALE COUNTY

CC.

- The County Commissioner – Kwale

- Sub County Director of Education – Matuga Sub County

- Director General - CEO

Appendix I: Published papers

Check for updates

Quality and human health risk assessment of uranium and other heavy metals in drinking water from Kwale County, Kenya

Pamella Kageliza Kilavi · M. I. Kaniu ·
J. P. Patel · I. T. Usman ⓞ

Abstract Heavy metal contamination in drinking water is a global health concern. Anthropogenic and geogenic activities exacerbate the concentrations of these metals in surface and groundwater. In this study, we sampled drinking water sourced from surface and groundwater resources at the environs of Mrima Hill and the Kwale heavy minerals sand deposit, Kwale County, Kenya. The concentrations of Cr, Ni, Cu, As, Cd, Pb, and U were measured using the inductively coupled plasma mass spectrometer. The water quality indices were evaluated using the weighted arithmetic index method, while the human health risks due to exposure to these heavy metals through the ingestion pathway were assessed using deterministic and probabilistic techniques. The concentrations of Cr and Cd in samples from both study areas exceeded the national and international maximum contaminant levels in drinking water. The concentration levels of Ni, Cu, As, and U in all samples from both study areas were within the recommended values in drinking water. Therefore, the quality of water from both study areas was unsuitable for human consumption due to Cd and Cr contamination. The non-carcinogenic risk assessment also showed that the hazard indices (HI) evaluated for both children and adults at the study areas were higher than unity. In addition, the estimated carcinogenic risks of both population groups were more than the recommended value of 10^{-4}. This study shows that the residents near Mrima Hill and the Kwale heavy minerals sand deposit remain susceptible to carcinogenic and non-carcinogenic health risks emanating from exposure to these heavy metals in drinking water.

Assessment of Heavy Metal Pollution in Soil and Associated Risks in the Environs Adjacent to a Heavy Mineral Sand Mine on the South Coast of Kenya

P. K. Kilavi · M. I. Kaniu · J. P. Patel · I. T. Usman

Abstract Heavy metal pollution is a global concern with significant ecological and health implications. However, limited studies have focused on assessing heavy metal pollution in soil resulting from heavy mineral sand (HMS) mining and processing activities, as well as its effects on ecology and human health. In this study, we assessed heavy metal concentrations in soil samples collected near an HMS mine on the south coast of Kenya using Agilent 7700s ICP-MS. Geoaccumulation index (I_{geo}), enrichment factor (EF), and pollution index (PI) were used to evaluate the extent of soil pollution. The non-carcinogenic (NCR) and carcinogenic (CR) health risk from metal exposure was also evaluated. The results showed moderate pollution by Ti, Mn, Zn, and Nb and high pollution by Cr and As. Mean Cr concentration exceeded the maximum allowable concentration (MAC) and trigger value (TV) by 135 and 61 times, respectively, in topsoil, while As exceeded MAC and TV by 8 and 2 times. Cr and As enrichment factors (EF) were ~200 and ~25 times higher than the EF threshold value of 1.5. The NCR assessment showed that the population was more susceptible to the effects of As, while the CR assessment indicated a higher risk from Cr and As. Notably, the CR values for both As and Cr exceeded the threshold value of 10^{-4}. The findings of this study are essential for developing regulations to monitor, control, and mitigate soil pollution from HMS mining activities and its impact on soil and human health.